

(Please see the last page of this document for a list of mistakes found)

UNIVERSITY OF CALIFORNIA, SAN DIEGO

**Temporal variability of atmospheric oxygen from both
continuous measurements and a flask sampling network:
Tools for studying the global carbon cycle**

A dissertation submitted in partial satisfaction of the
requirements for the degree Doctor of Philosophy in

Oceanography

by

Andrew C. Manning

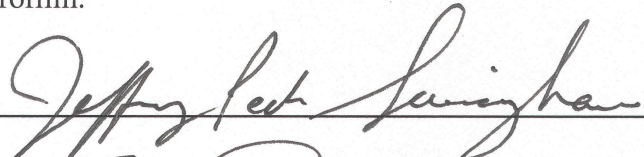
Committee in charge:

Professor Ralph F. Keeling, Chair
Professor Veerabhadran Ramanathan
Professor Jeffrey P. Severinghaus
Professor William C. Troglor
Professor Ray F. Weiss

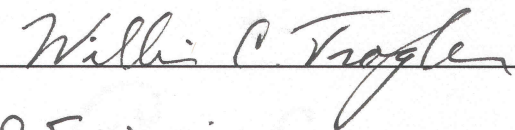
2001

Copyright
Andrew C. Manning, 2001
All rights reserved.

The dissertation of Andrew C. Manning is approved, and
it is acceptable in quality and form for publication on
microfilm:



C. Remoath



R. F. Wern

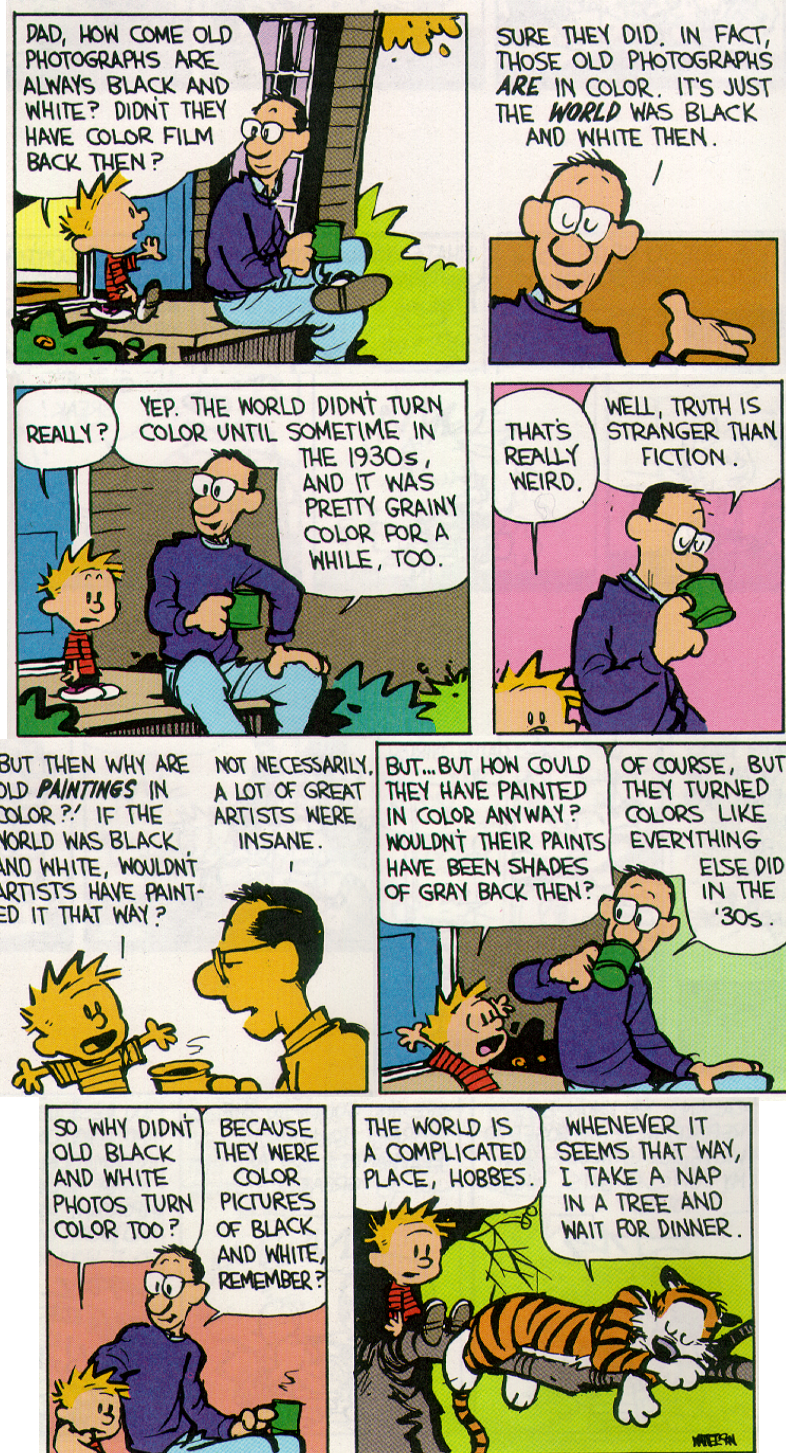


Chair

University of California, San Diego
2000

To Mum and Dad

Figuring Out a Complicated World



Calvin and Hobbes. Copyright 1991 Watterson. Reprinted with permission of UNIVERSAL PRESS SYNDICATE. All rights reserved

I have felt like taking many naps during the last seven years. Fortunately I didn't.

TABLE OF CONTENTS

Signature Page	iii
Dedication	iv
Epigraph	v
Table of Contents	vi
List of Figures and Tables	viii
Acknowledgements	x
Vita and Publications	xxiii
Abstract	xxiv
Chapter 1. Introduction	1
1.1. References	17
Chapter 2. Atmospheric oxygen in the 1990s from a global flask sampling network: Trends and variability pertaining to the carbon cycle	21
Abstract	22
2.1. Introduction	23
2.2. Sample Collection and Raw Data Analysis	30
2.2.1. Methods	30
2.2.2. Raw Data Presentation	33
2.2.3. Data Adjustments	38
2.3. First Order Interpretations of the Data	45
2.3.1. Seasonal Cycles	45
2.4. Interpreting Seasonal Cycles of O ₂ and CO ₂ at American Samoa ...	54
2.4.1. Unique Features Observed in Atmospheric Data Collected at Samoa	54
2.4.2. Land and Ocean Partitioning of Air Mass Influences at Samoa	59
2.4.3. Conclusions	66
2.5. Global Land Biotic and Oceanic Carbon Sinks	67
2.5.1. Update of <i>Keeling et al.</i> [1996]	72
2.5.2. Calculation for the Decade of the 1990s for the IPCC Third Assessment Report	74
2.5.3. Special Considerations in the IPCC Global Sinks Calculation	80
2.5.4. Comparisons With Other Results	85
2.6. Interannual Variability	88
2.6.1. Interannual Variability in Global Land and Ocean Carbon Sinks	88
2.6.2. Interannual Variability in Seasonal Cycles	88
2.7. References	94
Chapter 3. Precise atmospheric oxygen measurements with a paramagnetic oxygen analyzer	101
Abstract	102
3.1. Introduction	103
3.2. Paramagnetic Analyzer System Design and Testing	105
3.2.1. Paramagnetic Analyzer and Gas Handling Descriptions	105
3.2.2. Fine-Tuning Improvements	111

3.2.3. Experimental Testing	112
3.3. Preliminary Results of Continuous Oxygen Measurements	117
3.4. Discussion and Conclusions	123
3.5. References	126
Chapter 4. Oceanic and terrestrial contributions to atmospheric O ₂ and CO ₂ derived from continuous measurements at Baring Head, New Zealand	129
Abstract	130
4.1. Introduction	131
4.2. Methods	136
4.2.1. Paramagnetic analyzer improvements	136
4.2.2. O ₂ /N ₂ Ratio Fractionation at ‘Tee’ Junctions	142
4.2.3. Deployment of Paramagnetic Analyzer at Baring Head, New Zealand	145
4.2.4. Calibration Procedures and Results	153
4.3. The First Year of Data	162
4.3.1. Seasonal Cycle Observed at Baring Head	162
4.3.2. High Temporal Resolution Features in O ₂ and CO ₂ Concentrations	171
4.4. Anomalous Events	178
4.5. Determining the land biotic O ₂ :C ratio	185
4.5.1. Preliminary Analyses of Land Biotic O ₂ :C Ratios	186
4.5.2. Computational Techniques Used to Derive O ₂ :C Ratios	187
4.6. References	190
Appendix 1. Baring Head oxygen system LabVIEW programming	193
Appendix 2. Support	201

LIST OF FIGURES AND TABLES

Table 2.1.	Summary of Flask Sampling Stations in the Scripps O ₂ /N ₂ Network .	31
Figure 2.1.	Scripps Atmospheric O ₂ /N ₂ Ratio Flask Sampling Network	32
Figure 2.2.	Atmospheric O ₂ /N ₂ Ratios From All Stations	35
Figure 2.3.	Atmospheric CO ₂ Concentrations From All Stations	36
Figure 2.4.	Atmospheric Potential Oxygen From All Stations	37
Table 2.2.	Average Amplitudes of Seasonal Cycles	47
Figure 2.5.	Interannually Detrended APO From All Stations	48
Figure 2.6.	O ₂ /N ₂ Ratio Seasonal Cycle Amplitude From All Stations	50
Figure 2.7.	CO ₂ Concentration Seasonal Cycle Amplitude From All Stations.....	51
Figure 2.8.	Atmospheric Potential Oxygen Seasonal Cycle Amplitude From All Stations	52
Figure 2.9.	American Samoa O ₂ /N ₂ and CO ₂ Seasonal Cycles	55
Figure 2.10.	Air Circulation Patterns in the Region of American Samoa.....	57
Figure 2.11.	American Samoa CO ₂ Concentrations.....	59
Figure 2.12.	Oceanic and Land Biotic Influences on Air Masses Arriving at Samoa	60
Figure 2.13a.	APO Residuals from Curve Fit at Samoa	62
Figure 2.13b.	CO ₂ Residuals from Curve Fit at Samoa	63
Figure 2.14.	Deseasonalized O ₂ /N ₂ Ratios Subtracted from Cape Grim of All Stations	68
Figure 2.15.	Deseasonalized CO ₂ Concentrations Subtracted from Cape Grim of All Stations	69
Figure 2.16.	Deseasonalized APO Subtracted from Cape Grim of All Stations.....	70
Figure 2.17.	Vector Diagram of Global Land Biotic and Oceanic Carbon Sinks	73
Table 2.3.	Global Fossil Fuel Combustion Data for the 1990s.....	76
Table 2.4.	Globally and Annually Averaged Trends in the 1990s.....	77
Figure 2.18.	Seasonally Detrended APO From La Jolla and Alert	82
Table 2.5.	Uncertainties in Global Land Biotic and Oceanic Sink Calculations..	86
Figure 2.19.	APO Residuals from Curve Fit From La Jolla and Alert	87
Figure 2.20.	Interannual Variability in Land Biotic and Oceanic Carbon Sinks.....	89
Figure 2.21.	Interannual Variability in O ₂ /N ₂ Ratio Seasonal Amplitude	91
Figure 2.22.	Comparison of Two O ₂ /N ₂ Ratio Flask Sampling Programs.....	92
Table 3.1.	Molar Magnetic Susceptibilities of the Primary Constituents in Air...	107
Figure 3.1.	Paramagnetic Gas Handling Schematic	109
Figure 3.2.	Linearity of the Paramagnetic Analyser.....	115
Table 3.2.	Results From Linearity Test of the Paramagnetic Analyzer	116
Figure 3.3.	Continuous O ₂ /N ₂ and CO ₂ Data from Scripps Pier.....	119
Figure 3.4.	O ₂ /N ₂ and CO ₂ Correlation Plot	121
Figure 3.5.	Paramagnetic and Interferometer O ₂ /N ₂ and CO ₂ Data	122
Figure 4.1.	Location of Baring Head Station, New Zealand	134
Figure 4.2.	Typical Raw Data Output From Paramagnetic Analyzer	138
Figure 4.3.	Transient O ₂ /N ₂ Ratio Spikes Due to Cold Traps.....	140
Figure 4.4.	Baring Head Paramagnetic Analyzer System Gas Handling Schematic	146

Table 4.1.	Interferometric Declared Concentrations of Calibration Gases	154
Figure 4.5.	O ₂ /N ₂ Ratios of Calibration Gases	155
Figure 4.6.	Daily-Defined O ₂ /N ₂ Ratios of Working Gases	156
Figure 4.7.	Daily-Defined O ₂ Span of Paramagnetic Analyzer	158
Table 4.2.	Typical Uncertainties in Paramagnetic O ₂ Analyzer System	159
Figure 4.8.	Analysis of Calibration Gas Drift.....	161
Figure 4.9.	O ₂ /N ₂ Ratios and CO ₂ Concentrations from Baring Head	163
Figure 4.10.	APO from Baring Head.....	165
Figure 4.11.	Filtered O ₂ /N ₂ Ratios and CO ₂ Concentrations from Baring Head.....	167
Figure 4.12.	Filtered APO from Baring Head.....	168
Figure 4.13a.	APO, CO ₂ and Wind Direction for July and August 1999.....	172
Figure 4.13b.	APO, CO ₂ and Wind Direction for September and October 1999.....	173
Figure 4.13c.	APO, CO ₂ and Wind Direction for November and December 1999....	174
Figure 4.13d.	APO, CO ₂ and Wind Direction for January and February 2000	175
Figure 4.13e.	APO, CO ₂ and Wind Direction for March and April 2000	176
Figure 4.13f.	APO, CO ₂ and Wind Direction for May and June 2000	177
Figure 4.14.	O ₂ /N ₂ and CO ₂ for 3-5 July 1999	180
Figure 4.15.	O ₂ /N ₂ and CO ₂ for 3-5 July 1999 with Enlarged Scale.....	181
Figure 4.16.	Backward Wind Trajectory for 4 July 1999	182
Figure 4.17.	Land Biotic O ₂ :CO ₂ Ratio for 3-10 November 1999.....	187
Table 4.3.	Comparison of Techniques for Computing O ₂ :C Ratios.....	189

ACKNOWLEDGEMENTS

I hope that these several pages of acknowledgements do not appear over-indulgent. In terms of how much I have to be thankful for from the past seven years, these few pages can not come close to representing the amount of time, guidance, knowledge, help, support, patience, and love that has been given to me by so many people.

In the course of my Ph.D. studies, my life has changed immensely. I have grown up, matured, become wiser, I hope!, made friends, made wrinkles, and learnt a lot about the world, about people, and about atmospheric oxygen. During this same time, the lives of three people I knew were ended prematurely. My aunt, Diana Manning, was a person who was always full of energy and happiness and inspiring others to great things. I clearly remember enthusiastic encouragement she gave me, sometimes as long as 20 years ago, and her words still have an impact on me today. Diane Phillips was for a short time a fellow-Kiwi Scripps graduate student, and I regret that I did not have the chance to have a longer friendship with her. In her one year at Scripps before her death, I knew already that she was a very special person, and even with the brief contact we had, she managed to touch my life profoundly. Paul Fernandes was the younger brother of one of my closest and oldest friends, Neil. I never knew Paul very well, he was always simply 'my friend's brother', but I was in New Zealand in the months leading up to his death, and I saw the toll that this took on Neil and his family. I mention these three people here to give some perspective to my own life. This dissertation is the product of seven years of my life, and this, and my future career are very important to

me. However, these three tragic losses remind me that there are other things in life that are more important, and that life itself should never be taken for granted.

I am now the age my advisor, Ralph Keeling, was when we first met – a strange concept for me to consider! Ralph and I have had many ups and downs, and we have not always seen eye to eye. I was learning how to be a graduate student at the same time that he was learning how to be a professor, and we didn't always agree on the other's methods. However, after some bumpy initial years, we settled into a much more healthy relationship, and as I leave Scripps now, having been Ralph's employee or student for over eight years, more than one quarter of my life, it is with a sense of much sadness and loss. I have become very attached to both Ralph and his lab, and I will always have an active interest in knowing how he and his lab are doing. Even after eight years, Ralph's grasp and understanding of biogeochemistry and general scientific principles continue to amaze me. It is not often that you can find an advisor who is both an expert in laboratory and instrument development, and also at the forefront of his field from a scientific standpoint. Ralph is both of these. I very much hope that Ralph and I continue to collaborate together for many, many years to come.

I have not had much interaction with my original thesis committee, Ray Weiss, Ramanathan, Tom Haywood, and Kent Wilson, over the years, but I thank them for the help they did provide whenever I asked. And I thank Bill Trogler and Jeff Severinghaus for agreeing to step in as committee replacements at a very late date, and slogging through reading this long dissertation. Jeff, especially, is someone whom I look up to as the kind of scientist that I aspire to be. I find myself in an unusual position with respect

to Jeff, we were both students working together in Ralph's lab many years ago, now I am still a student, and he is a professor on my thesis committee!

The two people from Ralph's lab whom I owe a very big debt of gratitude to are Elizabeth McEvoy and Bill Paplawsky. Elizabeth was the glue that held our lab together, organising pizza lunches, making cakes, and keeping people happy working with each other with her very social, cheerful, and flamboyant personality. I also got to know Elizabeth outside the lab, and very much enjoyed the friendship that grew from this. I can't thank Bill Paplawsky enough for everything he has given me over the years. Bill has two qualities that make him the very best person any student could ever hope to have in their lab; first, he has an in-depth knowledge of just about everything, he can fix anything, explain how anything works, and give advice and suggestions on how to go about doing anything. Bill's second quality is that he is always very willing to share this knowledge and his time to help you out. Bill also helped me through a very tough time of my Ph.D. early on, for which I am very grateful. I only hope that I have been able to give something back with my friendship to him.

Several other people in Ralph's lab gave me much help and advice over the years. Laura Katz, Chris Atwood, Hernan Garcia, Max Hecksher, Anh Nguyen, Emily Fung, and Alex Chow helped out with a variety of things ranging from photocopying to helping with making figures to advice on C programming to filling compressed air cylinders.

In three trips to New Zealand during my Ph.D. studies, I spent a total of 10 months working in the laboratories of NIWA, the National Institute for Water and Atmospheric Research, and consequently I have a long list of people I must thank for

their helpfulness and generosity with their time, their friendships, their sharing of their offices, lab spaces, and scientific and technical expertise, and especially with putting up with yet another question of “Where can I find a spanner/drill/screw/nail/Snoop/screwdriver/voltmeter/resistor/computer keyboard/extension cord/...?”. Many thanks to Carolyn Walker, Dick Barr, Tony Bromley, Ross Martin, Rob Knobben, Rowena Moss, Mike Harvey, John MacGregor, Tracy Adamson, Sarah Bury, Mike Uddstrom, Bob Walker, Zhu Mei, Sylvia Nichol, Dom Ferretti, Jill Caine, and especially Kim Currie.

Also at NIWA, Antony Gomez, Gordon Brailsford, and Dave Lowe deserve special mention. Antony and Gordon have both worked hard at maintaining the paramagnetic oxygen analyser system at Baring Head over the last two years. I think that they have both learnt a lot more about the fickleness of atmospheric oxygen than they cared to in the process! In addition to oxygen related problems they have fought against lightning strikes, flooded rivers, bridge outages, wild pigs, and antsy farmers to keep my system running and for this I am very grateful. During my time in New Zealand they both provided more support than I had a right to ask for, with Antony writing a large chunk of the LabVIEW programming, and Gordon always very willing to share his expertise and knowledge on instrument development and gas handling.

Ten years ago, Dave Lowe was the person who inspired me to want to become an experimental scientist. His constant enthusiasm and motivation was infectious. It was impossible to ever feel down, or to think science was boring when working with Dave. After three weeks working in the lab one time, we finally solved a problem on the vacuum line that had been bugging the hell out of us, and Dave’s next step was to immediately crack open a couple of beers right there in the lab to celebrate. And so I

thank Dave for showing me how much fun science can be, and for being instrumental in sending me down the career path I now find myself on.

One thing about taking seven years to do a Ph.D. is that you have opportunities both to make a large number of friends, and to get quite attached to some of them. In both of these aspects, I feel that I have been very lucky during my time at Scripps. Of my friends, several I must mention specifically here.

Rain Bosworth owns the distinction of being the first deaf person (other than my sister) with whom I became friends. During my time in San Diego, in addition to my Ph.D. studies, I have learnt a huge amount about deaf culture, both from meeting other deaf people through Rain, from taking many sign language classes at UCSD and reading books, and from Rain herself, and for this I am very grateful. I have also been forced to re-examine and think about my own deafness in a new light, which has been a large part of my personal growth over the last few years.

In addition to having so much in common with Rain because of our deafness, we also have much in common in other parts of our lives, and she has always been a wonderfully supportive, motivational, and cheerful friend. Perhaps because it was the easiest way for us to communicate before I learnt sign language, Rain and I were always prolific email correspondents, often having a ‘conversation’ lasting an hour via a flurry of emails back and forth, on topics covering almost anything imaginable, even though we had offices only half a mile from each other. We both have an equal thirst for knowledge, and we both have an equal, deaf-induced, lack of general world and current affairs knowledge which we are trying to eliminate and which we weren’t embarrassed to admit to each other. These similarities gave us a deep understanding of each other,

and resulted in a very close friendship which I hope will continue until we are too old to type! Thank you, Rain, for everything you have taught me, about being deaf, and about myself.

Continuing with the deaf theme, I would like to thank Carol Padden and Tom Humphries. Carol and Tom are perhaps the two most well-known deaf people in the U.S., and they are both professors at UCSD. One day I found myself thinking, “Wow! They have invited me, me!, to dinner at their house!” They are a constant source of inspiration for me, proving by their own examples and in their quiet, modest ways, the great lengths to which deaf people can succeed in this hearing world.

Helen Perks was my officemate for almost six years. When you share an office with someone for such a long time, sometimes more than 12 hours a day, sometimes 7 days a week, it is impossible not to share intimate details about your personal lives, impossible not to share in your daily life experiences, all the good times and the bad times. Also being a fellow foreigner, Helen was able to commiserate whenever I felt alienated by something about American culture. Helen is something of an enigma, being very different from anyone else I have ever met, and this has also made it enjoyable and interesting getting to know her. Thank you for the many years of friendship, companionship, conversations, and the many, many dinners you cooked for me – they were all much better than you gave yourself credit for!

Until I met Britt Stephens I thought I knew everything there was to know about the art of procrastination. Britt, however, taught me that it is a constantly evolving art form, and requires a lot of hard work to stay on top of the game. At the same time, with our frequent 3am chats about oxygen fractionation or the reason for using ‘per meg’

units, we both taught each other a lot about our research. Only one thing is guaranteed with Britt, and that is, you will never be bored, whether working or playing, it is always an adventure. Britt has always been a really great friend: every time I tore shoulder or knee ligaments, or flew over the bike handlebars once again while trying to keep up with him, he was always right there to rush me off to hospital. But I'm telling you, you lost that sculling race!

Alison Shaw took over Helen's role as officemate, and she did a wonderful job, especially with putting up with an officemate who was often stressed-out and occasionally bordering on insanity through the last months of finishing this thesis. After some initial communication technical difficulties (Ali speaks at about 10 decibels lower than my threshold hearing!), we established a good understanding, and after a few months, I was able to figure out what she was actually talking to me about... usually. Ali also proved to be an excellent replacement for Britt as my procrastination partner, being very inventive and creative at finding ways of not working on your research, and also bringing a woman's touch to procrastinating, something I hadn't previously had the privilege to learn about. Thank you for always being a shining light in the office, and helping me through the final few months (even though you didn't realise!).

Graham Mortyn made an exception for me, and became close friends with someone who had never surfed in his life, nor had any intention to. Graham is the most stable and reliable person I know, and it was great to have him as a close friend for so many years. He helped to provide some much needed balance and stability to my own life at some important times, often without even knowing, for which I am very grateful. I very much look forward to continuing our friendship in Europe.

Aaron Thode was my flatmate for almost two years and one of the best of the 22 flatmates I have had. Aaron is also the most quirky person with whom I've become close friends, and I found myself often entertained by his unusual habits, ways of doing things, and ways of thinking about things. Sleeping on the roof for a week (for which he had to climb in and out of my bedroom window, sometimes while I was sleeping), was a good example. Thank you for your friendship, and I hope you never change.

This year, for the first time in 19 years, my life and that of Neil Fernandes have taken different paths. We have followed each other along very similar paths through intermediate school and high school in Lower Hutt, New Zealand, to university in first Wellington, and then Christchurch, and finally we both ended up in universities in southern California studying for our Ph.D.'s. Now we are about to end up on opposite sides of the planet, as Neil has just gone back to New Zealand and I am about to move to Europe. Our friendship has changed immensely over these 19 years, and yet throughout we have had an instant understanding of each other. Neil is someone with whom I can have no contact for six months, then see him again, and within five minutes immediately be as close as we have ever been. I am very much looking forward to the next 19 years of our friendship.

Veronique Hanssen has more confidence and belief in me than any other friend I have, certainly a lot more than I have myself, and far more than I deserve. I value her friendship for showing me life outside of academia, her uncanny ability to understand a person or a problem almost before she had met the person or heard the problem, for her unflagging belief in me, and for her untiring efforts of trying to get hold of me on the phone!

Anna Broome was a fellow-Kiwi who started graduate school in the US at the same time as me, and we shared some of the many difficulties of adjusting to the demands of graduate school life. Although we have drifted apart more recently, I have many treasured memories of our early times together, and I thank Anna for being there during those times, especially her way of delighting in the silliest little things in life.

Ulli Seibt I only knew in San Diego for six months, but in that short time we became very close friends. Ulli opened my eyes to many aspects of the world that I was previously ignorant of. And she constantly challenged me to perceive and think about things in a different light, and for that I say thank you. I hope that you will continue to keep me on my toes in Jena!

Conny Weyhenmeyer abandoned me by leaving Scripps after only three years. But if she hadn't, I would never have had the opportunity to visit Switzerland, Namibia, and Botswana, so I suppose I will forgive her! It is not possible to ask for anything more in a friend than Conny has given to me. Except perhaps to be in town more often! She is supportive and full of wise advice when you most need it, but will also point out that you are being stupid when you are, in fact... being stupid. Moving closer to Conny is the most attractive personal reason for me moving to Europe in a few short weeks.

With many of my friends graduating and abandoning me and San Diego, Kim Cobb was the one who took over, as my squash-playing, 39¢-cheeseburger-Sunday-at-McDonald's-eating, shoulder-to-cry-on, motivating-each-other, working-all-night companion. My friendship with Kim has continued to grow both closer and stronger throughout the last two years, and she constantly amazes me both with what a wonderful friend she is, and with the very wise words of advice she so often has to give me. In this

last crazy, stressful year of finishing, I can not imagine how I could have possibly survived without the constant, daily support Kim always unfailingly gave to me. Thank you, Kim, and I'm very sorry that I won't be here when you reach the same stage of finishing.

Of my other friends, I want to thank Rob Rhew for always being an inspiration on how to be a considerate person; Sonya Wainwright for teaching me about generosity; Kara Lavender for making so much banana bread for me; Meriah Arias for teaching me about different types of alcohol; Julianna Fessenden for the exciting 4am chair-race through Ritter Hall; Paul and Yvette Drayton for the food 'energy packs' they mailed from Chicago; Angie Knapp for the many supportive and entertaining emails from afar; Tegan Blaine for her help in the last weeks, and for making me feel wiser than I am; Nicole Cardoza for giving me a family away from home; Jane Teranes for being such a cheerful next-door office neighbour; Gladys Strong for her many wise words of advice and her infectious laughter; Kieran Peckston for his friendship from afar, and teaching me a good squash move; Nancy White for the conversations and showing me something of life outside academia; and Manu Di Lorenzo for the Matlab expertise, the incredible pasta he cooked, and the beginnings of a great friendship in my last few months.

Finally I thank my family. Both of my grandmothers, Gran and Umma, visited me in San Diego, an uncomfortable, 24 hour-long journey from New Zealand. I was delighted to be able to show them around my 'home' town, and show them where I lived and worked. Now I will have to ask them both to come even further to visit my new home, I really hope that they will both make it. In their very different ways from

each other, Gran and Umma are both examples to me that getting older is not actually so bad after all. They both have very full and rich lives because of their very strong will and desire to make it so, and I only hope that mine can be the same when I retire.

I have not seen nearly as much of my younger sisters, Victoria and Elizabeth, as I would have liked to over the last seven years, nor have I been very good at writing to either of them. Even when I was back in New Zealand, I spent more of my time hanging out with the Baring Head pigs than with Victoria and Elizabeth, which I regret, but which also seemed to be necessary at the time. I still often think of them both as young girls, and find it a bit of a surprise to discover that they are in fact young women. I know that they are both proud of me, and I hope that they know that I am very proud of both of them. Despite the fact that I am now about to move further away from home, I hope that as we three get older together, we can also become closer to each other. Perhaps now that my student days are over, I will have more time for you both, I hope so.

It is not possible for me to imagine more supportive parents than my Mum and Dad. Since the age of about six, they have brought me up to believe that you go to school, and one day many years later you finish, and you have this thing called a 'Ph.D.'. I was half-way through high school before I discovered that not everybody actually does this! This is not to say that I was in any way pushed into taking this path in my life; Mum and Dad would have been just as supportive no matter what I chose to do, as evidenced by their equal support of both Victoria and Elizabeth. I like to think that I have turned out as a reasonably well-balanced adult, and I give all credit for this to Mum and Dad, for the stability, support, and unconditional love that they have always

unquestioningly given to me. (Well okay, Mum often asked lots of questions, but that was just her intense curiosity!) There was nothing that Mum would not do for me, which she proved time and time again. In fact sometimes I had to make up things for her to do for me, just to keep her happy!

I did everything I could during my undergraduate career to **not** follow in my Dad's footsteps, so maybe it's in my genes, since now I find myself in exactly the same field, and with most of the continuous oxygen data presented in this thesis resulting from an analyser maintained by his group in New Zealand. I don't regret that fate or genes or whatever it was brought me to this position, and I feel much closer to Dad because of it. Dad was always a frequent source of ideas, insight, and helpful discussions while I was in New Zealand, and he contributed a lot to the final chapter of this thesis via many, many emails. But much more than these work aspects, Dad has been the most amazing father for almost 32 years now, and I have many, many memories of all the things he has done for me, and all the things he has taught me, or at least tried to teach me. As one example, I remember one time, I was maybe eight years old, Dad tried to explain these tiny things called atoms, which couldn't be seen, and of which many millions could fit on my thumbnail, he said. Literally for several years after this, I naïvely thought that I had a unique ability to 'see' atoms, but what I now know were small, suspended dust particles which I saw illuminated by a sunbeam shining through my bedroom window.

In day to day life, I almost never thank Mum and Dad for the unending help, patience, and love that they give me, so I hope that these few words of thanks and appreciation will remedy that just a little bit. As I said at my defence, a lot of children

will say about their parents, “they are the best”, but in my case, this really is true, there is no question in my mind.

In finishing, I thank everyone for contributing to making my life the amazing and wonderful journey it has been this far, and particularly for helping me through the last seven years while I worked on getting those two letters, ‘Dr.’ put in front of my name. Most of all, thank you, Mum and Dad.

Chapter 3 appeared in full as Manning, A.C., R.F. Keeling, and J.P. Severinghaus, Precise atmospheric oxygen measurements with a paramagnetic oxygen analyzer, *Global Biogeochemical Cycles*, 13 (4), 1107-1115, 1999. I was the primary investigator and lead author of this paper and conducted all analyses presented therein.

VITA

- 1990 B.E., University of Canterbury, New Zealand
- 1991-1992 Visiting Scientist,
National Center for Atmospheric Research, Boulder, CO
- 1993 Staff Research Associate,
University of California, San Diego
- 1993-2000 Graduate Research Assistant,
University of California, San Diego
- 2001 Ph.D., Scripps Institution of Oceanography,
University of California, San Diego

PUBLICATIONS

Manning, A.C., and R.F. Keeling, Correlations in short-term variations in atmospheric oxygen and carbon dioxide at Mauna Loa Observatory, in *Climate Monitoring and Diagnostics Laboratory, No. 22, Summary Report 1993*, edited by J.T. Peterson, and R.M. Rosson, pp. 121-123, NOAA Environmental Research Laboratories, Boulder, CO, 1994.

Keeling, R.F., A.C. Manning, E.M. McEvoy, and S.R. Shertz, Methods for measuring changes in atmospheric O₂ concentration, and their applications in southern hemisphere air, *Journal of Geophysical Research*, 103 (D3), 3381-3397, 1998.

Manning, A.C., R.F. Keeling, and J.P. Severinghaus, Precise atmospheric oxygen measurements with a paramagnetic oxygen analyzer, *Global Biogeochemical Cycles*, 13 (4), 1107-1115, 1999.

Tyler, S.C., G.A. Klouda, G.W. Brailsford, A.C. Manning, J.M. Conny, and A.J.T. Jull, Seasonal snapshots of the isotopic (¹⁴C, ¹³C) composition of tropospheric carbon monoxide at Niwot Ridge, Colorado, *Chemosphere: Global Change Science*, 1, 185-203, 1999.

Manning, A.C., R.F. Keeling, and L.E. Katz, Interpreting seasonal cycles of atmospheric oxygen and carbon dioxide concentrations at American Samoa Observatory, in *Climate Monitoring and Diagnostics Laboratory, Summary Report No. 25, 1998-1999*, edited by D.J. Hofmann, J.T. Peterson, and R.M. Rosson, U.S. Department of Commerce, NOAA Environmental Research Laboratories, Boulder, CO, *in press*, 2000.

ABSTRACT OF THE DISSERTATION

Temporal variability of atmospheric oxygen from both
continuous measurements and a flask sampling network:
Tools for studying the global carbon cycle

by

Andrew C. Manning

Doctor of Philosophy in Oceanography

University of California, San Diego, 2001

Professor Ralph F. Keeling, Chair

Atmospheric oxygen (O_2) measurements, together with carbon dioxide (CO_2), are useful tools for elucidating mechanisms that influence the global carbon cycle. This dissertation presents a synthesis of data from eleven years of measurements from a global network of flask sampling stations, describes a new method for achieving continuous atmospheric O_2 measurements, and presents one year of data from a field station deployment of this continuous measurement technique. The eleven-year record shows atmospheric O_2 decreasing, but slower than expected from fossil fuel combustion owing to the influence of land biota. From these data a global carbon budget is calculated for the period from January 1990 to January 2000: fossil fuel combustion

produced an average of 6.33 ± 0.38 Gt C/y of CO_2 , of which 3.21 ± 0.13 Gt C/y remained in the atmosphere, 1.44 ± 0.66 Gt C/y were taken up by land biota, and 1.68 ± 0.52 Gt C/y were taken up by oceans.

The rate of decrease in atmospheric O_2 and increase in CO_2 vary from year to year. Analysis of these covariations suggests that exchanges with land biota can account for most of the variation in the CO_2 growth rate. The amplitudes of the seasonal cycles of atmospheric O_2 also show interannual variations, suggesting that oceanic marine productivity rates vary interannually. Observations such as these highlight the value of long records and the need for higher temporal resolution atmospheric O_2 time series that together can capture variability on time-scales ranging from hours to decades.

The new continuous measurement technique employs an analyzer that utilizes the paramagnetic properties of molecular O_2 . The design and development of the analyzer system is discussed, and it is shown to achieve a precision of 1 per meg (≈ 0.2 ppm) from repeated measurements over a one-hour interval. This system was deployed at Baring Head, New Zealand, where it has collected data since June 1999. These data show high resolution features in the seasonal cycle, and high frequency variability that the land biota and oceans can induce in atmospheric O_2 and CO_2 concentrations.

This dissertation also discusses gas handling issues that are important to consider for accurate determination of precise atmospheric O_2 concentrations.

Chapter 1.

Introduction

It is becoming increasingly apparent that human activities are creating unprecedented and perhaps irreversible changes to the Earth's climate system and to marine and terrestrial ecosystems on regional and global scales. Therefore there is a growing sense of urgency that we must increase our understanding of how the modern Earth system functions, its mechanistic controls, influences and feedbacks - so that we can interpret "surprises" as they happen instead of long after the fact, predict future states of the Earth system, and mitigate changes in current human activities where such activities can be shown to be unarguably detrimental. The signing of the "Montreal Protocol" in 1987 by the governments of 175 nations of the world banning the production of stratospheric ozone-destroying chlorofluorocarbons (CFCs) is a landmark example of comprehensive and persuasive scientific research being successfully utilized to make proactive changes in public policy to safeguard our Earth.

One of the current scientific challenges is to determine the effects of increasing concentrations of greenhouse gases on climate and ecosystems on regional and global scales. Several recent studies have found persuasive evidence that globally averaged surface temperatures increased significantly over the 20th century, particularly towards the end of the century [e.g., *Hansen et al.*, 1997]. That this warming is anthropogenically-induced is increasingly becoming the scientific consensus. *Mann et al.* [1998] constructed a surface air temperature record extending back to the year 1400 that shows a remarkable increase in temperatures in the 20th century when compared to the previous five centuries. Furthermore, they concluded that this 20th century increase in temperature was predominantly caused by increased concentrations of anthropogenically produced greenhouse gas.

Levitus et al. [2000] showed a significant warming trend of the world's oceans since the 1950s, illustrating that when the Earth receives more heat, this heat can be distributed to the oceans as well as to the atmosphere. With such findings it becomes increasingly apparent that changes in greenhouse gas concentrations will result in substantial changes to our Earth system.

Actions such as the signing by 84 countries of the "Kyoto Protocol"¹ in 1999 indicate that governments are taking seriously the impact of greenhouse gases on climate, and with this comes several responsibilities for the scientific community. We must continue to improve our understanding of the effects that greenhouse gases have on our climate and ecosystems since there are still many uncertainties and gaps in our current knowledge. With increasing confidence and reliability we must be able to distinguish between natural and anthropogenically-induced climate variability. With the aid of global atmospheric and oceanic computer models, we must be able to confidently project current greenhouse gas concentrations into the future based on expected emission rates, and assess the expected changes to the Earth system. And we must develop accurate monitoring techniques in order to verify adherence to the stipulations and requirements of the Kyoto Protocol or other internationally agreed upon emissions reductions.

Precise atmospheric oxygen (O₂) measurements are one tool that can be used to

¹ The Kyoto Protocol is an international treaty where signatories have given provisional agreement to reduce greenhouse gas emissions. The overall goal of the treaty is to reduce greenhouse gas emissions by 5% from their 1990 levels by the period 2008-2012. Although ratification of the Kyoto Protocol has recently been put in doubt, it still demonstrates that policymakers are considering substantive measures to control greenhouse gas emissions.

help address these issues. In this dissertation I will show how two different methodologies for achieving such measurements - a global network of stations collecting flask samples over many years and automated, continuous O₂ measurements collected over a one-year period - can provide additional information on the global carbon cycle and atmospheric carbon dioxide (CO₂) concentrations. From this knowledge inferences about the anthropogenic forcing of global climate and ecosystem changes can be made.

Of all the anthropogenically produced greenhouse gases, CO₂ is by far the most important, contributing about 64% of the total change in radiative forcing since pre-industrial times [*Schimel et al.*, 1996]. Atmospheric CO₂ concentrations are increasing primarily due to combustion of fossil fuels and in the 1990s approximately 6.3 billion tonnes² of carbon were emitted as CO₂ every year [*Marland et al.*, 2000, H. Khesghi, personal communication]. However, of this only about half remained in the atmosphere. The remainder must have been soaked up by the land biota from a net increase in plant and soil biomass owing to net photosynthesis and growth, or by dissolving into the oceans [*Schimel et al.*, 1996]. In order to predict future atmospheric CO₂ concentrations, we need to be able to quantify how much fossil fuel-emitted CO₂ is absorbed by each of these two reservoirs, and to identify the mechanisms which control these quantities.

Currently no direct measurement techniques exist which can calculate these land

² Here and elsewhere, when I quantify the amount of CO₂ emitted from fossil fuel combustion I also include a small term accounting for CO₂ production from cement manufacture (in this case, 0.2 billion tonnes of carbon per year). These statistics are also included in the *Marland et al.* [2000] database.

biotic and ocean carbon uptake quantities on a global scale and they are poorly known. Complicating this picture, the amount of fossil-fuel emitted CO₂ that remains in the atmosphere exhibits a wide range of interannual variability, even though fossil fuel emissions are relatively constant from year to year [Marland *et al.*, 2000]. This implies that carbon uptake by the oceans or the land biota (or a combination of the two) must exhibit large variations from year to, and mechanisms to explain these variations must also be identified.

In recent years several different carbon-based methods have been devised to estimate this partitioning of the CO₂ absorbed by the oceans and the land biota [Heimann and Maier-Reimer, 1996; Keeling *et al.*, 1989; Quay *et al.*, 1992; Tans *et al.*, 1990]. Most of these carbon-based methods make use of ¹³C/¹²C ratio measurements of atmospheric CO₂. Due to differences in the relative uptake or release of ¹³CO₂ and ¹²CO₂ in land biotic processes compared to oceanic processes, it is possible to make quantitative estimates of the partitioning between these two reservoirs. A complicating factor in these methods, however, is a disequilibrium effect arising because land biotic respiration is occurring from carbon stocks that were assimilated up to several decades earlier.

Another CO₂ sink partitioning method for which disequilibrium effects are minimal in comparison involves making very precise measurements of atmospheric O₂ concentrations [Bender *et al.*, 1994; Keeling, 1988b]. Atmospheric O₂ and CO₂ concentrations are closely linked through the biogeochemical cycles of carbon and oxygen. The main processes affecting both gases are fossil fuel combustion, biomass burning, and photosynthesis and respiration. Stoichiometric differences in these

processes on land, and differences in the physical and chemical interaction of these gases with seawater enable us to obtain additional information about the global carbon cycle not obtainable from a study of carbon and its isotopes alone.

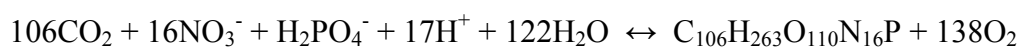
Fossil fuel combustion consumes O_2 and produces CO_2 and can be represented by the chemical equation: $CH_y + (1 + \frac{y}{4})O_2 \rightarrow \frac{y}{2}H_2O + CO_2$. From an extensive global database on the different types of fossil fuels used [Marland *et al.*, 2000, H. Kheshgi, personal communication] and a knowledge of the $O_2:C$ molar ratio for each fuel type [Keeling, 1988a], an average global $O_2:C$ ratio for fossil fuel combustion of 1.39 ± 0.04 moles of O_2 consumed per mole of CO_2 produced is calculated for the 1990s³. As CO_2 is added to the atmosphere by this fossil fuel combustion, the atmosphere-ocean equilibrium balance for CO_2 is shifted, driving a net flux of CO_2 into the oceans. However, because O_2 is much less soluble in seawater than CO_2 there is negligible corresponding outgassing of O_2 from the oceans in response to the fossil fuel-induced decreasing atmospheric O_2 concentrations. It is this difference between the sources and sinks of O_2 and CO_2 which makes it possible to distinguish how much atmospheric CO_2 is being absorbed by the land biota and how much by the oceans. Keeling and Shertz [1992] reported the first estimates of the global land biotic and oceanic carbon sinks derived from such an analysis. Their work has been updated with more recent data in Keeling *et al.* [1996b], Bender *et al.* [1996], and Battle *et al.* [2000].

Photosynthesis and respiration on land can be represented simplistically with the equation: $CO_2 + H_2O \leftrightarrow CH_2O + O_2$, where the forward reaction represents

³ This ratio also includes a consideration of CO_2 production from cement manufacture.

photosynthesis and the reverse reaction represents respiration. CH_2O is only an approximate representation for organic matter and the actual $\text{O}_2:\text{C}$ molar ratio in this equation is approximately 1.1 ± 0.05 moles of O_2 produced per mole of CO_2 consumed [Severinghaus, 1995]. If there is a net imbalance between photosynthesis and respiration then the total land biomass will increase or decrease, and atmospheric O_2 and CO_2 concentrations will change in this molar ratio. Biomass burning and other land-use changes will also affect atmospheric O_2 and CO_2 concentrations in approximately this ratio. Additional information can be obtained from studying the effects of land biotic photosynthesis and respiration on atmospheric O_2 and CO_2 . For example the seasonal cycles and latitudinal gradients in O_2 and CO_2 driven by these processes provide us with information on ecosystem productivity and the timing of growing seasons, interannual variability in these parameters, and information on atmospheric transport patterns [e.g. Keeling *et al.*, 1996a; Keeling *et al.*, 1995].

Photosynthesis and respiration also occur in the ocean biota and can be represented with the equation:



[Redfield *et al.*, 1963]. Here the average $\text{O}_2:\text{C}$ molar ratio is between 1.3 and 1.4 moles of O_2 produced per mole of CO_2 consumed [Keeling *et al.*, 1993]. However, dissolved CO_2 reacts to form carbonic acid and carbonate and bicarbonate ions, lowering the dissolved CO_2 partial pressure. The air-sea exchange of CO_2 is thus significantly buffered compared to O_2 , resulting in a much larger $\text{O}_2:\text{C}$ ratio observed in the flux to and from the atmosphere [Keeling *et al.*, 1993]. In addition, sea surface temperature effects tend to counteract influences on atmospheric CO_2 driven by the seasonal

photosynthesis and respiration cycle of CO₂ production and consumption, but reinforce the influences on atmospheric O₂. For example during spring and summer, with higher rates of photosynthesis there is more consumption of dissolved CO₂ but at the same time surface waters are warmer, reducing the solubility of CO₂. Thus the degree to which CO₂ becomes undersaturated is reduced and there is a diminished CO₂ demand on the atmosphere. In fall and winter the opposite occurs. Whereas in the case of O₂, dissolved O₂ is produced in spring and summer and at the same time the waters warm, decreasing the solubility. These effects combine to cause enhanced O₂ supersaturation and a flux from the ocean to the atmosphere. In fall and winter surface waters are colder and there is less photosynthetically-produced O₂ and these two effects combine to present an O₂ demand to the atmosphere.

Sea surface temperature and wind speed variability also cause changes in the depth of the mixed layer which can also affect air-sea gas fluxes. These two processes also show seasonal variations. For example, in fall and winter, surface waters cool and become more dense and wind speeds are generally higher. Denser surface waters and higher wind speeds both promote more vigorous water column overturning and cause a deepening of the surface mixed layer. As the mixed layer deepens it entrains waters where net respiration occurs, below the illuminated euphotic zone, therefore entraining waters that are O₂-depleted and CO₂-enriched. This effect also reinforces the seasonal air-sea exchange of O₂, while suppressing the exchange of CO₂.

From considerations of these seasonal-scale processes affecting atmospheric O₂, *Keeling and Shertz* [1992], *Bender et al.* [1996], and *Najjar and Keeling* [2000] were able to compute estimates of marine biotic new production. In addition, *Balkanski et al.*

[1999] used atmospheric O₂ seasonal cycle data to assess satellite ocean color data and the performance of an ocean biology model.

If there is any imbalance in the seasonal ingassing and outgassing of O₂ from the oceans when integrated over one year, these can appear as an artifact in calculations of the global land biotic and ocean carbon sink partitioning due to fossil fuel combustion. Perhaps the largest source of uncertainty arises from “stationary fluxes” [Bender *et al.*, 1996; Keeling *et al.*, 1993]. That is, the component of air-sea fluxes associated with oceanic production of organic matter in subtropical and temperate zones, respiration in the main thermocline, and ventilation at subpolar and higher latitudes. Organic matter production enhances O₂ supersaturation, whereas ventilation brings O₂ undersaturated waters to the surface. It is quite possible that these two processes are out of balance for several years, thus having an impact on the interannual atmospheric O₂ decrease [Bender *et al.*, 1996].

In summary, precise measurements of atmospheric O₂ can provide constraints on estimates of global budgets of land biotic and oceanic carbon sinks, and on marine biotic productivity. Additionally, such measurements can provide information on air-sea gas exchange rates [Keeling *et al.*, 1998], atmospheric transport patterns, and in assessing satellite data and ocean carbon cycle models [Balkanski *et al.*, 1999; Stephens *et al.*, 1998].

In this dissertation, I will expand on this existing groundwork of atmospheric O₂ measurements. I will present and discuss data from a network of flask sampling stations, and calculate improved estimates of land biotic and oceanic carbon sinks. I present the first time series of continuous atmospheric O₂ measurements and discuss the

information that can be gained from such high sampling frequency. And I describe many of the analytical and gas handling problems that I have encountered and solutions found over the last few years in my attempts to improve our analytical sampling and measurement strategies for atmospheric O₂ concentrations.

Chapter 2 presents records of atmospheric O₂ concentrations from our network of eleven sampling stations worldwide, in some cases going back to 1989, up to the present. I discuss sampling and laboratory procedural problems that we have discovered along the way, as we continued to learn more about the subtleties of high precision O₂ measurements, and I apply corrections to the data where needed. This information helps to assess the confidence that we have in our data and is pertinent to other researchers measuring atmospheric O₂.

I analyze and discuss interpretations of the seasonal cycles and secular trend observed at different stations, and I present the observed latitudinal gradient. The seasonal cycles are partitioned in terms of their land biotic and oceanic components, and relative amplitude and phasing differences between stations are discussed. Data from the American Samoa station (14°S, 171°W) are examined in detail. This station exhibits seasonal cycles out of phase with those observed at all other stations, and exhibits greater short-term variability. The degree of variability in CO₂ is found to be seasonally dependent, whereas in O₂ it is not, and reasons for this are suggested relating to atmospheric transport patterns and differences in the distribution of sources and sinks of O₂ in contrast to CO₂.

I calculate global land biotic and oceanic CO₂ sinks from our data for the decade of the 1990s. I calculate that of the $6.33 \pm 0.38 \text{ Gt C/y}^4$ of fossil fuel combusted in the

1990s, 3.21 ± 0.13 Gt C/y remained in the atmosphere, 1.44 ± 0.66 Gt C/y were absorbed by the land biota, and 1.68 ± 0.52 Gt C/y were absorbed by the oceans. This shows that the average land biotic and oceanic sinks were of roughly comparable magnitude.

These calculations incorporate a rough, preliminary estimate of the effect of long-term ocean warming on oceanic O₂ outgassing.

To assess the sensitivity and robustness of these global carbon sink calculations, I compared this result with results derived from several different computational techniques employed on our data, and with other results in the literature. Also, to gain a greater understanding of the processes involved I recomputed the data over one-year time intervals to determine the interannual variability in the land biotic and oceanic sinks. This analysis showed that the land biotic sink exhibits significantly greater variability than the oceanic sink. The oceanic sink shows very little variability, except for a period in 1992-1993, and there were brief periods when either the land or the ocean were in fact small sources of atmospheric CO₂. Finally in Chapter 2, I discuss the interannual variability observed in the amplitude of atmospheric O₂ seasonal cycles, and correlate the observed variability at the Cape Grim station (41°S, 145°E) with spatially averaged Southern Ocean wind fields.

In Chapter 3, I describe the design and development of a new technique for measuring atmospheric O₂ at high precision. Chapter 2 demonstrated the wealth of information that can be obtained from a global flask sampling network; however, it still leaves unanswered many questions concerning subtleties in the global oxygen and carbon cycles. Some of these issues can be addressed by the higher time resolution

⁴ 1 Gt C/y is equivalent to 1 billion tonnes of carbon per year, 1 Pg C/y, or 1×10^{15} g C/y.

sampling that would be possible from a continuous atmospheric O₂ monitoring program.

Previously only two analytical methods existed that could measure O₂ to the precision needed of about 1 ppm to be useful as a biogeochemical tool. These were an interferometric technique [Keeling, 1988a] and a mass spectrometric technique [Bender *et al.*, 1994]. Both of these techniques involve large, relatively expensive instruments not suitable for placement at remote atmospheric monitoring stations, and with their current designs require flask samples to be collected in order to make atmospheric O₂ measurements. The new technique I developed and describe in Chapter 3 is capable of continuous measurements and suitable for placement at a remote field site.

I took a commercially available paramagnetic oxygen analyzer, with factory-quoted specifications of ± 1000 ppm precision and improved this to a precision of ± 0.2 ppm over a one-hour interval. This improvement was achieved by incorporating high-precision active pressure control, stabilizing temperature, and by rapid (3 min) switching between a reference gas and sample air to nullify analyzer drift. I demonstrated the feasibility of applying this method to continuous sampling by running the analyzer semi-continuously on air sampled from the end of Scripps Pier, La Jolla, California, for several months. Data from one week are presented in this chapter, highlighting some of the information that can be obtained from high time resolution sampling of atmospheric O₂.

Chapter 3 appeared in full as Manning, A.C., R.F. Keeling, and J.P. Severinghaus, Precise atmospheric oxygen measurements with a paramagnetic oxygen analyzer, *Global Biogeochemical Cycles*, 13 (4), 1107-1115, 1999.

Chapter 4 describes further improvements made to the paramagnetic analyzer system, discusses deployment of the system in the field, and presents the first time series of continuous atmospheric O₂ data resulting from this deployment. I added high-precision active temperature control and made other modifications to the design, further improving the precision, drift rate and functionality of the analyzer. I installed this system at a remote background air monitoring station at Baring Head, Wellington, New Zealand, where a continuous atmospheric CO₂ measurement program already existed.

I present twelve months of O₂ data from this system. A seasonal cycle is observed, and is found to be in rough agreement with data from flask samples collected at Cape Grim, Tasmania, a southern hemisphere mid-latitude station which is a part of our global flask network. With the concurrent CO₂ measurements, partitioning of the relative influences of land biota and the oceans on air masses arriving at Baring Head is possible. This partitioning shows much greater variability attributable to land biotic effects, and diurnal cycles due to land biotic photosynthesis and respiration processes are observed. To assess the robustness of the land biotic O₂:C exchange ratio used in global carbon sink calculations, preliminary analyses of this ratio at selected time intervals were carried out on the Baring Head dataset.

The high temporal resolution of the data showed several features affecting atmospheric O₂ concentration that were not previously known. For example, there was at least one event observed during “baseline” conditions, when atmospheric O₂ and CO₂ concentrations are normally thought to be stable, where a decrease in O₂ concentration roughly equivalent to the amplitude of the annual seasonal cycle occurred in the space of only 18 hours. It is believed that an oceanic process was responsible for this

drawdown, probably due to upwelling of deeper, O₂-undersaturated, colder waters, but the exact mechanism is unclear. Because this event happened under what appeared to be baseline conditions when flask samples could potentially be collected, this observation of significant variability in atmospheric O₂ has implications for all flask sampling programs and highlights the importance of continuous monitoring programs.

Another important contribution in this dissertation relevant for other researchers with respect to achieving accurate measurements of precise atmospheric O₂ concentrations, is the knowledge I have gained related to gas handling for very high precision concentration measurements. Some of these aspects are also discussed in detail in Chapter 4. For example, there are a variety of conditions under which atmospheric O₂ can fractionate relative to N₂ which need to be avoided to prevent biases in reported O₂ concentrations. Chapter 4 discusses such fractionation processes occurring at 'tee' junctions where an incoming air stream divides into two, in air sampling intake lines, and in cryogenic cold traps. The procedures I implemented to overcome these problems are described, and explanations for the fractionation processes observed are suggested based on flow, temperature, and pressure considerations.

Appendix 1 briefly describes the data acquisition and processing programs written in LabVIEW which run the O₂ system at Baring Head in a fully automated mode. A software package, pcANYWHERE, in conjunction with the LabVIEW programs, allows me to directly control calibration and sample air cycles, download data, and diagnose problems from any network connection in the world.

In summary, this dissertation has widened the observational database for atmospheric O₂ measurements in two different directions. I have presented eleven years

of flask measurements, the longest dataset available, discussing new signals observed in these data, and refining existing analyses and interpretations. The second direction has been to implement the first time series of continuous measurements of atmospheric O₂. A one year record of these data highlight land biotic and oceanic influences on atmospheric O₂ concentrations on hourly, daily and seasonal time scales.

Very precise measurements of atmospheric O₂ are still a relatively new field [Keeling, 1988a] and we are continuing to learn more about the technical and analytical challenges faced in making these measurements, some of which are described and met in this dissertation. Additional work in this area is still needed, especially in establishing a more complete knowledge of the conditions under which fractionation of O₂ relative to N₂ can occur, and the physical processes causing this fractionation. More work is also needed in establishing collaborative inter-laboratory calibration comparison techniques so that the growing atmospheric O₂ measuring community is able to directly compare their data with each other, and can report and compare long-term trends in their data with confidence.

We are also still in the early learning stages of making use of atmospheric O₂ data to improve our knowledge of the biogeochemical cycles on Earth. For optimal use of atmospheric O₂ data we need to improve our knowledge in several key areas; estimates of the land biotic O₂:C exchange ratio; air-sea gas exchange processes; and atmospheric transport and oceanic circulation patterns. Describing, quantifying, and interpreting the causes of seasonal and interannual variability in O₂ concentrations are also important. Establishing continuous O₂ measuring programs at several other carefully selected sites around the world would greatly improve our understanding of

the carbon cycle and various terrestrial and oceanic biogeochemical processes at high temporal resolution on local, regional and global scales. This knowledge, in turn, will aid in the confidence with which we can assess and make predictions of the present and future impacts of anthropogenically-induced changes to Earth's climate and ecosystems.

1.1. References

- Balkanski, Y., P. Monfray, M. Battle, and M. Heimann, Ocean primary production derived from satellite data: An evaluation with atmospheric oxygen measurements, *Global Biogeochemical Cycles*, 13 (2), 257-271, 1999.
- Battle, M., M.L. Bender, P.P. Tans, J.W.C. White, J.T. Ellis, T. Conway, and R.J. Francey, Global carbon sinks and their variability inferred from atmospheric O₂ and δ¹³C, *Science*, 287 (5462), 2467-2470, 2000.
- Bender, M., T. Ellis, P. Tans, R. Francey, and D. Lowe, Variability in the O₂/N₂ ratio of southern hemisphere air, 1991-1994: Implications for the carbon cycle, *Global Biogeochemical Cycles*, 10 (1), 9-21, 1996.
- Bender, M.L., P.P. Tans, J.T. Ellis, J. Orchardo, and K. Habfast, A high precision isotope ratio mass spectrometry method for measuring the O₂/N₂ ratio of air, *Geochimica et Cosmochimica Acta*, 58 (21), 4751-4758, 1994.
- Hansen, J., M. Sato, R. Ruedy, A. Lacis, K. Asamoah, K. Beckford, S. Borenstein, E. Brown, B. Cairns, B. Carlson, B. Curran, S. deCastro, L. Druyan, P. Etwarrow, T. Ferede, M. Fox, D. Gaffen, J. Glascoe, H. Gordon, S. Hollandsworth, X. Jiang, C. Johnson, N. Lawrence, J. Lean, J. Lerner, K. Lo, J. Logan, A. Lueckert, M.P. McCormick, R. McPeters, R. Miller, P. Minnis, I. Ramberran, G. Russell, P. Russell, P. Stone, I. Tegen, S. Thomas, L. Thomason, A. Thompson, J. Wilder, R. Willson, and J. Zawodny, Forcings and chaos in interannual to decadal climate change, *Journal of Geophysical Research-Atmospheres*, 102 (D22), 25679-25720, 1997.
- Heimann, M., and E. Maier-Reimer, On the relations between the oceanic uptake of CO₂ and its carbon isotopes, *Global Biogeochemical Cycles*, 10 (1), 89-110, 1996.
- Keeling, C.D., J.F.S. Chin, and T.P. Whorf, Increased activity of northern vegetation inferred from atmospheric CO₂ measurements, *Nature*, 382, 146-149, 1996a.
- Keeling, C.D., S.C. Piper, and M. Heimann, A three-dimensional model of atmospheric CO₂ transport based on observed winds: 4. Mean annual gradients and interannual variations, in *Geophysical Monograph 55, Aspects of climate variability in the Pacific and the Western Americas*, edited by D.H. Peterson, pp. 305-363, American Geophysical Union, Washington D. C., 1989.
- Keeling, C.D., T.P. Whorf, M. Wahlen, and J. van der Plicht, Interannual extremes in the rate of rise of atmospheric carbon dioxide since 1980, *Nature*, 375, 666-670, 1995.

- Keeling, R.F., Development of an interferometric oxygen analyser for precise measurement of the atmospheric O₂ mole fraction, Ph.D. thesis, Harvard University, Cambridge, Massachusetts, U.S.A., 1988a.
- Keeling, R.F., Measuring correlations between atmospheric oxygen and carbon dioxide mole fractions: A preliminary study in urban air, *Journal of Atmospheric Chemistry*, 7, 153-176, 1988b.
- Keeling, R.F., R.P. Najjar, M.L. Bender, and P.P. Tans, What atmospheric oxygen measurements can tell us about the global carbon cycle, *Global Biogeochemical Cycles*, 7 (1), 37-67, 1993.
- Keeling, R.F., S.C. Piper, and M. Heimann, Global and hemispheric CO₂ sinks deduced from changes in atmospheric O₂ concentration, *Nature*, 381, 218-221, 1996b.
- Keeling, R.F., and S.R. Shertz, Seasonal and interannual variations in atmospheric oxygen and implications for the global carbon cycle, *Nature*, 358, 723-727, 1992.
- Keeling, R.F., B.B. Stephens, R.G. Najjar, S.C. Doney, D. Archer, and M. Heimann, Seasonal variations in the atmospheric O₂/N₂ ratio in relation to the kinetics of air-sea gas exchange, *Global Biogeochemical Cycles*, 12 (1), 141-163, 1998.
- Levitus, S., J.I. Antonov, T.P. Boyer, and C. Stephens, Warming of the world ocean, *Science*, 287 (5461), 2225-2229, 2000.
- Mann, M.E., R.S. Bradley, and M.K. Hughes, Global-scale temperature patterns and climate forcing over the past six centuries, *Nature*, 392 (6678), 779-787, 1998.
- Marland, G., T.A. Boden, R.J. Andres, A.L. Brenkert, and C.A. Johnston, Global, Regional, and National Fossil Fuel CO₂ Emissions, in *Trends: A Compendium of Data on Global Change*, Carbon Dioxide Information Analysis Center, Oak Ridge National Laboratory, U.S. Department of Energy, Oak Ridge, Tenn., U.S.A., 2000.
- Najjar, R.G., and R.F. Keeling, Mean annual cycle of the air-sea oxygen flux: A global view, *Global Biogeochemical Cycles*, 14 (2), 573-584, 2000.
- Quay, P.D., B. Tilbrook, and C.S. Wong, Oceanic uptake of fossil fuel CO₂: Carbon-13 evidence, *Science*, 256, 74-79, 1992.
- Redfield, A.C., B.H. Ketchum, and F.A. Richards, The influence of organisms on the composition of sea-water, in *The Sea*, edited by M.N. Hill, pp. 26-77, Wiley Interscience, New York, 1963.

- Schimel, D., D. Alves, I.G. Enting, M. Heimann, F. Joos, D. Raynaud, T.M.L. Wigley, M. Prather, R. Derwent, D. Ehhalt, P. Fraser, E. Sanhueza, X. Zhou, P. Jonas, R. Charlson, H. Rodhe, S. Sadasivan, K.P. Shine, Y. Fouquart, V. Ramaswamy, S. Solomon, J. Srinivasan, D. Albritton, R. Derwent, I. Isaksen, R. Lal, and D. Wuebbles, Radiative Forcing of Climate Change, in *Climate Change 1995: The Science of Climate Change, Contribution of Working Group I to the Second Assessment Report of the IPCC*, edited by J.T. Houghton, L.G. Meira Filho, B.A. Callander, N. Harris, A. Kattenberg, and K. Maskell, pp. 65-131, Cambridge University Press, Cambridge, U.S.A., 1996.
- Severinghaus, J.P., Studies of the terrestrial O₂ and carbon cycles in sand dune gases and in Biosphere 2, Ph.D. thesis, Columbia University, New York, U.S.A., 1995.
- Stephens, B.B., R.F. Keeling, M. Heimann, K.D. Six, R. Murnane, and K. Caldeira, Testing global ocean carbon cycle models using measurements of atmospheric O₂ and CO₂ concentration, *Global Biogeochemical Cycles*, 12 (2), 213-230, 1998.
- Tans, P.P., I.Y. Fung, and T. Takahashi, Observational constraints on the global atmospheric CO₂ budget, *Science*, 247, 1431-1438, 1990.

Chapter 2.

**Atmospheric oxygen in the 1990s from
a global flask sampling network:
Trends and variability pertaining to
the carbon cycle**

Abstract.

I present time series measurements of up to 11 years in length of atmospheric O₂ and CO₂ concentration data from eleven sampling stations worldwide. I discuss the temporal and spatial distributions of the seasonal cycles, interannual long-term trends, and latitudinal gradients observed. With these measurements I am able to distinguish between oceanic and land biotic effects and thus I discuss the temporal and spatial variability observed due to processes occurring in these two reservoirs. I examine data from the American Samoa station in the tropical Pacific in detail. Short-term variability in atmospheric CO₂ concentrations from this station, in contrast with O₂, exhibits a strong seasonal dependence. This can be explained by the unique meteorology in this region, and a difference in the sources and sinks of atmospheric O₂ in contrast to CO₂.

From a subset of these data I have calculated a global carbon budget for the decade of the 1990s. Fossil fuel combustion during this period released an average of 6.33 ± 0.38 Gt C/y, of which 3.21 ± 0.13 Gt C/y remained in the atmosphere, 1.44 ± 0.66 Gt C/y were taken up by the land biota, and 1.68 ± 0.52 Gt C/y were taken up by the oceans, illustrating that the land biota and oceans are roughly equally important for carbon uptake. I repeated this computational technique on shorter one year time-steps, and observed significant interannual variability particularly, in the land biotic carbon sink. El Niño effects appear to play a role in the land biotic sink, but they do not appear to affect the oceanic sink. Other mechanisms remain to be found to explain some of the observed variability. Temporal variability was also observed in the amplitude of the seasonal cycle of O₂, and I speculate that in the mid to high latitudes of the southern hemisphere, this results from variability in wind strength over the oceans.

2.1. Introduction

Evidence continues to grow supporting significant anthropogenic-induced changes in Earth's climate system [e.g. *Mann et al.*, 1998; *Tans et al.*, 1996]. One of the major players causing such changes is changes in atmospheric CO₂ concentrations, owing to the ability of CO₂ to close a portion of the otherwise open absorption window in the radiation spectrum, at 12-17 μm [*Peixoto and Oort*, 1992], preventing infrared radiation from escaping back into space, thus potentially warming the Earth [*Graedel and Crutzen*, 1993]. As anthropogenic CO₂ production continues to accelerate from the combustion of fossil fuels it becomes increasingly important to understand the partitioning of CO₂ into the atmospheric, terrestrial, and oceanic reservoirs so that reliable future projections of climate can be made.

Careful measurements of background atmospheric CO₂ concentrations from a large number of monitoring stations around the world provide us with spatial and temporal data on the increase of CO₂ in the atmospheric reservoir [e.g. *GLOBALVIEW-CO2*, 1999]. To quantify the partitioning of CO₂ uptake in the terrestrial and oceanic reservoirs no direct methods exist, but several different indirect carbon-based methods have been employed, including: use of surface ocean pCO₂ data [*Takahashi et al.*, 1999; *Tans et al.*, 1990]; several different approaches making use of atmospheric ¹³CO₂/¹²CO₂ data [*Bacastow et al.*, 1996; *Gruber and Keeling*, 1999; *Heimann and Maier-Reimer*, 1996; *Quay et al.*, 1992; *Tans et al.*, 1993]; use of inverse atmospheric transport models [*Enting et al.*, 1995; *Keeling et al.*, 1989; *Tans et al.*, 1990]; and use of ocean carbon models [several models are compared in *Orr*, 1997]. Each of these methods have inherent strengths and weaknesses. The oceanic pCO₂ method suffers

from a sparsity of data, particularly in the southern hemisphere, and from uncertainties in gas transfer velocities [Liss and Merlivat, 1986]. $^{13}\text{CO}_2/^{12}\text{CO}_2$ methods make use of the fact that during terrestrial photosynthesis uptake of carbon favors the lighter ^{12}C isotope whereas discrimination between the two isotopes in oceanic carbon uptake is very small [Ciavis *et al.*, 1995]. However, C_3 and C_4 plants discriminate against ^{13}C to differing degrees and the global relative distributions of C_3 and C_4 plants, especially in the tropics, is not well known. In addition a further complication is added by the disequilibrium effect discussed in Chapter 1. These methods also suffer from laboratory intercalibration problems. Heimann and Maier-Reimer [1996] showed that even with a factor of two reduction in the largest uncertainties in these ^{13}C methods, the uncertainty in the oceanic carbon sink will still be 0.8 Gt C/y or greater.

Atmospheric oxygen measurements provide an additional, independent land/ocean carbon sink partitioning method as first discussed by Machta [1980], and they can also provide additional information about the global carbon cycle not obtainable from a study of carbon and its isotopes alone [e.g. Bender *et al.*, 1998; Keeling *et al.*, 1993]. O_2 and CO_2 are inversely linked by the processes of photosynthesis, respiration, and combustion. For example, photosynthesis of land biota produces atmospheric O_2 and consumes atmospheric CO_2 , whereas combustion of fossil fuel or biomass burning consumes O_2 and produces CO_2 . However, several characteristics, all related to oceanic processes, result in decoupled changes in the atmospheric concentrations of O_2 and CO_2 . First, the characteristic most pertinent to distinguishing between the land and ocean partitioning of CO_2 is that a portion of the fossil fuel-derived CO_2 dissolves into the oceans, but the corresponding fossil fuel-

derived O_2 decrease is not offset by an O_2 flux from the oceans. This is because in the ocean-atmosphere system, 99% of the O_2 is in the atmosphere because O_2 is relatively insoluble in seawater [e.g. *Bender and Battle, 1999*], hence the relative changes in the atmospheric O_2 concentration is very small and results in no appreciable change in the equilibrium position with respect to the ocean. In contrast, 98% of the CO_2 in the ocean-atmosphere system is in the ocean [e.g. *Bender and Battle, 1999*], thus changes in atmospheric CO_2 are relatively significant and perturb the atmosphere-ocean equilibrium, driving a flux of CO_2 across the air-sea interface into the oceans.

Second, although biologically-induced seasonal changes in dissolved O_2 and dissolved CO_2 in the euphotic zone of the ocean are inversely coupled, the air-sea fluxes of these two species are decoupled owing to the CO_2 buffering effect created by reactions of CO_2 with water to form carbonic acid and carbonate and bicarbonate ions, whereas O_2 is geochemically neutral in the oceans. Therefore the partial pressure of dissolved CO_2 has a much smaller seasonal variation than it would if CO_2 were geochemically neutral, resulting in much less seasonal air-sea gas exchange of CO_2 .

Third, seasonal CO_2 fluxes across the air-sea interface are further suppressed because of the opposing effects of temperature-induced solubility changes and marine biotic photosynthesis and respiration. In fall and winter, for example, the mixed layer deepens incorporating CO_2 -enriched waters in surface waters and at the same time photosynthesis is less dominant over respiration, combining to increase surface water CO_2 concentrations. However, at the same time cooler surface waters increase gas solubilities and can hold more dissolved CO_2 without becoming supersaturated. In contrast, also in fall and winter, deepening of the mixed layer incorporates O_2 -depleted

waters in surface waters, less photosynthesis produces less O₂, and colder waters cause an increase in the undersaturation of O₂, driving a net flux of O₂ from the atmosphere into the oceans. During spring and summer these effects are opposite with a net O₂ flux out of surface waters. In summary, these two effects partially cancel each other for CO₂, but reinforce each other for O₂, causing an even greater flux of O₂ across the air-sea interface and a weakened CO₂ flux. The magnitude of these effects is dependent on latitude and region, but as a very rough estimate, the ocean temperature effects contribute about 15% of the observed atmospheric O₂ ratio seasonal cycle.

The fourth difference is similar to the third, but occurs on different spatial and temporal scales. Beneath the seasonal thermocline, in the main thermocline, falling organic matter is respired causing O₂ undersaturation. These waters are transported laterally along isopycnal (constant density) surfaces from low latitude waters, where they tend to be deep, to high latitudes where they outcrop and are ventilated. These waters are undersaturated in O₂ both from the respiration of organic matter that occurred at low latitudes and due to the lower temperatures at higher latitudes increasing solubility, therefore they present an O₂ demand to the atmosphere. As in the case above, however, these respiration and temperature-solubility effects cancel for CO₂. These lateral, main thermocline ocean ventilation processes occur on decadal time scales.

Finally, for processes on land, although O₂ and CO₂ are always inversely coupled, different processes have different O₂:CO₂ molar ratios and thus can be distinguished from each other. Fossil fuel combustion has a global average O₂:CO₂ ratio of about -1.39 [Keeling, 1988a] whereas land biotic photosynthesis and respiration has an average ratio of about -1.1 [Severinghaus, 1995]. These ratios can vary over

spatial and temporal scales, for example in regions with high natural gas usage such as The Netherlands values greater than -1.5 have been observed (H. Meijer, personal communication), whereas a study of diurnal cycling in Harvard Forest shows night-time ratios as low as -0.94 , when respiration is dominant (B. Stephens, personal communication).

For a more in-depth discussion of the physical, chemical and biological controls and influences on atmospheric O_2 concentrations, the reader is referred to *Bender and Battle* [1999] and *Bender et al.* [1998].

A landmark in early measurements of atmospheric O_2 concentrations are those of *Benedict* [1912] who used a chemical extraction technique followed by volumetric analysis. *Benedict* [1912] reported that atmospheric O_2 was constant to the precision he could attain of 60 ppm. Subsequent measurements by *Carpenter* [1937] with a similar measurement technique and *Machta and Hughes* [1970] with a paramagnetic technique, reaffirmed *Benedict's* [1912] results to approximately the same level of precision. Using a volumetric technique *Krogh* [1919] claimed a much higher level of precision of 5 ppm O_2 , but this result has been questioned [*Keeling*, 1988a; *Paneth*, 1937]. Despite this questionable precision, *Krogh* [1919] was able to clearly demonstrate variability in the O_2 mole fraction of the order of 70 ppm in air sampled in Copenhagen between Oct 1917 and Jan 1918 which was most probably related to local coal combustion.

More recently, several independent analytical techniques have been developed, some of which can measure atmospheric O_2 to a precision of 1 ppm or better. All of these techniques have been used to demonstrate atmospheric O_2 variability, and used in the study of geochemical processes such as those described above. The techniques that

have been developed are an interferometric technique [Keeling, 1988b]; a zirconium oxide electrode electrochemical technique [Bloom *et al.*, 1989]; a mass spectrometric technique [Bender *et al.*, 1994b]; a paramagnetic technique [Manning *et al.*, 1999, Chapter 3]; a vacuum ultraviolet absorption technique [Stephens, 1999]; and a gas chromatographic technique [Tohjima, 2000].

Keeling and Shertz [1992] presented the first time series of precise atmospheric O₂ measurements, showing data from three years of sampling at three different global locations. From these data they calculated land biotic and oceanic carbon sinks, and they gave an estimate of net production in the global ocean derived from the O₂ seasonal cycles observed. *Keeling et al.* [1996] updated the land biotic and oceanic sinks estimate with three more years of data, and also interpreted the latitudinal gradient of O₂ concentrations to estimate the hemispheric distribution of the land biotic sink. *Bender et al.* [1996] established an independent sampling program and from their data they calculated independent estimates of the land biotic and oceanic CO₂ sinks, and estimates for net oceanic production in the southern hemisphere. In a continuation of the same sampling program, *Battle et al.* [2000] updated the land biotic and oceanic sinks estimate to mid-1997 and compared these results with the sinks derived from an analysis of ¹³CO₂ data.

In order to estimate land biotic and oceanic CO₂ sinks prior to 1989 when atmospheric O₂ measurement flask programs first began, *Bender et al.* [1994a] and *Battle et al.* [1996] studied air in the firn of Antarctic ice sheets at Vostok and South Pole respectively. Another analysis of old air was carried out by *Langenfelds et al.* [1999] using the Cape Grim Air Archive, a suite of tanks filled with air samples

between 1978 and 1997. Unsuitable sampling techniques meant most of the samples contained artifacts in O₂ concentration, but despite this *Langenfelds et al.* [1999] were able to give an estimate of the land biotic and oceanic sinks for this time period.

Finally, atmospheric O₂ measurements have been used to improve our knowledge in other areas of geochemical interest. *Keeling et al.* [1998b] used O₂ data and an atmospheric transport model to improve estimates of air-sea gas-exchange velocities; *Stephen et al.* [1998] used the same data and transport model to compare and assess the performance of three different ocean carbon cycle models; and *Balkanski et al.* [1999] incorporated satellite ocean color data into an ocean biology model to estimate O₂ fluxes, then used an atmospheric transport model to calculate seasonal cycles of atmospheric O₂. By comparing to observed O₂ seasonal cycles *Balkanski et al.* [1999] were able to assess both the satellite data and the ocean biology model.

The remainder of this chapter will update and expand on the results of *Keeling and Shertz* [1992] and *Keeling et al.* [1996], showing five additional years of data and a larger network of sampling stations. Section 2.2 describes our flask sampling and analysis methods, presents the raw data, and discusses various manipulations and omissions I have made to the raw data, correcting for obvious technical and logistical reasons. Section 2.3 gives a first order discussion of the data, interpreting the observed seasonal cycles, secular trends, and latitudinal gradients. Section 2.4 looks in detail at data from American Samoa and finds that the observed differences in short-term variability between atmospheric O₂ and CO₂ is a result of the unique meteorology at this station, and of differences in the sources and sinks of O₂ in contrast to CO₂.

Section 2.5 calculates global land biotic and oceanic carbon sinks for the 1990s, and compares these results against several different computational techniques, and with other results published in the literature. Section 2.6 discusses the interannual variability observed in secular trends, in the amplitude of seasonal cycles, and in latitudinal gradients, and discusses possible mechanisms for these observations.

2.2. Sample Collection and Raw Data Analysis

2.2.1. Methods

The eleven field sampling stations in the Scripps O₂/N₂ network are shown in Table 2.1 and Figure 2.1. Stations were selected in a manner to achieve a globally representative network, and taking advantage of previously established sampling stations. Sampling ceased at Niwot Ridge (NWR) in April 1993, shortly after our O₂/N₂ laboratory was moved from the National Center for Atmospheric Research (NCAR) in Boulder, Colorado to Scripps Institution of Oceanography in La Jolla, California. The Macquarie Island (MCQ) record was obtained for only 17 months before it was stopped in January 1994 because of high costs of shipping.

Flask sampling methodology is described in detail in *Keeling et al.* [1998a]. Briefly, ambient air samples are collected at each station approximately biweekly, in triplicate, in 5 L glass flasks equipped with two stopcocks sealed with Viton o-rings. Prior to shipment to field stations, flasks contain dry air at approximately 1 bar. At each station air is drawn through an intake line mounted up a tower or mast. A small compressor pump maintains an air flow ranging from 2 to 5 STP L/min, depending on the station, flushing ambient air through each flask. Flushing continues until a

Table 2.1. Summary of Flask Sampling Stations in the Scripps O₂/N₂ Network

Station code	Station	Latitude	Longitude	Elevation (m a.s.l.)	Time period
ALT	Alert, Northwest Territories, Canada	82°27'N	62°31'W	210	Nov. 1989 – May 2000
CBA	Cold Bay, Alaska, USA	55°12'N	162°43'W	25	Aug. 1995 – May 2000
NWR	Niwot Ridge, Colorado, USA	40°03'N	105°38'W	3749	Apr. 1991 – Apr. 1993
LJO	La Jolla, California, USA	32°52'N	117°15'W	15	May 1989 – June 2000
MLO	Mauna Loa, Hawaii, USA	19°32'N	155°35'W	3397	Jan. 1991 – May 2000
KUM	Cape Kumukahi, Hawaii, USA	19°31'N	154°49'W	3	June 1993 – May 2000
SMO	Cape Matatula, American Samoa, USA	14°15'S	170°34'W	42/93*	June 1993 – Apr. 2000
CGO	Cape Grim, Tasmania, Australia	40°41'S	144°41'E	94	Jan. 1991 – Dec. 1999
MCQ	Macquarie Island, Australia	54°29'S	158°58'E	94	Sep. 1992 – Jan. 1994
PSA	Palmer Station, Antarctica	64°55'S	64°00'W	10	Sep. 1996 – Mar. 2000
SPO	South Pole Station, Antarctica	89°59'S	24°48'W	2810	Nov. 1991 – Dec 1999

* In May 1999 a new sampling intake was installed on a new tower, 93 m above sea level.

minimum of 15 flask volumes have passed through each flask, then the sample is sealed off, at a pressure of approximately 1 bar. A back pressure regulator is employed at stations located significantly above sea level to achieve 1 bar of pressure in the flasks. A cold trap at temperatures ranging from -55°C to -90°C, depending on the station, pre-dries the air to remove water vapor. Samples are collected in a temperature-controlled environment to minimize possible fractionation effects. Flask samples are shipped back to our laboratory in La Jolla for analysis. In the case of South Pole (SPO) and Macquarie Island, samples may be stored on site for as long as ten months before they are shipped back to La Jolla, and as long as two months at Palmer Station (PSA). All other stations ship samples back within three weeks of collection.

Flask samples are collected by station personnel during what are considered to be “clean, background air” conditions. The general criteria used to determine when these conditions are met is a pre-established wind direction and speed, and where

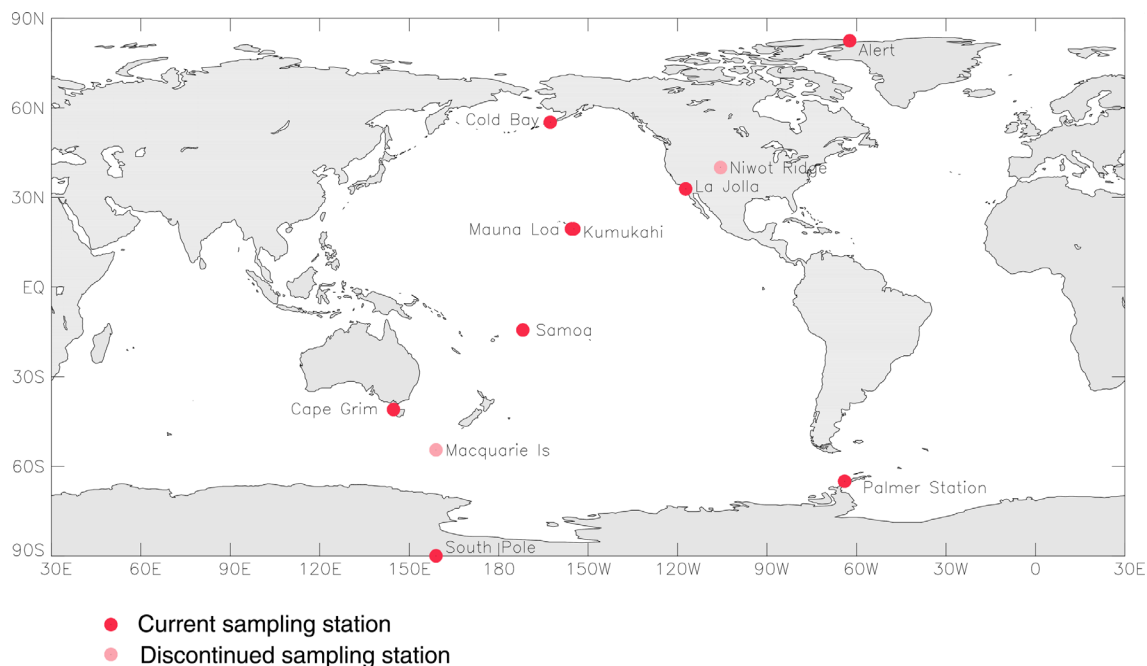


Figure 2.1. Map showing the locations of the eleven sampling stations in the Scripps O_2/N_2 network as listed in Table 2.1. Mauna Loa (MLO) and Cape Kumukahi (KUM) are shown as one point. Niwot Ridge (NWR) and Macquarie Island (MCQ) stations have now been discontinued. With the exceptions of Niwot Ridge (3749 m), Mauna Loa (3397 m) and South Pole (2810 m), all stations are approximately at sea level and coastal and therefore they are situated in the marine boundary layer.

available, relatively steady, non-fluctuating, *in situ* atmospheric CO_2 concentrations, or criteria based on other trace gas species which are measured *in situ*. We wish to sample air that has not been contaminated by local or regional anthropogenic or terrestrial processes.

In this manner we can observe synoptic and hemispheric-scale spatial trends, and seasonal and interannual temporal trends. Thus, for example, stations such as La Jolla (LJO) and Cape Grim (CGO), require a relatively narrow wind direction window (roughly westerlies for both stations) to meet these sampling requirements. Cape

Kumukahi (KUM) and American Samoa (SMO) on the other hand require the prevalent easterly trade winds.

In our laboratory flask samples are analyzed simultaneously for CO₂ concentration on a Siemens nondispersive infrared analyzer (NDIR), and for O₂/N₂ ratio on our interferometric analyzer [Keeling, 1988b]. Samples are analyzed relative to a working gas, which in turn is calibrated each day against a pair of secondary reference gases of pre-determined O₂/N₂ ratios and CO₂ concentrations. A suite of twelve primary reference gases are analyzed roughly every six months as a check on the long-term stability of the secondary reference gases in both O₂/N₂ ratios and CO₂ concentrations. (See Keeling *et al.* [1998a] for a detailed discussion on reference gases and calibration procedures). In early 2000 we updated our long term O₂/N₂ and CO₂ calibration scales based on observed eleven-year trends of these primary gases, and, for CO₂, based on careful comparisons over the same time period against the “Scripps 1999 manometric scale” maintained at the CO₂ laboratory of C. D. Keeling at the Scripps Institution of Oceanography.

2.2.2. Raw Data Presentation

Figures 2.2, 2.3, and 2.4 show data from all stations for O₂/N₂ ratios, CO₂ concentration, and Atmospheric Potential Oxygen (APO, defined below) respectively. Each data point represents averages of two or three replicates collected on the same day. Differences in O₂/N₂ ratios are expressed in “per meg” units, where

$$\delta(\text{O}_2/\text{N}_2) \text{ (per meg)} = \frac{(\text{O}_2/\text{N}_2)_{\text{sam}} - (\text{O}_2/\text{N}_2)_{\text{ref}}}{(\text{O}_2/\text{N}_2)_{\text{ref}}} \times 10^6, \quad (2.1)$$

where $(O_2/N_2)_{\text{sam}}$ is the ratio of the sample gas and $(O_2/N_2)_{\text{ref}}$ is the ratio of an arbitrary reference gas cylinder. 1 per meg is equivalent to 0.001 per mil, the unit typically used in stable isotope work. This ratio is used to define what is meant by O_2 concentration. Then by making the assumption that atmospheric N_2 concentrations are constant, this definition of O_2 concentration can be applied to compute O_2 fluxes⁵. In these units, 4.8 per meg are essentially equivalent to 1 ppm (i.e., 1 $\mu\text{mole } O_2$ per mole of dry air). CO_2 concentrations are expressed as the mole fraction of dry gas in ppm units. It is also useful (see *Stephens et al.* [1998]) to examine the tracer, Atmospheric Potential Oxygen, which is largely conservative with respect to O_2 and CO_2 exchanges of land biota. APO is defined as

$$\text{APO (per meg)} = \delta(O_2/N_2) - \frac{\alpha_B}{X_{O_2}} \Delta X_{CO_2}, \quad (2.2)$$

where α_B represents the O_2 :C exchange ratio for land biotic photosynthesis and respiration, X_{O_2} is the standard mole fraction of O_2 in dry air, and ΔX_{CO_2} is the difference in the CO_2 mole fraction of the sample from an arbitrary reference gas, in ppm. This definition is a simplified version of the formula presented in *Stephens et al.* [1998] since here I have neglected minor influences from CH_4 and CO oxidation. I use $\alpha_B = -1.1$ based on measurements of *Severinghaus* [1995], and $X_{O_2} = 0.20946$ from *Machta and Hughes* [1970]. Thus variations in APO can only be caused by air-sea exchanges of O_2 , N_2 , and CO_2 , and by combustion of fossil fuels, since the O_2 :C

⁵ Typical peak N_2 fluxes are 6% of O_2 fluxes, and because N_2 is approximately 4 times more abundant in the atmosphere, the impact on the atmospheric O_2/N_2 ratio is only 1.5% that of O_2 fluxes.

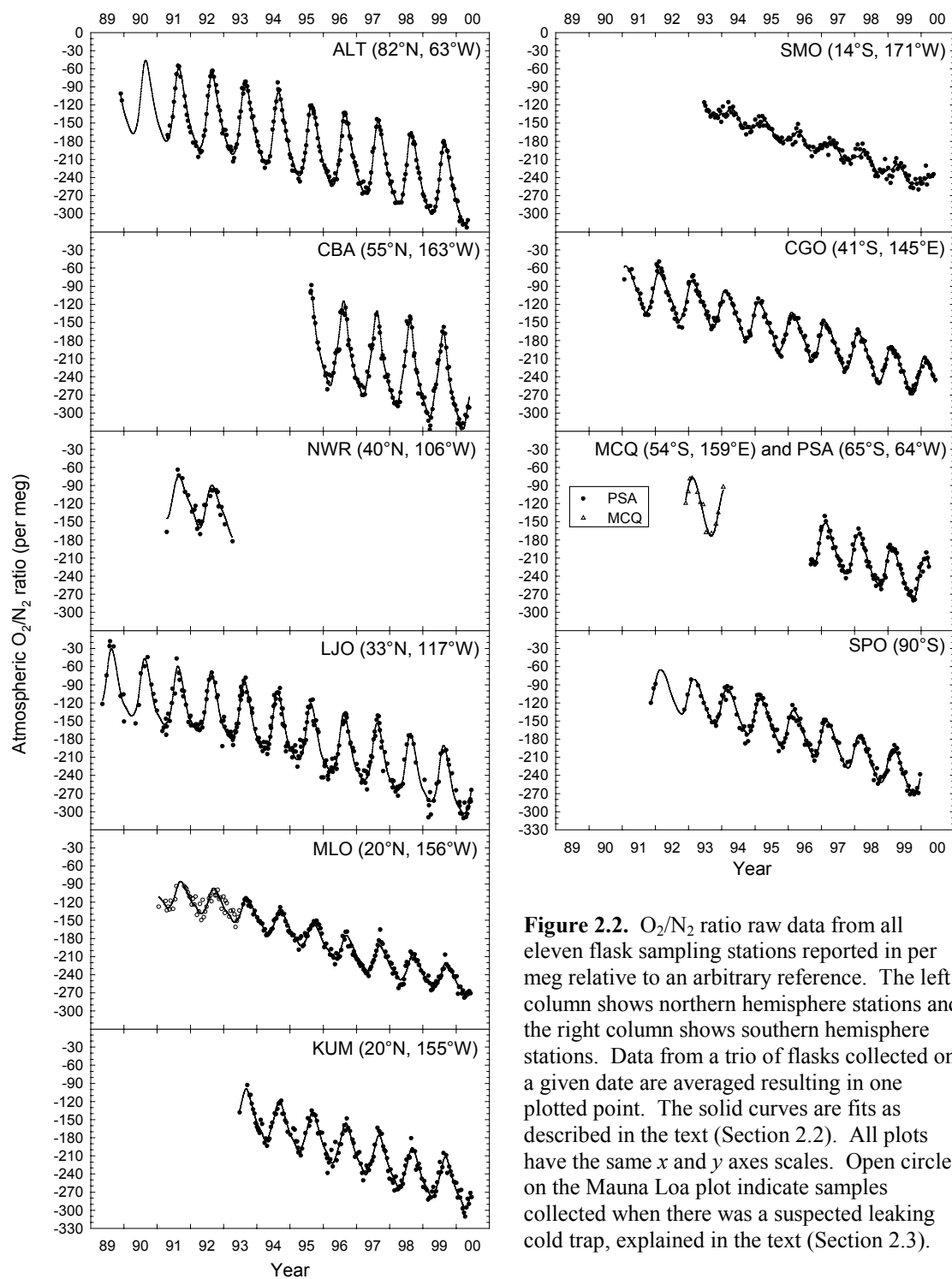


Figure 2.2. O_2/N_2 ratio raw data from all eleven flask sampling stations reported in per meg relative to an arbitrary reference. The left column shows northern hemisphere stations and the right column shows southern hemisphere stations. Data from a trio of flasks collected on a given date are averaged resulting in one plotted point. The solid curves are fits as described in the text (Section 2.2). All plots have the same x and y axes scales. Open circles on the Mauna Loa plot indicate samples collected when there was a suspected leaking cold trap, explained in the text (Section 2.3).

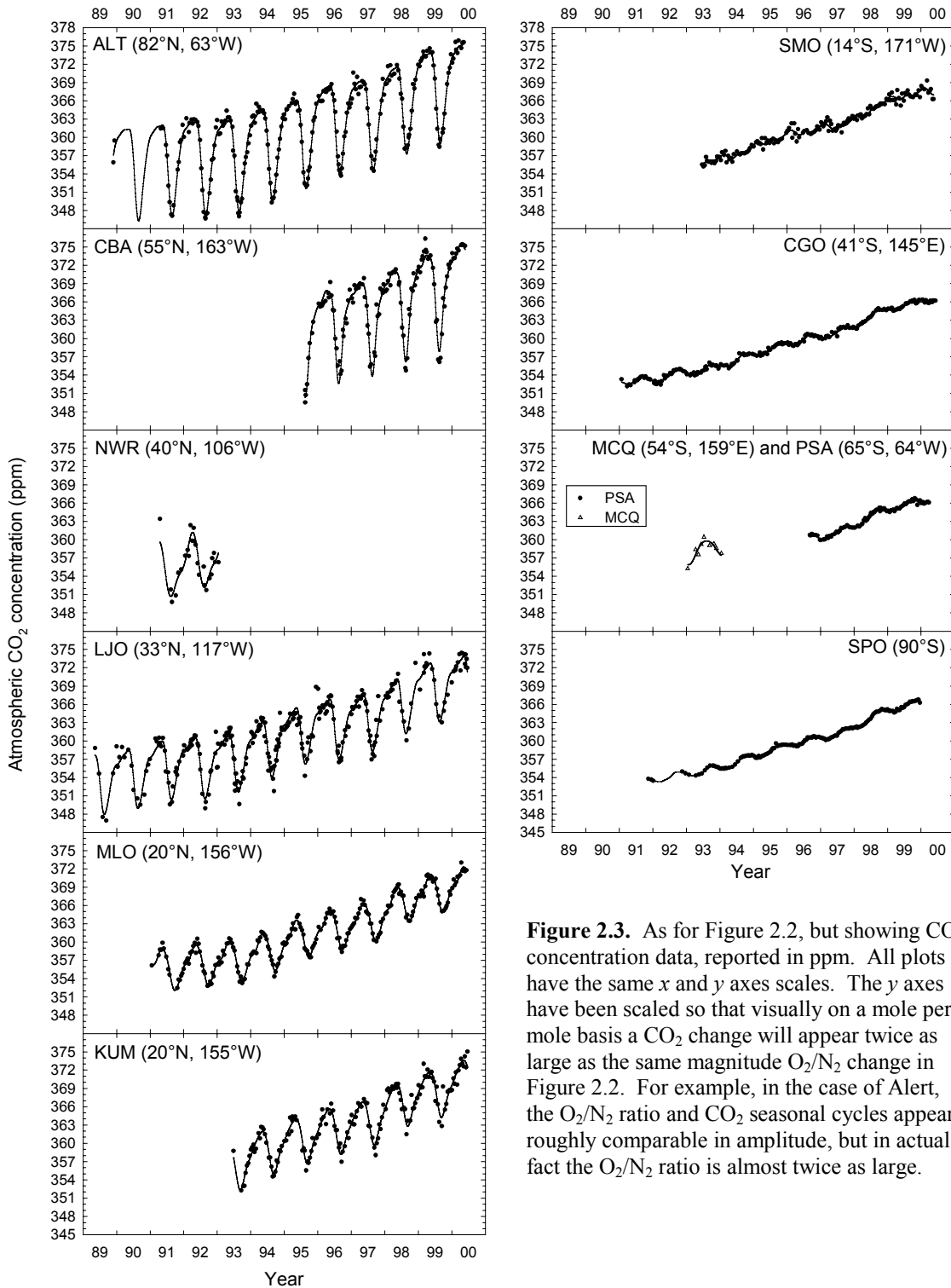


Figure 2.3. As for Figure 2.2, but showing CO₂ concentration data, reported in ppm. All plots have the same x and y axes scales. The y axes have been scaled so that visually on a mole per mole basis a CO₂ change will appear twice as large as the same magnitude O₂/N₂ change in Figure 2.2. For example, in the case of Alert, the O₂/N₂ ratio and CO₂ seasonal cycles appear roughly comparable in amplitude, but in actual fact the O₂/N₂ ratio is almost twice as large.

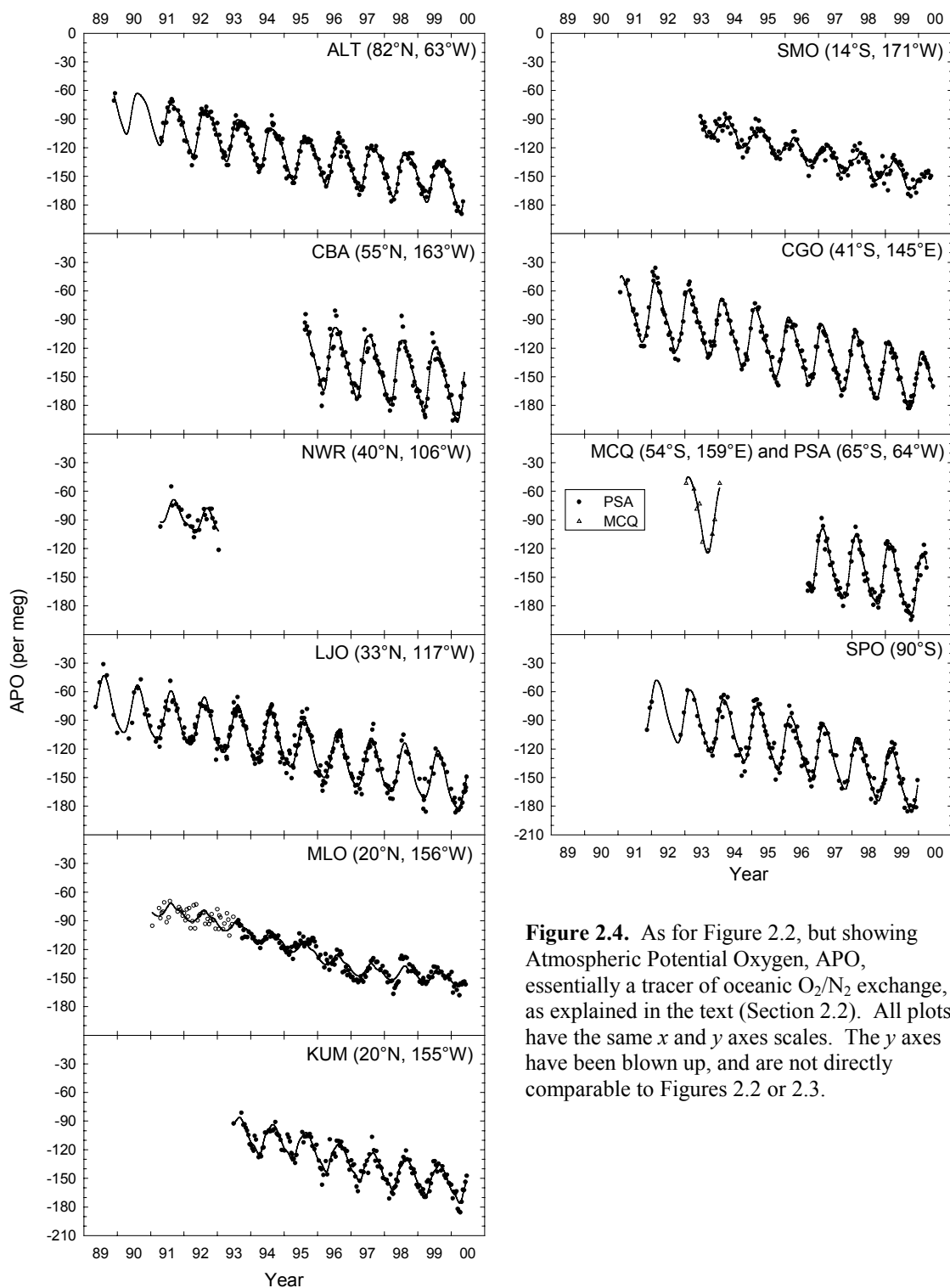


Figure 2.4. As for Figure 2.2, but showing Atmospheric Potential Oxygen, APO, essentially a tracer of oceanic O_2/N_2 exchange, as explained in the text (Section 2.2). All plots have the same x and y axes scales. The y axes have been blown up, and are not directly comparable to Figures 2.2 or 2.3.

exchange ratio for fossil fuels is approximately -1.4, different from the value of -1.1 for land biotic exchanges [Keeling *et al.*, 1998b; Stephens *et al.*, 1998].

Since 1989 when our flask sampling program began 5276 flask samples have been collected, of which 5014 have been analyzed in our laboratory, and 4653, 4772, and 4644 are presented in the plots of Figures 2.2, 2.3, and 2.4 respectively. Generally, flasks are collected in triplicate. Flasks collected on the same day from the same station are averaged and plotted as a single point in these figures. Reasons for non-analysis or exclusion from the plots include flask breakage, identified sampling problems in the field, and procedural problems in our laboratory. For each triplicate, outliers are rejected if they are more than ± 8 per meg from the triplicate mean.

All curve fits in Figures 2.2, 2.3, and 2.4, with the exception of Niwot Ridge and Macquarie stations, are computed as a least squares fit to the sum of a four harmonic annual seasonal cycle and a stiff *Reinsch* [1967] spline to account for the interannual trend and other non-seasonal variability. Owing to the shortness of the records, Niwot Ridge and Macquarie curve fits are computed as a least squares fit to the sum of a two harmonic annual seasonal cycle and a fixed linear trend.

2.2.3. Data Adjustments

Obtaining O₂/N₂ ratio measurements to an accuracy of 5 per meg or better (0.005 ‰) presents many logistical and technical challenges not faced in typical trace gas measurements. This can be understood conceptually by considering that we are attempting to observe changes in O₂ concentration of 1 part in 209,500. Thus over the years we have continued to discover additional problems and variables in both field

sampling and instrumental analysis techniques that can create artifacts in O₂/N₂ ratios. This section describes those findings only as they pertain to our flask sampling methods, and the subsequent corrections I have applied to the data, where possible.

At Mauna Loa, from inception in January 1991 through to July 1993 the O₂/N₂ data exhibit greater short-term variability than other stations (see Figure 2.2). This becomes even more apparent from the Mauna Loa APO plot in Figure 2.4. At first we reasoned that this scatter in the data could be illustrating real atmospheric variability [Manning and Keeling, 1994]. Heimann *et al.* [section 5.5, 1989] have shown that a significant fraction of the CO₂ variability observed at Mauna Loa is related to changing synoptic weather patterns particular to the area, further supporting this conclusion. Variations in north-south transport in the proximity of Mauna Loa have the potential to bring air masses of either northern hemisphere or southern hemisphere origin to the area. During much of the year because of both seasonal and anthropogenic effects, these different air masses have large differences in O₂/N₂ ratios and CO₂ concentrations and this could be reflected in greater variability of O₂/N₂ ratios and CO₂ concentrations from Mauna Loa flask samples. Indeed, a statistical analysis of these data supported this conclusion, showing that at least 37% of the scatter in the residuals of the flask data from the curve fits could be explained by real atmospheric variability and not by experimental artifacts [Manning and Keeling, 1994].

In July 1993, however, it became apparent from communication with Mauna Loa station personnel that the cold trap used to dry the incoming air stream was intermittently leaking. Mauna Loa personnel collect our air samples somewhat differently from all other stations in that the flasks are left flushing overnight for many

hours. During this time, ice builds up in the cold trap, causing an increase in the flow restriction and hence increasing the upstream pressure. This pressure could act on the tapered joint seal of the two-piece glass cold trap, periodically breaking the seal and causing intermittent leakage. The positive pressure in the cold trap would probably prevent contamination of room air into the sample, however O₂ and N₂ would escape from the leak at different rates, fractionating the O₂/N₂ ratio of the sample. Once this problem was identified, a new cold trap was sent to MLO with a different design that would not allow such leakage. Subsequent O₂/N₂ and APO data can be seen to exhibit less scatter (Figures 2.2 and 2.4). These suspect Mauna Loa data are shown as open circles in Figures 2.2 and 2.4, and are deleted from subsequent data analysis.

Concurrent CO₂ data for the same period are also discarded.

In 1998 I discovered that in a flowing air stream O₂ will fractionate relative to N₂ under many instances at a 'tee' junction, where an incoming air stream divides into two outlet air streams (Chapter 4 explains this phenomena in greater detail). Three of our sampling stations, Mauna Loa, Samoa, and La Jolla have had plumbing arrangements with such a tee. At each of these stations the division of flow existed because we shared our intake lines with independent continuous atmospheric CO₂ monitoring programs. Recognizing this problem, we set out to eliminate all tees.

At Mauna Loa, this tee was eliminated from the sampling system in June 1998 when we obtained a dedicated intake line. Flask samples were collected simultaneously on the old and new setup at that time and indicated that the tee was producing a -13.5 per meg artifact. This result is further supported by subsequent samples collected, shown in Figures 2.2 and 2.4, which appear to indicate a stepwise increase in the data in

June 1998 of the order of 10 to 15 per meg (somewhat difficult to see on the low resolution plots presented here). Based on my experiences of temporal variability in the degree of fractionation at a tee junction (see Chapter 4), we can not confidently apply a 13.5 per meg correction to all pre-June 1998 data. Instead, for subsequent data shown and discussed in this chapter I have treated Mauna Loa data as two separate time series, with the first terminating in June 1998, and the second beginning at this time. Clearly the first time series should be considered to contain greater uncertainty than the more recent record.

At Samoa I removed the tee and changed to a dedicated intake line in May 1999. At the same time I shifted the physical location of the intake line from the top of a mast at 42 m a.s.l. to the top of a newly constructed communications tower located approximately 100 m further inland and at a height of 93 m a.s.l. To assess any potential changes in the O₂/N₂ ratios or CO₂ concentrations of the sampled air created by the removal of the tee or shift in physical location of the inlet, I left the old setup in place and we began alternating our biweekly flask collection schedule between the two intakes starting in May 1999, and we plan to continue this for a two year period. A preliminary comparison of the first 12 months of data from this overlapping collection routine shows no discernible difference between the two intakes, although the higher atmospheric variability observed at Samoa, discussed in section 2.4 below, makes a definitive statement difficult.

Flask sampling at La Jolla has undergone a series of transitions. Up until March 1999 sampling took place in a laboratory maintained by C. D. Keeling, approximately 400 meters from the sample intake at the end of the Scripps Pier. Between September

1995 and October 1997, flask samples were also collected from our own laboratories in a different building approximately 100 meters further away from the intake, with different intake tubing and a different pumping module. These samples were collected in addition to and in most cases simultaneously with continued sampling in the C. D. Keeling laboratory. Both of these setups included tees in the intake lines. A comparison of the 32 samples collected simultaneously over this two year period shows a difference of 0.4 ± 3.0 per meg in O_2/N_2 ratio, and a difference of 0.03 ± 0.14 ppm in CO_2 concentration. These differences are smaller than the laboratory analytical precision. In March 1999, owing to our laboratory moving to a new building, and concerns about the setup in the C. D. Keeling laboratory, we began sampling directly off the end of the Scripps Pier and with no tee. Unfortunately we do not have any overlap of direct pier sampling with either of the old systems, however, a step change such as that observed in the data at Mauna Loa in June 1998 has not been observed at La Jolla.

The question may be asked, why did a tee in the intake line at Mauna Loa cause a -13.5 per meg step change in O_2/N_2 ratios whereas tees at Samoa and La Jolla appear to have little or no effect? From results discussed in Chapter 4, the answer appears to lie in the flow ratio at the tee junction. The greater the flow ratio of the two outlets of the tee, the greater the potential for O_2 fractionation relative to N_2 . At Mauna Loa, this ratio was typically 15:1.5 Lpm (10), whereas at Samoa and La Jolla it was typically 2:5 Lpm (0.4) and 15:3 Lpm (5) respectively.

CO_2 data from Macquarie is suspect owing to dry ice being used on site. This problem became apparent from an examination of the residuals of the CO_2 flask data points from the curve fit. Macquarie residuals exhibited a range of variability greater

than ± 1.0 ppm, whereas all other mid to high-latitude southern hemisphere stations varied over a range of only ± 0.5 ppm or less. Therefore subsequent plots and calculations in this chapter involving CO₂ and APO at Macquarie are either not shown at all, or are calculated by substituting Cape Grim CO₂ data as a proxy for this station.

There have been several identified procedural problems with the South Pole sampling program. Several of these have already been discussed in *Keeling et al.* [1998a]. More recently, we noticed excessive scatter in the 1997 and 1998 data. We found some flasks to show highly anomalous O₂/N₂ ratios. We speculated that these results may have been caused during storage after the flask sample had been collected. The flasks were stored outside in conditions well below freezing. Therefore the stopcock o-rings would have been frozen and it is possible that they did not make a completely leak tight seal against the glass of the flask. A small leak such as this would result in different leak rates for O₂ relative to N₂, biasing subsequent determinations of O₂/N₂ ratios. Therefore from February 1998 onward, all flask samples were stored in temperatures above freezing. Subsequent data exhibit less scatter, and appear to show a change in the long-term trend. Therefore as with Mauna Loa, I have treated the South Pole data set as two separate time series, before and after February 1998.

Of the six remaining stations in our network, Alert, Cold Bay, Niwot Ridge, Cape Kumukahi, Cape Grim, and Palmer Station, none have ever had a tee in their intake lines, nor have I identified any other sampling or procedural problems. The other potential sources of error or bias in reported flask concentrations are in our laboratory analysis procedures or from long-term drift in our calibration gases. *Keeling et al.* [1998a] give a detailed description of the results from our long-term calibration

procedures up to July 1996, and applicable corrections applied to the data. There are now four more years of calibration data and from these no evidence of long term drift in O_2/N_2 ratios in our calibration gases is apparent, thus no further corrections have been applied. For CO_2 our calibration scale has been updated to agree with the Scripps 1999 manometric scale maintained by the C. D. Keeling laboratory, also at Scripps Institution of Oceanography. I also noticed and corrected for a step change in the span of our CO_2 analyzer in March 1993 which coincided with the change in physical location of our laboratory from Boulder, Colorado, to La Jolla, California. This is perhaps not surprising since in Boulder the CO_2 analyzer was actively controlled to ambient pressure which is approximately 620 torr at the altitude of Boulder. When we moved to La Jolla, situated at sea level, we changed the gas handling design to continue to actively stabilize the CO_2 analyzer to 620 torr, but it appears that despite this, a change in the span of the analyzer occurred. This change was of the order of 0.4 ppm/Volt, which, for example, corresponded to a change in one reference gas of about 0.1 ppm CO_2 . No changes in O_2/N_2 ratios in calibration gases relative to each other were observed after the move to La Jolla.

During a two month period from September to November 1996 a diaphragm on a compressor pump in the analysis system was leaking. This pump is located downstream of the CO_2 analyzer and so did not affect CO_2 concentrations, but it resulted in a change in span of the interferometric O_2 analyzer. Because our primary calibration gases were analyzed during this period, a correction could be applied to the 136 flasks that were analyzed during this period and the data I show in Figures 2.3 and 2.4 have this correction applied.

2.3. First Order Interpretations of the Data

Several features of the data stand out in Figures 2.2, 2.3, and 2.4. All stations have a clear annual seasonal cycle and all stations exhibit a long-term interannual trend. For O_2/N_2 ratios the long-term trend shows decreasing O_2 concentrations, and the latitudinal gradient shows low O_2/N_2 ratios in the north, progressing to high O_2/N_2 ratios in the south. For the APO data of Figure 2.4 the seasonal cycle is generally smaller than the O_2/N_2 cycle, reflecting only the oceanic component of O_2/N_2 seasonality. The APO interannual downward trend is less steep than the O_2/N_2 trend, reflecting a small contribution from fossil fuel combustion owing to the higher $O_2:CO_2$ ratio of fossil fuel compared to land biota, and a contribution from fossil fuel combusted CO_2 that is taken up by the oceans. The APO latitudinal gradient is also smaller than that for O_2/N_2 . The CO_2 data of Figure 2.3 show similar features as O_2/N_2 except that the seasonal cycle is smaller, particularly in the southern hemisphere, and reversed in phase, and the interannual trend is increasing, but less steeply than O_2/N_2 is decreasing. Because the majority of fossil fuel combustion is in the northern hemisphere, the CO_2 latitudinal gradient exhibits high concentrations in the north and low in the south, but this gradient is smaller than the O_2/N_2 gradient reflecting either an oceanic sink of O_2 or CO_2 in the northern hemisphere, or an oceanic source of O_2 or CO_2 in the southern hemisphere. The remainder of this section discusses these features in greater detail.

2.3.1. Seasonal Cycles

Seasonal cycling in O_2/N_2 ratios is caused by a combination of land biotic O_2 exchanges, and O_2 and N_2 air-sea gas exchanges. Latitudinal variations in amplitude

can be seen in Figure 2.2 and are quantified in Table 2.2. By analyzing the seasonal amplitudes of CO₂ and APO (shown in Figures 2.3 and 2.4 respectively, and quantified in Table 2.2), I can separate and quantify the effects on the O₂/N₂ seasonal amplitude which are due to seasonal processes on the land and in the oceans respectively. At all stations in the northern hemisphere between half and two-thirds of the O₂/N₂ seasonal cycle is due to the land biota (Table 2.2). In the spring and summer photosynthesis dominates and atmospheric O₂/N₂ ratios increase, whereas in the fall and winter with lower temperatures and less solar irradiance, plant and soil respiration dominate over photosynthesis and there is a drawdown of O₂/N₂ ratios. In the southern hemisphere there is relatively little land cover in the temperate and high latitudes apart from the ice-covered Antarctic continent, and there is little seasonality in the tropics, therefore the southern hemisphere seasonal cycle of O₂/N₂ is dominated by ocean effects, with a land biotic effect of approximately 10%. A portion of this land biotic effect is in fact thought to be a northern hemisphere land biotic component from long-range transport with a lag time of 9 to 12 months, as proposed based on CO₂ data from Baring Head, New Zealand [Lowe *et al.*, 1979]. This northern hemispheric influence can be seen most dramatically at the low latitude station of Samoa (14°S) and is described in more detail in section 2.4 below.

The seasonal cycles in atmospheric CO₂, as shown in Figure 2.3, to a good approximation represent these land biotic influences [Keeling *et al.*, 1998b]. In general the CO₂ cycle is anti-correlated with the O₂/N₂ cycle, but is of smaller magnitude because there is almost no ocean effect on the CO₂ seasonality [Heimann *et al.*, 1989]. As explained in the introduction, this is because the marine biotic production and

Table 2.2. Average Amplitudes of Seasonal Cycles¹

Station code	Latitude	O ₂ /N ₂ (per meg)	CO ₂ (ppm)	APO (per meg)	APO (%) ²
ALT	82°N	125	15.1	47	38
CBA	55°N	146	14.3	80	55
NWR	40°N	76	9.5	27	36
LJO	33°N	101	9.8	53	53
MLO	20°N	46	7.0	16	34
KUM	20°N	71	8.0	33	46
SMO	14°S	22	1.2	29	131
CGO	41°S	72	1.2	67	93
MCQ	54°S	91	-	77	84
PSA	65°S	79	1.3	72	91
SPO	90°S	65	1.0	61	94

¹ O₂/N₂, CO₂ and APO seasonal amplitudes are calculated from curve fits approximately the same as those shown in Figures 2.2, 2.3, and 2.4. The data adjustments described in Section 2.3 were carried out on the datasets and curve fits were recomputed on these corrected datasets.

² APO as a percentage of the total O₂/N₂ seasonal cycle. This column represents the percentage of the total seasonal cycle due to all oceanic processes.

consumption cycle is approximately six months out of phase with the temperature-solubility effects on CO₂; because dissolved CO₂ produced from marine heterotrophic and autotrophic respiration reacts with seawater to form carbonate and bicarbonate ions and so does not reach saturation as easily as a geochemically neutral gas; and because the temperature induced seasonality of the mixed layer depth acts to dilute or concentrate the mixed layer in CO₂ out of phase with the temperature-solubility effects.

The oceanic contribution to the O₂/N₂ seasonal cycles is illustrated more clearly in Figure 2.5 which shows APO data only and with the interannual trend removed. This result was achieved by subtracting the spline component of the curve fit from each data point in Figure 2.4. Approximately 15% of the APO seasonal cycle in both hemispheres is due to ocean temperature-solubility effects. As surface waters warm in the spring and

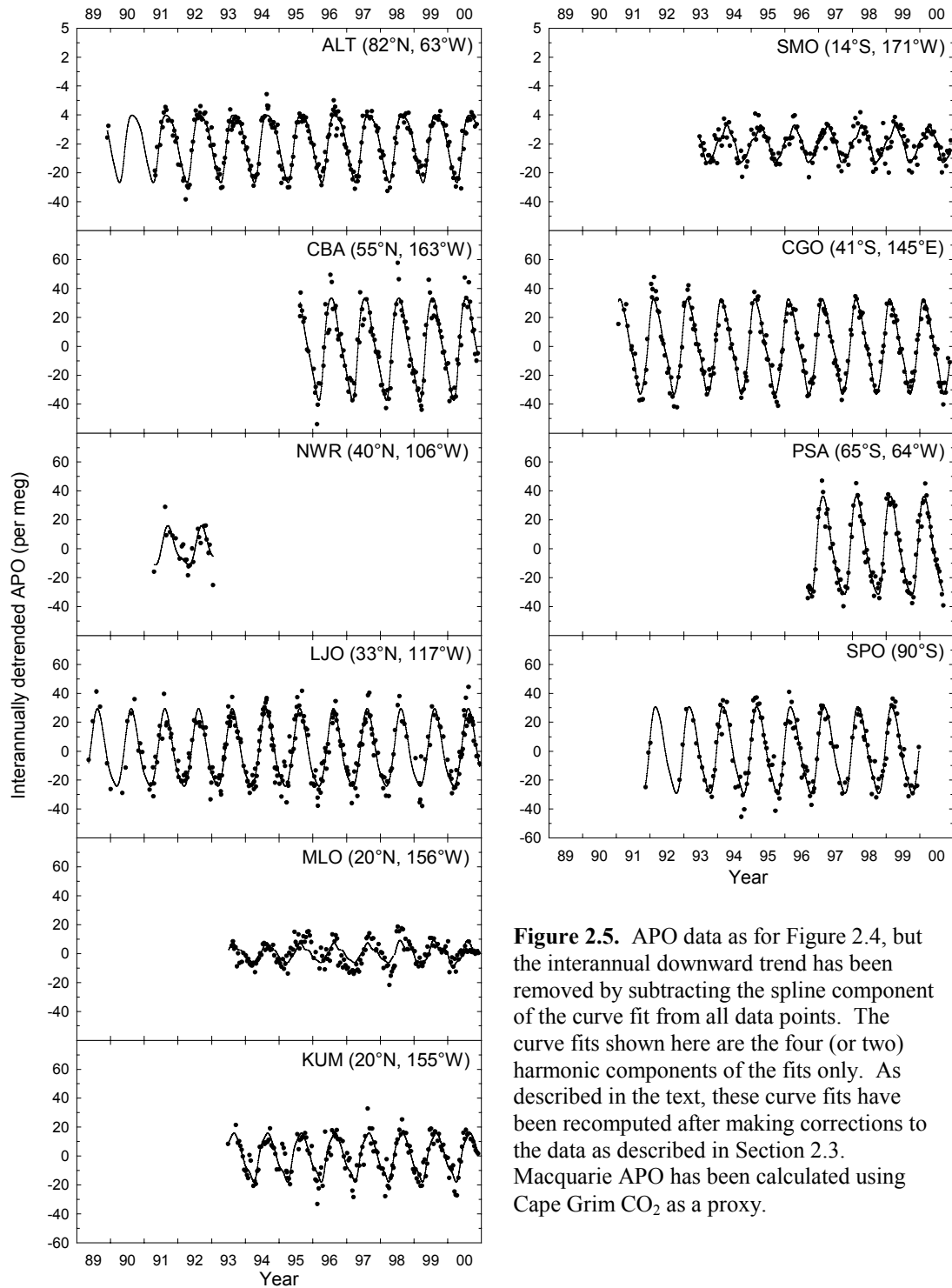


Figure 2.5. APO data as for Figure 2.4, but the interannual downward trend has been removed by subtracting the spline component of the curve fit from all data points. The curve fits shown here are the four (or two) harmonic components of the fits only. As described in the text, these curve fits have been recomputed after making corrections to the data as described in Section 2.3. Macquarie APO has been calculated using Cape Grim CO₂ as a proxy.

summer gas solubilities decrease driving a flux of O_2 and N_2 into the atmosphere. The N_2 solubility dependence on temperature is less than that of O_2 resulting in an increase in the O_2/N_2 ratio. During fall and winter surface waters cool, gas solubilities increase, and more O_2 re-dissolves than N_2 , decreasing the atmospheric O_2/N_2 ratio. The remaining 85% or so of the APO seasonal cycle is due to ocean biota. During fall and winter the mixed layer deepens as surface waters cool, become more dense and sink, entraining water that is undersaturated in O_2 . At the same time there is less net photosynthesis because of less solar irradiance and because the mixed layer is deeper than the euphotic zone, so phytoplankton spend less time in a region with available energy for photosynthesizing. These processes all combine to create a net atmospheric O_2 demand. In the spring and summer the mixed layer shoals, concentrating phytoplankton in the surface waters which receive the most sunlight, there is more net solar irradiance, and temperatures are warmer, all combining to result in higher net photosynthesis. Additionally, because of the shallow mixed layer, O_2 is concentrated in the surface waters. All of these processes result in O_2 -supersaturated surface waters and a flux of O_2 to the atmosphere.

Figures 2.6, 2.7, and 2.8 show respectively the O_2/N_2 , CO_2 , and APO harmonic curve fits for all stations superimposed on each other for comparison. Cold Bay exhibits the largest amplitude in O_2/N_2 ratio and in APO (Table 2.2), with O_2/N_2 ratio over 20 per meg higher than the next highest, Alert, and APO almost 30 per meg higher than the next highest in the northern hemisphere. I suspect that this large amplitude is owing to the proximity of Cold Bay to regions of highly active air-sea exchange of O_2 in the North Pacific and Bering Sea. This conclusion is further supported by data from an

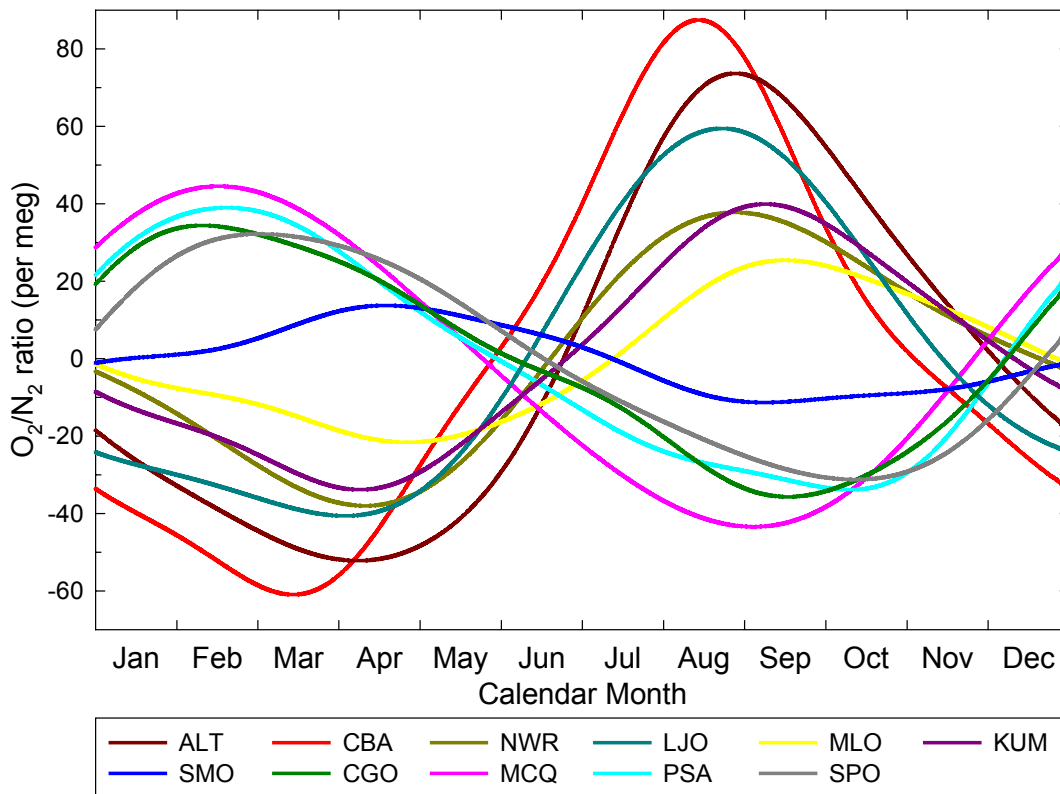


Figure 2.6. Shows the seasonal cycle component of the curve fits from Figure 2.2 for O₂/N₂ ratios for all stations, after correcting data as described in Section 2.2.3. Amplitude and phasing variations can be compared between different stations in this figure.

independent O₂/N₂ sampling program at Point Barrow, Alaska (71°19'N, 156°36'W), also in close proximity to the Bering Sea, where similar large seasonal amplitudes are observed (M. Bender, personal communication).

Cold Bay also shows a significantly earlier minimum in both O₂/N₂ ratios and APO and a slightly earlier maximum in CO₂ than other northern hemisphere stations (Figures 2.6, 2.7, and 2.8), indicating an earlier start of the “spring thaw” in both the marine and land biota. Alert exhibits the latest start in the spring thaw, as could be

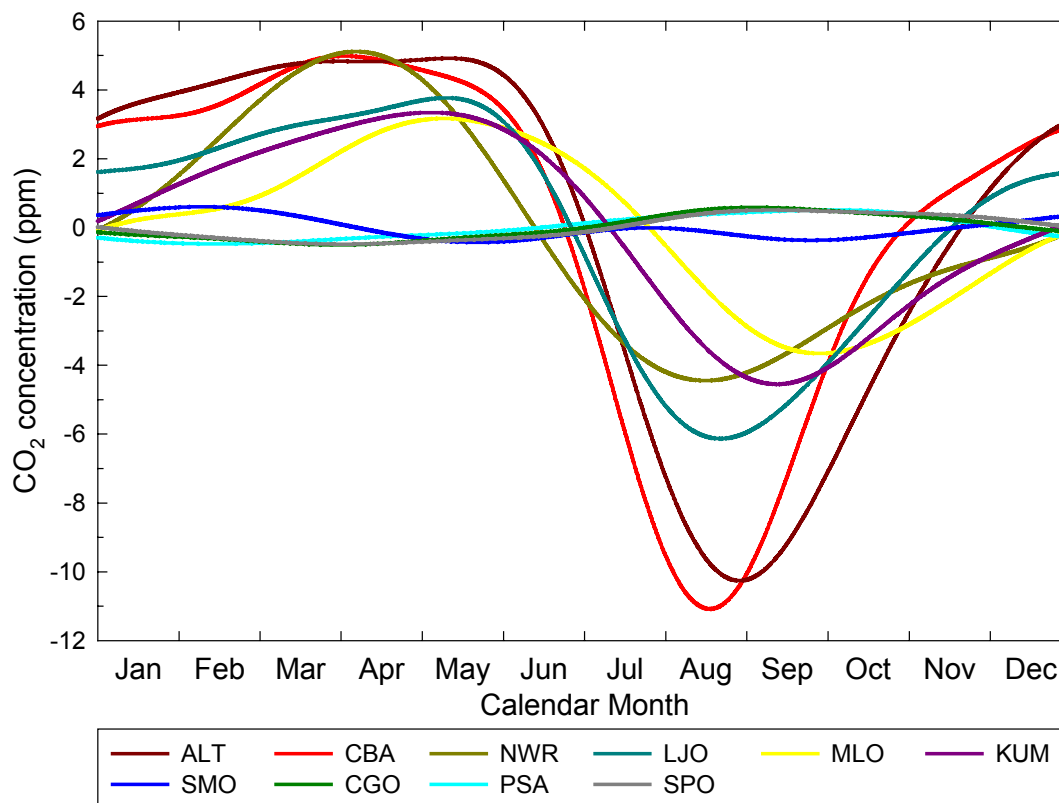


Figure 2.7. Shows the seasonal cycle component of the curve fits from Figure 2.3 for CO₂ concentration for all stations, after correcting data as described in Section 2.2.3.

expected by a high northern latitude station. The same reason given for Cold Bay exhibiting the largest amplitude, the proximity to sources and sinks, can also explain the significantly earlier spring rise and fall decrease in O₂/N₂ ratios. The Cold Bay APO signal shows greater asymmetry compared to other stations, particularly noticeable in the spring. This I attribute to the marine and land biota being slightly out of phase in this region in terms of the start of the spring thaw.

The seasonal APO cycles at Niwot Ridge and Mauna Loa are the smallest observed because both of these sites are situated at elevations that place them above the

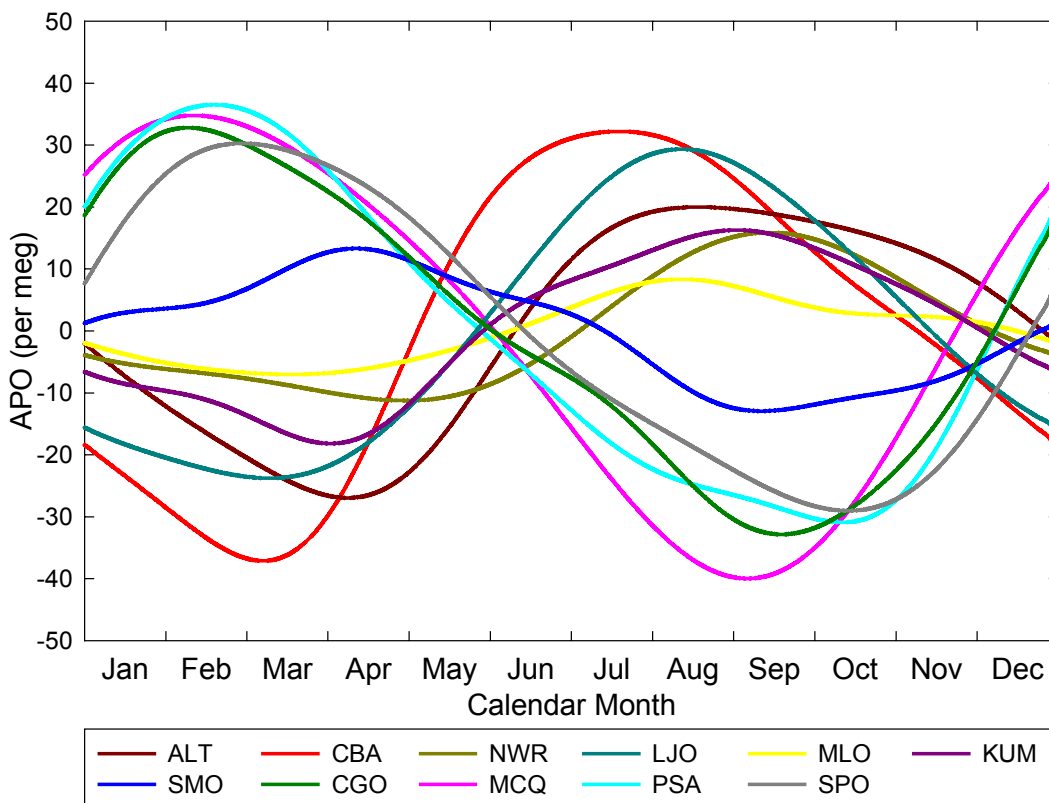


Figure 2.8. Shows the seasonal cycle component of the curve fits from Figure 2.4 for APO for all stations, after correcting data as described in Section 2.2.3.

marine boundary layer, and the surface-based ocean fluxes driving the seasonal cycles are attenuated at these altitudes. South Pole is also at higher elevation and shows some attenuation in APO compared to other mid- to high latitude southern hemisphere stations. The reason why South Pole does not exhibit the same attenuation as observed at Mauna Loa and Niwot Ridge is probably because it is surrounded by regions of active air-sea gas exchange.

The smallest seasonal cycles are observed in the tropical stations of Mauna Loa, Cape Kumukahi, and Samoa, as expected due to the low seasonality in these locations.

Cape Kumukahi shows larger APO and CO₂ seasonality than Mauna Loa because it is a coastal site in the marine boundary layer, whereas the Mauna Loa station is located at 3,400 m, above the boundary layer and thus further from the sources and sinks driving both the APO and CO₂ seasonal cycles. Data from Samoa are very different from all other stations. The APO seasonal cycle is actually larger than the O₂/N₂ cycle (see Table 2.2) by 7 per meg, indicating that the CO₂ seasonal cycle must have a similar phasing as O₂/N₂, rather than approximately six months out of phase as observed at all other stations. Additional complicating factors are found to be contributing to the Samoa signal, as I discuss in section 2.4 below.

In terms of maximum APO seasonal amplitude, Cold Bay is followed by the mid- to high latitude stations in the southern hemisphere, Macquarie, Palmer Station, Cape Grim, and South Pole in that order. The phasing and amplitude of O₂/N₂, CO₂, and APO in the mid- to high latitudes of the southern hemisphere are all roughly equal. At Palmer Station the CO₂ minimum occurs about 2 months earlier (January) and is about 0.2 ppm lower than observed at Cape Grim or South Pole. In addition, O₂/N₂ at Palmer Station closely follows the patterns observed at Cape Grim and South Pole except for a maximum about one month earlier (January) and about 12 per meg higher. I suspect that these differences at Palmer Station may be explained by oceanic influences on both O₂ and CO₂. Macquarie O₂/N₂ shows similar features as Palmer except for a 15 per meg lower minimum which occurs about one month earlier. Since we only have one year of data from Macquarie, this difference may not be statistically significant, but could represent a similar effect observed at Cold Bay, where Macquarie

is situated in a latitude band of highly active air-sea exchange of O_2 in the Southern Ocean.

2.4. Interpreting Seasonal Cycles of O_2 and CO_2 at American Samoa

2.4.1. Unique Features Observed in Atmospheric Data Collected at Samoa

When compared to other stations in our flask sampling network, data from Samoa are unusual, exhibiting higher short-term variability and seasonal cycles not in phase with other stations. The unusual seasonality is illustrated in Figure 2.9 which shows the four-harmonic seasonal component of the O_2/N_2 and CO_2 curve fits from the Samoa plots in Figures 2.2 and 2.3. The curves shown are the average seasonal cycles calculated from all data over the seven-year record. Also shown are the same curve fits calculated from data collected at Cape Grim and La Jolla which I will assume are broadly representative of mid-latitudes in the southern and northern hemispheres respectively. To illustrate the characteristics of the seasonal variability more clearly, the first six months of data are repeated in order to generate an 18 month-long record.

As shown in Figure 2.9a, the maximum O_2/N_2 ratio at Samoa occurs in April, approximately two months later than the peak at Cape Grim, which occurs in February. The minimum O_2/N_2 ratio at Samoa occurs in late August or early September, a few weeks earlier than Cape Grim. There is some evidence of a weak second maximum in late December at Samoa. CO_2 data in Figure 2.9b show an even larger contrast to typical southern hemisphere patterns. Maximum CO_2 at Samoa occurs in February in contrast to September for Cape Grim, whereas the minimum occurs in May at Samoa and April at Cape Grim. CO_2 also exhibits a clearer second maxima and minima at

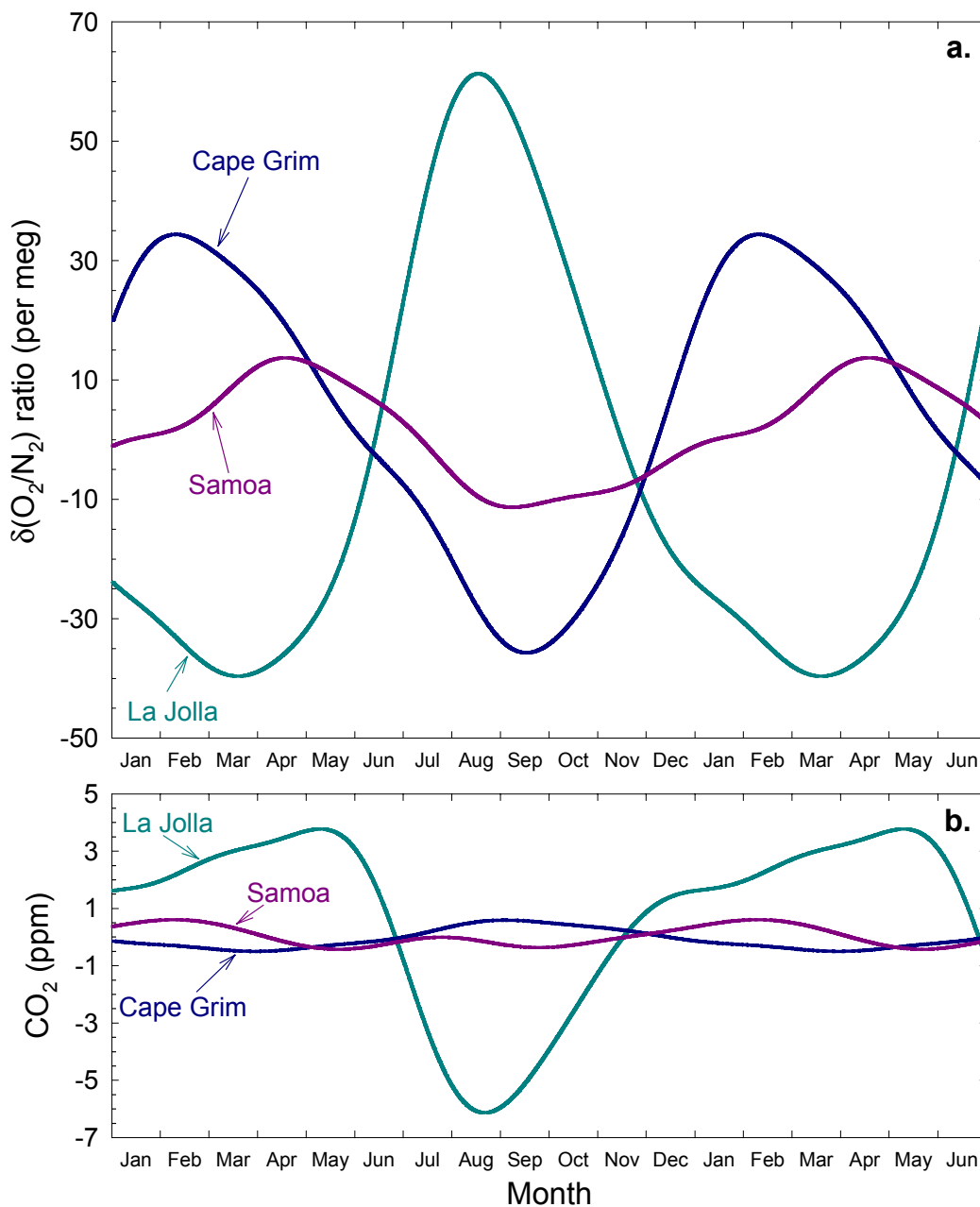


Figure 2.9. Four-harmonic seasonal components of the Samoa curve fits in Figures 2.2 and 2.3, showing O_2/N_2 ratios (a) and CO_2 concentrations (b). Also shown for comparison are similar seasonal curve fits calculated from Cape Grim and La Jolla, representing the mid-latitudes of the southern and northern hemisphere respectively. To show the seasonal characteristics more clearly, the first six months of each cycle are repeated. Southern hemisphere and northern hemisphere cycles are roughly six months out of phase with each other, whereas Samoa shows a more complicated signal. Plots a and b have been scaled so that changes in O_2 and CO_2 can be compared visually on a mole to mole basis.

Samoa, as seen in the figure. The La Jolla curves show that Samoa O_2/N_2 ratios and CO_2 concentrations are also not in phase with northern hemisphere trends. In addition, at each of La Jolla and Cape Grim, O_2/N_2 and CO_2 changes are to a good approximation anti-correlated with each other, whereas at Samoa this is clearly not the case.

The unique climatological conditions at Samoa and their impact on concentrations of atmospheric constituents have been noted before. *Halter et al.* [1988] presented three years of CO_2 data from 1979-1981. They discussed the seasonal dependence of the variability observed in their CO_2 data and related this to air masses arriving at Samoa from different source regions. Following the wind climatology at Samoa presented by *Bortniak* [1981] and from an analysis of wind backward trajectories, *Halter et al.* [1988] were able to show that the air arriving at Samoa came from one of three broadly-defined source regions centered on anticyclones named A_{NP} , A_{SP} , and A_{ANZ} , representing the north Pacific tropical anticyclone, the southeast Pacific tropical anticyclone, and the Australia-New Zealand anticyclone respectively. These source regions are shown in Figure 2.10.

Halter et al. [1988] further demonstrated that the observed Samoa CO_2 seasonal cycle was a superposition of three distinct seasonal cycles originating from each of these three air mass source regions. Because the seasonal cycle of CO_2 in the northern and southern hemispheres are out of phase, these cancel out partially, but not completely, at Samoa, resulting in the complex seasonal pattern which can be seen in Figure 2.9b. *Halter et al.* [1988] then showed that the seasonal dependence of the CO_2 variability observed at Samoa is a function of the seasonally varying interhemispheric gradient in CO_2 concentration, and also of the seasonally varying frequency of occurrence that air

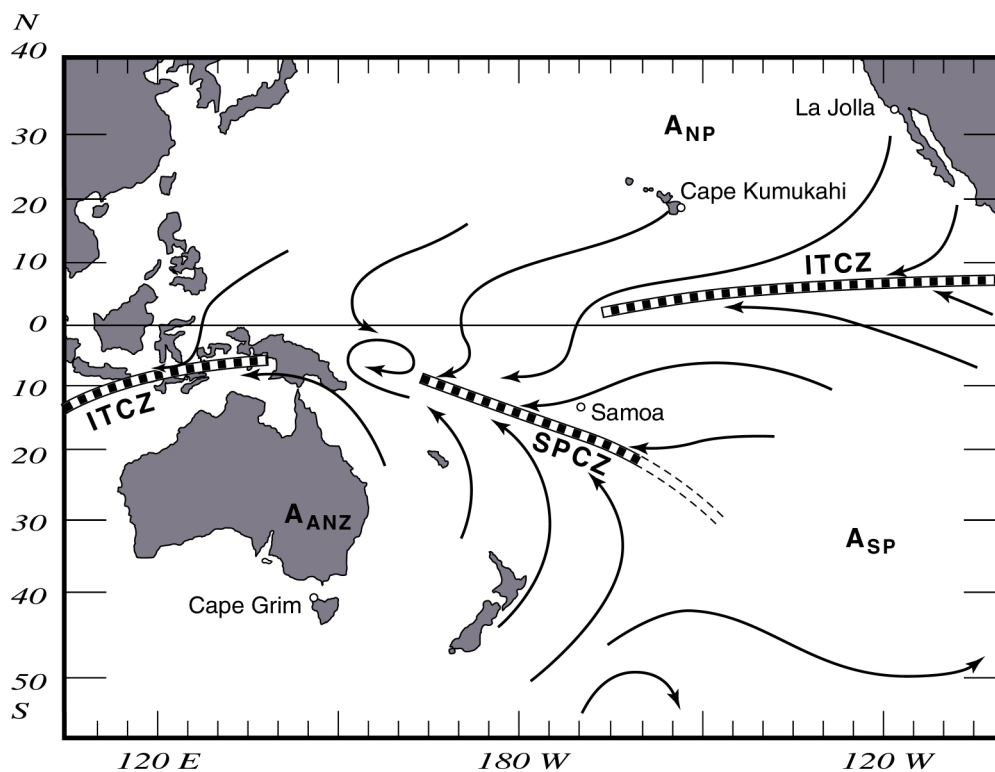


Figure 2.10. Average surface air circulation patterns in the region of Samoa, shown for austral summer. This figure is after *Bortniak* [1981] and *Halter et al.* [1988]. Lines labeled ITCZ and SPCZ are the axes of the Intertropical Convergence Zone and the South Pacific Convergence Zone respectively. In austral winter the ITCZ extends further westwards and the SPCZ shifts northwards, resulting in a lower frequency of occurrence of air from the anticyclone, A_{NP} , arriving at Samoa, and a higher frequency of air from anticyclone, A_{ANZ} . The third source of air to Samoa is from anticyclone A_{SP} . Also shown are the locations of Cape Grim, Tasmania, Cape Kumukahi, Hawaii, and La Jolla, California, from which atmospheric O_2 data are shown in this section.

arriving at Samoa originated from the northern hemispheric A_{NP} anticyclone. These two effects combine to result in greater CO_2 variability during austral summer and autumn.

The frequency of occurrence of air from A_{NP} varies because of seasonal variations in the position and strength of the Intertropical Convergence Zone (ITCZ) and the South Pacific Convergence Zone (SPCZ), shown in Figure 2.10. This figure shows the average position of the ITCZ and SPCZ in austral summer. In austral winter, by

contrast, the ITCZ extends further westwards, blocking air masses from the A_{NP} region from reaching Samoa.

Prinn et al. [1992] and *Hartley and Black* [1995] found relatively high short-term variability in methyl chloroform concentrations measured at Samoa during austral summers, but only in non-El Niño years. *Hartley and Black* [1995] showed that these observations could be explained by changes in large-scale atmospheric circulation patterns at Samoa similar to the seasonal changes described by *Halter et al.* [1988] and *Bortniak* [1981]. They demonstrated that the frequency of occurrence of air originating from the A_{NP} anticyclone during El Niño years was significantly reduced, explaining the lack of methyl chloroform variability in these years. In Figure 2.11, I show an enlarged version of the Samoa data in Figure 2.3. This shows that our CO_2 data support the conclusion of *Hartley and Black* [1995], showing that during the strong 1997-1998 El Niño, CO_2 variability during the austral summer is significantly reduced compared to other years.

Harris and Oltmans [1997] observed variability in tropospheric ozone concentrations at Samoa approximately six months out of phase with the variability in CO_2 described by *Halter et al.* [1988]. They also attributed these observations to summer-winter changes in atmospheric transport, in this case explaining the high austral winter variability not by variations in the latitudinal origin of the air masses arriving at Samoa, but by variations in the altitudinal origin which impacts the relative strengths of ozone sources and sinks, thus influencing the concentration of ozone in arriving air masses.

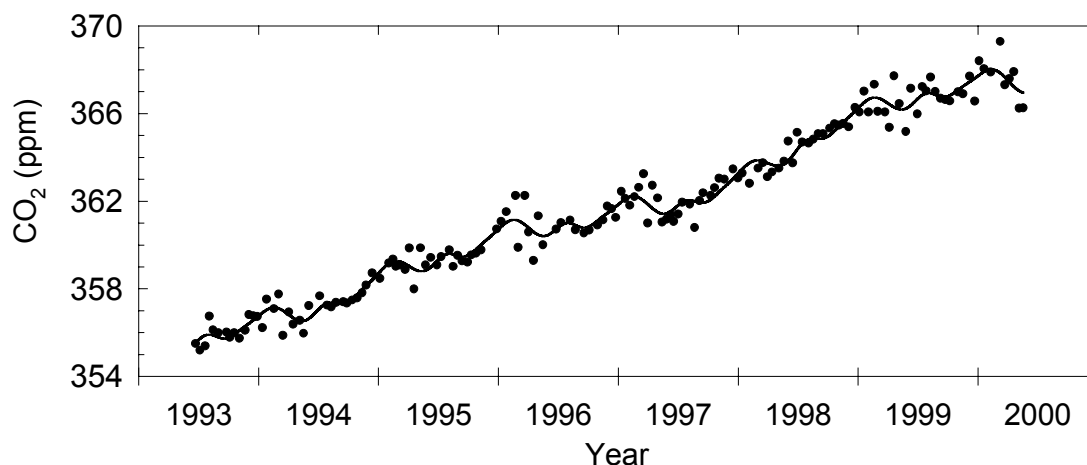


Figure 2.11. Samoa CO₂ data, as shown in Figure 2.3, enlarged here to show the contrast in variability between El Niño and non-El Niño years. During the strong El Niño of 1997-1998 a lack of variability during austral summer can be seen.

2.4.2. Land and Ocean Partitioning of Air Mass Influences at Samoa

In Figure 2.12, I show plots of APO and CO₂ concentrations representing oceanic and land influences at Samoa respectively. The symbols on each plot show all flask samples collected at Samoa from June 1993 to June 2000, where all samples have been collapsed into one calendar year. The curves shown are the four-harmonic seasonal component of the curve fits to data from Cape Grim and Cape Kumukahi, representing the nearest sampling stations from which I have data in the southern and northern hemispheres respectively. Typically, data that have been interannually detrended are centered on zero and have no absolute frame of reference. Here, in order to compare detrended data across different stations, I have normalized all data to the Cape Grim interannual trend. In other words, the Samoa flask data shown are the raw data points from the Samoa plots of Figures 2.4 and 2.3 with the interannual spline component of the Cape Grim curve fit subtracted. Because of slight variability from

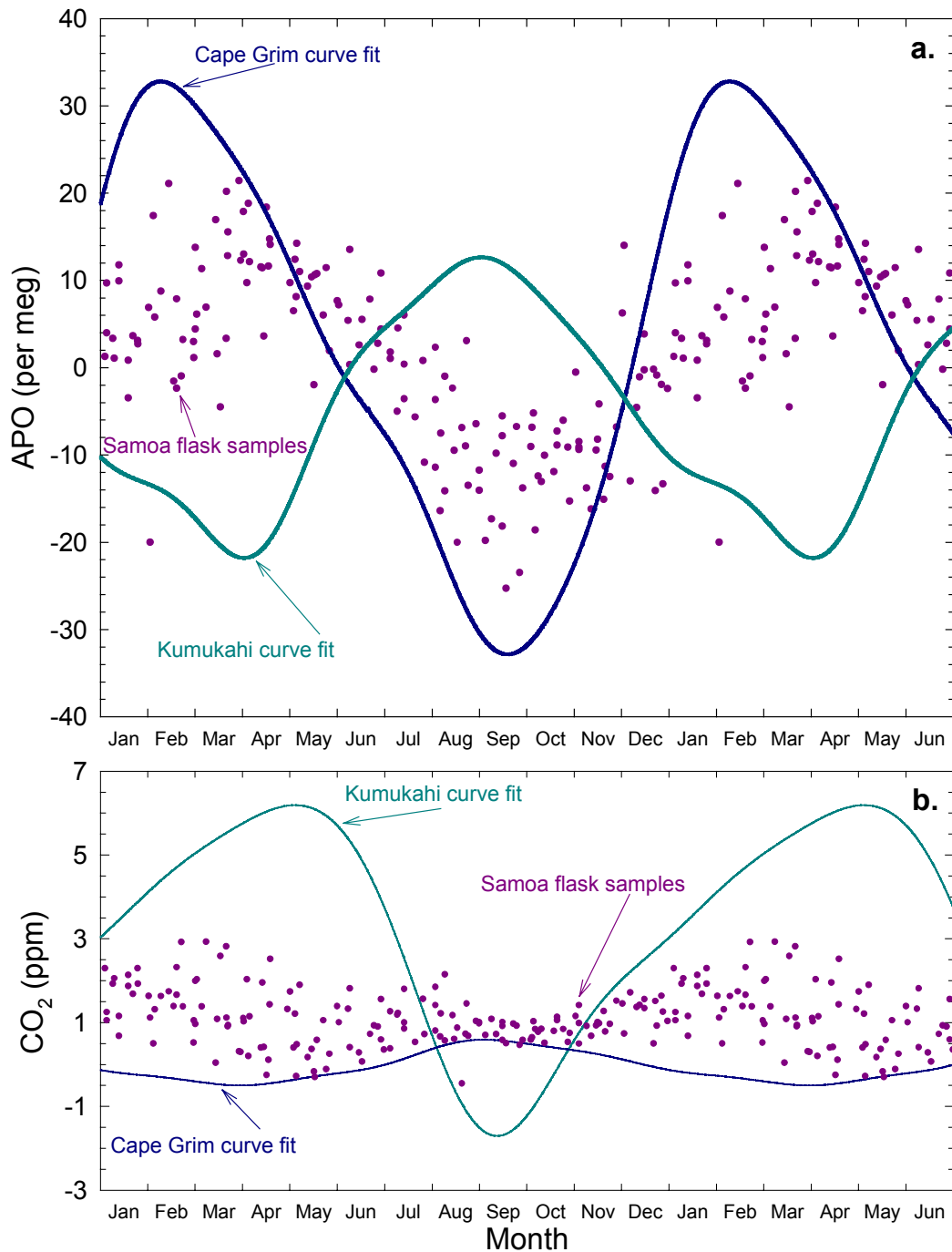


Figure 2.12. Shows oceanic (a) and land biotic (b) influences on the air masses arriving at Samoa. Atmospheric Potential Oxygen (APO), defined in the text (section 2.2.2), is essentially not influenced by land biotic processes and therefore represents oceanic influences. The seasonal component of the Samoa flask samples are shown, as well as seasonal curve fits from Cape Grim and Cape Kumukahi, representing the nearest stations from which I have data in the southern and northern hemisphere respectively. Data have been normalized as described in the text. As with Figure 2.9, the first six months of each cycle are repeated, and the plots have been scaled to be able to visually compare mole to mole changes in APO and CO₂ concentrations.

year to year in the interannual trends, I am not able to show the Kumukahi four-harmonic curve fit in the same manner. Instead, I calculated the average offset between the Kumukahi and Cape Grim spline components from 1993 to 2000 ($\Delta\text{O}_2/\text{N}_2 = -3.6$ per meg; $\Delta\text{CO}_2 = 2.8$ ppm) and added this offset to the Kumukahi four-harmonic curve fit, resulting in the Kumukahi curves shown in Figures 2.12a and b. The Cape Grim curves shown are simply the Cape Grim four-harmonic components of the Cape Grim curve fits. As with Figure 2.9, the first six months are repeated to generate 18 months of data, and APO and CO_2 changes are comparable visually on a mole to mole basis.

There are several prominent features apparent in Figure 2.12. Samoa CO_2 data in Figure 2.12b agree very well with the earlier data presented by *Halter et al.* [1988], showing greater variability in the austral summer and autumn. However, based on additional information from our APO data, I suggest a slightly different hypothesis of source air mass origins to explain this variability. For periods of May, June, and December in the APO signal, and from August to October in the CO_2 signal, Samoa data exhibit persistently higher concentrations than seen in air masses either to the north or to the south. I believe that these data represent recirculated air, perhaps as a component of the Pacific Walker cell circulation, in other words air not recently originating from the north or the south, but from the tropics at some point in the past.

To further support this hypothesis, in Figure 2.13 I present the statistical variability in the data. I calculated the residuals of all Samoa flask samples from the plots in Figures 2.4 and 2.3 from the curve fits also shown in the Samoa plots of Figure 2.4 and 2.3. I then calculated the standard deviation of these residuals for each month, where, for example, all January samples from 1993 to 2000 have been binned together.

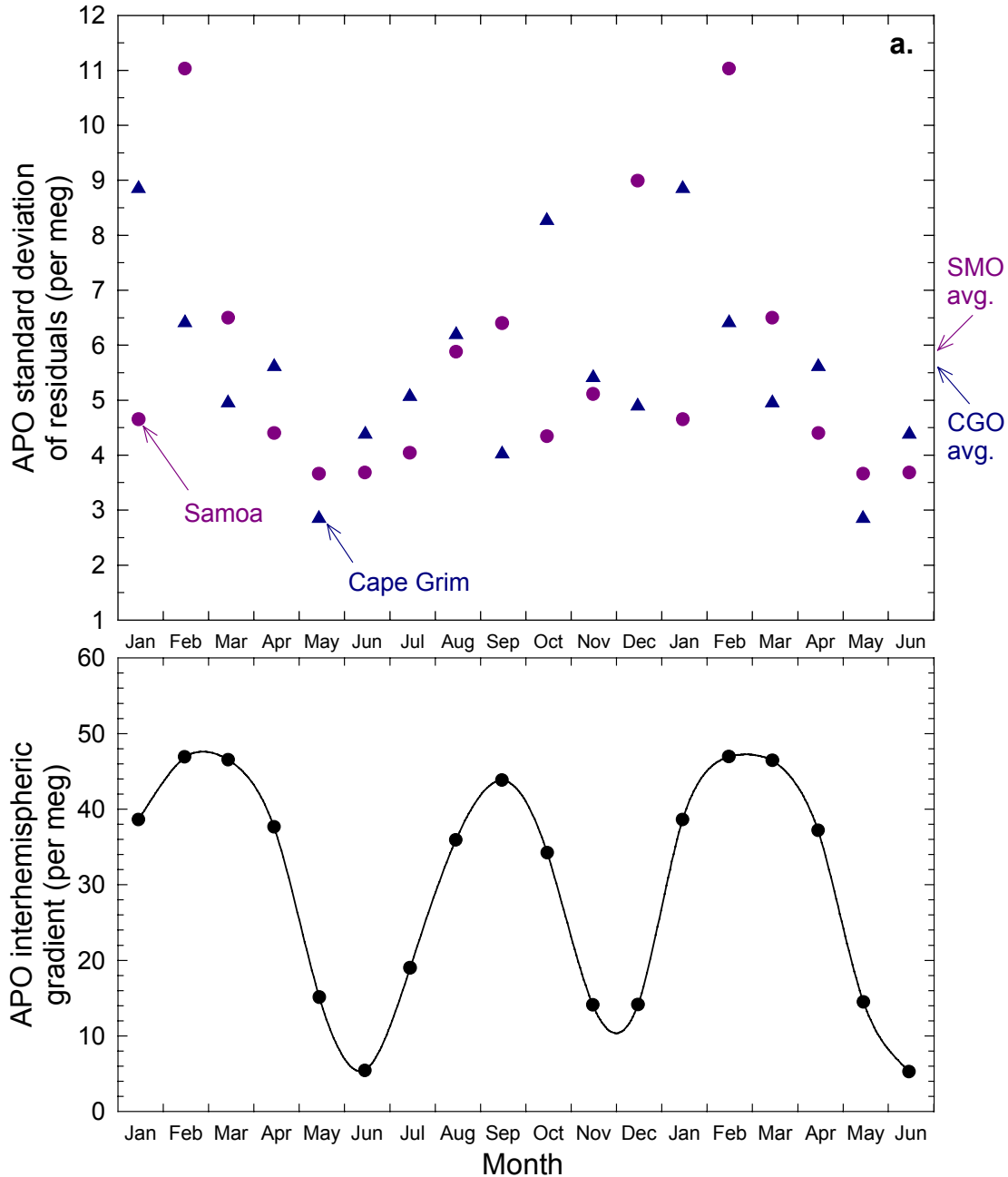


Figure 2.13a. The top plot shows APO monthly standard deviations of the residuals of the flask data from Figure 2.4 from the curve fits in the same figure. Results are shown for both Samoa and Cape Grim, and the first six months are repeated. The annual average residual at each station is indicated on the right. There is little to distinguish between Samoa and Cape Grim, and there is only weak evidence of a seasonal trend in the residuals at both stations. The bottom plot shows the absolute magnitude of the north-south interhemispheric gradient, calculated each month, and using Cape Grim and Cape Kumukahi data as representative of the southern and northern hemisphere respectively to calculate the gradient.

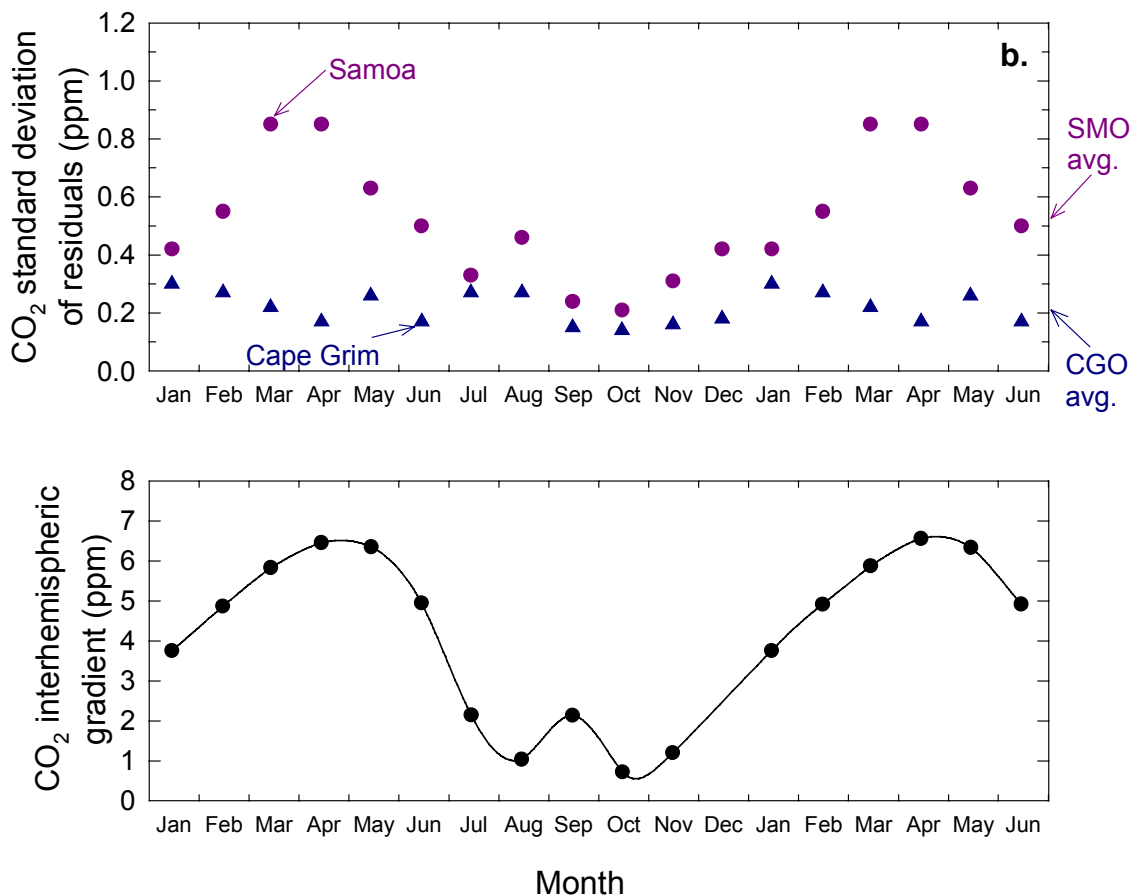


Figure 2.13b. Top and bottom plots as for Figure 2.13a, except showing CO₂ concentration. As for Figures 2.9 and 2.12, APO and CO₂ changes are visually comparable between Figures 2.13a and b. In contrast to APO, CO₂ shows a clear seasonal pattern in variability at Samoa, indicated here with higher standard deviations, whereas Cape Grim does not appear to show any seasonality. The pattern at Samoa appears to correlate well with the north-south interhemispheric gradient. Contrasting the magnitude of APO variability with CO₂, it can be seen that the APO signal is much “noisier”, reflecting the presence of larger sources and sinks for O₂ in the southern hemisphere compared to CO₂.

These standard deviations for each month are shown in the top plots of Figures 2.13a and 2.13b for APO and CO₂ respectively. Thus these plots give a statistical measure of the variability in APO and CO₂ at monthly time intervals. To provide a comparison,

Cape Grim data are calculated in the same manner. As for Figures 2.9 and 2.12, the first six months are repeated.

Figure 2.13b shows what was readily apparent in Figure 2.12b, a clear seasonal pattern to the variability in the CO₂ signal. The figure also shows a good correlation of this variability with the north-south interhemispheric gradient, shown in the bottom plot of Figure 2.13b. In contrast, the top plot of Figure 2.13b shows that Cape Grim does not exhibit such seasonal variability, and that during the austral winter and spring, Samoa variability is similar to that at Cape Grim. Figure 2.13a shows that there may also be a seasonal component to the APO variability. However, such seasonality is much less readily apparent than the CO₂ seasonality, is not of the same phasing as CO₂, and is almost equally apparent in Cape Grim APO as it is in Samoa APO.

With the exception of APO in December, all of the months described above in Figure 2.12 exhibiting APO or CO₂ concentrations higher than present in the northern or southern hemisphere for that month also show relatively low monthly standard deviations in Figure 2.13. This lower variability also suggests that this air has had more time to mix and become homogenized, and has not been influenced to the same extent by air masses from the north or the south, supporting the hypothesis of recirculated tropical air.

Figures 2.12 and 2.13 both show a clear difference in the pattern of variability in the APO signal compared with the CO₂ signal. APO does not show such a clear seasonal distinction in variability as CO₂, and does not show significant differences from Cape Grim variability (Figure 2.13). The top plots of Figure 2.13 have been scaled to enable direct comparison of the magnitude of variability of APO with CO₂. Thus it is

clear that APO exhibits about twice the magnitude of variability of CO₂. These differences between APO and CO₂ can not be directly explained either by the seasonally varying interhemispheric gradient, or by the seasonally varying frequency of occurrence of the different air masses arriving at Samoa, both of which can be expected to affect APO in a similar manner as CO₂. In addition, the bottom plots of Figure 2.13, which have also been scaled to be comparable mole to mole, show that the magnitude of the APO interhemispheric gradient is only slightly larger than the magnitude of the CO₂ interhemispheric gradient, and not large enough to explain the much greater APO variability observed.

There is, however, a difference in the southern hemisphere with respect to APO and CO₂. Regional sources and sinks for CO₂ are relatively small, whereas sources and sinks for APO are comparable to those in the northern hemisphere. Therefore from July to November CO₂ variability is lowest both because of a smaller interhemispheric gradient (Figure 2.13b, bottom plot) and because of a lower frequency of occurrence of A_{NP} air masses arriving at Samoa [Halter *et al.*, 1988] owing to the position of the ITCZ (Figure 2.10). By contrast, even when air masses are entirely of southern hemisphere origin, APO variability is still high because regional sources and sinks prevent the air from becoming as well homogenized in APO. Figure 2.13a shows little distinction in APO variability between Samoa and Cape Grim, further supporting this conclusion. In addition, the backward wind trajectory analyses of Harris and Oltmans [1997] showed that air masses originating from the southern hemispheric A_{ANZ} anticyclone arriving at Samoa were more variable in their originating altitude than air masses arriving from A_{NP} or A_{SP}. Because the source and sink mechanisms for APO occur via air-sea gas

exchange at the sea surface, this altitudinal variability in air mass origin will contribute further to the variability observed in the APO signal at Samoa. Furthermore, because of a northward shift in the SPCZ (Figure 2.10), the frequency of occurrence of air arriving from the A_{ANZ} anticyclone is higher during austral winter and spring, resulting in greater APO variability and coinciding with the time of lowest CO_2 variability.

2.4.3. Conclusions

When compared to other stations in our flask sampling network, data from Samoa are unusual, exhibiting higher short-term variability and seasonal cycles not in phase with other stations. This has been noted previously from measurements of CO_2 , methyl chloroform, and ozone, and has been attributed to the unique geographical position of Samoa in relation to the IPCZ and SPCZ, whose positions vary seasonally, resulting in different air masses arriving at Samoa at different times of year. Our atmospheric O_2 data, expressed as Atmospheric Potential Oxygen, APO, exhibit characteristics different from these other atmospheric gases. The main differences are greater magnitude in the short-term variability, but, in contrast, almost no seasonal pattern to this variability. This I explain by significant regional sources and sinks existing for APO in both hemispheres, in contrast to CO_2 , and related to this, a dependence on the altitudinal origins of air masses arriving at Samoa in addition to a dependence on the latitudinal origins. Thus APO variability is a function of the interhemispheric gradient, the frequency of occurrence of air masses originating from A_{NP} when this gradient is large, and also a function of the frequency of occurrence of air masses originating from A_{ANZ} . These three effects, combined with regional sources and

sinks of comparable magnitude in both hemispheres, combine to result in higher variability in the APO signal than the CO₂ signal, and very little if any seasonal pattern to this APO variability.

2.5. Global Land Biotic and Oceanic Carbon Sinks

As discussed in Section 2.1, precise measurements of atmospheric O₂, along with concurrent CO₂ measurements, allow estimates of global land biotic and oceanic carbon sinks to be derived. In this section I present calculations of these sinks made over different time periods and using data from different stations, and I compare my results with results from other researchers.

The primary contribution to the interannual downward trend in O₂/N₂ ratios (and upward trend in CO₂ concentrations) is anthropogenic combustion of fossil fuels. Other processes can also affect this trend such as biomass burning, other anthropogenic land use changes, net uptake by the land biota, and oceanic ventilation processes occurring on interannual time scales. In Figures 2.14, 2.15, and 2.16, I show the interannual trends at all stations (except Niwot Ridge) in O₂/N₂ ratios, CO₂ concentrations, and APO respectively. These plots are shown as differences from the spline component of the Cape Grim curve fit. Both the deseasonalized flask data and the deseasonalized curve fit for each station are subtracted from the Cape Grim spline. Therefore these figures are a measure of the consistency both temporally and between stations of the long-term interannual trends. Most records show relatively flat trends. Several stations show a sharp increase or decrease in the last year or so of the record. This can most

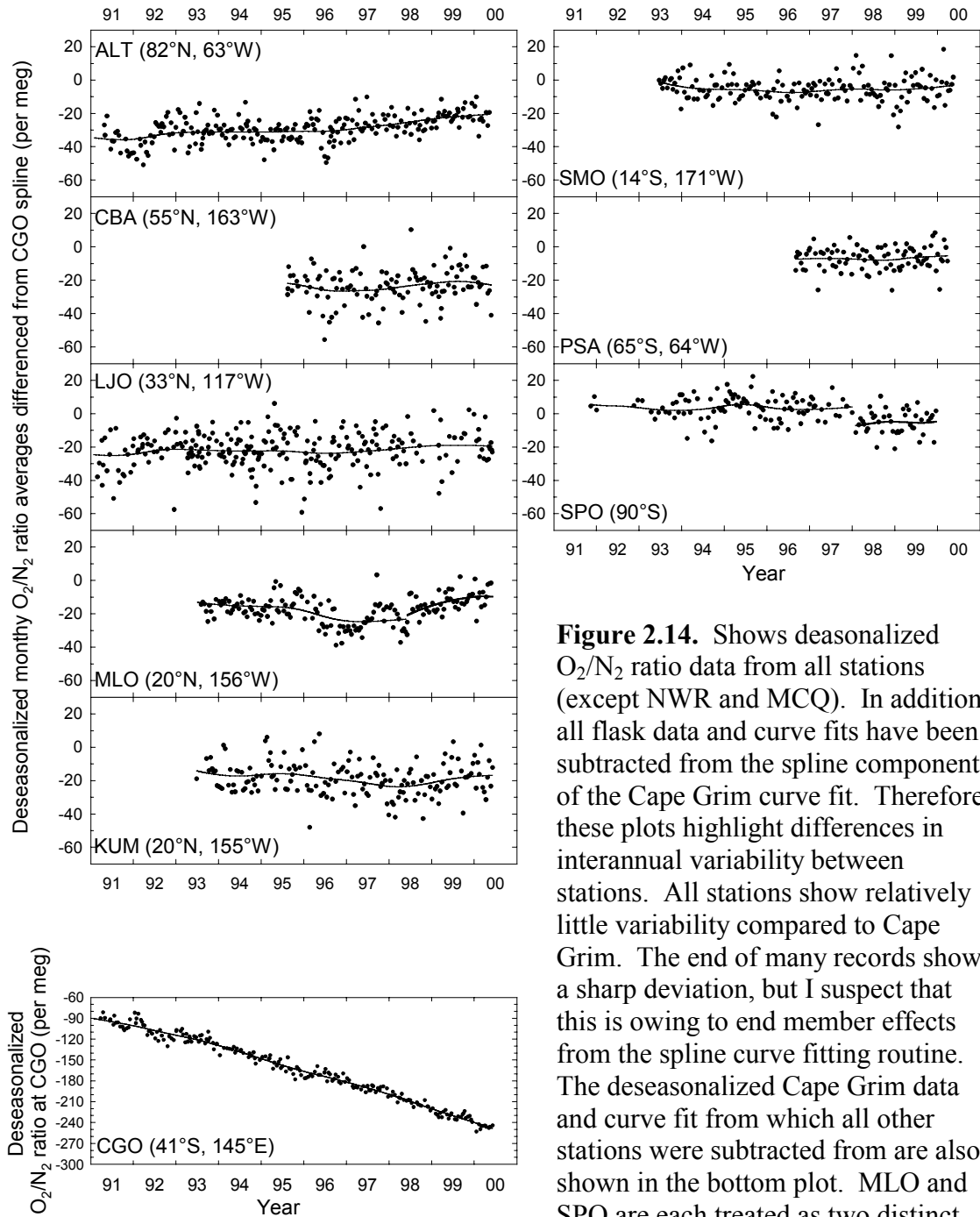


Figure 2.14. Shows deseasonalized O_2/N_2 ratio data from all stations (except NWR and MCQ). In addition, all flask data and curve fits have been subtracted from the spline component of the Cape Grim curve fit. Therefore these plots highlight differences in interannual variability between stations. All stations show relatively little variability compared to Cape Grim. The end of many records shows a sharp deviation, but I suspect that this is owing to end member effects from the spline curve fitting routine. The deseasonalized Cape Grim data and curve fit from which all other stations were subtracted from are also shown in the bottom plot. MLO and SPO are each treated as two distinct time series, as described in section 2.2.3.

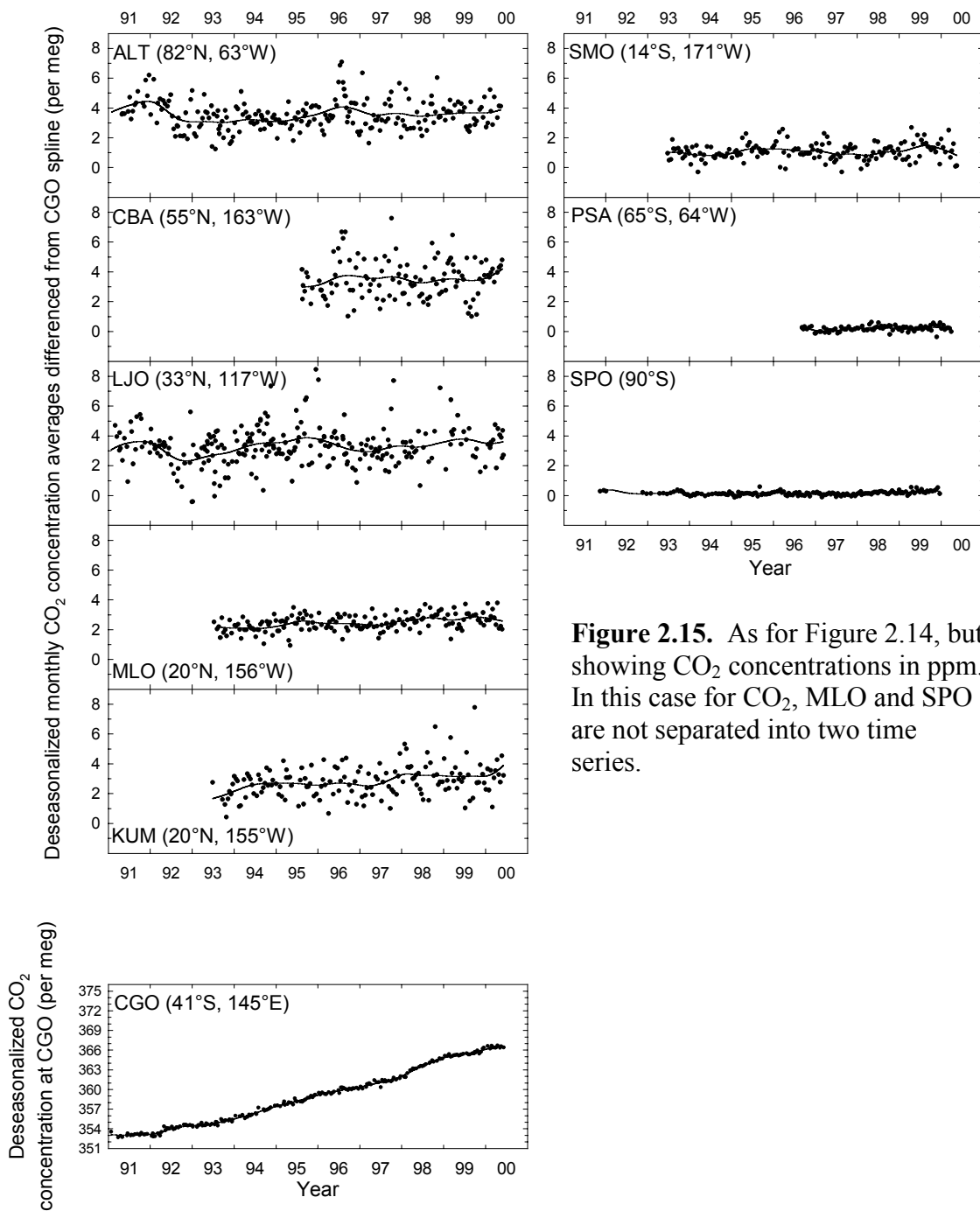


Figure 2.15. As for Figure 2.14, but showing CO₂ concentrations in ppm. In this case for CO₂, MLO and SPO are not separated into two time series.

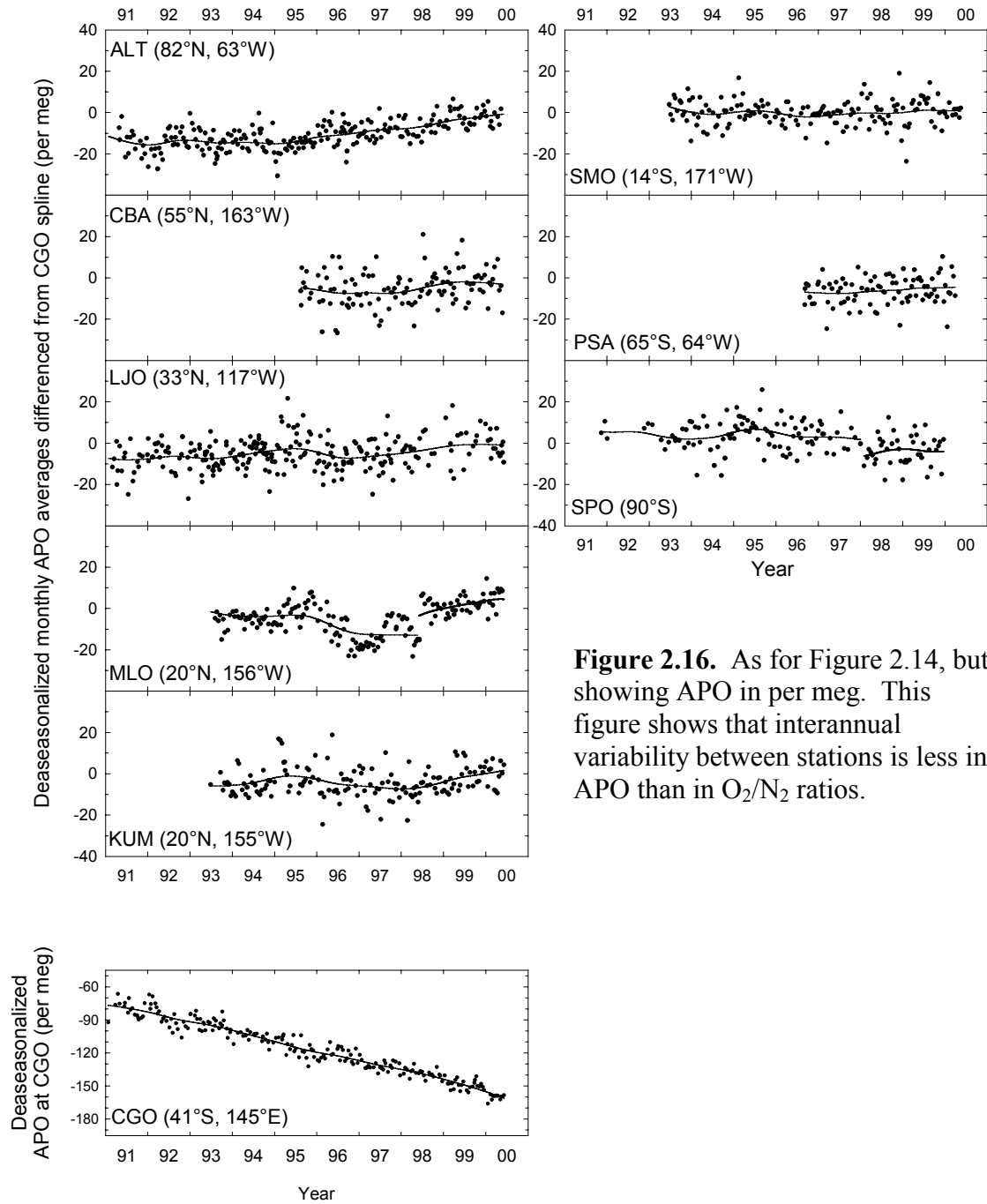


Figure 2.16. As for Figure 2.14, but showing APO in per meg. This figure shows that interannual variability between stations is less in APO than in O_2/N_2 ratios.

likely be attributed to end member effects of the spline curve fitting routine, and therefore these trends probably do not represent real atmospheric variability.

The global budgets for atmospheric CO₂ and O₂ can be respectively represented by

$$\Delta\text{CO}_2 = F - O - B, \text{ and} \quad (2.3)$$

$$\Delta\text{O}_2 = \alpha_F F - \alpha_B B, \quad (2.4)$$

where ΔCO_2 is the observed change in atmospheric CO₂ concentration, ΔO_2 is the observed change in atmospheric O₂ concentration, F is the source of CO₂ emitted from fossil fuel combustion (and cement manufacture), O is the oceanic CO₂ sink, B is the land biotic CO₂ sink, α_F is the average O₂:C molar exchange ratio for fossil fuels, and α_B is the average O₂:C molar exchange ratio of land biota. All quantities, except for the exchange ratios, α_F and α_B , are expressed in units of moles per year. As discussed in the Introduction, there is no oceanic term in the O₂ budget because O₂ is much less soluble in the oceans than CO₂.

In all calculations below, a value of -1.1 ± 0.05 is used for α_B [Severinghaus, 1995]. A value of -1.39 ± 0.04 is used for α_F which was calculated from a knowledge of the amount of the different fossil fuel types combusted from year to year [Marland *et al.*, 2000], from the average O₂:C oxidative ratios for full combustion of each fuel type [Keeling, 1988a]. This value for α_F was found to change only negligibly in any of the different time periods considered in the sections below.

2.5.1. Update of *Keeling et al.* [1996]

In this section I calculate global land biotic and oceanic carbon sinks in a similar manner to *Keeling et al.* [1996], using O₂/N₂ ratio and CO₂ concentration data from Alert, La Jolla, and Cape Grim. For each station I use the curve fits to the flask data shown in Figures 2.2 and 2.3 to adjust all flask data to the 15th of each month, then I calculate monthly means. Months with no flask data are filled in using the curve fits. I average twelve consecutive monthly means to compute an annual mean for O₂/N₂ ratio, repeating this calculation at six-month time steps centered on 1 January and 1 July of each year. I then average the annual means of Alert and La Jolla as a proxy for the northern hemisphere, $(\delta\text{O}_2/\text{N}_2)_{\text{NH}}$, and I use the annual means of Cape Grim as a proxy for the southern hemisphere, $(\delta\text{O}_2/\text{N}_2)_{\text{SH}}$. Finally I compute global annual means as $(\delta\text{O}_2/\text{N}_2)_{\text{Global}} = ((\delta\text{O}_2/\text{N}_2)_{\text{NH}} + (\delta\text{O}_2/\text{N}_2)_{\text{SH}})/2$. I calculate similar annual means for CO₂ concentration and the resultant data points are shown as solid circles in Figure 2.17. These data points show the expected trends of increasing CO₂ concentrations over time and decreasing O₂/N₂ ratios.

I calculate the amount of CO₂ produced from fossil fuel combustion and cement manufacture from data in *Marland et al.* [2000] through to the end of 1997, and from British Petroleum data for 1998 and 1999 (H. Kheshgi, personal communication). I calculate the amount of O₂ consumed from a knowledge of the relative fraction of the different fossil fuel types combusted each year and the O₂:C oxidative ratios given for each fuel type in *Keeling* [1988a], assuming full combustion of fossil fuel carbon to CO₂. For the eight year period from July 1991 to July 1999 these fossil fuel emissions resulted in an average of 6.35 ± 0.38 Gt C/y of CO₂ released to the atmosphere, and, if no

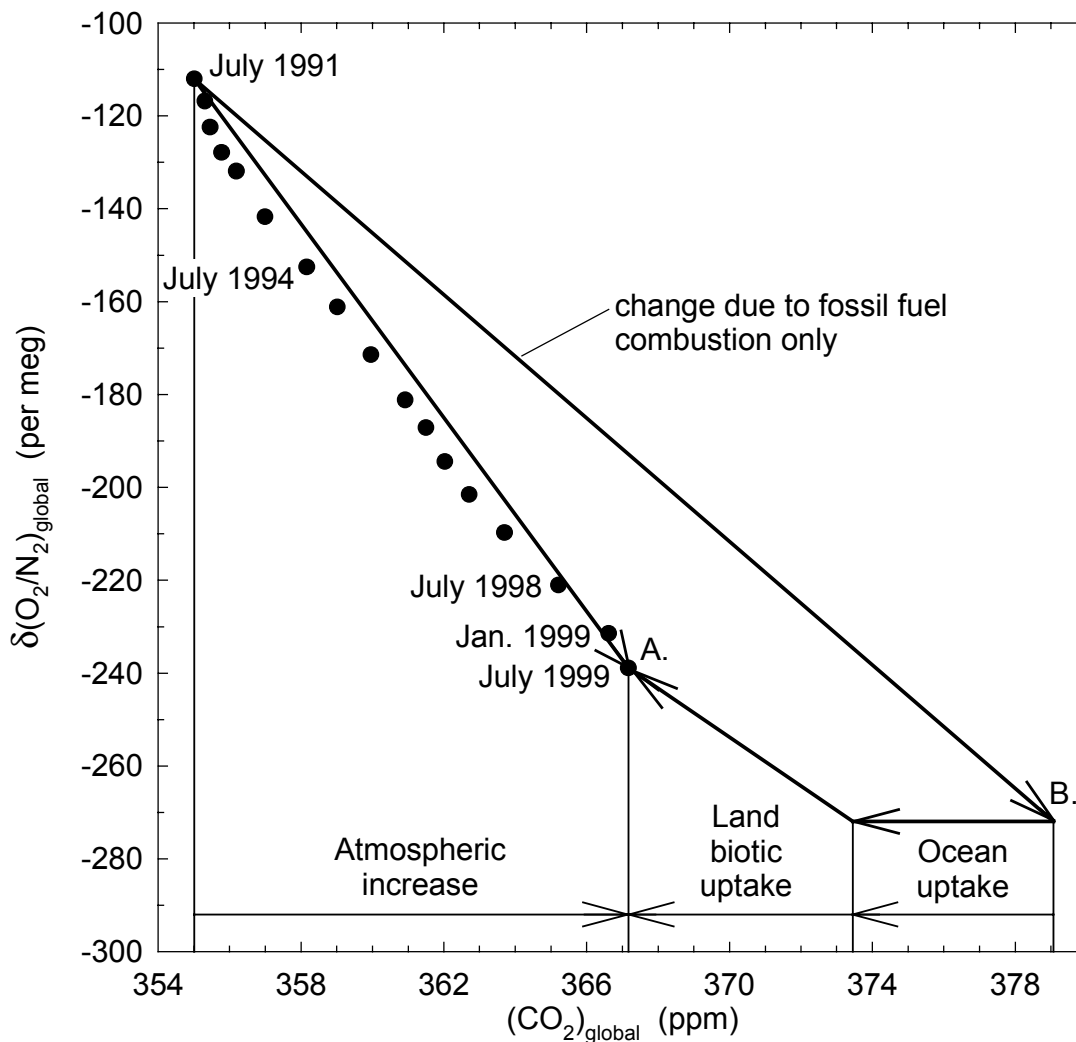


Figure 2.17. Vector diagram showing the calculation of the global land biotic and oceanic carbon sinks. Solid circles are annual averages of the observed O_2 and CO_2 concentrations, calculated from global averages of Alert, La Jolla, and Cape Grim. Also shown is a fossil fuel combustion line, representing the change in atmospheric O_2 and CO_2 concentrations that would have occurred if all CO_2 emitted remained in the atmosphere. The slope for the land biotic sink is fixed to an $O_2:C$ molar ratio of -1.1 , the best estimate of the ratio observed for land photosynthesis and respiration processes, whereas the oceanic sink assumes that there is no effect on O_2 , as described in the text.

other processes were involved, would have resulted in a total atmospheric CO_2 increase of 23.9 ± 1.4 ppm and an O_2/N_2 decrease of 158.9 ± 9.6 per meg. This hypothetical change is shown in Figure 2.17 as a straight line labeled “change due to fossil fuel

combustion only". The observed changes over this eight year period were an atmospheric CO₂ increase of 12.16±0.26 ppm (3.23±0.07 Gt C/y), and an O₂/N₂ decrease of 126.9±6.0 per meg. To determine the partitioning of the unaccounted for CO₂, I assume that there is no oceanic uptake or release of oxygen on interannual time scales and that the O₂:C land biotic exchange ratio is -1.1 [Severinghaus, 1995]. Then using equations 2.3 and 2.4 above I calculate global carbon sinks, resulting in, from July 1991 to July 1999:

Land biotic carbon sink = 1.62±0.58 Gt C/y, and

Oceanic carbon sink = 1.51±0.41 Gt C/y.

This solution is also shown graphically in Figure 2.17. Point 'A' on the figure shows the observed global atmospheric O₂/N₂ ratio and CO₂ concentration in July 1999, and point 'B' shows the atmospheric concentrations expected if all fossil fuel-emitted CO₂ remained in the atmosphere. A unique solution can then be found for the land biotic and oceanic uptakes by drawing a line with slope -1.1 mol O₂ per mol CO₂ representing the land biotic uptake, and a horizontal line representing the oceanic uptake. As shown on the figure, these uptakes are in units of ppm CO₂, but they have been converted to Gt C/y above.

2.5.2. Calculation for the Decade of the 1990s for the IPCC Third Assessment Report⁶

The calculations above were computed over the longest time period for which atmospheric O₂ measurements exist from at least one station in each hemisphere. The IPCC (Intergovernmental Panel for Climate Change), in their Third Assessment Report,

wish to report global land biotic and oceanic carbon sinks for the entire decade of the 1990s so as to compare these results with similar calculations computed for the 1980s decade. Because our Cape Grim station did not start collecting flask samples until January 1991 (Table 2.1), a different computational methodology is needed to estimate a 1990s average.

Eleven years of atmospheric O₂/N₂ and CO₂ data are needed in order to calculate land biotic and oceanic carbon sinks for the ten year period from 1 January 1990 to 1 January 2000 using the above technique. The technique subtracts an annual average centered on 1 January 2000 from an annual average centered on 1 January 1990, and therefore requires measurements spanning the period from 1 July 1989 to 1 July 2000. La Jolla is the only station for which such a dataset exists. The Alert record comes close, with samples collected on two dates in 1989, in November and December, and with recent samples processed through to May 2000. Therefore my strategy will be to use both the La Jolla and Alert records, with a slightly different method of calculating the endpoints of the Alert record. After presenting the data and results in this section, the next section will assess the robustness of the Alert endpoint calculation, comment on the lack of having data from a southern hemisphere station, and describe other considerations that were necessary to arrive at these particular results.

Table 2.3 shows the CO₂ emissions from fossil fuel combustion and cement manufacture, taken from *Marland et al.* [2000] through to the end of 1997, and from

⁶ The data and results in this section will be referenced in the IPCC Third Assessment Report, 2000. Therefore in this section I have explained my calculations more thoroughly, and provided additional tables of data so that my calculations may be duplicated by other researchers.

Table 2.3. Global Fossil Fuel Combustion Data for the 1990s

Year	CO ₂ produced ¹ (10 ⁶ tonnes) ²	O ₂ consumed ³ (10 ⁶ tonnes)	O ₂ :C molar ratio
1990	6.104	22.581	1.389
1991	6,183	22,955	1.394
1992	6,095	22,546	1.388
1993	6,073	22,514	1.391
1994	6,221	23,029	1.389
1995	6,407	23,752	1.392
1996	6,517	24,181	1.393
1997	6,601	24,517	1.394
1998	6,566	24,339	
1999	6,521	24,172	
Total	63,288	234,587	1.391 ⁴
Total (10 ¹⁴ mol)	52.70	73.32	

¹ Data from 1990 to 1997 inclusive are from *Marland et al.* [2000], and include CO₂ produced from solid, liquid, and gas fuel, as well as from flared gas and cement manufacture. Data from 1998 and 1999 are from British Petroleum statistics (H. Kheshgi, personal communication).

² 10⁶ tonnes is equivalent to 0.001 Gt, or 0.001 Pg.

³ O₂ consumed is calculated assuming full combustion of all fossil fuel types, and using O₂:C molar ratios for each fuel type from *Keeling* [1988a]. That is, O₂:C is 1.17 for solid fuel; 1.44 for liquid fuel; 1.95 for gas fuel; and 1.98 for flared gas. (Cement manufacture does not consume O₂.) Because British Petroleum data are split into different fuel type categories, the O₂ consumed in 1998 and 1999 was calculated by using the average O₂:C ratio from 1990 to 1997. As can be seen in the table, this ratio varies little, hence this is a reasonable approximation.

⁴ Average O₂:C molar ratio from 1990 to 1997.

British Petroleum data for 1998 and 1999 (H. Kheshgi, personal communication). The amount of atmospheric O₂ consumed is calculated from a knowledge of the relative fraction of the different fossil fuel types combusted each year (not shown in the table), and the O₂:C ratio for complete combustion of each fuel type. In Table 2.4, I show annual means of O₂/N₂ and APO for Alert and La Jolla, calculated every six months, and the annual averages of the two stations. For reasons detailed in section 2.5.3 below,

Table 2.4. Globally and Annually Averaged Trends in the 1990s¹

Year	Alert O ₂ /N ₂ (per meg)	La Jolla O ₂ /N ₂ (per meg)	Average O ₂ /N ₂ (per meg)	Alert APO ² (per meg)	La Jolla APO ² (per meg)	Average APO ² (per meg)
1990.0	-111.1	-95.7	-103.4	-75.6	-74.7	-75.1
1990.5	-117.7	-107.3	-112.5	-81.5	-79.9	-80.7
1991.0	-123.3	-113.8	-118.6	-87.2	-83.5	-85.4
1991.5	-131.4	-125.1	-128.2	-93.2	-89.3	-91.3
1992.0	-140.8	-127.9	-134.4	-100.2	-90.7	-95.4
1992.5	-141.6	-129.0	-135.3	-102.6	-94.1	-98.3
1993.0	-142.1	-134.7	-138.4	-103.3	-98.9	-101.1
1993.5	-149.3	-140.6	-144.9	-109.0	-101.6	-105.3
1994.0	-158.4	-150.4	-154.4	-113.6	-106.5	-110.1
1994.5	-168.3	-162.4	-165.3	-117.2	-110.1	-113.7
1995.0	-180.2	-169.3	-174.8	-125.3	-112.5	-118.9
1995.5	-191.5	-178.5	-185.0	-131.2	-115.7	-123.4
1996.0	-197.0	-192.3	-194.6	-130.9	-123.8	-127.4
1996.5	-204.7	-196.9	-200.8	-132.9	-129.8	-131.3
1997.0	-211.2	-201.8	-206.5	-136.7	-132.9	-134.8
1997.5	-216.1	-209.9	-213.0	-139.1	-136.1	-137.6
1998.0	-225.4	-217.8	-221.6	-143.4	-139.1	-141.2
1998.5	-236.2	-229.4	-232.8	-146.7	-143.0	-144.9
1999.0	-244.6	-239.9	-242.2	-147.1	-145.1	-146.1
1999.5	-250.8	-245.3	-248.0	-150.8	-147.2	-149.0
2000.0	-260.4	-255.7	-258.1	-157.0	-154.4	-155.7
Trend ³	-149.4	-160.0	-154.7	-81.43	-79.73	-80.58
Trend (10 ¹⁴ mol) ⁴	-55.36	-59.31	-57.34	-30.18	-29.55	-29.87

¹ All data are annual averages, calculated every six months, centered on 1 January and 1 July of each year, as described in the text (section 2.5.1). The average columns are the average of Alert and La Jolla.

² APO, Atmospheric Potential Oxygen, is defined in section 2.2.2, and is essentially the O₂/N₂ data added to 1.1 times the CO₂ data. APO is an approximately conservative tracer with respect to the land biota.

³ Global trends for the 1990s are calculated simply as the 1990.0 annual averages subtracted from the 2000.0 averages.

⁴ Uses total moles of dry air equal to 1.769×10^{20} , and an atmospheric O₂ mole fraction of 0.2095 [Machta and Hughes, 1970].

I chose to calculate the land biotic and oceanic carbon sinks with a slightly different method from that outlined in section 2.5.1 above.

Combining equations 2.2, 2.3 and 2.4 gives

$$\Delta\text{APO} = (\alpha_F - \alpha_B)F + \alpha_B O. \quad (2.5)$$

Using this equation, and from the APO and fossil fuel data in Tables 2.4 and 2.3 respectively, I can calculate the oceanic carbon sink. The value for ΔAPO is found simply by subtracting the 1990.0 mean from the 2000.0 mean (see Table 2.4, bottom row). The value for F is shown in the bottom row of Table 2.3. Once the oceanic sink has been determined, the land biotic sink is then calculated from equation 2.3 and atmospheric CO_2 data. In this calculation of the land biotic sink, I have not used the CO_2 data from our laboratory. Instead I have used NOAA/CMDL data [Conway *et al.*, 1994]. In this manner, I am able to use a more robust CO_2 global average since the NOAA dataset includes many more sampling stations, including southern hemisphere stations which extend back in time to at least 1990. Using a 2-D atmospheric transport model described in Tans *et al.* [Tans *et al.*, 1989], a global value for ΔCO_2 of 3.21 ± 0.13 Gt C/y is calculated for the 1990s (P. Tans, personal communication). This results in:

Land biotic carbon sink = 1.54 ± 0.65 Gt C/y, and

Oceanic carbon sink = 1.59 ± 0.52 Gt C/y.

It should be stated explicitly that this calculation technique effectively determines a global oceanic carbon sink from northern hemisphere data only, then using this result, the land biotic sink is calculated from globally averaged CO_2 data.

In these calculations I have assumed that there is no net air-sea gas exchange of O_2 on interannual time scales. In terms of exchange owing to the atmosphere-ocean equilibrium shift from decreasing atmospheric O_2 concentration driven by fossil fuel combustion, this assumption holds well, because O_2 is much less soluble in seawater than CO_2 , as explained in Chapter 1. However, there is another process that can cause

significant net air-sea gas exchange and that is net ocean warming (or cooling).

Recently, *Levitus et al.* [2000] showed that the global oceans have warmed significantly since 1948. For example, they calculated that the temperature of the 0 to 300 meter layer of the global ocean increased by 0.31°C over 40 years. Hence, as a direct result of this warming, net O₂ degassing from the oceans most probably occurred, offsetting the observed atmospheric decrease.

I will attempt to correct for this probable outgassing by assuming a 1 W/m² warming rate over the global oceans during the 1990s (M. Heimann, personal communication). This corresponds to a 0.71 W/m² warming over the entire surface of the Earth. Because of the uncertain nature of this calculation, I will assign a 100% uncertainty to this correction factor. 1 W/m² results in a total of 1.14 x 10²³ J of energy being absorbed by the oceans in the decade of the 1990s. Using an O₂ solubility temperature dependence of 5.818 x 10⁻⁶ mol/kg/K [*Weiss*, 1970], this results in a total of 1.59 x 10¹⁴ mol O₂ outgassed from the oceans in the 1990s. Net N₂ degassing from the oceans will also occur, offsetting the increase in the atmospheric O₂/N₂ ratio. I calculate that 2.58 x 10¹⁴ mol N₂ outgassed from the oceans in the 1990s, or 0.69 x 10¹⁴ mol O₂ equivalent. Therefore 0.90 x 10¹⁴ mol O₂ were effectively outgassed after applying this N₂ correction. Recalculating the land biotic and oceanic carbon sinks in the 1990s then results in:

Land biotic carbon sink = 1.44±0.66 Gt C/y, and

Oceanic carbon sink = 1.68±0.52 Gt C/y.

These data show that the land biotic and oceanic sinks are of approximately comparable magnitude and importance in the global carbon budget. These results also show an

approximate 0.1 Gt C/y shift in the land biotic and oceanic carbon sinks when allowance is made for an ocean warming effect with subsequent O₂ outgassing. It is probable that the ocean warming trend results in more O₂ outgassing than calculated here. I have applied a correction based solely on gas solubility dependences on temperature. In addition, it is likely that there is a biological response to ocean warming, probably resulting in more net O₂ outgassing. It is beyond the scope of this work to estimate such an effect, but it should be kept in mind that this will introduce additional uncertainty in the calculated global land biotic and oceanic carbon sinks.

2.5.3. Special Considerations in the IPCC Global Sinks Calculation

In this section I will give further details on special considerations that were necessary to arrive at the final global sink calculations in the previous section. I will also detail how I arrived at the uncertainty quoted for these sinks. In the La Jolla dataset I discarded some data resulting from flask samples collected in 1990. This is pertinent to any comparison made to *Keeling and Shertz* [1992], where our 1990 data were also used. In 1989 and 1990, some of the stopcocks on the glass flasks sealed with Teflon o-rings, rather than Viton o-rings. *Keeling and Shertz* [1992], observing very low O₂ concentrations in some flask samples, realized that they were contaminated, and attributed this problem to preferential diffusion of O₂ relative to N₂ through the Teflon o-rings. *Keeling and Shertz* [1992] discarded many, but not all, of the samples collected in these flasks. With the longer dataset now available, I was able to show that the Teflon flasks retained by *Keeling and Shertz* [1992] also exhibited a small negative O₂ anomaly from the apparent baseline. Therefore I discarded all remaining samples

collected in Teflon flasks. Although CO₂ concentrations were not affected by the Teflon flasks, I removed CO₂ data obtained from the same flasks also, so as not to cause inconsistent aliasing of the two datasets. This removed seven sampling dates in 1990 from the dataset, leaving a total of five dates when samples were collected from La Jolla in 1989 and three in 1990 (in 1991 our regular sampling program was initiated and, for example, in this year 18 samples were collected). The raw data retained are shown in Figure 2.18a. Here I have shown APO data only, and I have seasonally detrended the data, removing the four-harmonic component of the curve fit from all data points. Therefore this figure shows the actual flask data used to compute the annual means.

Because of the sparseness of the early part of the La Jolla record, I then proceeded to look in more detail at the Alert record. If the Alert record shows a similar long-term trend as La Jolla, then this will provide greater confidence in the La Jolla data. Flask samples were collected on two dates at Alert in 1989, none in 1990, and 15 in 1991 when a regular sampling program was begun. Figure 2.18b shows the Alert seasonally detrended APO.

In order to include the Alert data in the land and ocean sink calculations, annual averages centered on 1 January 1990, and 1 January 2000 are needed, therefore requiring data back to 1 July 1989, and up to 1 July 2000 in the normal calculation methods. Since in 1989 I only have data from samples collected in November and December, my procedure to calculate an “annual” average was as follows: The computer program used for calculating curve fits to the data also reports monthly values of the curve fit on the 15th of each month, and reports deseasonalized values for each month. Therefore I averaged four deseasonalized monthly values, from November and

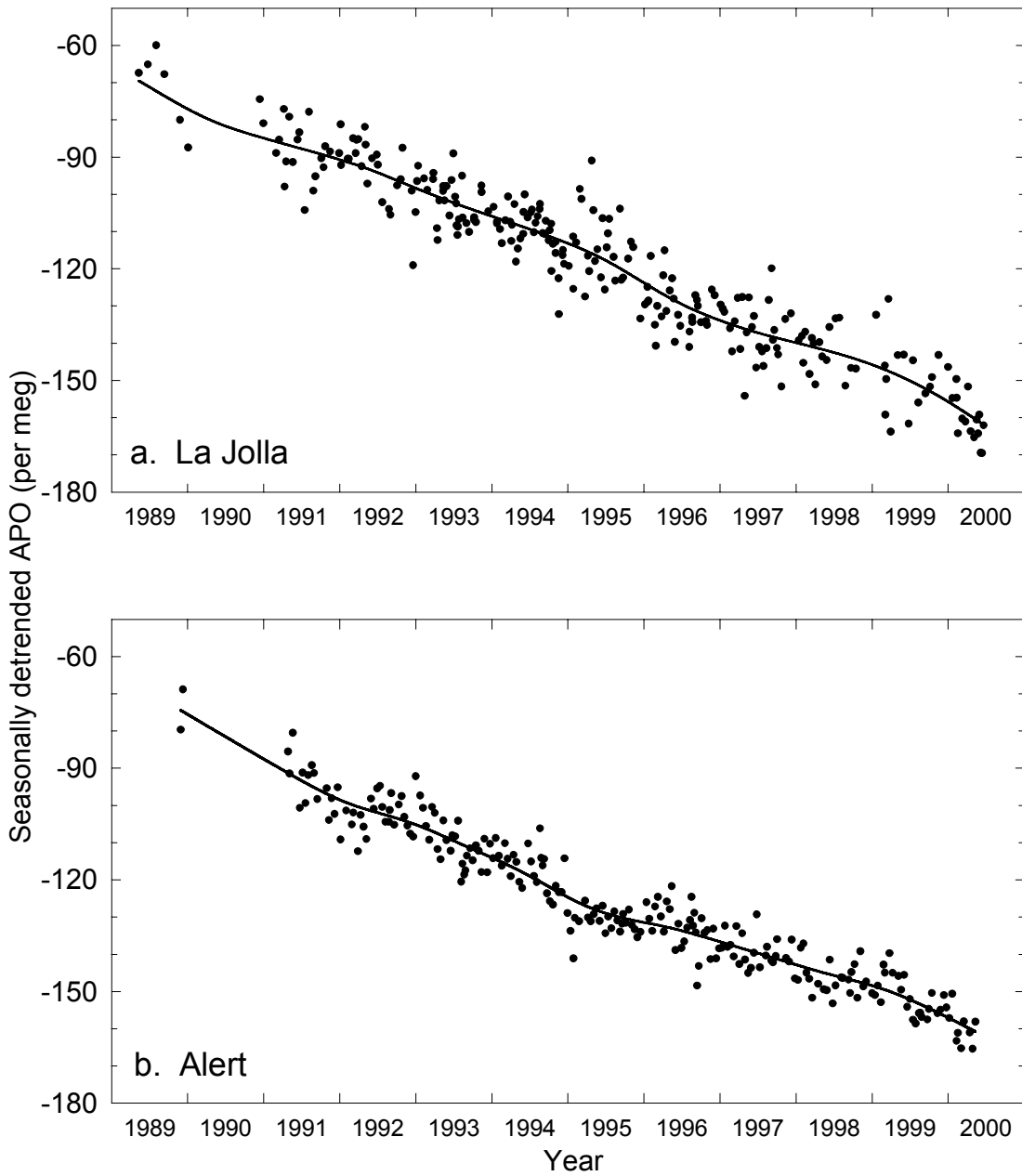


Figure 2.18. Deseasonalized APO data from La Jolla and Alert, used in the computation of global land biotic and oceanic carbon sinks in the 1990s for the IPCC.

December 1989, based on flask samples, and from January and February 1990, based on interpolated monthly values of the curve fit, resulting in an average centered on 1

January 1990. To obtain an average for 1 January 2000, because recent data is only processed up to May 2000, I averaged the deseasonalized monthly values for the ten month period from August 1999 to May 2000, giving an average centered on 1 January 2000.

The next decision made was to calculate the oceanic sink using APO data. There were several reasons for this decision. First, the uncertainty calculated from a quadrature sum of errors for the oceanic sink is minimized by using this calculation technique. Second, uncertainty is further reduced because short-term (daily to seasonal) atmospheric variability is less in APO than in either O_2/N_2 ratios or CO_2 concentrations. Third, this technique conforms with the recent *Battle et al.* [2000] paper, where similar global sink calculations were derived from atmospheric O_2 measurements (over a shorter six year time period. A full comparison and discussion of results from this paper is made in the following section). And fourth, I expect interannual variability in APO to be reduced compared to O_2/N_2 ratios because the APO signal is not affected by interannual variability in the land biotic sink, and indeed the APO data shown in Figure 2.16 appear to confirm this, exhibiting less variability than the O_2/N_2 ratio data in Figure 2.14.

This last fact becomes much more important because of two other considerations unique to this calculation. First, it improves the robustness of the interpolation of the Alert data, and using less than twelve months to determine “annual” averages. And second, the interhemispheric gradient in APO exhibits less temporal variability. The improved APO interpolation becomes apparent when I compare the Alert and La Jolla trends. I compared these trends in O_2/N_2 ratio over the nine year time period when we

have a full dataset from both stations and found that they differed by about 5 per meg over nine years. Whereas with the interpolated Alert dataset, and the sparse early record of La Jolla added, the difference in the trends doubled to 10 per meg over ten years. However, APO trend data over the same intervals (illustrated in Figure 2.18) show a 2 per meg difference in the Alert and La Jolla trends over nine years, and also a 2 per meg difference over the longer ten year period. These findings provide confidence both in the use of APO data, and in the Alert interpolation technique and subsequent averaging of Alert and La Jolla stations to obtain a northern hemisphere proxy.

The final consideration in this calculation is the lack of southern hemisphere O_2/N_2 data in computing “global” carbon sinks. Not only is there an interhemispheric gradient in O_2/N_2 ratios and APO [Stephens *et al.*, 1998], but as shown in section 2.6 of this chapter, these gradients show significant interannual variability. This makes it more problematic to use only northern hemisphere stations in reporting a global average. I attempted to quantify this additional error by comparing the Cape Grim trend to the Alert and La Jolla trends over the time period for which we have Cape Grim data, which is a 9.5 year measurement period from January 1991 to July 2000. Over this time period, the O_2/N_2 ratio at Cape Grim decreased by about 15 per meg more than at the two northern hemisphere stations. In APO the difference was less, but still high at about 10 per meg. Since in a true global calculation the southern hemisphere would contribute a weighting of one-half to the global trend, I decided to add ± 3 per meg uncertainty to the reported APO trend because of this lack of southern hemisphere data.

A summary of the uncertainties assigned to the different variables needed in the global sinks calculation is shown in Table 2.5. The uncertainty in the global O_2/N_2

trend used in section 2.5.1 was ± 6 per meg over a nine year measurement period. In this section I use ± 8.2 per meg uncertainty. This was derived from a quadrature sum of the ± 6 per meg uncertainty for a typical global O_2/N_2 (or APO) trend computation, ± 3 per meg attributed to the lack of southern hemisphere data, ± 3.4 per meg additional uncertainty attributed to sparse data in the early Alert record and the Alert interpolation, and ± 3.2 per meg attributed to the sparse La Jolla data in 1989 and 1990. These latter two uncertainties were calculated from considering the residuals of the flask data from the curve fits of the full Alert and La Jolla records. These residuals are shown in Figure 2.19. The standard deviation of these residuals was calculated for the full record, then the standard error was calculated by considering how many flask samples were used in deriving the 1990 annual averages. Figure 2.19 also verifies that the 1989 and 1990 data are not unusual in terms of their residuals from the fitted curves.

2.5.4. Comparisons With Other Results

Recently, *Battle et al.* [2000] reported land biotic and oceanic carbon sinks from an independent O_2/N_2 sampling network. They constructed global trends in a similar manner presented here, using our data from Alert in 1991 and 1992 and Point Barrow, Alaska ($71^\circ 19'N$, $156^\circ 36'W$) from 1993 onward as a northern hemisphere proxy, and using Cape Grim data from their own flask collection program as a southern hemisphere proxy. Their results are reported over a different time period, from July 1991 to July 1997, for which they calculated 1.4 ± 0.8 Gt C/y and 2.0 ± 0.6 Gt C/y for the land biotic and oceanic sinks respectively.

Table 2.5. Uncertainties in Global Land Biotic and Oceanic Sink Calculations

Quantity	Value	Uncertainty	Source
α_B	1.1	± 0.05	[Severinghaus, 1995]
α_F	1.391	± 0.04	[Keeling, 1988a]
Fossil fuel emissions	6.33 Gt C/y	± 0.38 Gt C/y	[Marland <i>et al.</i> , 2000]
CO ₂ trend	3.21 Gt C/y	± 0.13 Gt C/y	[Tans <i>et al.</i> , 1989; Conway <i>et al.</i> , 1994]
Oceanic O ₂ degassing	1.64×10^{13} mol/y	$\pm 1.64 \times 10^{13}$ mol/y	This study
APO trend:			
- from “typical” trend calculation		± 6 per meg	This study
- lack of southern hemisphere data		± 3 per meg	This study
- additional La Jolla		± 3.2 per meg	This study
- additional Alert		± 3.4 per meg	This study
- total	-80.4 per meg	± 8.2 per meg	This study

When I recalculate our data for the same time period (according to the methodology in section 2.5.1), I find 2.0 ± 0.6 Gt C/y and 1.4 ± 0.4 Gt C/y for the land biotic and oceanic sinks respectively. Although the estimates agree within the error margins, the size of this discrepancy is larger than expected from the uncertainty attributed to the atmospheric trends in O₂/N₂ ratios and CO₂ concentrations. A close examination of the two results shows differences in the reported atmospheric changes between the two labs. For the six year period, *Battle et al.* [2000] report a 0.9 ppm smaller CO₂ increase and a 7 per meg greater O₂/N₂ decrease.

In Figure 2.17 and in all carbon sink calculations derived here I computed the atmospheric trend by drawing a line through the first and last annual means for the time period of interest. I believe that this is a more accurate method of depicting the changes observed in the atmosphere between two end points, rather than a linear least squares fit to the O₂/N₂ and CO₂ data which was used by *Battle et al.* [2000].

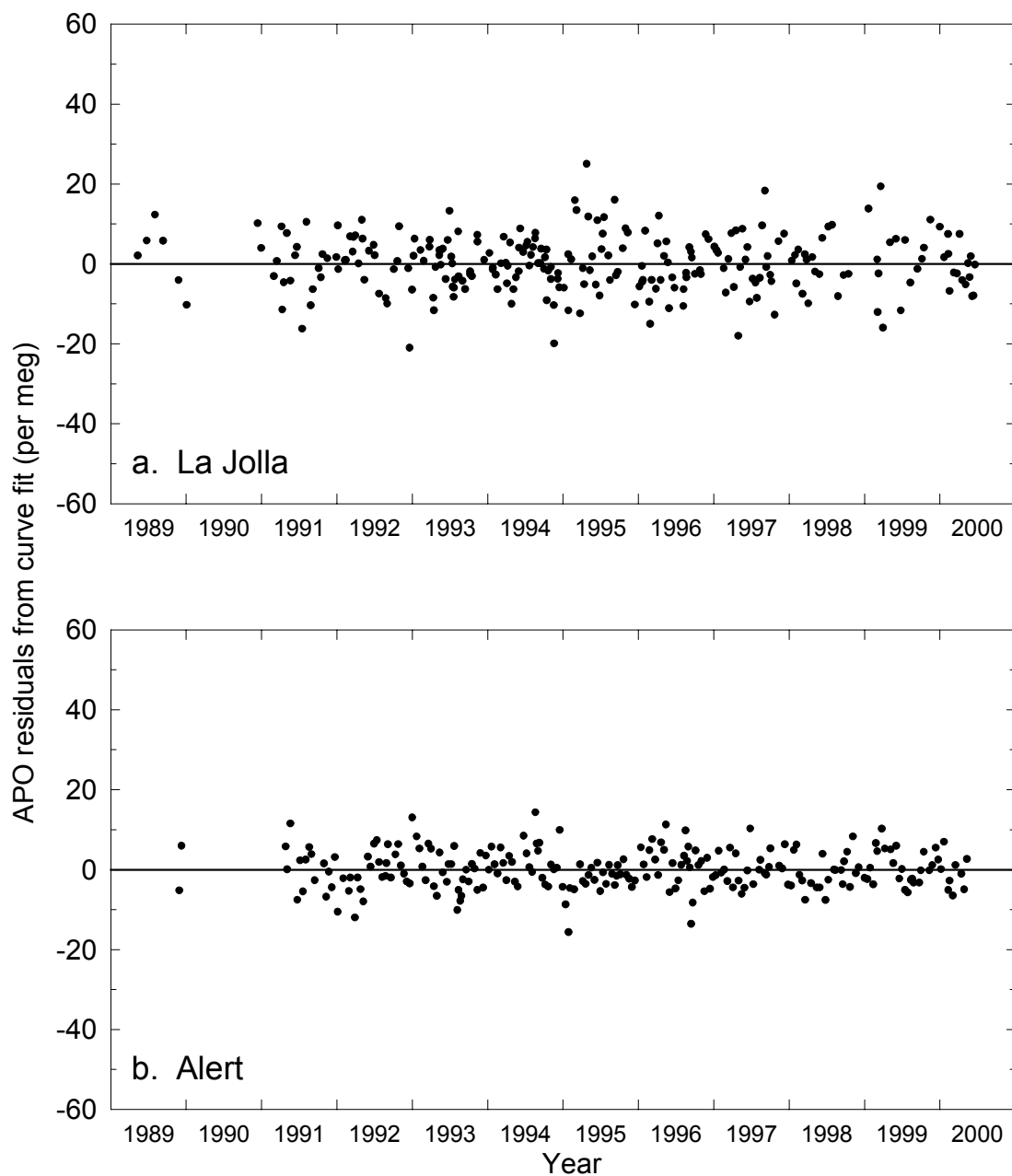


Figure 2.19. APO flask residuals from the curve fits of Figure 2.4 for La Jolla and Alert. These residuals give a measure of the uncertainty to assign in the calculation of global land biotic and oceanic carbon sinks. The figure also shows that early 1989 data are not more variable than more recent parts of the record.

2.6. Interannual Variability

2.6.1. Interannual Variability in Global Land and Ocean Carbon Sinks

An important point to be made in this study of land biotic and oceanic carbon sinks, is to realize that there is significant interannual variability, especially in the land biotic sink, and therefore deriving average sinks for time frames such as every decade does not give a complete picture. A more informative analysis is to show the variability from year to year, as shown in Figure 2.20. I computed this plot with similar calculations as Figure 2.17, using Alert, La Jolla, and Cape Grim data to calculate global means in O_2/N_2 ratios and CO_2 concentrations. The difference is that the land biotic and oceanic sinks are calculated over one-year intervals every six months rather than on the full record. The most striking feature of this graph is to observe that the land biotic sink varies more than twice as much as the oceanic sink on these interannual time scales. In the early 1990's the land biota was a relatively large carbon sink, drawing down 4-5 Gt C/y, whereas for periods in the mid- and late 1990's the land biota was approximately in balance, neither a net carbon sink nor source.

The oceanic sink by contrast varies only from 0 – 3 Gt C/y for the whole record in the 1990's, and does not appear to be influenced by either of the 1990's El Niño events from 1991-1994 or 1997-1998.

2.6.2. Interannual Variability in Seasonal Cycles

Temporal variability is also seen in the amplitude of the seasonal cycles. *Bender et al.* [1996] were the first to quantify and discuss possible reasons for the interannual

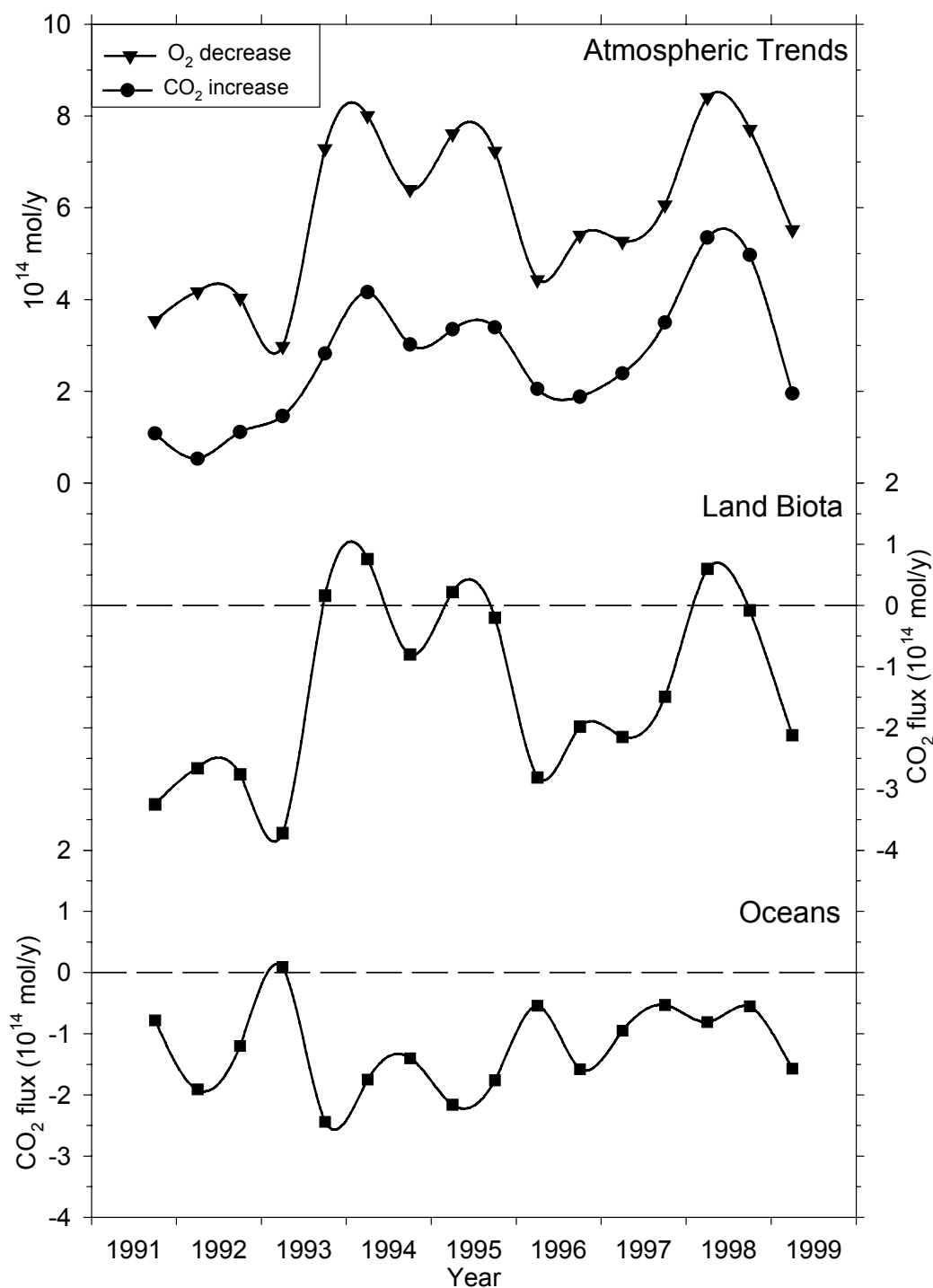


Figure 2.20. Land biotic and oceanic carbon sinks calculated on an annual basis with the same computational technique used in Figure 2.17. The triangles and circles on the top plot show the atmospheric O₂ and CO₂ trends respectively. This plot shows increases of CO₂ to the atmosphere, and decreases of O₂. Because O₂ changes can not be expressed in units of Gt C/y, all units in this figure are in 10¹⁴ moles. Throughout the 1990s atmospheric O₂ decreased at a faster rate than CO₂ increased. The land biotic sink exhibits much greater interannual variability than the oceanic sink.

variability in the atmospheric O₂/N₂ seasonal cycle. They presented O₂/N₂ ratio data from 1991 to mid-1994 from flask samples taken from Cape Grim, and from Baring Head, New Zealand (BHD). In one year intervals centered approximately on February, they found large interannual variations, with seasonal amplitudes of 86, 68, and 56 per meg in 1992, 1993, and 1994, respectively. Approximately 80% of the seasonal cycle in atmospheric O₂/N₂ ratios at Cape Grim and Baring Head is attributed to marine biotic processes, hence *Bender et al.* [1996] hypothesized that regulators on the bioavailability of the nutrients, NO₃⁻, PO₄³⁻, and Fe, could be affecting seasonal variability. They further hypothesized that the most likely nutrient-regulating candidate is surface winds, since winds drive the convection that brings nutrient-rich deep waters into the euphotic zone, and they transport Fe-bearing mineral aerosols from the continent to the open ocean. Thus, they believe that high variability in the seasonal cycle of atmospheric O₂/N₂ ratios is to be expected, as they observed.

Our extended Cape Grim O₂/N₂ dataset, however, shows a marked decrease in interannual variability in the seasonal amplitude of O₂/N₂ after 1994, shown in Figure 2.21, and suggests that the years 1992 through to 1994 were anomalous years. I have derived estimates of our seasonal amplitudes using an independent sampling program and a different computational technique from that used in *Bender et al.* [1996], thus I must first prove that a comparison of the two results is valid. The solid circles in Figure 2.21 show the seasonal amplitudes calculated in *Bender et al.* [1996], and the solid squares show the amplitudes from our own CGO dataset over the same interval, and calculated in exactly the same fashion. That is, a straight line was drawn by hand through the annual wintertime minimums in 1991, 1992, and 1993, then the amplitude

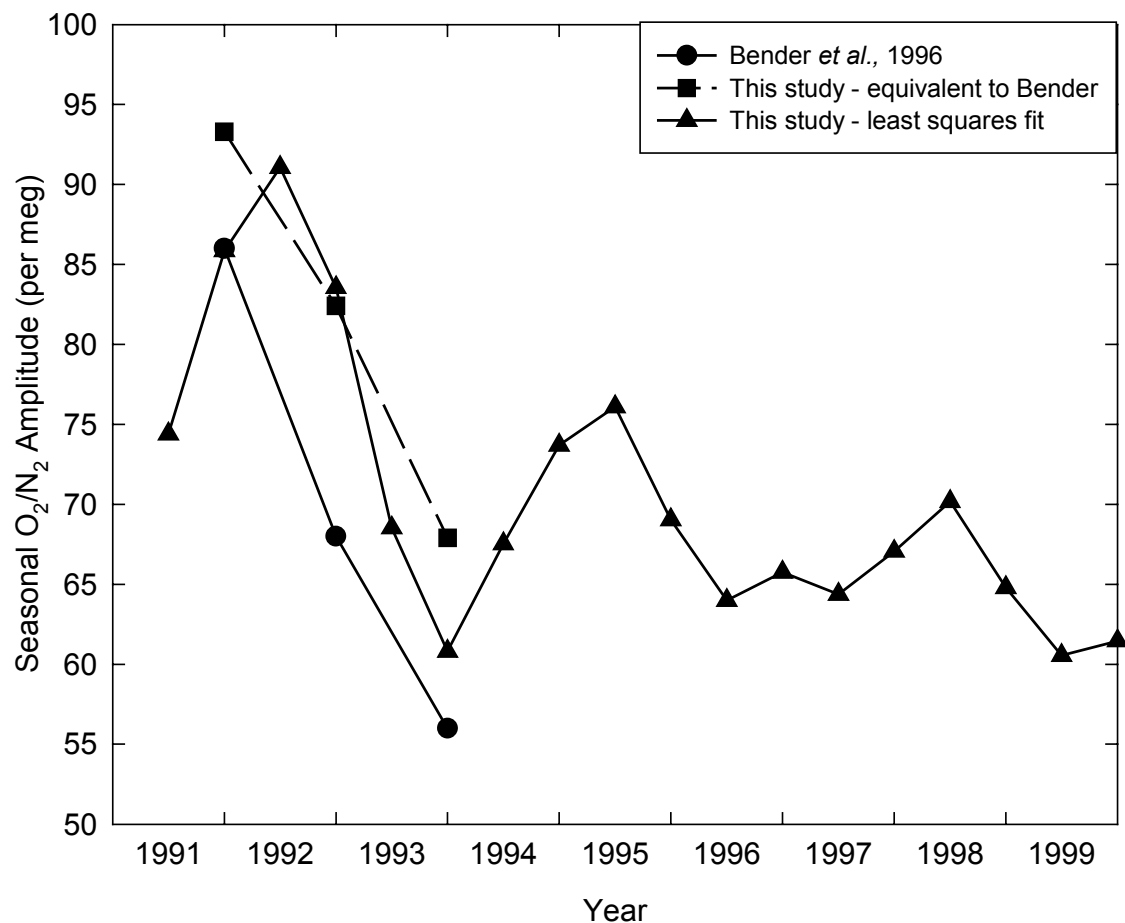


Figure 2.21. Shows the interannual variability in the amplitude of the seasonal cycle observed at Cape Grim. A comparison is made with earlier results from *Bender et al.* [1996]. Variability has decreased significantly since the early 1990s which the *Bender et al.* [1996] study examined.

in per meg up to the summertime maximum value was measured. Although there is an offset in the two results of about 10 per meg, both show similar features. My results are slightly less variable, as indicated by the standard error on the three measurements of 7.4 per meg, compared to 8.7 per meg from the *Bender et al.* [1996] dataset. The reason for the offset can be seen by studying Figure 2.22 which shows the raw atmospheric O₂/N₂ ratio data collected by both programs. Note that for comparison purposes, the

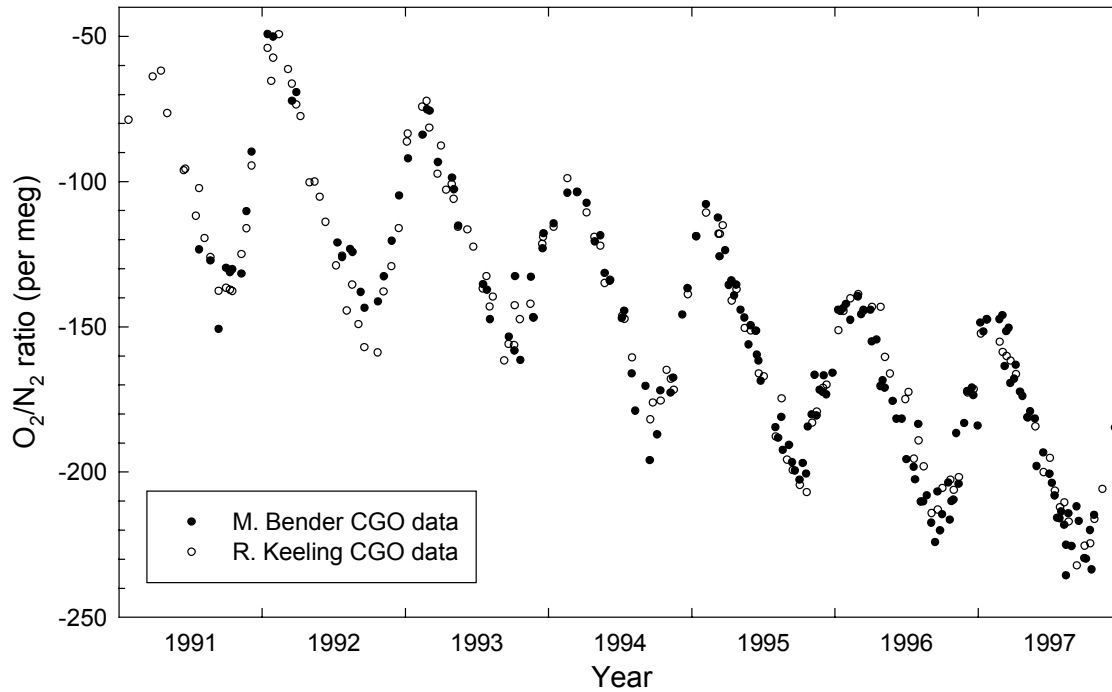


Figure 2.22. O_2/N_2 ratio data from flask samples collected at Cape Grim, Tasmania, Australia, by two independent programs run by M. Bender at Princeton University, and R. Keeling at Scripps Institution of Oceanography. All flask samples are collected by the same station personnel under identical criteria for appropriate sampling conditions.

Bender et al. [1996] data has been adjusted by -70 per meg because of different arbitrary reference gases used in the definition of the per meg scales (Equation 2.1). Agreement is good, especially at the summertime maximums. However, there is a notable exception in the wintertime minimum of 1992, where our values dip about 12 per meg lower. This resulted in a lower baseline through the wintertime minimums, and hence higher seasonal amplitude values as seen in Figure 2.21. I am unsure of the discrepancy between the two datasets, and it is particularly puzzling because the flask samples for both programs were collected on exactly the same days before and after this wintertime minimum. Ongoing intercalibration efforts between the two laboratories

seek to reduce the frequency of such discrepancies. I note that the BHD data shown in *Bender et al.* [1996] agree with our lower CGO results during this time period, but *Bender et al.* [1996] appear to have ignored this BHD data in calculating their wintertime baseline.

Having shown that despite an offset in the absolute magnitude of the seasonal amplitude the interannual variability is approximately the same, I now proceed to examine this variability over our longer dataset, and using what I believe is a less subjective computational technique. I have taken data over a one year period and scaled the four harmonic fit by a constant factor such that the sum of the squares of the residuals of the data from the scaled fit over the one year period is a minimum. I repeat this computation for one year periods at six month intervals centered on January 1 and July 1 of each year. This results in the solid triangles shown in Figure 2.21, demonstrating that after 1994, there was significantly less interannual variability in the seasonal amplitudes at Cape Grim. The standard error of this technique, which is a measure of the variability independent of the length of the record, for the period 1992-1994 was 5.7 per meg whereas from 1994-1999 it was 1.1 per meg.

2.7. References

- Bacastow, R.B., C.D. Keeling, T.J. Lueker, M. Wahlen, and W.G. Mook, The ^{13}C Suess effect in the world surface oceans and its implications for oceanic uptake of CO_2 : Analysis of observations at Bermuda, *Global Biogeochemical Cycles*, 10 (2), 335-346, 1996.
- Balkanski, Y., P. Monfray, M. Battle, and M. Heimann, Ocean primary production derived from satellite data: An evaluation with atmospheric oxygen measurements, *Global Biogeochemical Cycles*, 13 (2), 257-271, 1999.
- Battle, M., M. Bender, T. Sowers, P.P. Tans, J.H. Butler, J.W. Elkins, J.T. Ellis, T. Conway, N. Zhang, P. Lang, and A.D. Clarke, Atmospheric gas concentrations over the past century measured in air from firn at the South Pole, *Nature*, 383, 231-235, 1996.
- Battle, M., M.L. Bender, P.P. Tans, J.W.C. White, J.T. Ellis, T. Conway, and R.J. Francey, Global carbon sinks and their variability inferred from atmospheric O_2 and $\delta^{13}\text{C}$, *Science*, 287 (5462), 2467-2470, 2000.
- Bender, M., T. Ellis, P. Tans, R. Francey, and D. Lowe, Variability in the O_2/N_2 ratio of southern hemisphere air, 1991-1994: Implications for the carbon cycle, *Global Biogeochemical Cycles*, 10 (1), 9-21, 1996.
- Bender, M.L., M. Battle, and R.F. Keeling, The O_2 balance of the atmosphere: A tool for studying the fate of fossil-fuel CO_2 , *Annu. Rev. Energy Environ.*, 23, 207-223, 1998.
- Bender, M.L., and M.O. Battle, Carbon cycle studies based on the distribution of O_2 in air, *Tellus Series B-Chemical and Physical Meteorology*, 51 (2), 165-169, 1999.
- Bender, M.L., T. Sowers, J.M. Barnola, and J. Chappellaz, Changes in the O_2/N_2 ratio of the atmosphere during recent decades reflected in the composition of air in the firn at Vostok Station, Antarctica, *Geophysical Research Letters*, 21, 189-192, 1994a.
- Bender, M.L., P.P. Tans, J.T. Ellis, J. Orchardo, and K. Habfast, A high precision isotope ratio mass spectrometry method for measuring the O_2/N_2 ratio of air, *Geochimica et Cosmochimica Acta*, 58 (21), 4751-4758, 1994b.
- Benedict, F.G., *The Composition of the Atmosphere with Special Reference to its Oxygen Content*, Carnegie Institution of Washington, 1912.

- Bloom, A.J., R.M. Caldwell, J. Finazzo, R.L. Warner, and J. Weissbart, Oxygen and carbon dioxide fluxes from barley shoots depend on nitrate assimilation, *Plant Physiology*, 91 (1), 352-356, 1989.
- Bortniak, J.C., The wind climatology of American Samoa, pp. 67, NOAA Environ. Res. Lab., Boulder, Colorado, 1981.
- Carpenter, T.M., The constancy of the atmosphere with respect to carbon dioxide and oxygen content, *J. Amer. Chem. Soc.*, 59, 358-360, 1937.
- Ciais, P., P.P. Tans, J.W.C. White, M. Trolier, R.J. Francey, J.A. Berry, D.R. Randall, P.J. Sellers, J.G. Collatz, and D.S. Schimel, Partitioning of ocean and land uptake of CO₂ as inferred by $\delta^{13}\text{C}$ measurements from the NOAA Climate Monitoring and Diagnostics Laboratory Global Air Sampling Network, *Journal of Geophysical Research*, 100 (D3), 5051-5070, 1995.
- Conway, T.J., P.P. Tans, L.S. Waterman, K.W. Thoning, D.R. Kitzis, K.A. Masarie, and N. Zhang, Evidence for interannual variability of the carbon cycle from the NOAA/CMDL global air sampling network, *Journal of Geophysical Research*, 99 (D11), 22,831-22,855, 1994.
- Enting, I.G., C.M. Trudinger, and R.J. Francey, A synthesis inversion of the concentration and $\delta^{13}\text{C}$ of atmospheric CO₂, *Tellus Series B-Chemical and Physical Meteorology*, 47 (1-2), 35-52, 1995.
- GLOBALVIEW-CO₂: Cooperative Atmospheric Data Integration Project - Carbon Dioxide, CD-ROM, NOAA/CMDL, Boulder, Colorado. [Also available on Internet via anonymous FTP to ftp.cmdl.noaa.gov, Path: ccg/co2/GLOBALVIEW], 1999.
- Graedel, T.E., and P.J. Crutzen, *Atmospheric change: an Earth system perspective*, 446 pp., W. H. Freeman and Company, New York, 1993.
- Gruber, N., and C.D. Keeling, The isotopic air-sea disequilibrium and the oceanic uptake of anthropogenic CO₂, in *Proceedings of the 2nd International Symposium, CO₂ in the Oceans*, Center for Global Environmental Research, National Institute for Environmental Studies, Tsukuba, Japan, 1999.
- Halter, B.C., J.M. Harris, and T.J. Conway, Component signals in the record of atmospheric carbon dioxide concentration at American Samoa, *Journal of Geophysical Research*, 93 (D12), 15,914-15,918, 1988.
- Harris, J.M., and S.J. Oltmans, Variations in tropospheric ozone related to transport at American Samoa, *Journal of Geophysical Research-Atmospheres*, 102 (D7), 8781-8791, 1997.

- Hartley, D.E., and R.X. Black, Mechanistic analysis of interhemispheric transport, *Geophysical Research Letters*, 22 (21), 2945-2948, 1995.
- Heimann, M., C.D. Keeling, and C.J. Tucker, A three-dimensional model of atmospheric CO₂ transport based on observed winds: 3. Seasonal cycle and synoptic time scale variations, in *Geophysical Monograph 55, Aspects of climate variability in the Pacific and the Western Americas*, edited by D.H. Peterson, pp. 277-303, American Geophysical Union, Washington D. C., 1989.
- Heimann, M., and E. Maier-Reimer, On the relations between the oceanic uptake of CO₂ and its carbon isotopes, *Global Biogeochemical Cycles*, 10 (1), 89-110, 1996.
- Keeling, C.D., S.C. Piper, and M. Heimann, A three-dimensional model of atmospheric CO₂ transport based on observed winds: 4. Mean annual gradients and interannual variations, in *Geophysical Monograph 55, Aspects of climate variability in the Pacific and the Western Americas*, edited by D.H. Peterson, pp. 305-363, American Geophysical Union, Washington D. C., 1989.
- Keeling, R.F., Development of an interferometric oxygen analyzer for precise measurement of the atmospheric O₂ mole fraction, Ph.D. thesis, Harvard University, Cambridge, Massachusetts, U.S.A., 1988a.
- Keeling, R.F., Measuring correlations between atmospheric oxygen and carbon dioxide mole fractions: A preliminary study in urban air, *Journal of Atmospheric Chemistry*, 7, 153-176, 1988b.
- Keeling, R.F., A.C. Manning, E.M. McEvoy, and S.R. Shertz, Methods for measuring changes in atmospheric O₂ concentration and their applications in southern hemisphere air, *Journal of Geophysical Research*, 103 (D3), 3381-3397, 1998a.
- Keeling, R.F., R.P. Najjar, M.L. Bender, and P.P. Tans, What atmospheric oxygen measurements can tell us about the global carbon cycle, *Global Biogeochemical Cycles*, 7 (1), 37-67, 1993.
- Keeling, R.F., S.C. Piper, and M. Heimann, Global and hemispheric CO₂ sinks deduced from changes in atmospheric O₂ concentration, *Nature*, 381, 218-221, 1996.
- Keeling, R.F., and S.R. Shertz, Seasonal and interannual variations in atmospheric oxygen and implications for the global carbon cycle, *Nature*, 358, 723-727, 1992.
- Keeling, R.F., B.B. Stephens, R.G. Najjar, S.C. Doney, D. Archer, and M. Heimann, Seasonal variations in the atmospheric O₂/N₂ ratio in relation to the kinetics of air-sea gas exchange, *Global Biogeochemical Cycles*, 12 (1), 141-163, 1998b.

- Krogh, A., The composition of the atmosphere, *Det Kgl. Danske Videnskabernes Selskab.*, 1 (12), 1-19, 1919.
- Langenfelds, R.L., R.J. Francey, L.P. Steele, M. Battle, R.F. Keeling, and W.F. Budd, Partitioning of the global fossil CO₂ sink using a 19-year trend in atmospheric O₂, *Geophysical Research Letters*, 26 (13), 1897-1900, 1999.
- Levitus, S., J.I. Antonov, T.P. Boyer, and C. Stephens, Warming of the world ocean, *Science*, 287 (5461), 2225-2229, 2000.
- Liss, P.S., and L. Merlivat, Air-sea gas exchange rates: Introduction and synthesis, in *The Role of Air-Sea Exchange in Geochemical Cycling*, edited by P. Buat-Menard, pp. 113-127, D Reidel, Norwell, Mass, 1986.
- Lowe, D.C., P.R. Guenther, and C.D. Keeling, The concentration of atmospheric carbon dioxide at Baring Head, New Zealand, *Tellus*, 31, 58-67, 1979.
- Machta, L., Oxygen depletion, in *Proceedings of the International Meeting on Stable Isotopes in Tree Ring Research*, edited by G.C. Jacoby, pp. 125-127, 1980.
- Machta, L., and E. Hughes, Atmospheric oxygen in 1967 to 1970, *Science*, 168, 1582-1584, 1970.
- Mann, M.E., R.S. Bradley, and M.K. Hughes, Global-scale temperature patterns and climate forcing over the past six centuries, *Nature*, 392 (6678), 779-787, 1998.
- Manning, A.C., and R.F. Keeling, Correlations in short-term variations in atmospheric oxygen and carbon dioxide at Mauna Loa Observatory, in *Climate Monitoring and Diagnostics Laboratory, No. 22, Summary Report 1993*, edited by J.T. Peterson, and R.M. Rosson, pp. 121-123, U.S. Department of Commerce, NOAA Environmental Research Laboratories, Boulder, CO, 1994.
- Manning, A.C., R.F. Keeling, and J.P. Severinghaus, Precise atmospheric oxygen measurements with a paramagnetic oxygen analyzer, *Global Biogeochemical Cycles*, 13 (4), 1107-1115, 1999.
- Marland, G., T.A. Boden, R.J. Andres, A.L. Brenkert, and C.A. Johnston, Global, Regional, and National Fossil Fuel CO₂ Emissions, in *Trends: A Compendium of Data on Global Change*, Carbon Dioxide Information Analysis Center, Oak Ridge National Laboratory, U.S. Department of Energy, Oak Ridge, Tenn., U.S.A., 2000.
- Orr, J.C., *Ocean Carbon-Cycle Model Intercomparison Project (OCMIP)*, 27 pp., 1997.

- Paneth, F.A., The chemical composition of the atmosphere, *Quart. J. Roy. Meteorol. Soc.*, 63, 433-438, 1937.
- Peixoto, J.P., and A.H. Oort, *Physics of climate*, 520 pp., American Institute of Physics, New York, 1992.
- Prinn, R., D. Cunnold, P. Simmonds, F. Alyea, R. Boldi, A. Crawford, P. Fraser, D. Gutzler, D. Hartley, R. Rosen, and R. Rasmussen, Global average concentration and trend for hydroxyl radicals deduced from ALE/GAGE trichloroethane (methyl chloroform) data for 1978-1990, *Journal of Geophysical Research*, 97, 2445-2462, 1992.
- Quay, P.D., B. Tilbrook, and C.S. Wong, Oceanic uptake of fossil fuel CO₂: Carbon-13 evidence, *Science*, 256, 74-79, 1992.
- Reinsch, C.M., Smoothing by spline functions, *Num. Math.*, 10, 177-183, 1967.
- Severinghaus, J.P., Studies of the terrestrial O₂ and carbon cycles in sand dune gases and in Biosphere 2, Ph.D. thesis, Columbia University, New York, U.S.A., 1995.
- Stephens, B.B., Field-based atmospheric oxygen measurements and the ocean carbon cycle, Ph. D. thesis, University of California, San Diego, La Jolla, California, U.S.A., 1999.
- Stephens, B.B., R.F. Keeling, M. Heimann, K.D. Six, R. Murnane, and K. Caldeira, Testing global ocean carbon cycle models using measurements of atmospheric O₂ and CO₂ concentration, *Global Biogeochemical Cycles*, 12 (2), 213-230, 1998.
- Takahashi, T., R.H. Wanninkhof, R.A. Feely, R.F. Weiss, D.W. Chipman, N. Bates, J. Olafsson, C. Sabine, and S.C. Sutherland, Net sea-air CO₂ flux over the global oceans: an improved estimate based on the sea-air CO₂ difference, in *Proceedings of the 2nd International Symposium, CO₂ in the Oceans*, pp. 9-14, Center for Global Environmental Research, National Institute for Environmental Studies, Tsukuba, Japan, 1999.
- Tans, P.P., P.S. Bakwin, and D.W. Guenther, A feasible global carbon cycle observing system: A plan to decipher today's carbon cycle based on observations, *Global Change Biology*, 2, 309-318, 1996.
- Tans, P.P., J.A. Berry, and R.F. Keeling, Oceanic ¹³C/¹²C observations: a new window on ocean CO₂ uptake, *Global Biogeochemical Cycles*, 7 (2), 353-368, 1993.
- Tans, P.P., T.J. Conway, and T. Nakazawa, Latitudinal distribution of the sources and sinks of atmospheric carbon dioxide derived from surface observations and an

atmospheric transport model, *Journal of Geophysical Research*, 94 (D4), 5151-5172, 1989.

Tans, P.P., I.Y. Fung, and T. Takahashi, Observational constraints on the global atmospheric CO₂ budget, *Science*, 247, 1431-1438, 1990.

Tohjima, Y., Method for measuring changes in the atmospheric O₂/N₂ ratio by a gas chromatograph equipped with a thermal conductivity detector, *Journal of Geophysical Research-Atmospheres*, 105 (D11), 14575-14584, 2000.

Weiss, R.F., The solubility of nitrogen, oxygen and argon in water and seawater, *Deep-Sea Research*, 17, 721-735, 1970.

Chapter 3.

Precise atmospheric oxygen measurements with a paramagnetic oxygen analyzer

Abstract.

A methodology has been developed for making continuous, high-precision measurements of atmospheric oxygen concentrations by modifying a commercially available paramagnetic oxygen analyzer. Incorporating several design improvements, an effective precision of 0.2 ppm O₂ from repeated measurements over a 1-hour interval was achieved. This is sufficient to detect background changes in atmospheric O₂ to a level that constrains various aspects of the global carbon cycle. The analyzer was used to measure atmospheric O₂ in a semicontinuous fashion from air sampled from the end of Scripps Pier, La Jolla, California, and data from a 1-week period in August 1996 are shown. The data exhibit strongly anticorrelated changes in O₂ and CO₂ caused by local or regional combustion of fossil fuels. During periods of steady background CO₂ concentrations, however, we see additional variability in O₂ concentrations, clearly not due to local combustion and presumably due to oceanic sources or sinks of O₂. This variability suggests that in contrast to CO₂, higher O₂ sampling rates, such as those provided by continuous measurement programs, may be necessary to define an atmospheric O₂ background and thus aid in validating and interpreting other O₂ data from flask sampling programs. Our results have also demonstrated that this paramagnetic analyzer and gas handling design is well suited for making continuous measurements of atmospheric O₂ and is suitable for placement at remote background air monitoring sites.

3.1. Introduction

Despite several decades of study and many recent advances in our understanding of the physical and geochemical processes involved, significant uncertainties still exist in the magnitude of terrestrial and oceanic sources and sinks in the global carbon cycle and in the processes affecting it [*Schimel et al.*, 1995]. For example, the impact of marine biota is poorly constrained and interannual variations are not quantified nor are their reasons understood [*Bender et al.*, 1996]; the concentration of atmospheric CO₂ is rising at a slower rate than predicted by the rate of increasing fossil fuel usage [*Keeling et al.*, 1995]; anthropogenic land use changes are adding significant but uncertain amounts of CO₂ to the atmosphere [*Schimel et al.*, 1995]; and the oceans and undisturbed parts of the land biota are CO₂ sinks of uncertain magnitude. Vigorous debate continues as to the relative magnitude, spatial distribution, and physical processes involved in the partitioning of these CO₂ sources and sinks [e.g., *Ciais et al.*, 1995], and in global marine productivity estimates [e.g., *Bender et al.*, 1996].

One method for improving our understanding of the contemporary carbon cycle involves measuring changes in atmospheric O₂ concentrations [*Bender et al.*, 1996; *Keeling et al.*, 1993, 1996; *Keeling and Shertz*, 1992]. Photosynthesis and respiration processes produce coupled changes in O₂ and CO₂ concentrations from both the land and ocean biota. However, differences in the physical and chemical interactions of these gases with seawater cause the fluxes across the air-sea interface to be largely decoupled. Because of these differences, information about the fluxes can be gained from measurements of both atmospheric O₂ and CO₂ that is not achievable from CO₂ measurements alone. There are two key differences. First, atmospheric CO₂ uptake by

the oceans can occur with no corresponding O₂ flux, both because O₂ is relatively insoluble in seawater and because uptake of CO₂ by the oceans in response to increasing atmospheric CO₂ levels involves inorganic reactions that do not involve O₂. This implies that on interannual timescales, land biotic and oceanic sinks for the excess atmospheric CO₂ can be separated and quantified from measurements of O₂ [*Keeling and Shertz, 1992; Sarmiento et al., 1998*]. Second, pertinent to seasonal timescales, air-sea CO₂ exchange due to oceanic changes is heavily suppressed by the seawater chemistry that interconverts dissolved CO₂ with other dissolved carbonate forms.

An analytical measurement precision and accuracy of about 1 ppm O₂ is required [*Keeling et al., 1993*] to be able to put useful constraints on these carbon and oxygen fluxes and to address the issues mentioned above (note that by ppm O₂, we mean μmole O₂ per mole of dry air on a CO₂-free basis). To date, two independent measurement techniques have been developed which can measure atmospheric O₂ to this level of precision. *Keeling* [1988a] developed an interferometric method, where small variations in the refractive index of air are measured and related to changes in air composition. Correcting for a CO₂ interference effect and with some plausible assumptions on the other gases in whole air, changes in the refractive index can be related to atmospheric O₂ concentration and expressed in terms of changes in the O₂/N₂ ratio [*Keeling et al., 1998*]. *Bender et al.* [1994] developed a second method, modifying a Finigan MAT 251 isotope ratio mass spectrometer to simultaneously measure atomic masses 29 (¹⁵N¹⁴N) and 32 (¹⁶O₂), also effectively measuring atmospheric O₂/N₂ ratios. Both of these techniques require relatively expensive, dedicated instruments and, with their current design, require flask samples to be collected in order to make remote

background atmospheric O₂ measurements.

Atmospheric O₂ has also been previously measured using paramagnetic oxygen analyzers [*Machta and Hughes, 1970; Taylor, 1968*]. However the best precision achieved (based on multiple aliquots from a flask sample) was of the order of 10 ppm, and due to the reproducibility obtained from reference gas calibrations, these workers were unable to report data with an accuracy better than 60 ppm. In this paper we describe a methodology which incorporates high precision gas handling techniques, allowing us to make substantial improvements to the analytical precision of a paramagnetic analyzer and achieving better than the required level of precision of 1 ppm O₂. This new method complements the two existing methods and provides certain advantages such as lower cost and allows for continuous remote background atmospheric O₂ measurements.

The remainder of this paper is divided into two main sections. The first discusses the operating principle of the paramagnetic analyzer, the design improvements we have made to it, and results from experimental testing of the method. The second presents preliminary results and interpretations from ambient air sampled in a semicontinuous fashion from the end of Scripps Pier, La Jolla, California.

3.2. Paramagnetic Analyzer System Design and Testing

3.2.1. Paramagnetic Analyzer and Gas Handling Descriptions

The commercially available “Paramagnetic Oxygen Sensor, Paramax 101” from Columbus Instruments International Corporation measures oxygen concentrations by utilizing the paramagnetic properties of molecular oxygen, first discovered by M.

Faraday in 1851 [*Kocache*, 1986]. The heart of the oxygen sensor is in fact a “PM1155B” oxygen transducer cell manufactured by Servomex Limited and described in detail by *Kocache* [1986]. This cell contains a small glass dumbbell suspended in a strong, nonuniform magnetic field. Paramagnetic molecules tend to align their magnetic moments with the field and to be attracted to areas of higher field strength. This attraction creates an air pressure gradient in the cell, which produces a torque on the dumbbell. The PM1155B employs a “self-nulling” mechanism whereby deflections of the dumbbell are detected and used to regulate an electric current flowing through a wire wrapped around the dumbbell, which produces an electromagnetic force resulting in a countervailing torque, thereby keeping the dumbbell in its original position. The output signal of the PM1155B is essentially equal to this regulating current, which is linear to the magnetic susceptibility of the air stream (the net effect from all paramagnetic and diamagnetic molecules). Table 3.1 shows that the O₂ molecule has by far the largest magnetic moment of common molecules in air, and variations in O₂ will dominate the variation in magnetic susceptibility of dry air. Taking into consideration typical ambient concentration changes, CO₂ is the next most important gas, contributing an interference effect typically $\leq 0.6\%$ (mol per mol) that of O₂. Hence to a good approximation, we can directly correlate the electric current to the paramagnetic susceptibility of O₂ alone and hence to the O₂ partial pressure of the incoming air stream.

The factory specifications for the Columbus Instruments paramagnetic analyzer quote a repeatability of ± 1000 ppm O₂ and a drift rate of 100 ppm O₂/h, whereas in our work we need a precision in O₂ mole fraction of 1 ppm or better. Paramagnetic susceptibilities are inversely proportional to absolute temperature [*Kocache*, 1986], and

Table 3.1. Molar Magnetic Susceptibilities of the Primary Constituents in Air

Species	Mole Fraction in Dry Air/ppm ^a	Molar Magnetic Susceptibility/x10 ⁻⁶ cgs ^d
N ₂	780,840	-12.0
O ₂	209,460	3449.0 (at 293 K)
Ar	9,340	-19.6
CO ₂	354 ^b	-21.0
Ne	18.18	-6.74
He	5.24	-1.88
CH ₄	1.72 ^b	-12.2
Kr	1.14	-28.8
H ₂	0.5	-3.98
N ₂ O	0.310 ^b	-18.9 (at 285 K)
CO	0.02-0.25	-9.8
O ₃	0.0-0.1	6.7 (liquid)
NO	0.028 ^c	1461.0 (at 293 K)
NO ₂	0.035 ^c	150.0 (at 408 K)
H ₂ O	0-30,000	-12.97 (liquid, at 293 K)

^a Concentration data taken from *Keeling* [1988a], unless otherwise noted.

^b From *Graedel and Crutzen* [1993].

^c From *Logan et al.* [1981].

^d Data taken from *Lide* [1992]. Gives the molar magnetic susceptibilities of the listed element or compound expressed in cgs units. A positive value indicates a paramagnetic element or compound whereas a negative value indicates a diamagnetic element or compound. Measurements at 1 atm, 298 K, unless otherwise noted.

clearly, O₂ partial pressure is directly proportional to the total pressure in the cell; so to improve the precision of the analyzer, the temperature and pressure in the cell and the flowrate of the inlet air stream need to be controlled to a very high degree of constancy. In addition to these dynamic parameters, the analyzer has a very high sensitivity to vibration and a long memory effect from shock, hence it must be carefully protected against these to reduce instrumental noise.

We interfaced the Columbus Instruments paramagnetic analyzer to the gas-handling system shown in Figure 3.1. The cell pressure was kept constant by using

active differential pressure control. We maintained the cell at about 200 torr above ambient because it is easier to establish and maintain control at a pressure somewhat above ambient pressure. As shown in Figure 3.1, the required pressure elevation was achieved by passing sample gas through a diaphragm compressor pump (Neuberger, model N05). Any incoming air stream had been predried, but to ensure that all samples enter the analyzer with a common dewpoint, we passed the air stream through a cryogenic, stainless steel cold trap at -80°C . The air stream then passed through a preliminary, or “coarse,” active pressure control which acts as protection against pressure “pulsing” effects from the compressor. For independent reasons, we maintained this coarse pressure regime at about 1800 ± 10 torr, achieved using a 10,000 torr differential pressure gauge (Sensotec) and a solenoid valve (V1 in Figure 3.1; MKS, 248 Control Valve) servoed to an electronic controller (MKS, Type 250C Controller).

After passing through a four-way valve (V2; discussed below), the sample gas passed through a manual needle valve (V3 in Figure 3.1). This valve served two purposes; first, it isolated the two pressure control regimes from each other, and second, it protected the paramagnetic analyzer against any transient flow pulses above the maximum allowable flowrate of 200 std mL/min, which could extensively damage the paramagnetic cell. Further protection was provided by the relief valve and V4 at the outlet of the analyzer.

Pressure control of the paramagnetic analyzer cell was established with a ± 1 torr (full scale) differential pressure gauge (MKS, Baratron 223BD) and a solenoid valve (V5 in Figure 3.1, MKS, 248 Control Valve) servoed to a second electronic controller (MKS, Type 250C Controller). The reference side of the differential pressure gauge

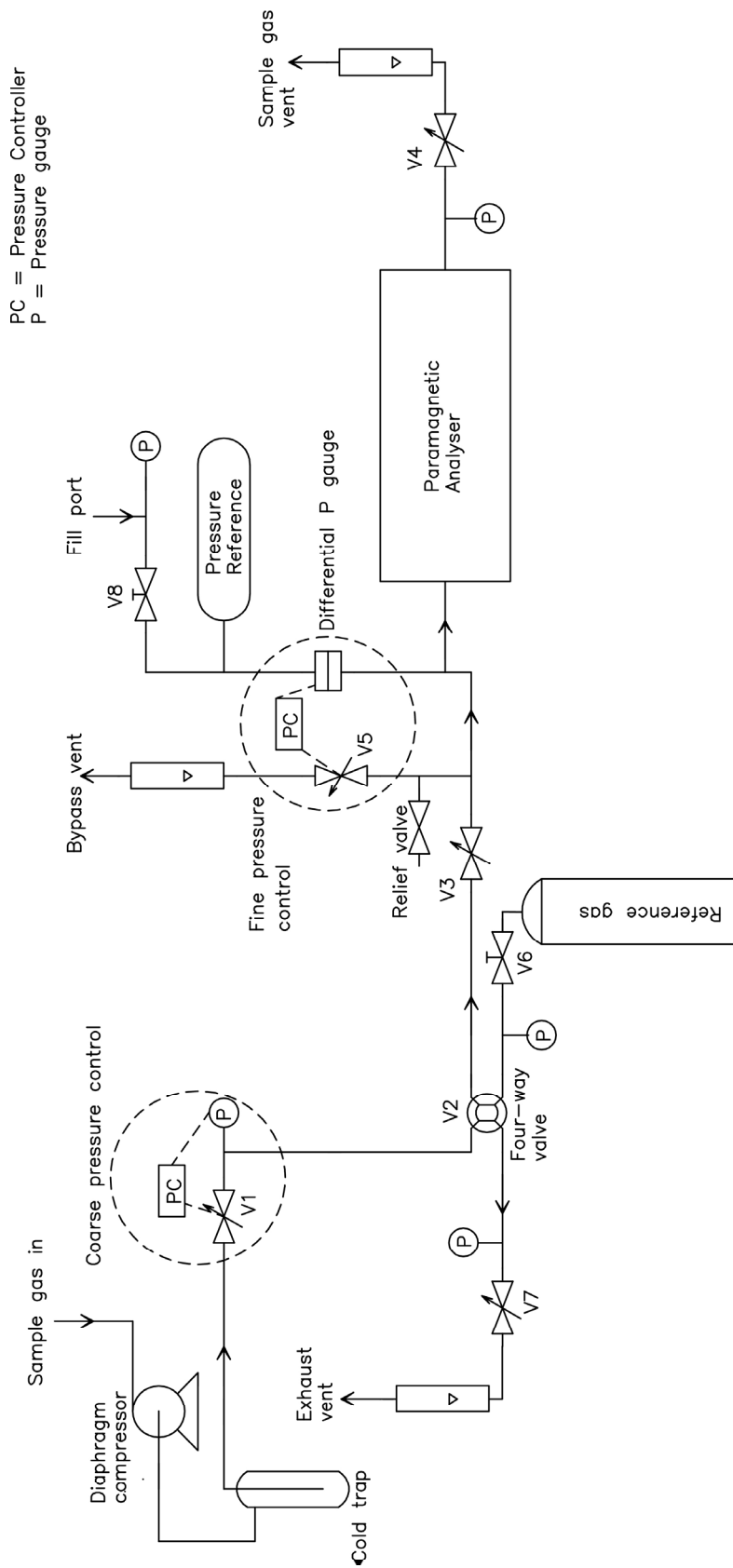


Figure 3.1. Schematic showing the gas-handling system used for making continuous atmospheric oxygen measurements with the Columbus Instruments paramagnetic oxygen analyzer. The “sample gas in” was either air from the Scripps Pier or a calibration gas. The “reference gas” was switched in and out with the sample gas every 2.5 min and was used to correct for the analyzer drift problem discussed in the text.

consisted of a “Pressure Reference” volume filled with air to about 960 torr (V8 normally closed). The MKS controller maintained a zero pressure differential (precise to 0.0005 torr) across the pressure gauge by adjusting the solenoid control valve, V5. The plumbing design maintained constant flow and pressure at the inlet to the analyzer by means of an adjustable bypass flow. Controlling in this way ensured that differences in the delivery pressures of reference gases or sample air would not affect the flowrate or pressure in the analyzer. V3 and V4 were set so that the flowrate through the analyzer was 120 mL/min and the bypass flowrate was 15 mL/min, as measured by downstream rotameter type flowmeters. An additional mechanical pressure gauge was located at the outlet of the analyzer as a diagnostic measure of cell pressure.

The paramagnetic analyzer, the ± 1 torr differential pressure gauge, and the “Pressure Reference” volume were all housed in a well-insulated enclosure, with the “Pressure Reference” volume further packed in polyurethane insulation. With this arrangement the analyzer response drifted on a quasi-diurnal cycle with an amplitude of about 400 ppm O₂, apparently linked to the diurnal temperature cycle in our laboratory of 1°C. To reduce the effect of this instrumental drift, the sample gas was replaced every 2.5 min with a reference gas, by means of a pneumatically operated four-way valve (V2). A solenoid valve, triggered by a computer to switch every 2.5 min controlled the pneumatic actuator. By computing concentration changes relative to this reference gas, we were able to null out the effect of analyzer drift on timescales longer than approximately 5 min. The gas stream not passing through the analyzer at any given time was vented through the second exit port of the four-way valve. This switching technique reduced transient pressure fluctuations induced by switching between two gas

streams and maintained constant conditioning of the walls of all inner tubing surfaces. A manual needle valve (V7) was adjusted to balance the venting flowrate to the flowrate through the analyzer. In addition, the delivery pressure of the reference tank was adjusted to match the 1800 torr delivered by the sample line. We found that a two-stage high pressure cylinder regulator (Scott Specialty Gases, Model 14 series) was sufficiently precise to achieve this.

In our laboratory, data were acquired from the paramagnetic analyzer with a computer-interfaced voltmeter (Keithley), which was programmed to read the analyzer output voltage 6 times in each 30-s interval. The average of the six readings was stored in an output file. Hence in a 2.5-min switch interval, which we call a “sample jog” or a “reference jog,” five data points were stored. When processing the data we threw out the first data point of each jog to avoid sweepout transients, which had a duration of about 20 s, and averaged the four remaining data points of each jog. We then linearly interpolated the two reference gas values on either side of a sample gas value and computed the difference between this interpolated value and the sample gas value.

3.2.2. Fine-Tuning Improvements

To improve the flushing characteristics of the differential pressure gauge, we placed a length of capillary tubing inside the 1/8th inch tubing, forcing any incoming air stream to travel to the pressure gauge diaphragm and eliminating most of the dead volume. The paramagnetic analyzer was so sensitive to pressure changes that very small leaks on the reference volume side of the ± 1 torr differential pressure gauge, of the order of 10^{-7} mbar L s⁻¹, were problematic. Welding all fittings on this reference

side eliminated these leaks. From extensive testing, we showed that the model N05 compressor did not detectably alter either the O₂ or CO₂ composition of an air stream which passed through it. However, as supplied by the factory, these pumps were found to leak at the Teflon flapper plate seals, so we modified the pump heads, sealing the leak using four Viton O-rings, two on either side of the flapper plate at the inlet and outlet bore holes of the pump head.

During the design-testing phase, we discovered a source of noise with a period of about 17 s and an amplitude of 3.2 ppm O₂, which was present when sample gas passed through the analyzer but not when reference gas passed through (during which time the baseline noise was about 0.8 ppm). We eliminated this source of noise simply by adding a short coil of 1/4 inch diameter polyethylene-aluminum composite tubing (Dekoron) between the N05 compressor and the cold trap which added approximately 10 mL of buffer volume. We speculate that the noise was caused by interactions between flow pulsations attributable to the compressor and thermal diffusive fractionation within the cold trap [Severinghaus *et al.*, 1996]. This resulted in concentration differences between adjacent “parcels” of air, and because the flow was laminar, these concentration differences were maintained and propagated through to the paramagnetic analyzer cell.

3.2.3. Experimental Testing

To test the precision, accuracy, and linearity of the paramagnetic analyzer system described above, we conducted two main experiments. The first experiment was primarily a linearity test. Calibration gas from a suite of ten gas cylinders spanning a

range of O₂ concentrations was passed through the sample side of the paramagnetic system for a period of 1 hour each. As with normal sampling protocol, the pneumatic four-way valve switched between a reference gas and each calibration gas at 2.5-min intervals. In this manner, twelve 2.5-min averaged values of O₂ concentration differences from the reference gas were obtained for each calibration cylinder. The interferometric oxygen analyzer also concurrently analyzed gas from each cylinder. In an extensive array of tests, described by *Keeling* [1988b] and *Keeling et al.* [1998], the interferometric analyzer has been proven to be both highly linear and accurate at reporting atmospheric O₂ concentrations. Additionally, the CO₂ concentration for each gas was determined from analysis on a Siemens Ultramat II CO₂ analyzer.

Variations in O₂ concentrations are typically reported as changes in the O₂/N₂ ratio according to methods described by *Keeling et al.* [1998]. Values are expressed in per meg units, where

$$\delta(\text{O}_2/\text{N}_2) \text{ (per meg)} = \frac{(\text{O}_2/\text{N}_2)_{\text{sam}} - (\text{O}_2/\text{N}_2)_{\text{ref}}}{(\text{O}_2/\text{N}_2)_{\text{ref}}} \times 10^6,$$

where $(\text{O}_2/\text{N}_2)_{\text{sam}}$ is the ratio of the sample gas and $(\text{O}_2/\text{N}_2)_{\text{ref}}$ is the ratio of an arbitrary reference gas cylinder. In these units, 4.8 per meg are essentially equivalent to 1 ppm (i.e., 1 μmole O₂ per mole of dry air). To express the paramagnetic analyzer output in per meg units, we use the formula:

$$\delta(\text{O}_2/\text{N}_2) \text{ (per meg)} = aV + \frac{\Delta X_{\text{CO}_2}}{(1 - X_{\text{O}_2})},$$

where V is the voltage output from the paramagnetic analyzer, expressed as a difference between sample gas and a reference gas as described above, a is the span factor in units

of per meg/V, calculated from analyzing two cylinders with known O₂ concentrations (called “high span” and “low span”), ΔX_{CO_2} is the difference in CO₂ mole fraction of the sample from an arbitrary reference gas, in ppm, and X_{O_2} is the standard mole fraction of O₂ in dry air (here we use 0.20946 [Machta and Hughes, 1970]). The ΔX_{CO_2} term accounts for the dilution effect of CO₂ changes on the O₂ partial pressure in the analyzer cell, at constant total pressure. This formula assumes that dilution caused by variations in trace gas species other than CO₂ is negligible.

Results from this linearity test are shown in Figure 3.2 and Table 3.2 and show that the paramagnetic analyzer is highly linear ($r^2 = 0.999$) over at least the range of 0 to -400 per meg, covering the range of concentrations observed in atmospheric O₂ due to natural and most anthropogenic perturbations. Table 3.2 also provides secondary information on the precision of the paramagnetic analyzer system. The average difference between the two instruments for the eight gas cylinders was 1.1 per meg, with a standard deviation of 2.8 per meg. These values incorporate inherent measurement errors in both analytical instruments.

The second series of experiments we called the “null” experiments. In one such experiment, reference gas was passed through the system continuously with no switching of the four-way valve. Data were then processed as if the four-way valve had been switching between a sample and reference gas. A series of 214 “sample jogs” were distributed about a mean difference of -0.2 per meg with a standard deviation of ± 3.1 per meg. This result corresponds to the theoretical precision that can be achieved by the paramagnetic transducer itself and how well a 2.5-min switching rate can null out the

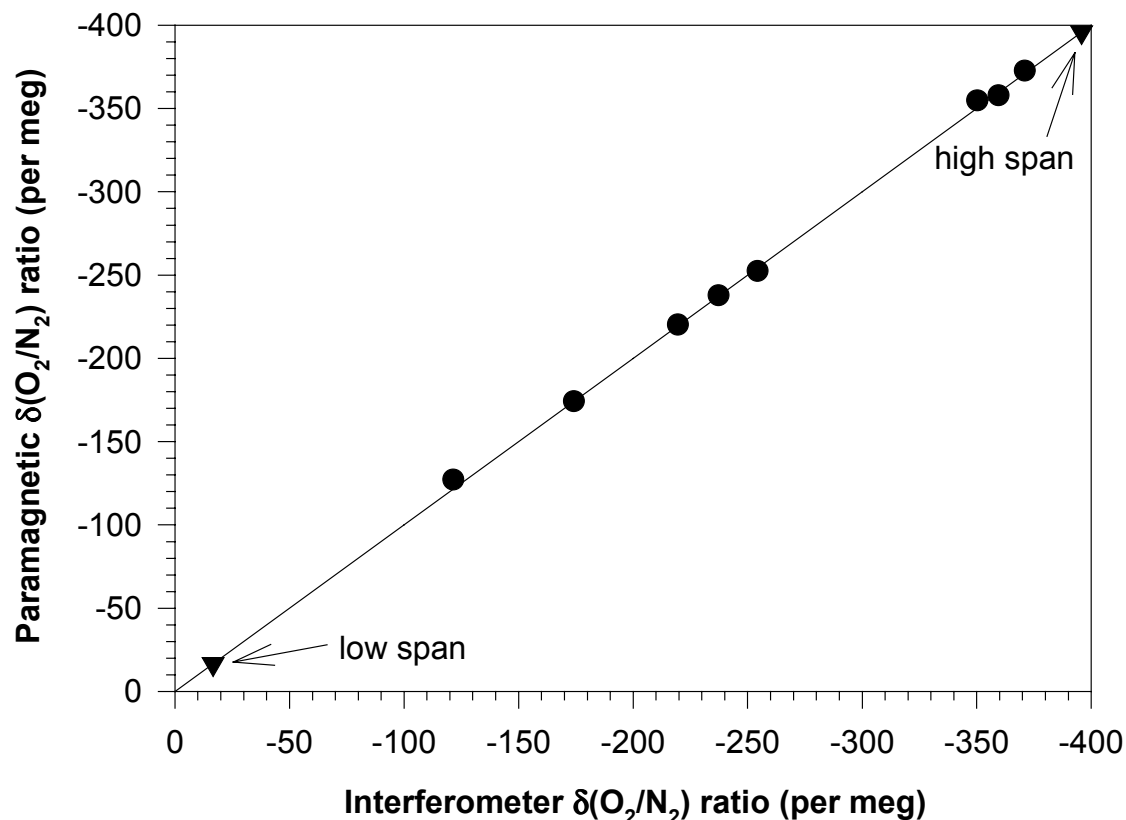


Figure 3.2. Results from a test on the linearity of the response of the paramagnetic analyzer for the range of O_2/N_2 ratios expected in ambient air. The solid line is $x = y$. Triangles indicate the paramagnetic “high span” and “low span” cylinders, which were used to define the span of the analyzer, hence they were forced to be equal to the interferometer-defined ratios. The ratios of the other eight cylinders were then determined from this span.

effect of sensor drift, assuming that no noise is introduced by the valve switching.

We also examined the possibility of a modified switching protocol that would double the lifetime of the reference gas. Analyzing the same data as above but assuming a switching protocol of 2.5 min of reference gas, followed by 7.5 min of sample gas, then 2.5 min of reference gas, etc., we obtained a mean difference of 0.1 per meg and a standard deviation of ± 3.5 per meg. To statistically compare these two

Table 3.2. Results From Linearity Test of the Paramagnetic Analyzer

Tank I.D.	Interferometer O ₂ /N ₂ Ratio, per meg	Paramagnetic O ₂ /N ₂ Ratio, per meg	Difference, per meg ^c
ND01540 (high span)	-16.6	-16.6 ^a	-
ND02729 (low span)	-395.8	-395.8 ^a	-
ND02702	-237.3 ^b	-237.8	0.5
ND02701	-174.2 ^b	-174.2	0.0
635872	-359.6	-357.8	-1.8
ND06875	-219.6	-220.1	0.5
CC106697	-254.4	-252.2	-2.2
ND02705	-371.1	-372.7	1.6
ND01598	-121.5	-127.2	5.7
465062	-350.3	-354.8	4.5

^a These two values were forced to be equal to the interferometer values, to define the span of the paramagnetic instrument. All other values were then calculated from this defined span.

^b These two tanks are used to define the span for the interferometer. As such, their measured interferometer O₂/N₂ ratios given here are not in fact values measured on the day of the test but rather are predetermined values that have been assigned to these two tanks based on the calibration protocol in the Scripps O₂ laboratory [Keeling *et al.*, 1998].

^c The mean difference of all cylinders is 1.1 ± 2.8 per meg.

results, we calculated the standard error based on a frequency of reporting data once per hour, resulting in ± 0.9 per meg for the 2.5-2.5 min switching scheme and ± 1.4 per meg for the 2.5-7.5 min switching scheme. This suggests that it is worthwhile investigating such reference gas saving methods further.

Another type of null experiment was designed to place a limit on the precision achievable with the entire gas handling system and not merely the analyzer transducer and the gas switching scheme. In normal operation, the pneumatic four-way valve shown in Figure 3.1 was used to switch between sample gas and a reference gas, whereas in this null experiment, gas derived from the same reference tank entered on both sides of the four-way valve. From previous work [Keeling *et al.*, 1998], we have

found dividing the flow from a high-pressure gas line into two pathways to be problematic, with measured O_2/N_2 differences between the two pathways resulting from fractionation. This problem was minimized by constructing a “T” made from a monolithic block of brass, connected directly to the reference cylinder with two high-pressure gas regulators connected to the block [Keeling *et al.*, 1998]. This reduced thermal gradients where the gas path divides in two, reducing O_2/N_2 fractionation.

Data for this “T” experiment were processed in the same manner as before, using a 2.5 min/2.5 min switching protocol and determining the difference in concentrations between two nominally identical gas streams. A series of 208 sample jogs were distributed about a mean difference of -4.7 per meg with a standard deviation of ± 3.1 per meg (and a standard error of ± 0.9 per meg if reporting data hourly). This standard error shows that effectively no additional imprecision was introduced by our gas handling system. The offset of -4.7 per meg shows that there was, however, a systematic offset introduced in dividing the flow. We did not identify the source of this offset, but it is clear that it involved the gas-handling system upstream of the analyzer and was not intrinsic to the paramagnetic analyzer itself.

3.3. Preliminary Results of Continuous Oxygen Measurements

One of the foreseeable applications of this paramagnetic oxygen analyzer is in measuring atmospheric O_2 in a continuous fashion at remote background air-monitoring sites. To test the feasibility of this application, we ran the analyzer semicontinuously for a period of 3 months in 1996. Ambient air was drawn from the end of Scripps Pier, La Jolla, California, located about 300 m from the shoreline and 15 m above sea level. Air

was drawn into our lab, a total distance of approximately 490 m from the end of the pier, through 1/2 inch outside diameter polyethylene-aluminum composite tubing (Dekoron). The air flowed first through the Siemens Ultramat II CO₂ analyzer, then divided into two streams, one of which went to the paramagnetic analyzer, the other to the interferometric analyzer. All three instruments were calibrated daily during a 4-hour calibration procedure in the early morning. A 10-min calibration was additionally carried out every hour on all three instruments, and for the paramagnetic analyzer, a reference gas was switched in every 2.5 min as described above. A computer controlled all necessary valve switching and data acquisition.

We present here a sample of the data, from August 10-16, 1996. Figure 3.3 shows O₂ data measured by the paramagnetic analyzer and converted to O₂/N₂ ratios and also concurrent CO₂ data from the same air stream. The O₂/N₂ data exhibit large daily variations, and the rapidity of these variations indicate that local sources and sinks are the predominant influences on the air. The daily pattern observed is most likely due to the prevailing on-shore, off-shore wind pattern present at La Jolla. In the night and early morning, off-shore winds bring air impacted by local fossil fuel combustion with low-O₂/N₂ ratios and high-CO₂ concentrations, whereas during the day cleaner on-shore winds are present, driving up O₂/N₂ ratios and driving down CO₂ concentrations. As expected, changes in these two gases anticorrelate, as is shown more clearly in Figure 3.4, and the data have an r^2 value of 0.88. The slope of the best-fit line through the data of Figure 3.4 is -6.22 ± 0.09 per meg/ppm, or 1.30 ± 0.02 moles of O₂ consumed per mole of CO₂ produced. The high variability of the data in Figure 3.3 indicates that all of the air sampled in this week (with the possible exception of the end of August 12) was

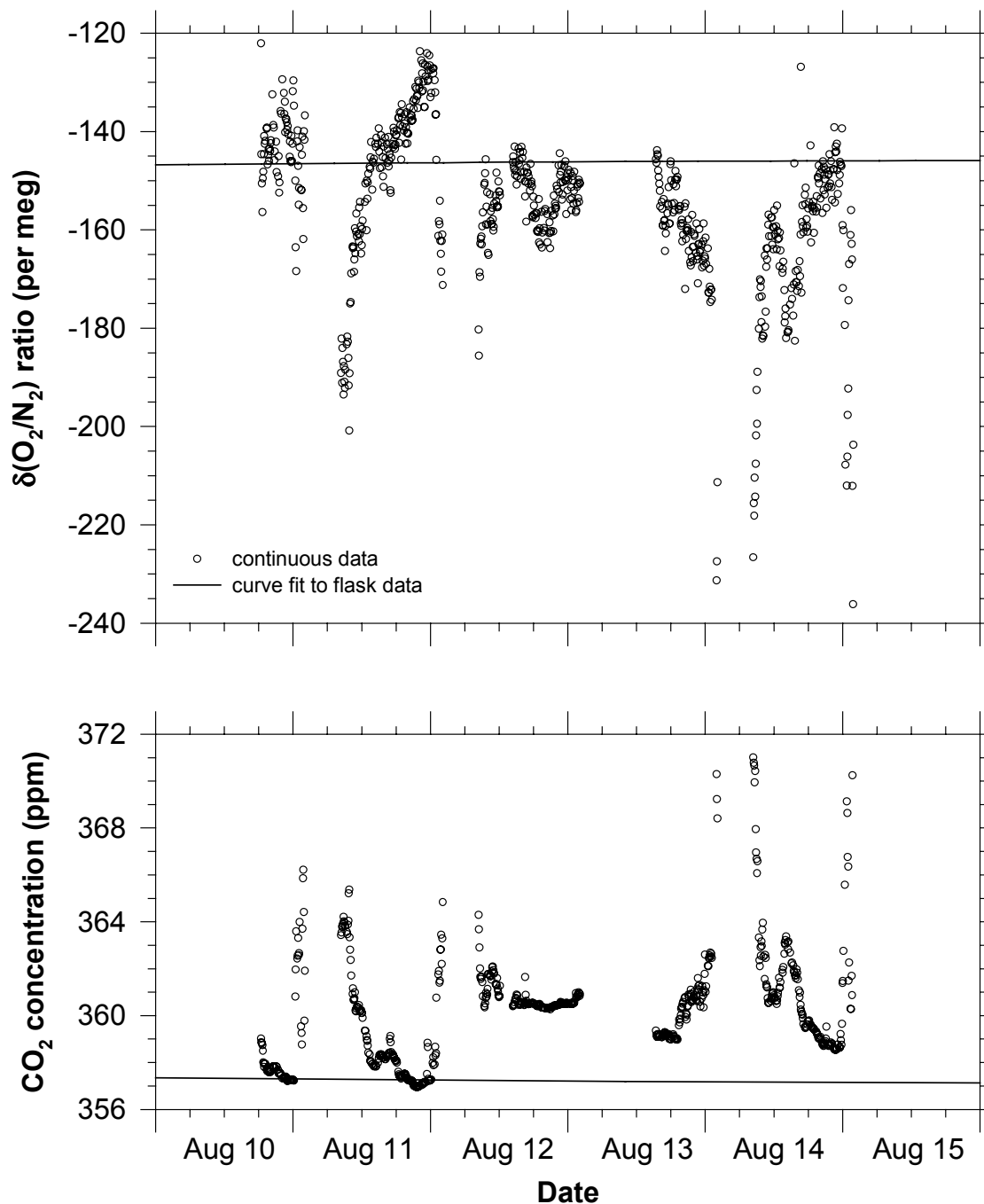


Figure 3.3. Continuous O_2/N_2 and CO_2 measurements sampled from the end of the Scripps Pier for a 1-week period in August 1996. The y axes have been scaled so that O_2/N_2 and CO_2 changes can be compared visually on a mole to mole basis. Data points shown are 2.5-min averages, with one point every 5 min. Gaps in the data are during 4-hourly daily calibration runs or downtime for other logistical reasons. Also shown are the curve fits to the La Jolla flask data (collected at approximately 2 week intervals and analyzed on the interferometric oxygen analyzer), based on a four harmonic seasonal cycle and a stiff spline interannual trend.

polluted or contaminated air, and the expected largest source of pollution in the La Jolla area is from the combustion of “liquid” fossil fuels, which when fully combusted have a ratio of 1.44 ± 0.03 moles of O_2 consumed per mole of CO_2 produced [Keeling, 1988a]. The lower value we observed of 1.30 can most probably be explained by small dilution effects from exchanges with either land biota ($O_2:C = 1.1$ [Severinghaus, 1995]) or oceans. Figure 3.3 also shows curve fits to the La Jolla flask data series. A comparison of these curves with the actual day to day variability in O_2 and CO_2 concentrations highlights the somewhat ambiguous nature of flask sampling methods.

The scatter of the residuals from the linear fit to the data in Figure 3.4 represents more than instrumental scatter and illustrates that O_2/N_2 ratios and CO_2 concentrations in ambient air are not always anticorrelated. The most significant example of this can be seen in Figure 3.3 on August 12 from approximately 1500-0000 local time. During this period, the CO_2 concentration was relatively steady, while the O_2/N_2 ratio first sharply decreased and then increased again to close to its earlier value. Such phenomena can be explained only by influences from oceanic sources or sinks. For example, there may have been a local upwelling event that brought oxygen-depleted waters to the surface, or there may have been a shift in air mass circulation. Because for air-sea gas exchange the CO_2 equilibration time is an order of magnitude longer than the O_2 equilibration time [Keeling *et al.*, 1993], only O_2 would have been affected by such an event.

Figure 3.5 shows the O_2/N_2 ratios derived from the paramagnetic analyzer and the concurrent O_2/N_2 ratios derived from the interferometric analyzer for the same one week period in August 1996. As can be seen, there is a small systematic offset of

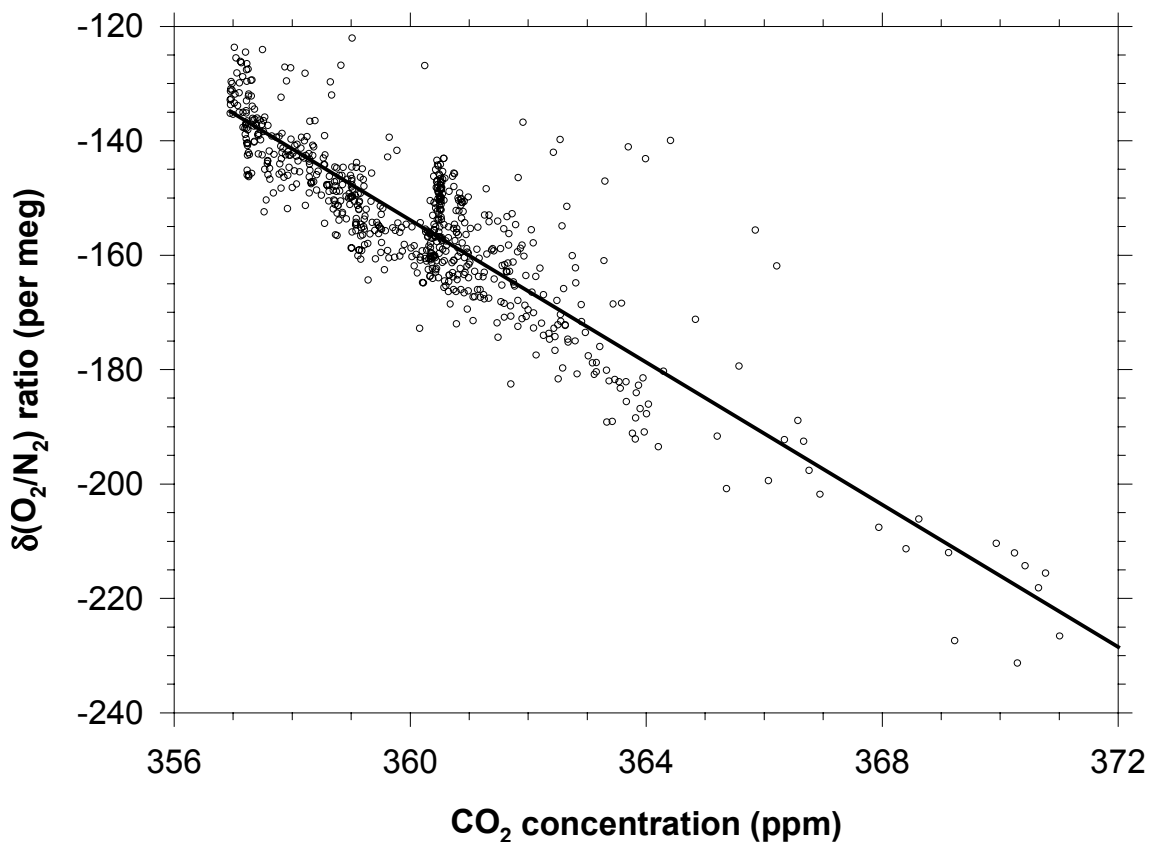


Figure 3.4. O₂/N₂ and CO₂ data from Figure 3.3 plotted against each other. The correlation is good, with an r^2 of 0.88. The slope of the best-fit line is -6.22 ± 0.09 per meg/ppm, or 1.30 ± 0.02 mol O₂ consumed per mol CO₂ produced, close to but lower than a value of 1.44 that would be expected if all the air was polluted by fossil fuel combustion from petroleum based fuels only. The residuals from the linear fit are larger than expected from instrumental imprecision, illustrating that O₂/N₂ and CO₂ are not always anticorrelated in ambient air.

approximately 2.1 per meg. This offset is most likely another manifestation of the offset discovered above in the null test using the brass “T”, and is clearly the result of gas-handling difficulties rather than analyzer problems. The two analyzer show the same features in the data with similar precision.

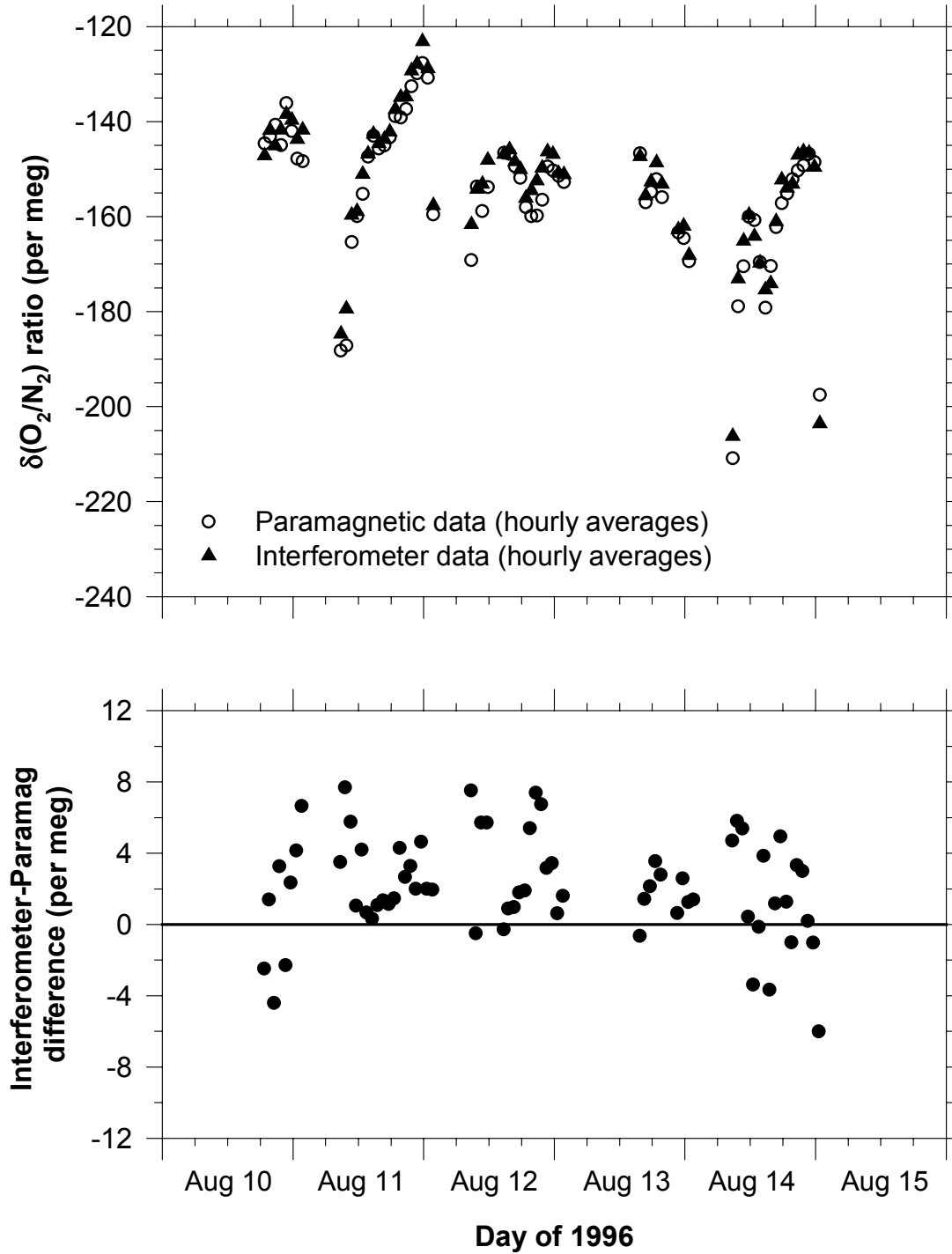


Figure 3.5. For the same period of continuous data collection on the paramagnetic analyzer, concurrent interferometer O_2/N_2 ratio data were collected. Apart from a small calibration offset, the two analyzers show the same features with similar precision. Note that the interferometer outputted one data point per hour, so the paramagnetic data were binned and averaged accordingly for this graph.

3.4. Discussion and Conclusions

The event on August 12 discussed in section 3.3 highlights one of the advantages of a continuous O₂ dataset over flask sampling programs that are currently in operation [*Bender et al.*, 1996; *Stephens et al.*, 1998; R. Francey, personal communication, 1997]. Flask samples take a “snap-shot” sample and are to some extent “blind” to the nature of the air being sampled. The criteria used in collecting background air for O₂/N₂ flask samples typically stipulate wind direction in a particular sector and greater than a certain threshold speed and stipulate ambient CO₂ concentration being steady. The afternoon of August 12 may well have satisfied such criteria at La Jolla, but depending on whether a flask sample was collected at 1500 or 1800 local time, the O₂/N₂ ratio could have been different by 20 per meg or almost 20% of the annual seasonal cycle. This demonstrates that the current practice of defining an atmospheric O₂ background using the same criteria as that used to define a CO₂ background may not be adequate, and other conditions need to be taken into account. Continuous O₂ data from a sampling station can highlight local meteorological and oceanic events on hourly, daily, and seasonal timescales and can show their effects on, and help to define, background atmospheric O₂ concentrations. This information can then be used to better interpret flask data or can be used on its own to construct a background, clean air O₂ signal for that station.

We are continuing to improve the performance of this paramagnetic analyzer. In the most elaborate improvement we hope to create a precisely controlled constant temperature environment by means of an active temperature control system. We are optimistic that this modification will reduce the 40 ppm/h temperature-induced drift rate

substantially, which would reduce the rate of reference gas usage, which is a logistical concern at any remote background air sampling station.

We envisage that this analyzer could also be used for a host of other applications. For example, in experiments on the potential CO₂ fertilization effect on plants, it is not practical to measure the photosynthetic CO₂ flux since CO₂ itself is being artificially introduced to the environment; hence O₂ measurements represent a viable alternative. This analyzer could also be used in other plant physiology studies and to study plant photosynthesis and respiration patterns, including measuring the photosynthetic and respiratory quotients. Finally, from analysis of the anticorrelation between O₂ and CO₂ concentrations (see Figure 3.4), it may be possible to separate effects of fossil fuel and natural CO₂ emissions from a region or country (assuming minimal complications from ocean influences). The analyzer is not suited, however, for measurements from a moving platform because of vibration and motion sensitivity.

In summary, the paramagnetic oxygen analyzer, when incorporated with the gas-handling design discussed in this paper, is well suited for measuring atmospheric O₂ in a continuous fashion, and is capable of an hourly precision of ± 0.9 per meg (± 0.2 ppm). Through extensive testing we have shown that the analyzer has a linear response for oxygen concentrations in the range of variations observed in ambient air. Finally we have shown that the analyzer can operate successfully for many months at a time with little or no maintenance and that resultant data are in good agreement with results from the interferometric oxygen analyzer.

This chapter appeared in full as Manning, A.C., R.F. Keeling, and J.P. Severinghaus, Precise atmospheric oxygen measurements with a paramagnetic oxygen analyzer, *Global Biogeochemical Cycles*, 13 (4), 1107-1115, 1999. I was the primary investigator and lead author of this paper and conducted all analyses presented therein.

3.5. References

- Bender, M.L., P.P. Tans, J.T. Ellis, J. Orchardo, and K. Habfast, A high precision isotope ratio mass spectrometry method for measuring the O₂/N₂ ratio of air, *Geochim. Cosmochim. Acta*, 58(21), 4751-4758, 1994.
- Bender, M., T. Ellis, P. Tans, R. Francey, and D. Lowe, Variability in the O₂/N₂ ratio of southern hemisphere air, 1991-1994: Implications for the carbon cycle, *Global Biogeochem. Cycles*, 10(1), 9-21, 1996.
- Ciais, P., P.P. Tans, M. Trolier, J.W.C. White, and R.J. Francey, A large northern hemisphere terrestrial CO₂ sink indicated by the ¹³C/¹²C ratio of atmospheric CO₂, *Science*, 269, 1098-1102, 1995.
- Graedel, T.E., and P.J. Crutzen, *Atmospheric change: an Earth system perspective*, 446 pp., W. H. Freeman, New York, 1993.
- Keeling, C.D., T.P. Whorf, M. Wahlen, and J. van der Plicht, Interannual extremes in the rate of rise of atmospheric carbon dioxide since 1980, *Nature*, 375, 666-670, 1995.
- Keeling, R.F., Development of an interferometric oxygen analyzer for precise measurement of the atmospheric O₂ mole fraction, Ph.D. thesis, Harvard Univ., Cambridge, Mass., 1988a.
- Keeling, R.F., Measuring correlations between atmospheric oxygen and carbon dioxide mole fractions: A preliminary study in urban air, *J. Atmos. Chem.*, 7, 153-176, 1988b.
- Keeling, R.F., and S.R. Shertz, Seasonal and interannual variations in atmospheric oxygen and implications for the global carbon cycle, *Nature*, 358, 723-727, 1992.
- Keeling, R.F., R.P. Najjar, M.L. Bender, and P.P. Tans, What atmospheric oxygen measurements can tell us about the global carbon cycle, *Global Biogeochem. Cycles*, 7(1), 37-67, 1993.
- Keeling, R.F., S.C. Piper, and M. Heimann, Global and hemispheric CO₂ sinks deduced from changes in atmospheric O₂ concentration, *Nature*, 381, 218-221, 1996.
- Keeling, R.F., A.C. Manning, E.M. McEvoy, and S.R. Shertz, Methods for measuring changes in atmospheric O₂ concentration, and their applications in southern hemisphere air, *J. Geophys. Res.*, 103(D3), 3381-3397, 1998.
- Kocache, R., The measurement of oxygen in gas mixtures, *J. Phys. E Sci. Instrum.*, 19, 401-412, 1986.
- Lide, D.R., *CRC Handbook of Chemistry and Physics*, CRC Press, Boca Raton, Fla.,

1992.

Logan, J.A., M.J. Prather, S.C. Wofsy, and M.B. McElroy, Tropospheric chemistry: A global perspective, *J. Geophys. Res.*, 86(C8), 7210-7254, 1981.

Machta, L., and E. Hughes, Atmospheric oxygen in 1967 to 1970, *Science*, 168, 1582-1584, 1970.

Sarmiento, J.L., T.M.C. Hughes, R.J. Stouffer, and S. Manabe, Simulated response of the ocean carbon cycle to anthropogenic climate warming, *Nature*, 393, 245-249, 1998.

Schimel, D., I.G. Enting, M. Heimann, T.M.L. Wigley, D. Raynaud, D. Alves, and U. Siegenthaler, CO₂ and the carbon cycle, in *Climate Change 1994: Radiative forcing of climate change and an evaluation of the IPCC IS92 emission scenarios*, edited by J.T. Houghton et al., pp. 35-71, Cambridge Univ. Press, New York, 1995.

Severinghaus, J.P., Studies of the terrestrial O₂ and carbon cycles in sand dune gases and in Biosphere 2, Ph.D. thesis, Columbia Univ., New York, 1995.

Severinghaus, J.P., M.L. Bender, R.F. Keeling, and W.S. Broecker, Fractionation of soil gases by diffusion of water vapor, gravitational settling, and thermal diffusion, *Geochim. Cosmochim. Acta*, 60(6), 1005-1018, 1996.

Stephens, B.B., R.F. Keeling, M. Heimann, K.D. Six, R. Murnane, and K. Caldeira, Testing global ocean carbon cycle models using measurements of atmospheric O₂ and CO₂ concentration, *Global Biogeochem. Cycles*, 12(2), 213-230, 1998.

Taylor, J.K., (Ed.), Microchemical Analysis Section: Summary of activities July 1967 to June 1968, Nat. Bureau of Stand., Washington D.C., 1968.

Chapter 4.
Oceanic and terrestrial contributions
to atmospheric O₂ and CO₂ derived
from continuous measurements
at Baring Head, New Zealand

Abstract.

I present the first time series of continuous atmospheric O₂ measurements from a background air monitoring station. One year of data are shown from June 1999 to June 2000 sampled at Baring Head, Wellington, New Zealand. These data, along with concurrent CO₂ measurements made at the site, allow partitioning of land biotic and oceanic influences on the air masses arriving at Baring Head. Processes occurring on hourly, daily, and seasonal time scales are observed. As expected, the land biota play a greater role in atmospheric variability, but the oceans are found to have a greater influence on short (hourly) time scales than previously observed.

I present calculations of the O₂:C exchange ratio derived from calculations when changes in this ratio are thought to be influenced only by the land biota. These calculations result in a ratio of 1.13, in agreement with the value of 1.1 ± 0.05 in the literature. Such analyses are preliminary, however, and further work is needed.

In addition, this chapter presents many of the technical and gas handling problems faced in precise measurements of atmospheric O₂, particularly as they pertain to achieving continuous measurements. Fractionation artifacts of O₂ relative to N₂ are discussed at 'tee' junctions, in cryogenic cold traps, and in sampling intake systems.

4.1. Introduction

In order to predict future climate and assess ongoing climate change on our planet, an in-depth understanding of the global carbon cycle and the mechanistic controls and influences on it is essential. One of the least understood regions of the world from this perspective is the Southern Ocean. Relatively little scientific research is carried out in this region, with a paucity of datasets available for interpreting the impact that the Southern Ocean can have on global climate and climate change. On the other hand many researchers speculate that the Southern Ocean may play a significant role in global climate and in the global carbon cycle, highlighting the need for additional observational datasets. For example, *Sarmiento et al.* [1998], using a coupled global atmosphere-ocean model and allowing changes in ocean circulation and biology, found large changes in oceanic uptake of carbon, with changes in the Southern Ocean dominating. *Murnane et al.* [1999] showed that the Southern Ocean appears to exist in a delicate balance between being a source of atmospheric CO₂ owing to ventilation of CO₂-depleted waters formed by the biological pump, and being a sink for CO₂ owing to colder waters having higher gas solubilities. Thus any changes such as increasing atmospheric CO₂ concentrations from anthropogenic input, ocean warming, or changes in the vertical mixing or stratification of the Southern Ocean have the potential to cause significant changes in the net effect of the oceans on the global carbon budget.

The observed latitudinal gradient in atmospheric CO₂ is less than expected when consideration is given to the geographic asymmetry of fossil fuel combustion and the barrier to interhemispheric atmospheric mixing owing to the Intertropical Convergence Zone. Several hypotheses have been presented to explain this observation.

Perhaps the most popular explanation is that the northern hemisphere land biota is a relatively large carbon sink [*Ciais et al.*, 1995; *Keeling et al.*, 1996; *Myneni et al.*, 1997; *Rayner et al.*, 1999]. *Fan et al.* [1998] argued that almost all of this northern hemisphere sink was in North America, but *Schimel et al.* [2000], and *Houghton et al.* [1999] contested this, showing with different approaches that the uptake of carbon by the North American land biota was in fact much smaller. These results could perhaps be extrapolated to question the initial hypothesis of the large northern hemisphere land biotic sink, thus suggesting that the reason for the discrepancy in the latitudinal gradient lies elsewhere.

One other process, for example, discussed by *Keeling et al.* [1996] which can influence both the atmospheric O₂/N₂ and CO₂ interhemispheric gradients is the North Atlantic thermohaline pump, which transports both O₂ and CO₂ southward. Another possible scenario is that the contemporary Southern Ocean could be a net source of atmospheric CO₂. Indeed, analyses of air trapped in ice cores indicate that the pre-industrial CO₂ interhemispheric gradient was reversed, with higher CO₂ concentrations in the southern hemisphere, which could be explained by a net source of atmospheric CO₂ from the Southern Ocean. The work of *Sarmiento et al.* [1998] and *Murnane et al.* [1999] also demonstrated the Southern Ocean as a source of atmospheric CO₂ as a potential future scenario. Additional recent research applying WOCE (World Ocean Circulation Experiment) datasets to an ocean circulation model further suggests that the Southern Ocean could be a significant source of atmospheric CO₂ (P. Robbins, personal communication).

The Southern Ocean is the region of the world's oceans with the strongest winds, and the greatest variability in wind speed and direction [*Gille et al.*, 2000]. Therefore it can be expected that this region will be both sensitive to, and a player in, global climate change. Thus increased efforts to monitor various aspects of the climate system in the region of the Southern Ocean are important, as stressed by *Sarmiento et al.* [1998].

Atmospheric O₂/N₂ ratio variations in the southern hemisphere are generally much larger than CO₂ variations, therefore it is possible to observe seasonal and interannual variability in processes connected with atmospheric CO₂ uptake and release that would not be apparent from measurements of CO₂ alone. Additionally, recent data from our atmospheric O₂/N₂ ratio flask sampling program (Chapter 2) indicate that in the mid- to high latitudes of the southern hemisphere the troposphere is not as well mixed as previously thought, further supporting increased efforts for additional atmospheric monitoring from stations in this region.

These issues were a primary motivating factor in choosing Baring Head, New Zealand as the first site to establish a continuous atmospheric O₂ monitoring program. As discussed in Chapter 1, atmospheric O₂ measurements together with concurrent atmospheric CO₂ measurements can aid in elucidating land biotic and oceanic influences on the global carbon cycle, thus a monitoring program at Baring Head will aid in interpreting and understanding signals derived from the Southern Ocean.

As shown in Figure 4.1, Baring Head (BHD) is located at 41.4°S, 174.9°E on a southeastern tip of the North Island of New Zealand, about 10 km southeast of Wellington, a metropolitan city with a population of about 200,000. New Zealand is

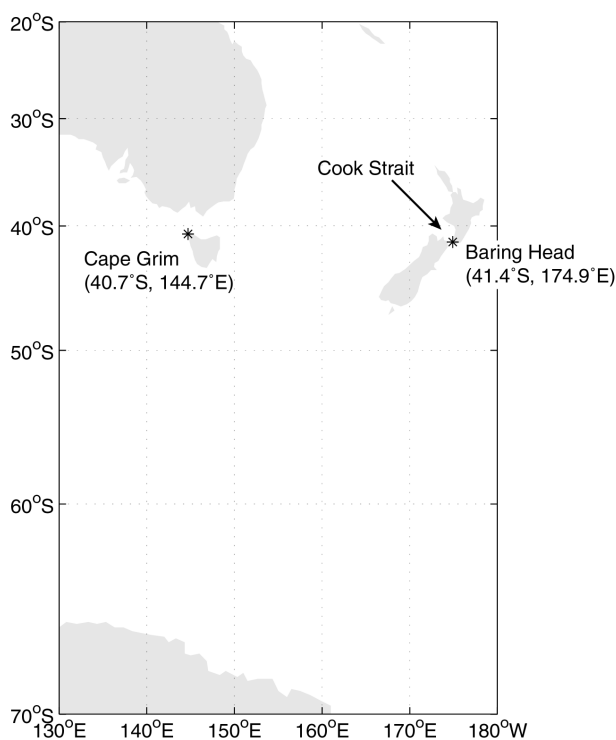


Figure 4.1. Map showing the location of Baring Head, New Zealand. The majority of air masses arriving at Baring Head are either southerlies derived from the Southern Ocean and not having recently passed over any land mass, or northerlies which have recently passed over the North Island of New Zealand, but which do not have a strong anthropogenic influence.

remote from all other major land masses except Australia, and experiences almost continuous oceanic weather with prevailing westerly winds.

Baring Head station has a well established atmospheric monitoring program that has been in operation since 1972 when continuous CO₂ measurements were first begun [Lowe, 1974]. Other measurements routinely made include local meteorological conditions, including archiving of backward wind trajectories every 12 hours, ¹³CO₂ and

$^{14}\text{CO}_2$ isotopic ratios, methane (CH_4) concentrations and $^{13}\text{CH}_4$ and $^{14}\text{CH}_4$ isotopic ratios, carbon monoxide (CO) concentrations and ^{13}CO , ^{14}CO and C^{18}O isotopic ratios, non-methane hydrocarbon concentrations, surface ozone concentrations, condensation nuclei concentrations, and atmospheric radionuclide concentrations [*Gomez, 1996*].

Near Baring Head, local winds are strongly influenced by the funneling action of the Cook Strait. When the regional air flow is from the west, the local wind at Baring Head is from the north or northwest, and when the regional air flow is from the south or southwest, the local wind at Baring Head is from the south or southeast [*Lowe et al., 1979*]. Approximately 30% of the time [*Gomez, 1996*] the regional air flow is from the south, and wind backward trajectories show that generally such air masses have not traveled across the South Island of New Zealand and are representative of large regions of the Southern Ocean [*Lowe et al., 1979*].

The paramagnetic oxygen analyzer described in Chapter 3 was improved further and deployed at the Baring Head site. I now have one year of O_2/N_2 ratio data from this system from June 1999 to June 2000. In conjunction with the existing continuous CO_2 measurements I can use these data to infer land biotic and oceanic influences on the air masses arriving at Baring Head. With these continuous measurements, such analyses can be performed over hourly, daily, and seasonal time scales. The $\text{O}_2:\text{C}$ land biotic exchange ratio, a crucial factor in calculations of global carbon sinks, is not well known [*Severinghaus, 1995*]. Continuous measurements of O_2 and CO_2 are one approach that can be used to improve estimates of this ratio. Baring Head is well situated for obtaining such measurements, frequently receiving winds from the north that for the most part have only been influenced by land biotic processes.

In the remainder of this chapter, section 4.2 discusses improvements I made to the paramagnetic analyzer system in addition to those discussed in Chapter 3. I discuss mechanistic causes of O₂ fractionation in air relative to N₂ that I have discovered during my research and the implications that these have for both flask and continuous sampling programs. Then I describe the deployment of my paramagnetic analyzer system at Baring Head, and I discuss the calibration procedures that I have employed and present results from the first year of calibration analyses. In section 4.3, I show one year of data collected from ambient air measurements from June 1999 to June 2000 at Baring Head. From these data I obtain a seasonal cycle in O₂/N₂ ratios which I compare to results from our flask sampling station at Cape Grim, Tasmania, and I analyze the high temporal resolution of the data in monthly plots. In section 4.4 I discuss an unusual event observed in the data in July 1999. Finally section 4.5 discusses and gives an example of a computation of O₂:C ratios over time periods when changes in O₂ and CO₂ concentrations are assumed to be owing only to land biotic exchanges.

4.2. Methods

4.2.1. Paramagnetic analyzer improvements

I made several modifications and improvements to the paramagnetic analyzer system described in Chapter 3. An active temperature-control system was incorporated into the design, controlling the temperature of the Servomex paramagnetic analyzer cell at about 40°C to a precision of ±0.01°C. Comparisons with results obtained in Chapter 3 when the entire analyzer system was housed in a statically-insulated box show an improvement in the overall drift rate from approximately 5,000 per meg/h to

approximately 10 per meg/h. The analyzer cell was housed in a custom-made aluminum box, 14 inches square, 8 inches high, with 0.5 inch thick walls. 1.5 inch thick PVC foam insulation was added to the exterior of the box with flexible heaters (Omega Engineering, Kapton KH series) covering all interior walls. A temperature controller (Omega Engineering, Fuzzy Logic controller model CN4801) responded to the output from two thermistor elements (Omega Engineering, model 44032) and adjusted the voltage applied across the flexible heaters between 0 and 24 Volts to maintain the temperature to within $\pm 0.01^\circ\text{C}$. Two small fans mounted at diagonally opposite corners inside the aluminum box ensured a well-mixed and homogeneous temperature. Very small fluctuations of pressure inside the sealed “Pressure Reference” volume (Figures 3.1 and 4.4) caused by temperature variability were found to be an even greater source of baseline drift in the analyzer signal than temperature-induced variability acting on the paramagnetic analyzer sensor itself. Therefore this pressure reference volume was also housed inside the aluminum box, as was the ± 1 torr MKS Baratron differential pressure gauge (Figures 3.1 and 4.4) to improve its stability.

As described in Section 3.2.1 “working gas” (called “reference gas” in Chapter 3) is passed through the analyzer periodically to null out the effect of analyzer drift on time scales longer than approximately 5 min. With the active temperature control and resulting improvement in drift rate I was able to decrease the frequency of passing working gas through the analyzer, thus saving on valuable working gas. I changed from a 2.5-min sample, 2.5-min working gas switching protocol utilized in Chapter 3, to a 9-min sample, 6-min working gas protocol at Baring Head. A typical raw data stream under normal operating conditions is shown in Figure 4.2. This shows six hours of data

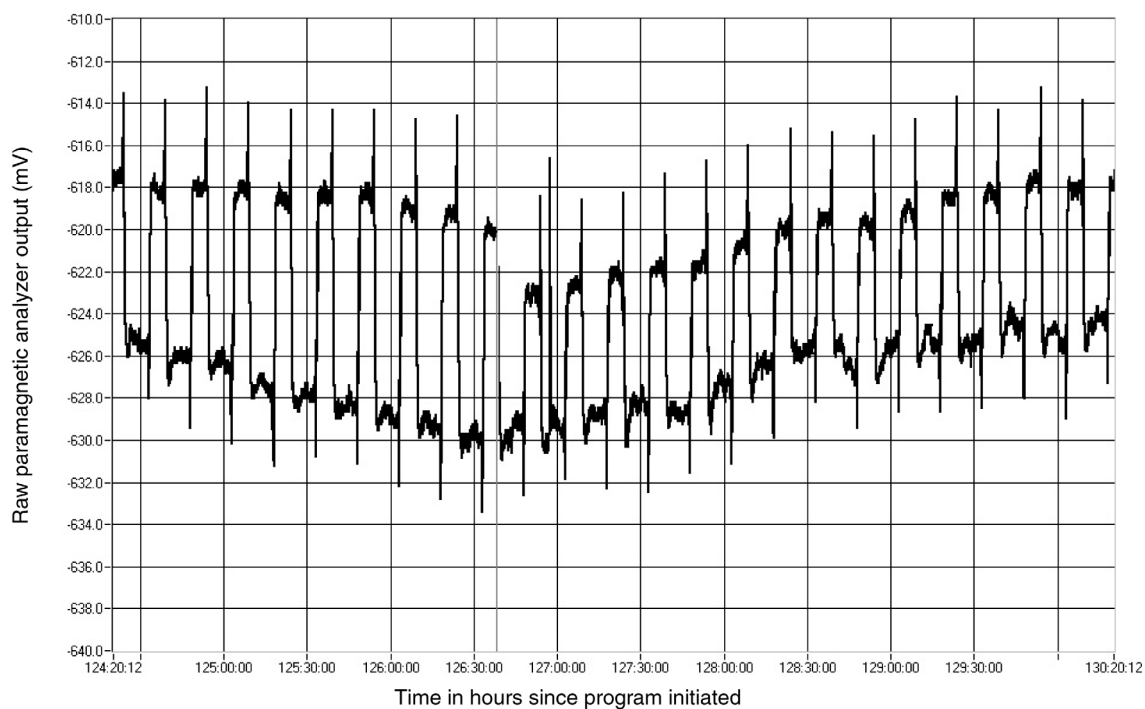


Figure 4.2. An example of the output signal from the paramagnetic analyzer. The top ‘jogs’ show 6 minute working gas jogs and the bottom jogs show 9 minute sample air jogs. Six hours of data are shown, with data points recorded every second. The analyzer signal is shown in mV units, where 1 mV is roughly equal to 5 per meg, thus the full scale shown is approximately 150 per meg. Spikes occurring at the end of each jog are electrical and mechanical impulses owing to switching of valves. A break appears at approximately 126:40, showing the current position of the trace.

from 8 July 2000 with the above switching protocol between a working gas and sample air. Sample air jogs are the lower jogs shown in the figure. The y-axis is in mV, the raw data output from the paramagnetic analyzer concentration, where 1 mV is roughly equal to 5 per meg, therefore full scale on this figure represents approximately 150 per meg. Data shown are reported every 1 sec, whereas data written to data files are reported only once every 30 sec by taking an average of 30 one-second points. The spikes shown are a combination of electrical and pressure pulses caused by the system

switching between working gas and sample air and vice versa. These spikes are filtered out in subsequent data processing.

Under the operating conditions employed in Chapter 3, when working gas was not flowing through the analyzer it was flushing through the purge side of the four-way valve to prevent transient pressure fluctuations induced by switching between the two gas streams and to maintain constant conditioning of the walls of inner tubing surfaces. Because 9 min now elapses between working gas jogs, I am able to turn off the working gas purge for the first 5 min of this air jog. Purging of the working gas is then turned on 4 min before it is sent through the analyzer and I demonstrated that this was enough time to recondition the walls of inner tubing and regulator surfaces. This new switching procedure allowed me to save 20 min worth of working gas every hour increasing the lifetime of a cylinder by 33%, a very important saving at a remote field station.

At Baring Head I found it necessary to employ this longer 6-min working gas jog because, compared to the setup in La Jolla, there was a much bigger sweepout transient after switching the four-way valve to pass working gas through the analyzer, as shown in Figure 4.3. This figure shows one hour of data from 22 May 1999, with data points shown every one second, as for Figure 4.2. The y axis is again shown in mV, and full-scale in this figure is equivalent to approximately 100 per meg. The transient observed on switching to working gas produces a spike of about 10 per meg, and sometimes took as long as 2 min to disappear and for the O_2 concentration to return to the true working gas concentration. An example can be seen at time 27:15. (In the figure shown, the system was running particularly well, and the transient dissipated more quickly).

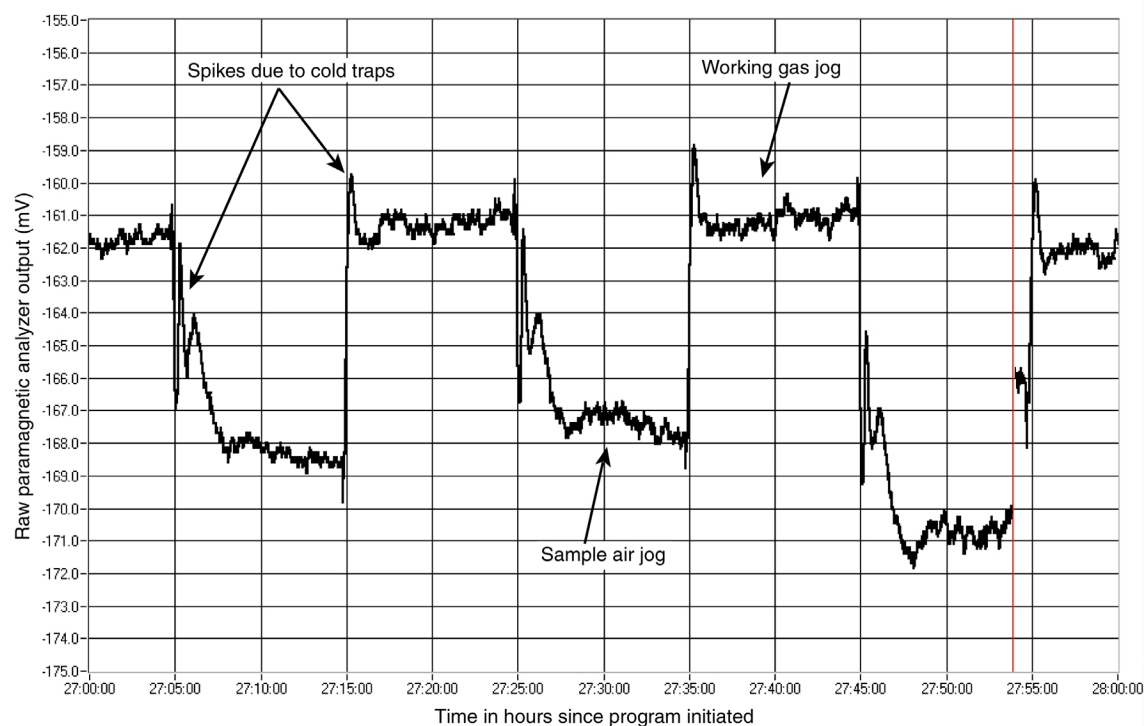
O₂ Spikes Due to Cold Trap and Switching Four-Way Valve

Figure 4.3. As for Figure 4.2, raw analyzer output signal is shown with a data point every second and 1 mV roughly equal to 5 per meg. Thus full scale in this figure is 100 per meg, and one hour of data are shown. This figure illustrates the transient spikes in O₂ concentrations that are caused when valve switching disturbs the O₂/N₂ ratio gradient equilibrium that is set up in the cryogenic cold traps.

The reason for this transient was because an additional cold trap has been added to the system (cold trap T6 in Figure 4.4) that was not present in La Jolla. I suspect that the transient is related to the same phenomena discussed in Section 3.2.2. Within the cold trap a large temperature gradient exists, from -80°C to roughly ambient temperature at the exit, resulting in an O₂/N₂ ratio gradient building up, since relative to N₂, O₂ will diffuse to colder regimes by thermal diffusion because it is a heavier molecule [Severinghaus *et al.*, 1996]. Under steady flow and pressure conditions this

thermal diffusion effect reaches steady state, and the O_2/N_2 ratio (and hence O_2 concentration) of any gas passing through the cold trap is not affected. However, switching the four-way valve immediately upstream of the cold trap (V14 in Figure 4.4) creates a brief pressure pulse through the system, disturbing the thermal diffusive fractionation equilibrium, and sending a pulse of high O_2/N_2 ratio air through the analyzer.

Figure 4.3 also shows an even larger transient of about 20 per meg immediately after switching back from working gas to sample air. An example of this can be seen at time 27:05. This transient in fact exhibits a double peak, and is caused by both cold trap T6, and also cold trap T5, upstream of the four-way valve, which is being used for drying the sample air stream. I did not observe such a transient at La Jolla because the equivalent trap used was much smaller (90 mL at La Jolla compared to 220 mL at Baring Head), and the time taken for this diffusive equilibrium to re-establish itself is very sensitive to the volume of the trap.

The larger cold trap at Baring Head was necessary because NIWA personnel could only guarantee traveling to the Baring Head station once every two weeks to replace the trap (necessary because it is slowly filling with ice), whereas at La Jolla such personnel limitations had not been a concern. I tried several different techniques to remove or reduce this pressure pulse and associated O_2/N_2 sweepout transient. Filling the cold traps with glass beads reduced the cold trap volume and resulted in a much quicker return to stable O_2/N_2 ratios. Carefully balancing the flowrate of the working gas flush to equal the flowrate through the analyzer system also reduced the spikes. However, this working gas flush flowrate is not controlled by an active feedback

controller, therefore it may drift over time, and can be influenced by variations in upstream pressure. Therefore I could not rely on these transients spikes never being present, hence my final solution was to have a longer 6-min working gas jog and I programmed the data processing routines to discard the first 3 min of the working gas jog, and the first 4 min of the sample air jog.

The relief valve used in the system in Chapter 3 was of a spring-loaded, o-ring sealing design. If pressure builds up it counteracts the spring causing the valve to open, protecting the sensitive paramagnetic analyzer cell. I was concerned about the integrity of the tightness of the o-ring seal, so I removed the relief valve from the system and incorporated new valves, V17 and V19 in Figure 4.4, which would not allow high flowrates that could damage to analyzer to pass through.

4.2.2. O₂/N₂ Ratio Fractionation at ‘Tee’ Junctions

Plumbing systems for ambient air analysis commonly employ a ‘tee’ junction, where an incoming flow divides into two branches. There are two primary reasons for dividing flow with such a tee. The first is to allow two different gas analyzers, or a gas analyzer and a flask collection system, to sample the same incoming air stream. The second reason is that in many cases the flowrate required or desired to pass through the gas analyzer is relatively low, and significantly lower than necessary for sufficient flushing of inlet tubing, hence a tee is employed, taking a small portion of the flow for the gas analyzer, and allowing the remainder to vent. I have found that in standard tee designs, O₂ molecules fractionate relative to N₂. Depending on various operating conditions, O₂ molecules preferentially flow through one branch compared to N₂.

I conducted experiments to diagnose this effect at Scripps Institution of Oceanography, using the Scripps Pier intake setup described in Chapter 3, section 3.3. Air was drawn through 1/2 inch outside diameter Dekoron tubing a length of approximately 500 m at a flowrate of about 15 Lpm with a diaphragm pump (Cole Parmer, model “Air Cadet 400”). Upstream of the pump, a 3/8 inch Swagelok stainless steel tee divided the flow, delivering 280 mL/min through one branch to the interferometric analyzer, and about 15 Lpm through the second branch, exhausting through the Cole Parmer pump. The interferometric analyzer branch utilized a KNF Neuberger diaphragm pump (model N05) to achieve the necessary flowrate and pressure drop. O₂/N₂ ratio fractionation through this tee was found to fluctuate in a seemingly random manner to the order of ±30 per meg. The degree of fractionation was determined from independent tests and comparisons with flask samples. It was not immediately clear why the degree of fractionation varied and was not constant.

My first attempts at eliminating this fractionation focussed on isolating the tee junction from pulsations in flow caused by the two pump diaphragms. I achieved this isolation simply by separating the two pumps from the tee junction with 30 m coils of 1/2 inch Dekoron tubing. Tests showed 30 m to be the minimum coil length required to achieve sufficient isolation to eliminate all O₂/N₂ ratio fractionation (to a level of 2-3 per meg or better).

Unfortunately, some time after this design improvement, intermittent O₂/N₂ ratio fractionation was again observed in a comparison of flask samples with direct measurements from the end of the Scripps Pier. A careful investigation of our flask sampling methods did not demonstrate any problems with these procedures, suggesting

that we still had a fractionation problem at the tee junction. At this point I became suspicious of temperature effects. I then found that holding my hand on the Swagelok tee produced an 80 per meg jump in the O_2/N_2 ratio fractionation. Therefore it was likely that even in an air conditioned laboratory, temperature swings, in conjunction with pump pulsations, were responsible for the observed O_2/N_2 ratio fractionation.

I attempted to prevent the temperature-induced fractionation simply by placing the Swagelok tee, together with about 5 m of Dekoron tubing attached to each of the three arms of the tee, in a 20 L water bath kept at room temperature. This appeared to eliminate all observable fractionation, until several months later when some evidence of fractionation of the order of 10 per meg resurfaced.

From these experiences it is clear that in order to be confident that we do not have any O_2/N_2 ratio fractionation in our air sampling systems, we must either design more elaborate protections against fractionation at tee junctions, or we must eliminate such tee junctions from the system entirely. In the case of the Baring Head system, I decided to eliminate all tee junctions, meaning a total flowrate through the intake lines of only 100 mL/min. Because these intake lines are relatively short (40 m), I am confident that this is a satisfactory solution.

As mentioned in Chapter 2, several of our flask sampling programs have made use of tee junctions at certain times, therefore these recent fractionation findings resulted in concern as to the integrity of many years of our flask sample data. Fortunately, my tests also showed that O_2/N_2 ratio fractionation is highly sensitive to the flow ratio of the two outlet branches of the tee. In the case of continuous measurements drawn from the end of the Scripps Pier, the tee flow ratio is 15 Lpm to 280 mL/min, a

ratio greater than 50. Apart from Mauna Loa, the largest flow ratio present in any flask sampling program at any time has been 5, and we are confident that such a flow ratio has not presented any O₂/N₂ ratio fractionation problems at the limit of our detectability.

4.2.3. Deployment of Paramagnetic Analyzer at Baring Head, New Zealand

Continuous measurements of atmospheric CO₂ have been made at Baring Head since 1972 continuing to the present [Lowe, 1974; Lowe *et al.*, 1979; Manning *et al.*, 1999; Manning *et al.*, 1994]. Initially I planned to interface my paramagnetic O₂ analyzer system with the existing CO₂ analyzer system. However, it soon became apparent that different flow and pressure stability criteria and different calibration procedures precluded the sharing of intake lines, calibration gases, or computer hardware. Therefore a completely independent system was built as described below. Minor exceptions to this include ambient room, refrigerator, and chiller temperatures, and meteorological data, all of which are acquired by the computer controlling the CO₂ system and sent to the computer controlling the O₂ system via an Ethernet connection. In addition, the O₂ computer receives data on the CO₂ analyzer output.

The sample air intake system differs in several respects from the intakes employed at our flask sampling stations. Generally we have an inlet comprising of an approximate 1 foot long section of 2 inch diameter PVC pipe filled with glass wool and inverted to prevent rainwater entering the tubing. The primary purpose of this pipe is to serve as a filter to prevent particulate matter and small insects from entering the analyzer system. Initially I built a similar intake for my system at Baring Head but after

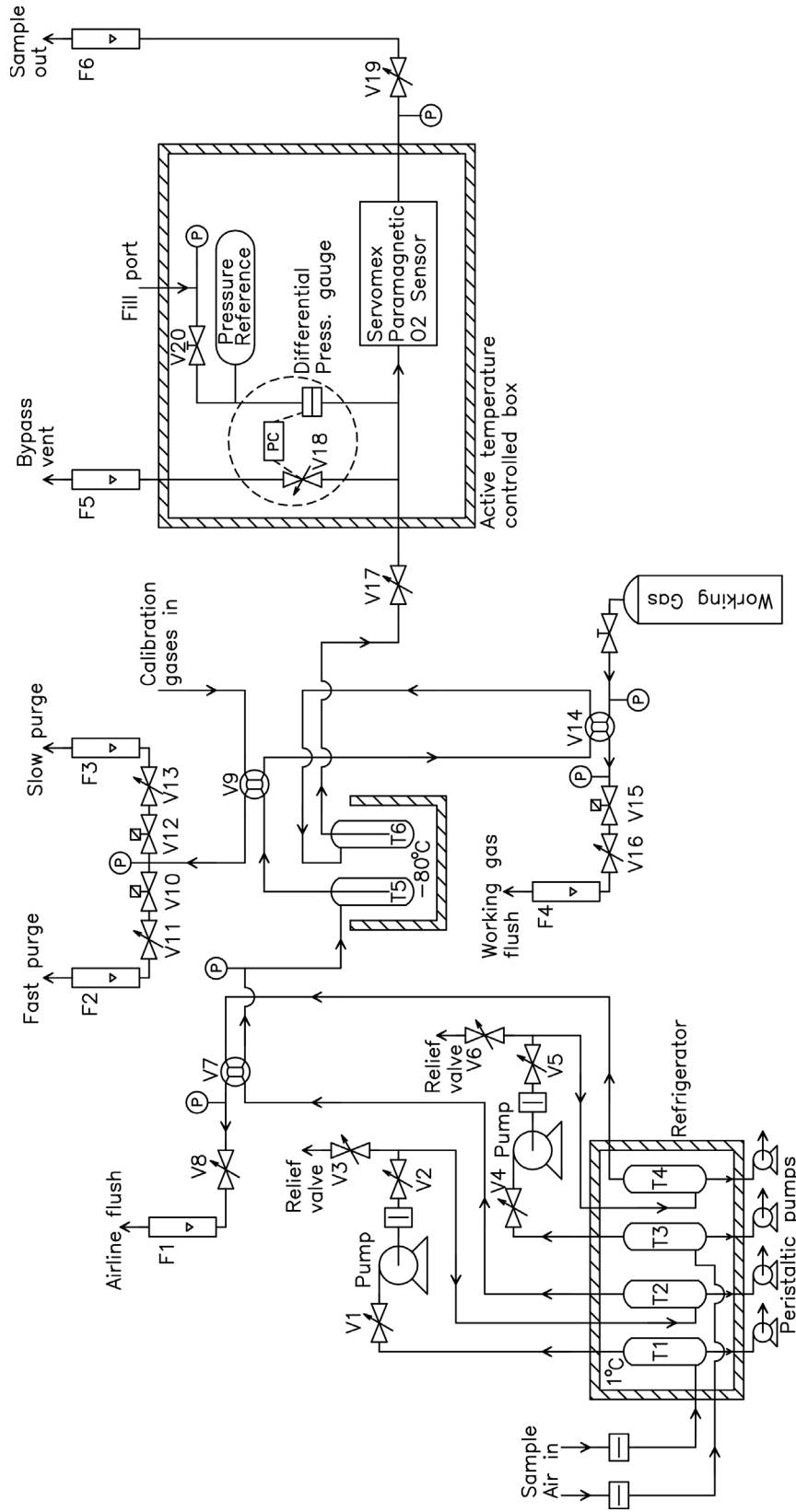


Figure 4.4. Gas handling schematic of the paramagnetic analyzer system set up at Baring Head, New Zealand. A ‘V’ label denotes a solenoid, pneumatic, or manual valve, ‘F’ a flowmeter, ‘T’ a thermometer, and ‘P’ a pressure gauge.

extensive testing I was able to show that the presence of the PVC pipe was inducing a seemingly randomly-fluctuating O_2/N_2 artifact which in one recorded experiment exhibited a range of 20-30 per meg over a one-hour period when the O_2/N_2 ratio was expected to be constant. I suspect that the low flowrate of my system, approximately 100 mL/min compared with 3 to 15 Lpm used at our flask sampling stations, was resulting in fractionation of O_2 relative to N_2 in the PVC pipe. This was probably occurring because of fluctuating temperature gradients in the pipe which in turn were a result of the low flowrate and the long residence time in the pipe of about 5 minutes, compared with less than 10 seconds for our flask sampling systems. I solved this problem simply by removing the pipe altogether. Inside the laboratory I added an inline 7μ Swagelok filter immediately upstream of the first refrigerator cold trap (see Figure 4.4 and description below) to remove any particulate matter entering the intake line.

Another difference between this intake system and our flask sampling intakes is the low flowrate itself. In the past our sampling systems have always used relatively high flowrates, and we had no prior experience with low flowrate intake systems. Our past reasoning behind establishing this protocol was that maintaining a relatively high flowrate is ideal for flushing the intake lines and for ensuring that any temperature, pressure, or concentration gradients that may arise are more likely to quickly reach an equilibrium state, and are less likely to vary as a result of fluctuations driven by external influences. Indeed, the PVC pipe problem demonstrated exactly this sort of problem. However, because of the fractionation at tee junctions described in section 4.2.2. above, and the inability to satisfactorily remove this artifact under all potential operating conditions, I decided to design the Baring Head intake system with a low flowrate, thus

avoiding the necessity for any tee junctions in the system. The only exception to this is the bypass vent flow (see Figure 4.4) immediately before sample gas enters the paramagnetic analyzer. I am not concerned about possible fractionation effects at this tee junction, because any fractionation that occurs will occur equally to sample air, and working and calibration gases, and thus will be cancelled out in the data processing procedures. In addition I am confident that any fractionation at this tee will be constant over time, since this regime is subject to very constant temperature, pressure and flow conditions.

My intake lines are relatively short because the Baring Head field laboratory is located immediately below the sample air inlet, thus by using 1/4 inch diameter tubing, even at the low flowrate employed of 100 mL/min, the time for ambient air to travel from the inlet to the paramagnetic analyzer is only 3.5 min.

Sample air enters from an inlet mounted at the top of a flagpole, 9.3 m above ground level and 90 m above sea level at the brink of a cliff overlooking the eastern part of the Cook Strait and the southwest Pacific Ocean as shown in Figure 4.1. I have two independent intake lines which I alternate sampling from so that I can diagnose potential problems when a discrepancy between the two lines occurs in O₂/N₂ ratios. 16 m of 1/4 inch outside diameter polyethylene-aluminum composite tubing (Dekoron) connects the flagpole inlet to the sampling setup in the field laboratory. From inside the laboratory all tubing is 1/8th inch 316L stainless steel tubing (Tube Service Company, cleaned with "Process C"). As shown in Figure 4.4 sample air passes through an inline 7 μ filter (Swagelok), then through a glass cold trap filled with glass beads located in a household refrigerator at 1°C. This trap removes the bulk of the water vapor in the sample air. A

peristaltic pump (Cole Parmer, model Masterflex L/S) draws off liquid water through the bottom of this trap at a flowrate of 0.2 mL/min. Sample air then passes through a diaphragm compressor pump (KNF Neuberger, model N05), modified as described in Section 3.2.2, which continuously draws the sample air in from the flagpole inlet. A pressure regulator (valves V2 and V5 in Figure 4.4; Valco, model Condyne PR50A15Z2) downstream of the pump regulates the pressure further downstream to be constant (set to 10 psig), thus smoothing out variability in pump performance. Because these pressure regulators were found to be very sensitive to minute particulate matter, another inline 7 μ filter was placed between the pump and the pressure regulator.

The sample air then travels through a second, identical glass cold trap filled with glass beads, mounted in the same refrigerator and with a peristaltic pump drawing off liquid water formed. Because the line pressure is now 10 psig, the efficiency of a 1°C cold trap is greater, and I am able to remove more water vapor at this stage. The purpose of both of these refrigerator traps is to greatly extend the lifetime of a -80°C cold trap further downstream which slowly fills with ice and needs to be cleaned out periodically. The first refrigerator trap was found to be necessary because water adversely affected the performance of the Valco pressure regulator. A 20 psig relief valve (V3 and V6) upstream of this glass trap exists as a safety precaution, in case of inadvertently over-pressurizing the line. After this cold trap sample air travels to a pneumatically operated four-way valve (V7) which selects between the two different intake lines. A solenoid valve (not shown) triggered by a computer controls the pneumatic actuator. Because I wish to always have both lines flushing continuously, the line not being sampled is bled off as exhaust with a flowrate and pressure controlled by

a manually-set needle valve and monitored with a rotameter type flowmeter and mechanical pressure gauge (valve, V8 and flowmeter, F1). The intake line selected as sample air then passes through a 220 mL cryogenic, stainless steel cold trap at -80°C , and then to a second pneumatically operated, solenoid-controlled, four-way valve (V9). This valve selects between sample air or a calibration gas. From V9, sample air or calibration gas continues on to the paramagnetic analyzer. The air stream not continuing to the analyzer has the potential to be flushed at two different flowrates, controlled by valves V10, V11, V12 and V13. When calibration gases are being analyzed, flushing before and during analysis occurs via this exhaust setup. When sample air is being analyzed, both solenoid valves V10 and V12 are closed and nothing is flushed through this port.

Finally, a third pneumatically operated four-way valve (V14) selects between the sample air/calibration gas stream or the working gas stream. The gas stream not passing through the analyzer at any given time is vented through the second exit port of this four-way valve. The system downstream of this four-way valve is almost identical to the system described in Chapter 3, Section 3.2.1, and shown in Figure 3.1 from valve V2 onwards and therefore is only very briefly discussed here. From this point the air stream to be analyzed travels to the Servomex paramagnetic analyzer sensor housed in the active temperature controlled aluminum box. Very precise pressure control in the analyzer cell is achieved with a ± 1 torr full scale differential pressure gauge and a solenoid valve (V18) servoed to an electronic pressure controller. The reference side of the differential pressure gauge consists of a "Pressure Reference" volume filled with air to about 960 torr. Differences from the setup in Chapter 3 include removal of the relief

valve as discussed above; no “coarse” active pressure control; an additional cold trap at -80°C (T6); and an additional solenoid valve on the purging side of four-way valve (V15). The coarse pressure control was excluded as a cost-saving measure and because I found it to be unnecessary once I employed the Valco pressure regulators (V2 and V5). The additional cold trap is a small, 40 mL trap which serves the purpose of ensuring that all calibration gases, working gas, and sample air passing through the analyzer are dried to the same dewpoint. Previously, working gas did not pass through a cold trap and this was shown to be problematic. The solenoid valve, V15, was added to enable shutting off of the working gas purge flow during the first 5 min of a sample air jog, as described above.

Calibration gases are housed horizontally in a thermally-insulated enclosure similar to that described in *Keeling et al.* [1998]. Each calibration gas is connected to a two-stage high pressure cylinder regulator (Scott Specialty Gases, Model 14 Series). These regulators are mounted on a manifold on top of the insulated enclosure and are connected to the high pressure cylinders with 1/16th inch Nickel alloy tubing (Valco Instruments, Nickel 200). Presently I have only four calibration gases, but the system has been designed to be expandable to eight. 1/8th inch stainless steel tubing travels from the low pressure side of each regulator to an 8-position multi-port selector valve (Valco Instruments, Model ESD8MZ-220) interfaced to the computer which can select one of the eight gas lines. The outlet from the multi-port valve is connected to the four-way valve, V9, described above.

Prior to analyzing a calibration gas, it is flushed through F2 at a flowrate of 300 mL/min for 10 min which I call the “fast purge”. Typically a calibration gas will be

analyzed over five separate 6-min jogs with 6-min working gas jogs between calibration gas jog. After the initial fast purge of calibration gas, whichever gas is not being analyzed at any given time is flushed at a “slow purge” flowrate of 100 mL/min, roughly equivalent to the flowrate through the analyzer side of the system. Details on the results obtained from analysis of all calibration gases during the period from June 1999 to June 2000 are given in section 4.2.4 below.

A computer program written in LabVIEW controls the paramagnetic O₂ system. The program handles all switching of solenoid valves, acquisition of data from the paramagnetic O₂ analyzer, acquisition of other important system parameters such as temperatures, pressures, and flowrates in the system, and acquisition of meteorological data and CO₂ concentration data which is sent from another computer running the Baring Head continuous CO₂ system. In addition the program generates five different types of output files, including data processed with relevant calibration information in order to present final results in per meg units. These output files are discussed in Appendix 1.

A modem and software package called pcANYWHERE allow dial-in from anywhere in the world, and full, remote control of the Baring Head O₂ computer. The LabVIEW program includes a user-interface that provides the user with manual control of all solenoid valves, allowing diagnostic tests and valve switching to be carried out remotely. Most critical system variables including pressures, temperatures and flowrates in the system are also displayed on the computer screen by the LabVIEW program. In this manner I am able to diagnose and solve many problems remotely from the U.S.A. A gateway computer situated at NIWA and connected to the internet provides a link to

the Baring Head computer, thus necessitating only a local telephone call to the Baring Head O₂ computer modem, avoiding the prohibitive costs of long-distance phone calls, and increasing the speed of transmission.

4.2.4. Calibration Procedures and Results

Before I present and discuss ambient data collected at Baring Head I will show results from measurements of the various calibration gases used at Baring Head. From this analysis, information on the precision and long term stability of the paramagnetic analyzer can be obtained. The suite of calibration gases consists of working gases, high span (HS) and low span (LS) gases, and several long-term archives. Working gas cylinders last between two and three months before they need to be refilled, HS and LS cylinders are expected to last approximately two years, and long term archives are expected to last 20 years or longer. Currently I have only two archive cylinders, but at the time of writing two more are about to be added to the system. Phasing in of new HS and LS cylinders will be staggered so that no two cylinders are ever replaced simultaneously. In this way I can perpetuate an independent “per meg scale” at Baring Head. Initially my scale was locked-in to the scale defined in Ralph Keeling’s laboratory at Scripps Institution of Oceanography. The first two HS and LS cylinders, two working gas cylinders, and the two archive cylinders were analyzed for O₂/N₂ ratios a series of times over a four-month period in 1997 on the interferometric analyzer in the Keeling laboratory. The results from these measurements are shown in Figure 4.5. Table 4.1 shows the mean and standard deviation for each cylinder derived from these measurements. CO₂ data are also shown in the table, calculated from concurrent CO₂

Table 4.1. Interferometric Declared Concentrations of Calibration Gases

Cylinder ID	Description	O ₂ /N ₂ (per meg)	σ (per meg)	CO ₂ (ppm)	σ (ppm)
CC66591	Archive	-291.8	1.7	366.55	0.01
CC66736	Archive	-197.8	2.9	366.40	0.01
ND10274	HS	-40.8	3.1	357.84	0.02
ND10277	LS	-428.7	2.9	358.13	0.01
ND10273	WT1	-231.4	2.6	359.41	0.02
ND10280	WT2	-230.1	2.7	359.57	0.02

measurements made on a Siemens NDIR analyzer at Scripps. With all six cylinders having standard deviations in O₂/N₂ of 3 per meg or less over the four-month measurement period, I felt confident in transporting these cylinders to New Zealand and beginning an independently maintained per meg scale on-site.

Two methods will be used to verify that the Baring Head scale and Keeling laboratory scale remain comparable over time. First, flask sample measurements will be obtained approximately once every two months at Baring Head, sent back to Scripps, and analyzed on the interferometric analyzer. Results from these flask analyses will be compared with the continuous measurements obtained from the paramagnetic analyzer at Baring Head. Second, approximately annually, one or two of the archive cylinders will be transported back to Scripps and also analyzed on the interferometric analyzer to verify that their concentrations have not changed over time. Unfortunately technical and logistical constraints have prevented such analyses thus far. In the coming months after my Ph.D. is completed, I expect both methods to be actively employed.

Every day five jogs each of the HS and LS are run against the working gas. From the declared O₂/N₂ ratios of the HS and LS defined by the interferometric analyses

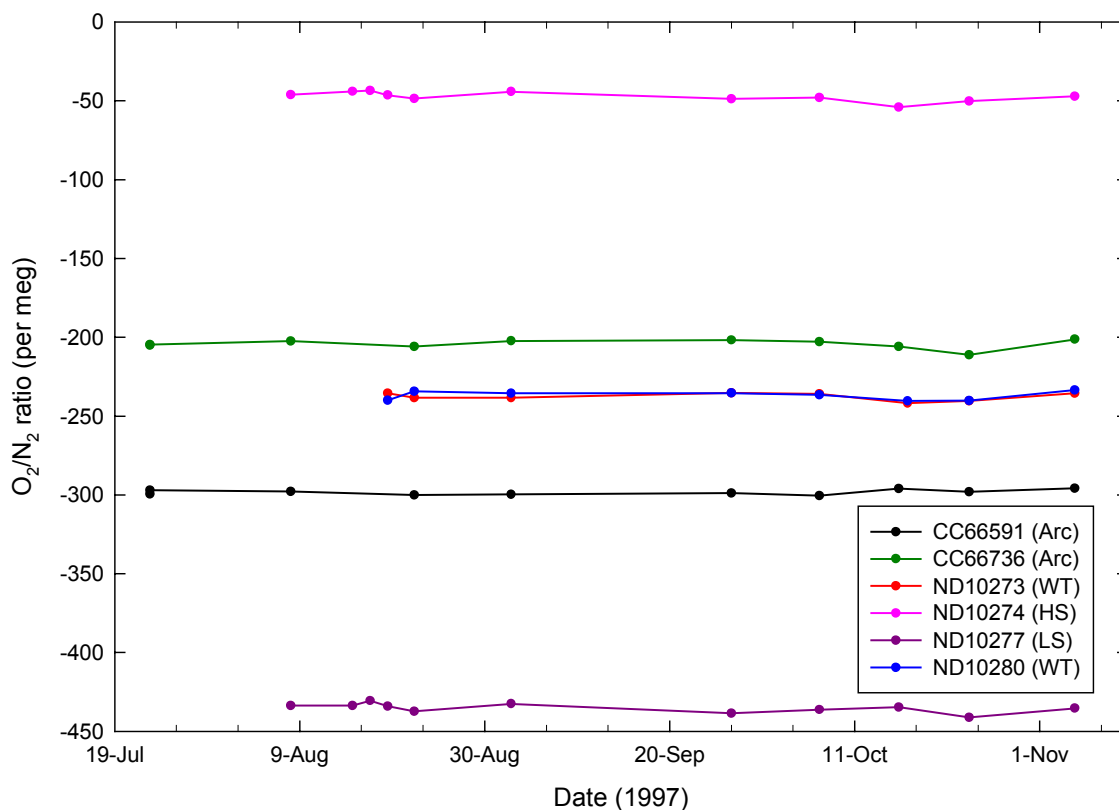


Figure 4.5. Shows the O_2/N_2 ratios calculated on the interferometric analyzer at Scripps of the calibration gases used at Baring Head. “Arc” indicates long-term archive gas cylinders, “WT” indicates working gases, and “HS” and “LS” are high span and low span gases respectively. All gases show good stability in O_2/N_2 ratios over a three to four month period.

(Table 4.1), I can then calculate a daily value for the O_2/N_2 ratio of the working gas. I assign this value for the next 24 hours, until the next HS/LS calibration runs and recalculates the working gas ratio. Figure 4.6 shows the results of these calculations. Five different working gases have been used in the first 12 months of operation, and these are shown labeled above the data in the figure. Small downward trends are apparent in the working gas concentrations over time. This is probably demonstrating a real change in O_2/N_2 ratio in the cylinders and is most likely owing to decreasing

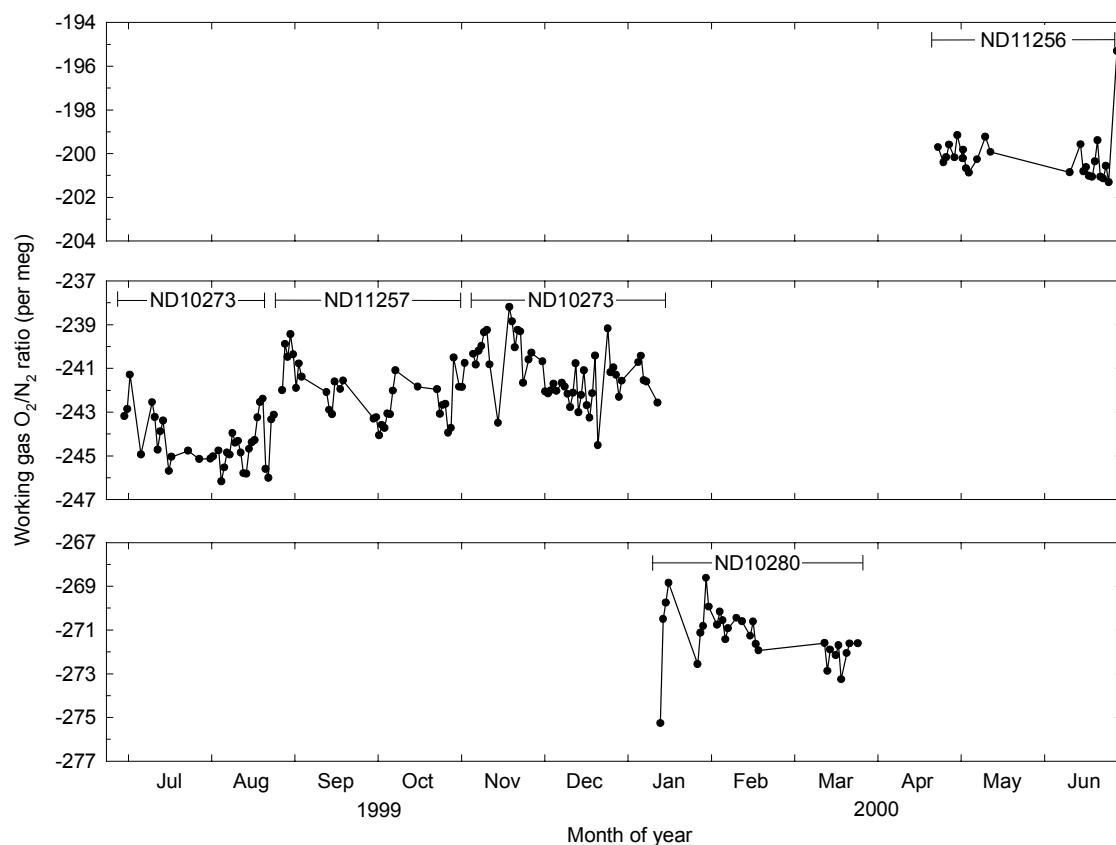


Figure 4.6. Working gas O₂/N₂ ratios as calculated from daily calibrations of the working gas against the high span and low span cylinders. Five different working gases have been used in the first year of operation at Baring Head, as labeled in the figure. Each panel shows a 10 per meg range, showing that the working gases are very stable over their lifetime.

cylinder pressure resulting in desorption from the tank walls, as discussed in *Keeling et al.* [1998]. Standard deviations of each working gas over its lifetime range between ± 1.2 and ± 1.3 per meg, with between 30 and 50 total daily calibration analyses. Several gaps can be seen in the record of Figure 4.6. These are because of ‘bad’ calibrations, or analyzer down-time. Continuous atmospheric O₂ measurements are in their infancy, and technical and programming problems continue to arise. With the very limited personnel support that NIWA was able to provide, only traveling to the station once

every two weeks, problems could not always be addressed and fixed immediately, resulting in the gaps shown in Figure 4.6, and also in the data itself shown in section 4.3 below. I am confident that in the near future as we continue to learn more about the system and improve various programming and technical designs, these problems and associated bad calibrations and down-times will become relatively infrequent.

The second purpose of the daily HS/LS calibration is to define the “span” or the “sensitivity” of the paramagnetic analyzer. From the declared O₂/N₂ ratios of HS and LS I calculate the difference in concentration between these two gases and by relating this to the difference observed from each daily calibration in mV from the analyzer output, I obtain a daily value for the O₂ span of the analyzer. Figure 4.7 shows the results of this calculation and shows the paramagnetic analyzer span to be remarkably constant over time. The standard deviation on one year of daily calculations of the O₂ span was 0.017 per meg/mV, or 0.4% of the mean.

Table 4.2 summarizes typical uncertainties obtained with the paramagnetic analyzer system at Baring Head over different time periods and different subsets of data. Raw data are written to output files once every 30 seconds, and are a mean of 30 one-second readings. Typical uncertainty for such a reading is 0.7 per meg. A working gas jog runs for 6 min, but I remove the first 3 min from the data analysis as described above, and a typical uncertainty for the mean of this final 3-min period is 0.9 per meg. As discussed above, typical standard deviations for the working gas concentration derived from the daily HS/LS calibration over the entire lifetime (two to three months) of the working gas is 1.3 per meg, remarkably close to the uncertainty calculated for one 3-min jog. This shows that my working gases are very stable over time intervals of days

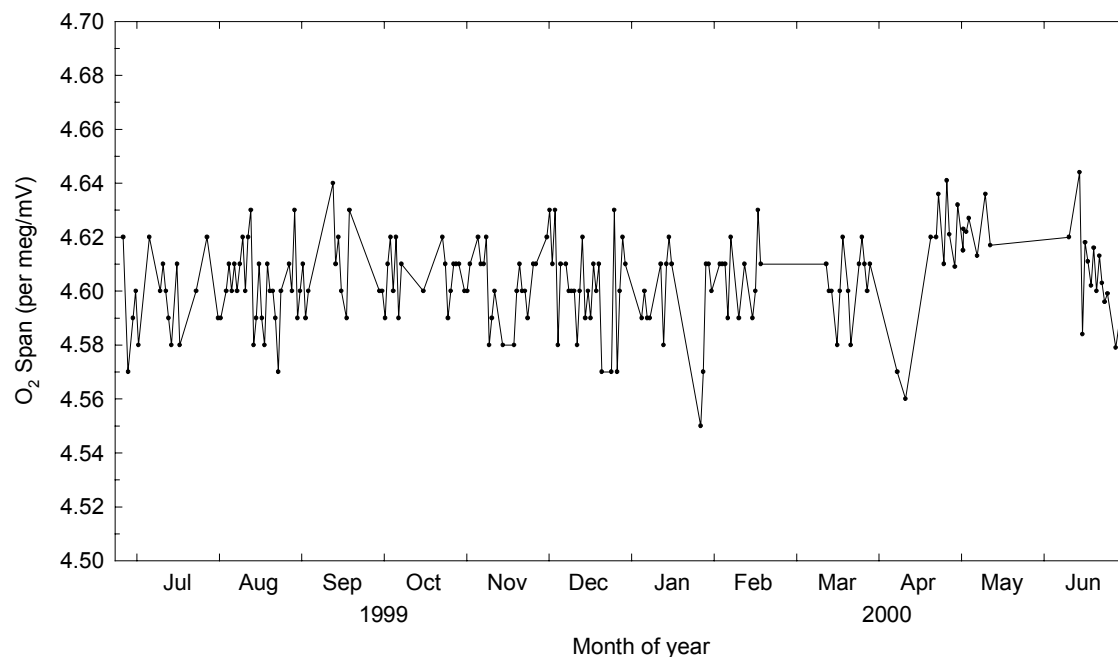


Figure 4.7. Paramagnetic O₂ analyzer span, in units of per meg/mV, calculated daily from the calibration with the high span and low span cylinders. The range of the analyzer span over a full year of operation is less than 2% of the average. Note that the span was reported to only two decimal places prior to 22 April 2000, accounting for the apparent discretized nature of changes in span from day to day prior to this date.

to months. Finally I calculate a typical uncertainty of 1.5 per meg for reporting 5 min “clean” air jogs. In a similar manner as for working gas jogs, the first 4 min of each 9-min air jog is removed from this analysis. This uncertainty is derived as the quadrature sum of uncertainties from both working gas jogs on either side of the air jog, and the air jog uncertainty itself. I calculated this value by analyzing data when ambient air was stable thus minimizing real air variability from contributing to this uncertainty calculation.

The purpose of the archive tanks is to assess whether the O₂/N₂ ratios of the HS and LS cylinders change over time. The method I use for calculating O₂/N₂ ratios from

Table 4.2. Typical Uncertainties in Paramagnetic O₂ Analyzer System

Description	Uncertainty ¹ (per meg)
30 sec mean of 1-sec readings	0.7
3 min working gas jog	0.9
working gas over its lifetime (approximately 2 months)	1.3
5 min “clean” ambient air jog	1.5
O ₂ span (one year period from June 1999 to June 2000)	.017 ²

¹ All uncertainties are calculated as 1- σ standard deviations.

² Units are per meg/mV

ambient air is based on the daily calibration of the working gas against the HS and LS cylinders and depends on the declared O₂/N₂ ratios for the HS and LS cylinders as calculated from the analyses carried out on the interferometric analyzer in 1997 (Figure 4.5 and Table 4.1). Periodic analyses of the archive cylinders provide a cross-check on the long term stability of the HS and LS cylinders and thus the per meg scale as defined by these two cylinders. The most likely cause of drift in the HS and LS cylinders is owing to desorption from the tank walls, which in turn is more likely to happen as the cylinder pressure decreases. Therefore analyzing these cylinders against archive cylinders which are still at relatively high pressures checks for this possibility.

With only one year of data it is too early to assess whether these cylinders or the per meg scale have drifted. I have analyzed the two archive cylinders six times in the first year. The results show one of the cylinders (CC66736) to be 51±19 per meg lower than the declared value from the interferometric analyzer in 1997. This result is troubling, and at the time of writing I am in the process of investigating possible causes of the offset and high variability from analyses of this cylinder, and I will probably ship it back to Scripps for further testing. The six analyses of the second archive cylinder

(CC66591) resulted in a mean concentration of -289.0 ± 9.0 per meg. This compares very favorably with the mean value of -291.8 ± 1.7 derived from the analyses on the interferometric analyzer at Scripps in 1997.

The large standard deviation of ± 9.0 per meg is of concern, however. When I examined the results more closely, it became apparent that the five jogs measured on a given day of this archive gas became successively more negative in O_2/N_2 ratio. This trend was consistently observed for all six analyses of this cylinder over the one-year period. An example of this observation is shown in Figure 4.8, showing data output from both archive cylinders from an analysis on 26 November 1999. In this figure, working gas concentration, at around -240 per meg, displays the typical variability I expect from a cylinder analysis. Both archive cylinders exhibit significantly greater variability than this, and CC66591 shows a persistent downward trend from one jog to the next, with a range of 25 per meg. Note that each archive cylinder was measured over 5 six-minute jogs. The figure also shows ten minute jogs prior to the first of each archive cylinder jog, and this is in fact ambient air which is passed through the analyzer while the archive cylinder is being flushed. I believe that the reason for this persistent trend observed in CC66591 is because of insufficient flushing of the archive cylinders before they are analyzed. Future analyses will address this problem, and hopefully more precise values will result.

Flushing of the archive cylinders follows the same protocol as flushing for HS and LS cylinders described above. No flushing problems, however, were observed for HS and LS cylinders. This demonstrates that the problem most likely lies with the conditioning of the interior walls of the stainless steel and nickel tubing used to deliver

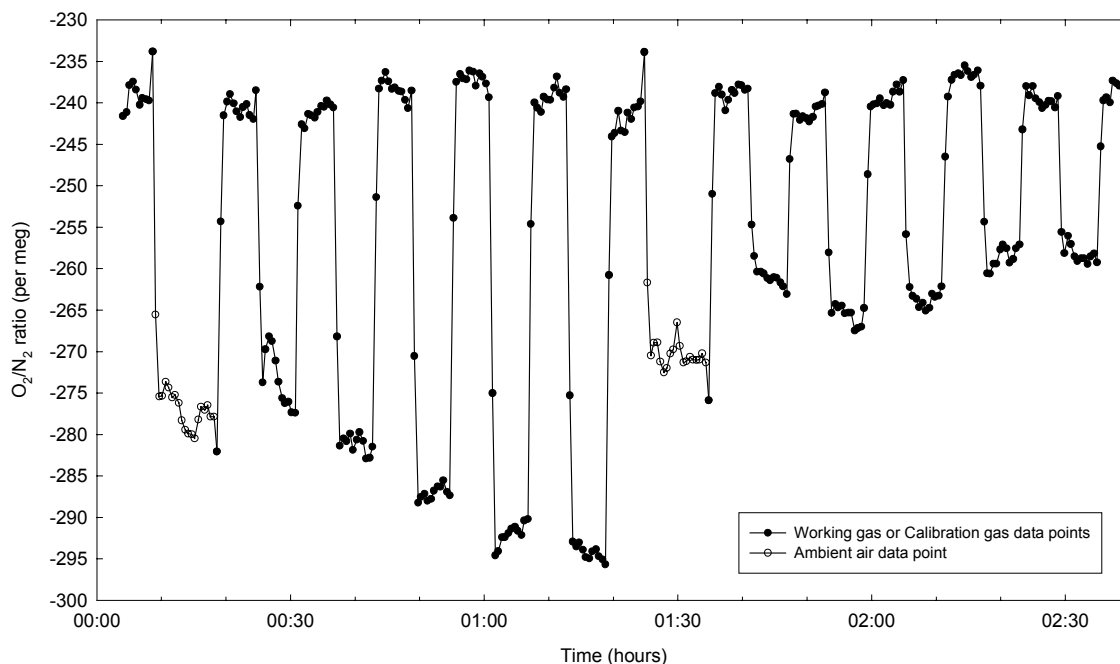


Figure 4.8. Illustrates the pronounced drift in one of the Archive calibration gases, where a downward drift of 25 per meg can be seen from the first to the fifth jog. In comparison, the working gas jogs, at approximately -240 per meg, show much greater stability over time. In contrast to Figures 4.2 and 4.3, data points shown here are not every second, but 30 second averages.

these gases to the system. Each cylinder has a length of tubing unique to that cylinder, from the cylinder valve to the multi-port Valco valve. In the case of the HS and LS cylinders, the gas in this tubing remains in a static state for a maximum of one day, whereas for the archive cylinders, the gas can remain static in the tubing for up to two months, therefore it is plausible that these archive cylinders require a longer flushing period.

4.3. The First Year of Data

4.3.1. Seasonal Cycle Observed at Baring Head

Figure 4.9a shows the full O_2/N_2 ratio dataset collected from Baring Head from inception on 26 June 1999 to 1 July 2000. As explained earlier, gaps in the data are owing to unsuccessful calibrations or analyzer downtimes. I am optimistic that continued improvements to the setup at Baring Head and the knowledge that I have gained from the first year of operation will result in a significant reduction in the size and frequency of these gaps in future years.

In general, data are concentrated at higher values, with episodic events of large decreases in O_2/N_2 ratio of up to 100 per meg. These low O_2/N_2 events typically correspond with high CO_2 events, as shown in Figure 4.9b, which shows concurrent atmospheric CO_2 measurements made at Baring Head with a Siemens NDIR analyzer. These plots have been scaled so that O_2/N_2 ratios and CO_2 concentrations can be compared visually on a mole to mole basis. Usually these episodic events are caused by diurnal cycling in land biotic photosynthesis and respiration processes. Net respiration during the night causes a decrease in O_2/N_2 ratios and an increase in CO_2 concentrations, whereas during the day there is net photosynthesis and the reverse occurs. Occasionally, when the winds at Baring Head are from the west or northwest, an anthropogenic influence from the city of Wellington results in a similar decrease in O_2/N_2 ratios and increase in CO_2 concentrations. The meteorological conditions at Baring Head do not often result in winds from this sector, however, and most often the concentration changes observed can be attributed to land biotic processes.

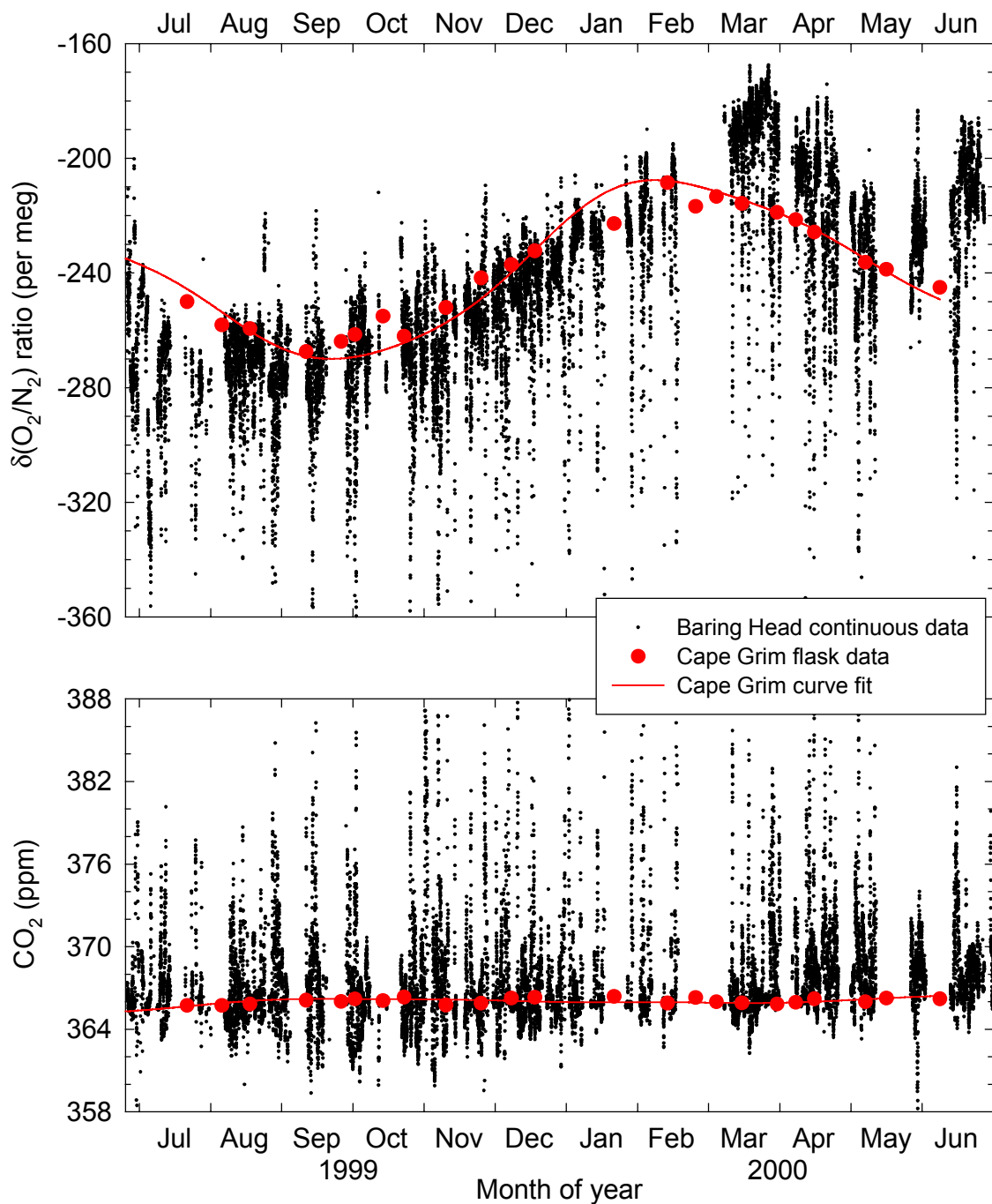


Figure 4.9. Shows all O_2/N_2 ratio and CO_2 concentration data collected at Baring Head from June 1999 to July 2000. Each black data point is an average over 15 minutes. Red data points show flask samples collected at Cape Grim, Tasmania (see Figure 4.1) during clean, background air conditions as a part of the Scripps O_2/N_2 flask sampling network. The red line is a curve fit to the Cape Grim data.

A clear seasonal cycle can be seen in O_2/N_2 ratios with a minimum occurring at the end of winter, in late August or early September, and a maximum occurring in late March, at the end of summer. No seasonal cycle is apparent in the CO_2 data, at least not at the scale shown in Figure 4.9b. This suggests that almost all of the seasonal cycle in O_2/N_2 can be explained by oceanic processes, and this is confirmed in Figure 4.10 which shows the oceanic-only influence on the O_2/N_2 ratios, as defined by Atmospheric Potential Oxygen (APO, see section 2.2.2. for a definition) showing a similar amplitude in the seasonal cycle of APO as in O_2/N_2 ratios. O_2/N_2 ratios (and APO) increase in spring and summer because of increased photosynthetic activity in the oceans producing dissolved O_2 , and because of shoaling of the mixed layer of the ocean which acts to concentrate this O_2 in the surface waters, supersaturating these waters, and driving a net flux of O_2 into the atmosphere. In addition, warming of the surface ocean in the spring and summer reduces the solubility of the water, causing further O_2 supersaturation and adding to the O_2 flux to the atmosphere. This activity peaks in March, then biological activity decreases producing less O_2 , the surface ocean cools becoming more soluble, and the mixed layer deepens, incorporating O_2 -depleted waters into the surface layer. These processes all act together to produce a net demand of O_2 to the atmosphere and the O_2/N_2 ratio (and APO) is observed to decrease.

Whereas O_2/N_2 ratio and CO_2 concentration data display asymmetric patterns, with O_2/N_2 ratio scatter falling below the baseline and CO_2 concentration scatter occurring above the baseline, APO data in Figure 4.10 shows more symmetric scatter, and less overall scatter to the data. This observation further demonstrates that for the most part, O_2/N_2 ratios and CO_2 concentrations are anti-correlated.

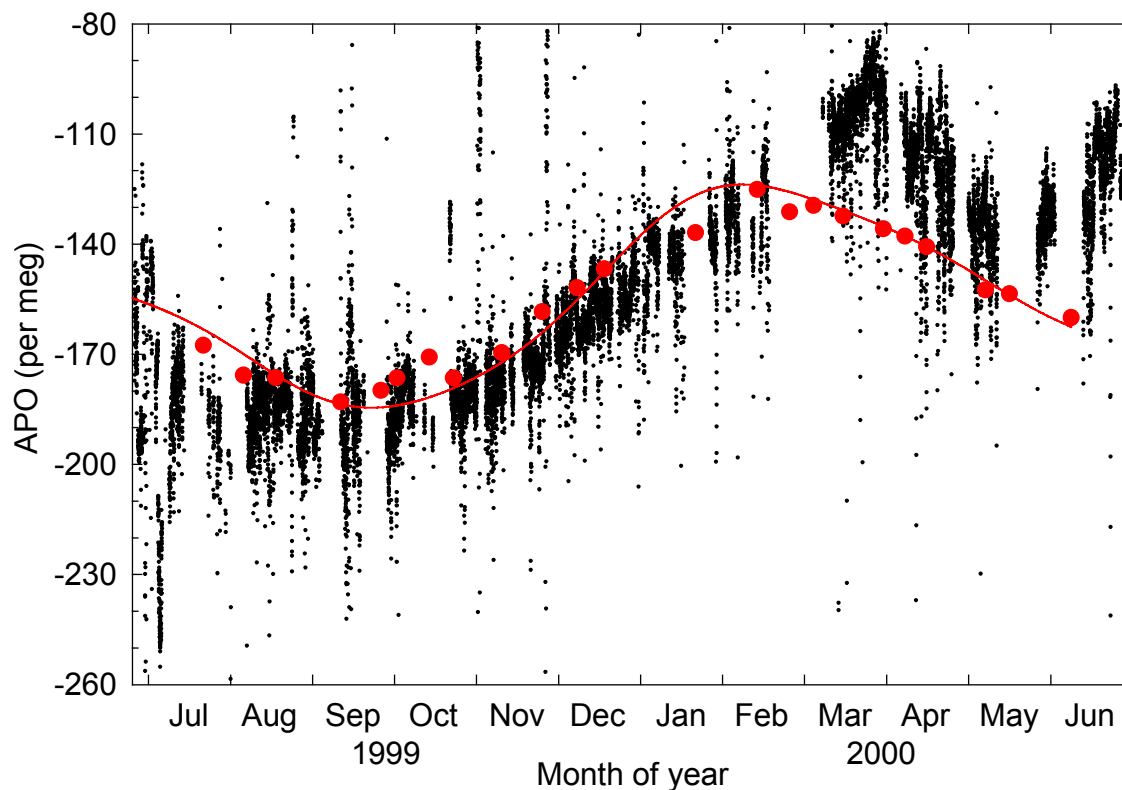


Figure 4.10. Atmospheric Potential Oxygen, APO, at Baring Head from June 1999 to July 2000. This shows the oceanic influence on the air arriving at Baring Head.

Also shown in Figures 4.9 and 4.10, as red symbols, are flask samples collected at Cape Grim, Tasmania (40.7°S, 144.7°E) as part of our global flask sampling network (Chapter 2). These flask samples are shipped back to our laboratory in La Jolla, California, where they are analyzed for O_2/N_2 ratio on our interferometric analyzer [Keeling, 1988] and for CO_2 concentration on a Siemens NDIR analyzer. Curve fits to the Cape Grim data are also shown, consisting of the sum of a four-harmonic seasonal cycle and a stiff spline. The curve fits were calculated from a longer dataset not shown, extending back to 1991.

Cape Grim flask samples are collected only when meteorological conditions are such that the air sampled is thought to be representative of a large, regional area of the mid-latitudes of the southern hemisphere, not influenced by local or regional anthropogenic or land biotic processes. Therefore, because Cape Grim is at a similar latitude as Baring Head, I can expect reasonable agreement between the two stations, when Baring Head data are also not influenced by these processes. Therefore, in general, I would expect the high O_2/N_2 ratios and low CO_2 concentrations from Baring Head to show reasonable agreement with the Cape Grim data. As illustrated in Figure 4.9a, such agreement for O_2/N_2 ratios is true from July 1999 to February 2000. In March 2000 the Baring Head trend departed significantly from the Cape Grim trend, showing O_2/N_2 ratios elevated by as much as 40 per meg. A similar trend is seen in the comparison of the APO data. From the CO_2 data in Figure 4.9b, it is difficult to determine if Baring Head and Cape Grim records are in agreement.

To investigate the comparison between the two stations in greater detail I have filtered the Baring Head data to only retain data collected under southerly wind conditions, when the local wind direction was between 135° and 225° , and when the local wind speed was greater than 20 km/h. For the most part, these data will be uninfluenced by anthropogenic or land biotic processes, representing air masses recently originating from the Southern Ocean, and thus comparable to Cape Grim flask data. Figure 4.11 shows these filtered data for O_2/N_2 ratios and CO_2 concentrations, and Figure 4.12 shows APO filtered data. Both figures include the same Cape Grim data and curves.

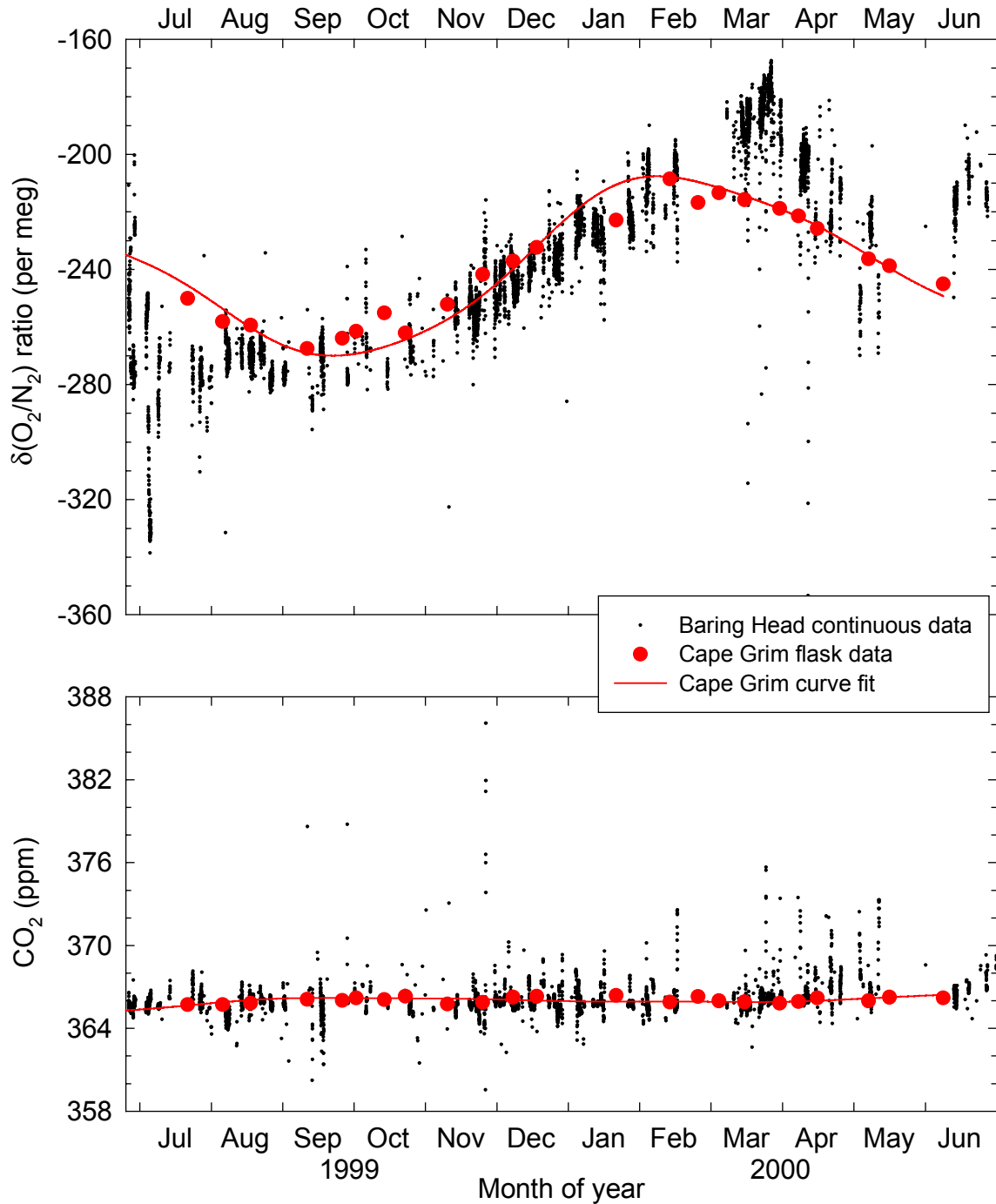


Figure 4.11. As for Figure 4.9, except data have now been filtered to only show data when conditions are thought to be representative of clean, background air. That is, the wind direction is between 135° and 225° , and the wind speed is greater than 20 km/h.

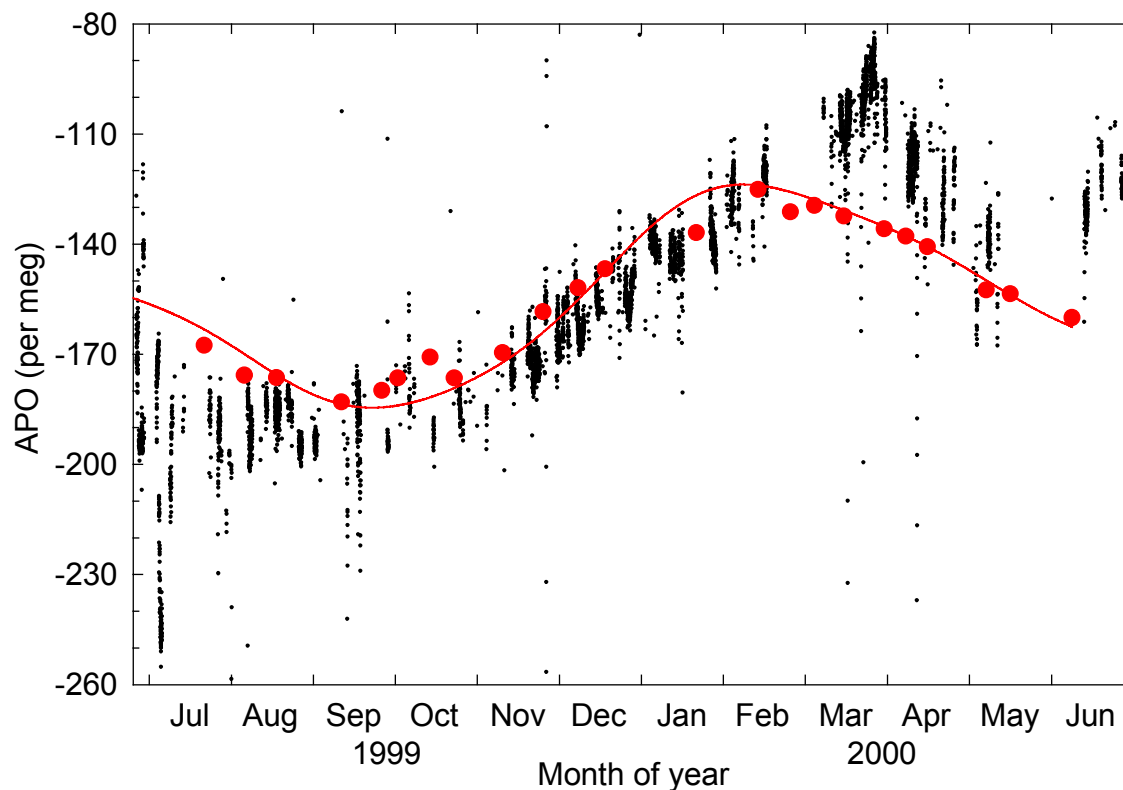


Figure 4.12. As for Figure 4.10, except data have now been filtered to only show data when conditions are thought to be representative of clean, background air, as in Figure 4.11. That is, the wind direction is between 135° and 225° and the wind speed is greater than 20 km/h.

Baring Head CO_2 data now show reasonably good agreement with Cape Grim for the one year record. O_2/N_2 ratio and APO data still show the same prominent differences observed in Figures 4.9a and 4.10. Ignoring for the moment data in June 2000, the March, April, and May 2000 data appear to indicate a later summertime O_2/N_2 (and APO) peak at Baring Head than Cape Grim and a subsequent faster drawdown of O_2/N_2 (and APO) in autumn. In addition, at the beginning of the record, in June and July 1999, there is tentative evidence for an earlier wintertime minimum in O_2/N_2 ratio

and APO. These two observations taken together suggest a more asymmetric seasonal cycle than observed from Cape Grim data. In addition, Baring Head data appear to show a larger seasonal cycle in O_2/N_2 ratio and APO. From Table 2.2, the average O_2/N_2 ratio seasonal amplitude at Cape Grim is 72 per meg, whereas the Baring Head data show a cycle of approximately 100 per meg.

Differences between Baring Head and Cape Grim such as discussed here could be owing to one of two things. There could be real differences in the air masses arriving at the two stations. Owing to the geographical position of the two stations, Baring Head receives “clean, background” air when the prevailing winds are meridional, coming from the south. Cape Grim on the other hand, although also receiving air derived from the Southern Ocean, requires zonal winds coming from the west for background conditions. This meteorological difference could contribute to observed differences between the two stations, where Baring Head receives air that is more recently derived from higher southern latitudes. This could explain the higher seasonal amplitude at Baring Head, whereby air masses arriving at Baring Head have recently been in contact with active zones of the Southern Ocean, thus experiencing high rates of air-sea exchange of O_2 . This possibility is analogous to the hypothesis given in section 2.3.1 to explain the large seasonal amplitude at Cold Bay, Alaska. However, it is interesting to note that an O_2/N_2 seasonal amplitude of 100 per meg at Baring Head is greater than that observed at any southern hemisphere station in our flask sampling network, including Macquarie Island at 55°S, which exhibited a seasonal amplitude of 91 per meg (in 1993).

Second, the differences observed could be partially due to the higher resolution features apparent in the Baring Head continuous record, compared with the discrete flask samples collected at Cape Grim. Even when Cape Grim flask samples are collected at the same time when there are Baring Head continuous data, because the two stations are sampling different air, a direct comparison is not very meaningful. Therefore a continuous record would be needed at Cape Grim to provide a good comparison of the two stations.

Baring Head data in June are particularly puzzling, exhibiting a rise in O_2/N_2 ratios of the order of 20 to 30 per meg at a time when this ratio is expected to continue decreasing. For a sustained period of several weeks in May and June, the region around Baring Head experienced very atypical weather conditions, with winds predominantly from the east and northeast and a stationary high pressure zone over much of New Zealand. In contrast, Cape Grim did not experience these unusual meteorological conditions.

Because the June 2000 data are recent, I have not completely ruled out the possibility of a calibration or other analytical problem being responsible for the anomalous O_2/N_2 ratios. However, preliminary checks of diagnostic parameters (temperatures, pressures, and flowrates in the system) and of calibration gas runs (see for example Figures 4.6 and 4.7 in June 2000) have not shown any problems with the June data. I will examine these data further in the near future, and I expect that the forthcoming July and August data will shed more light on this issue.

4.3.2. High Temporal Resolution Features in O₂ and CO₂ Concentrations

Figures 4.13 a through to f show monthly plots of APO and CO₂ concentration. For each month, I show oceanic (APO) and land biotic (CO₂) influences on the air masses arriving at Baring Head. For ease of comparison, all monthly plots have the same APO and CO₂ ranges. In addition, the y axes of APO and CO₂ have been scaled so that changes in O₂ and CO₂ are directly comparable visually on a mole to mole basis. Also shown for each month is the wind direction, shown as the cosine of the direction in degrees. Unfortunately there was a programming bug which resulted in northerly winds sometimes being misreported in these wind direction plots. The October 1999 plot in Figure 4.13b illustrates a good example of this problem, where horizontal “bands” can be seen for much of the month. In actuality, winds during the time where bands are shown were almost always northerlies. Despite this inconsistency I believe that the most important feature of these wind plots is still apparent, which is to distinguish between northerly and southerly winds. It should be noted that for the entire year-long dataset, 89% of all winds fall into the category of northerly or southerly, where northerly is defined as local wind direction between 315° and 45°, and southerly is defined as local wind direction between 135° and 225°. In other words, one half of the possible wind directions account for 89% of the observed winds. On 22nd April 2000, I installed a new version of the LabVIEW programming code and subsequent wind data shown are correct.

In general, these high resolution data show greater variability in CO₂ than APO, illustrating the faster response time of the atmosphere to changes in the land biota compared to changes in the ocean, where responses are significantly muted owing to the

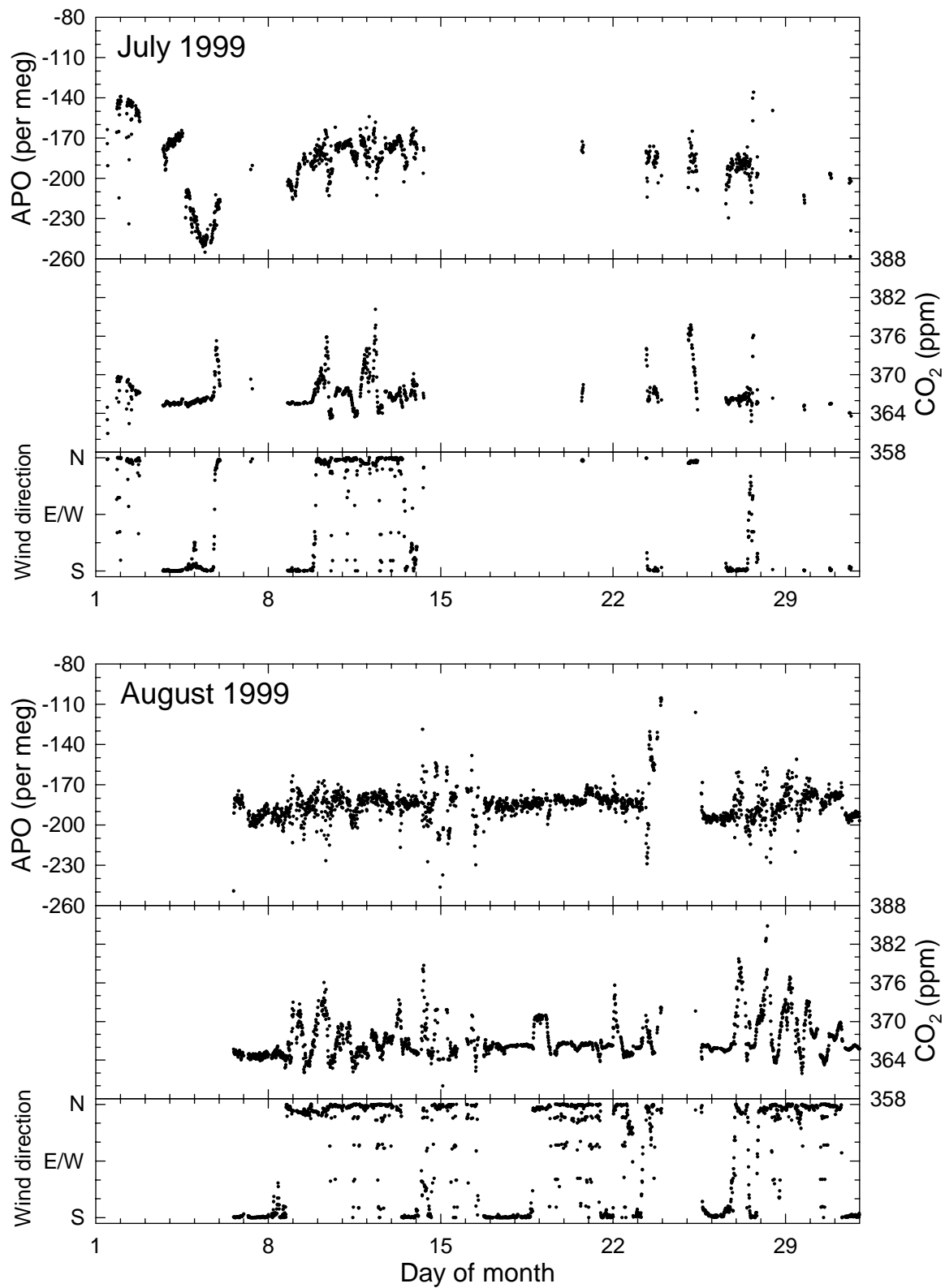


Figure 4.13a. APO, CO₂ and wind direction at Baring Head for July and August 1999. Wind direction is shown as the cosine of the direction in degrees.

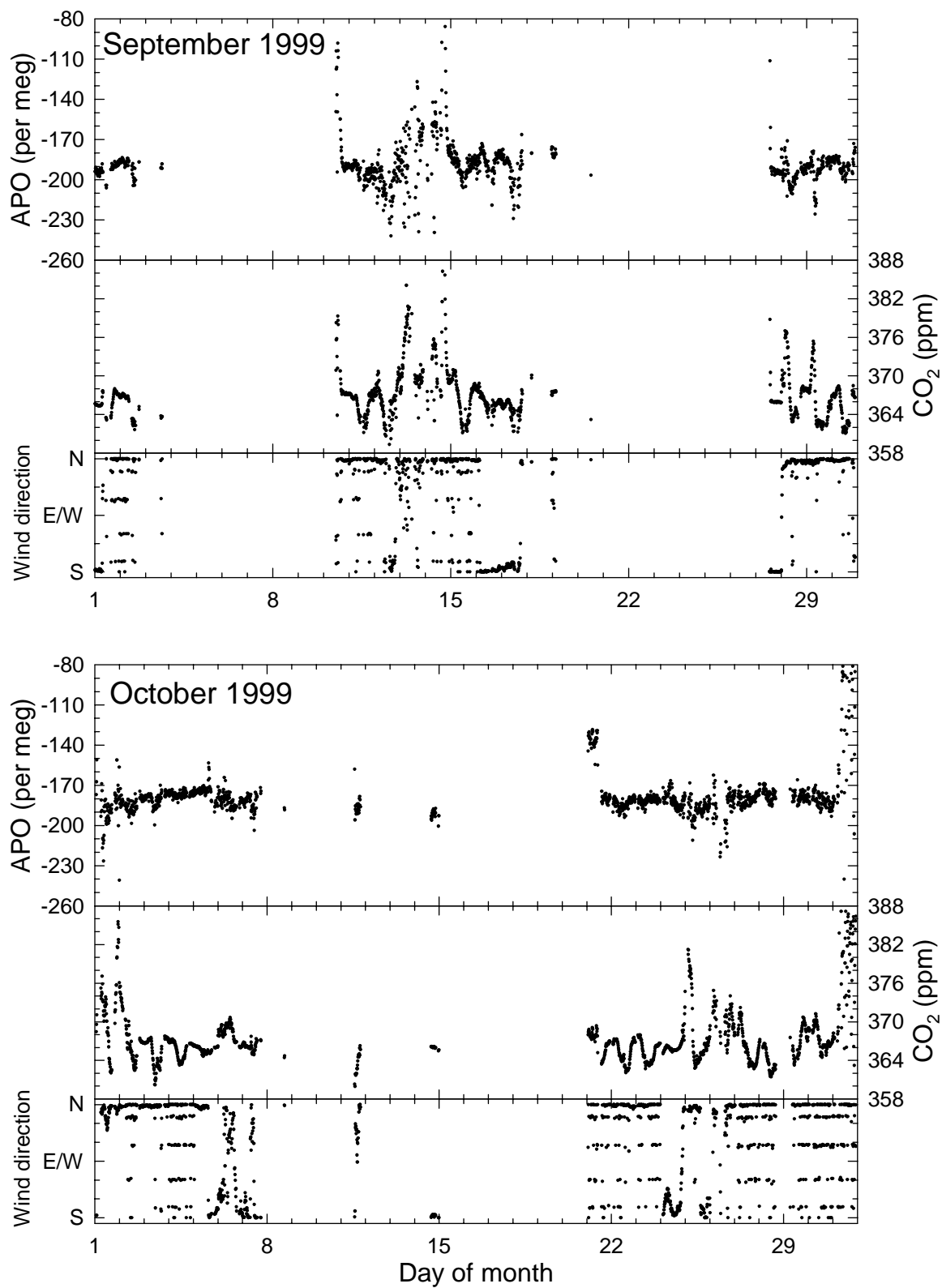


Figure 4.13b. APO, CO₂ and wind direction at Baring Head for September and October 1999.

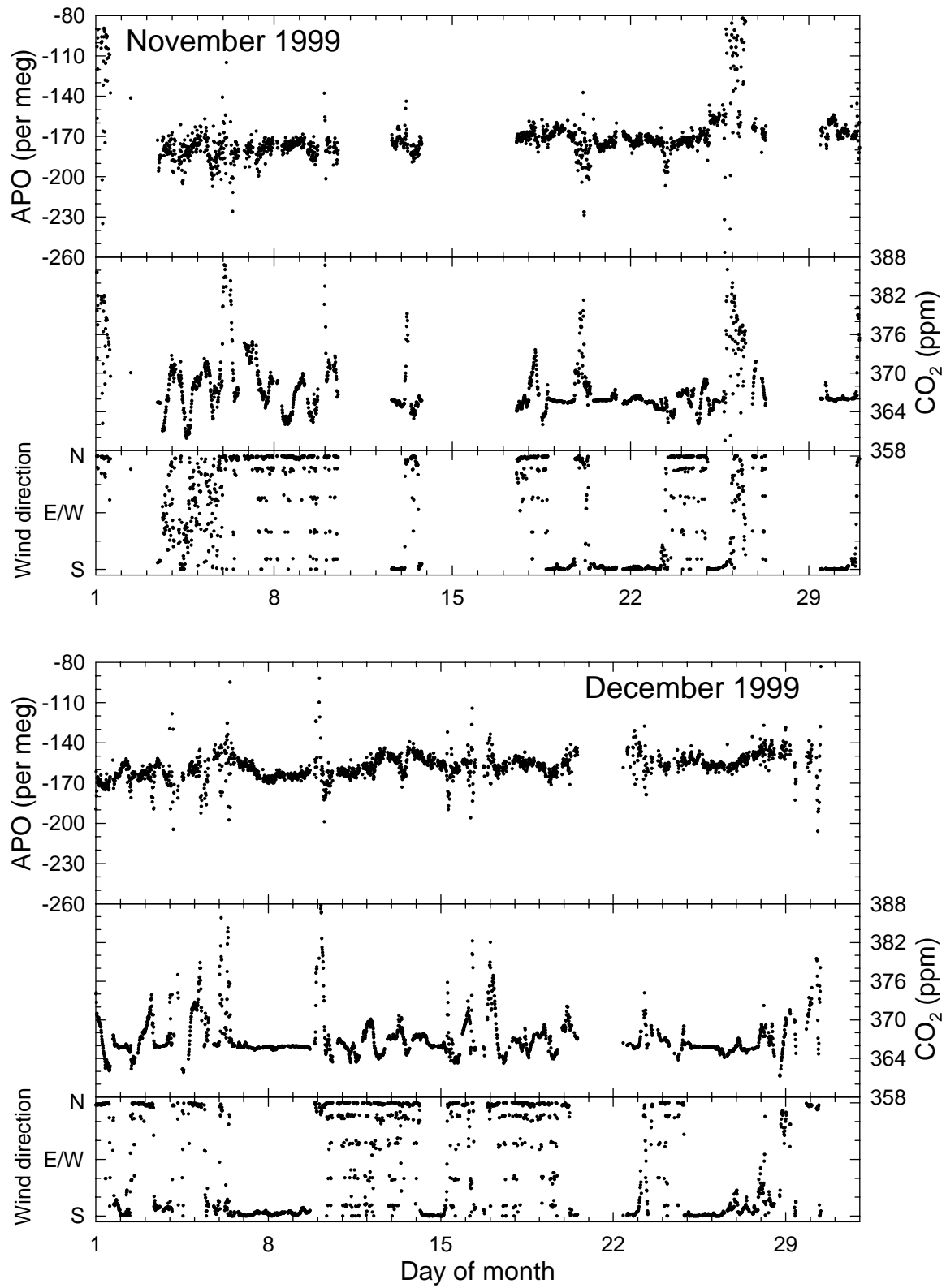


Figure 4.13c. APO, CO₂ and wind direction at Baring Head for November and December 1999.

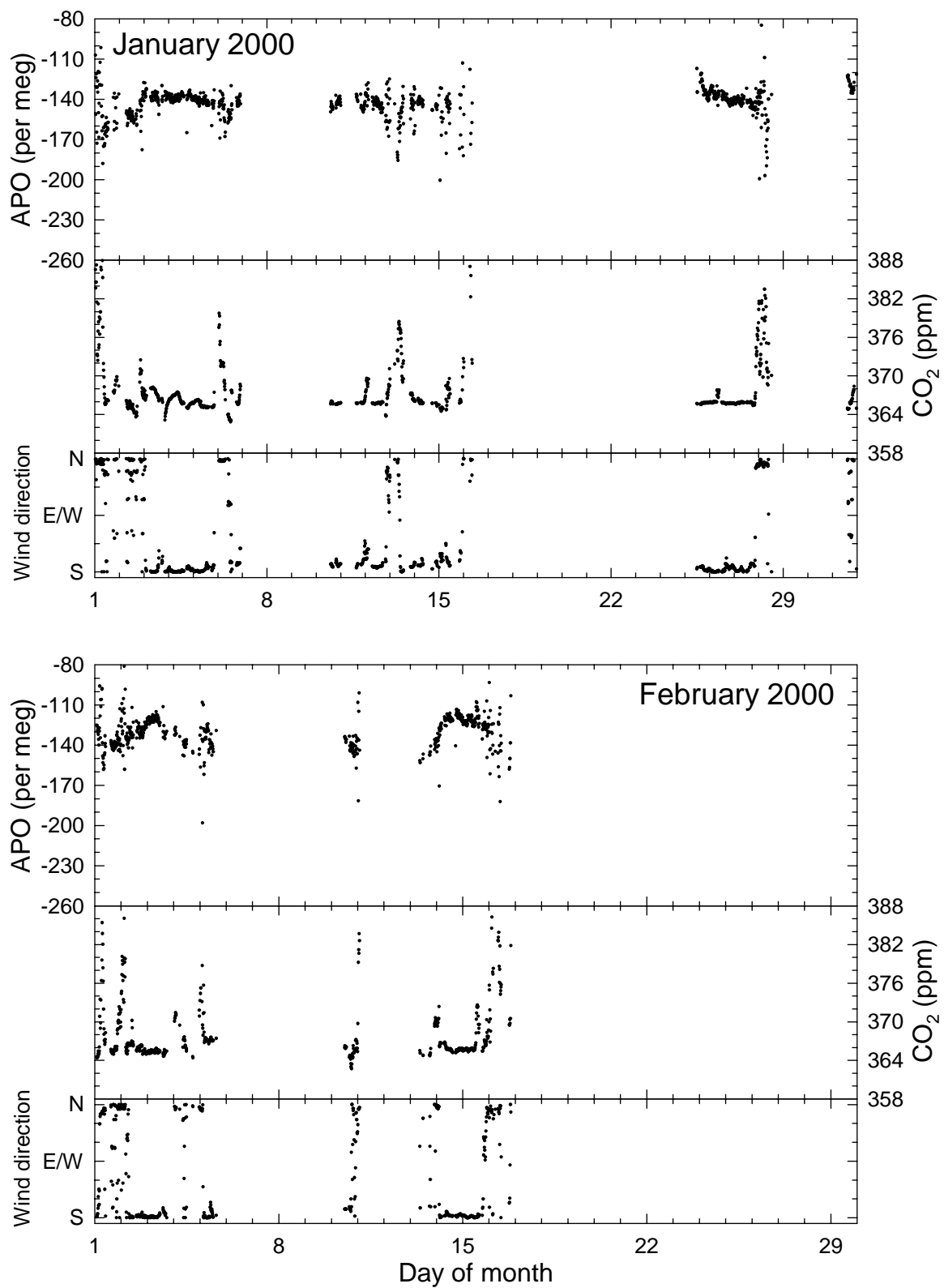


Figure 4.13d. APO, CO₂ and wind direction at Baring Head for January and February 2000.

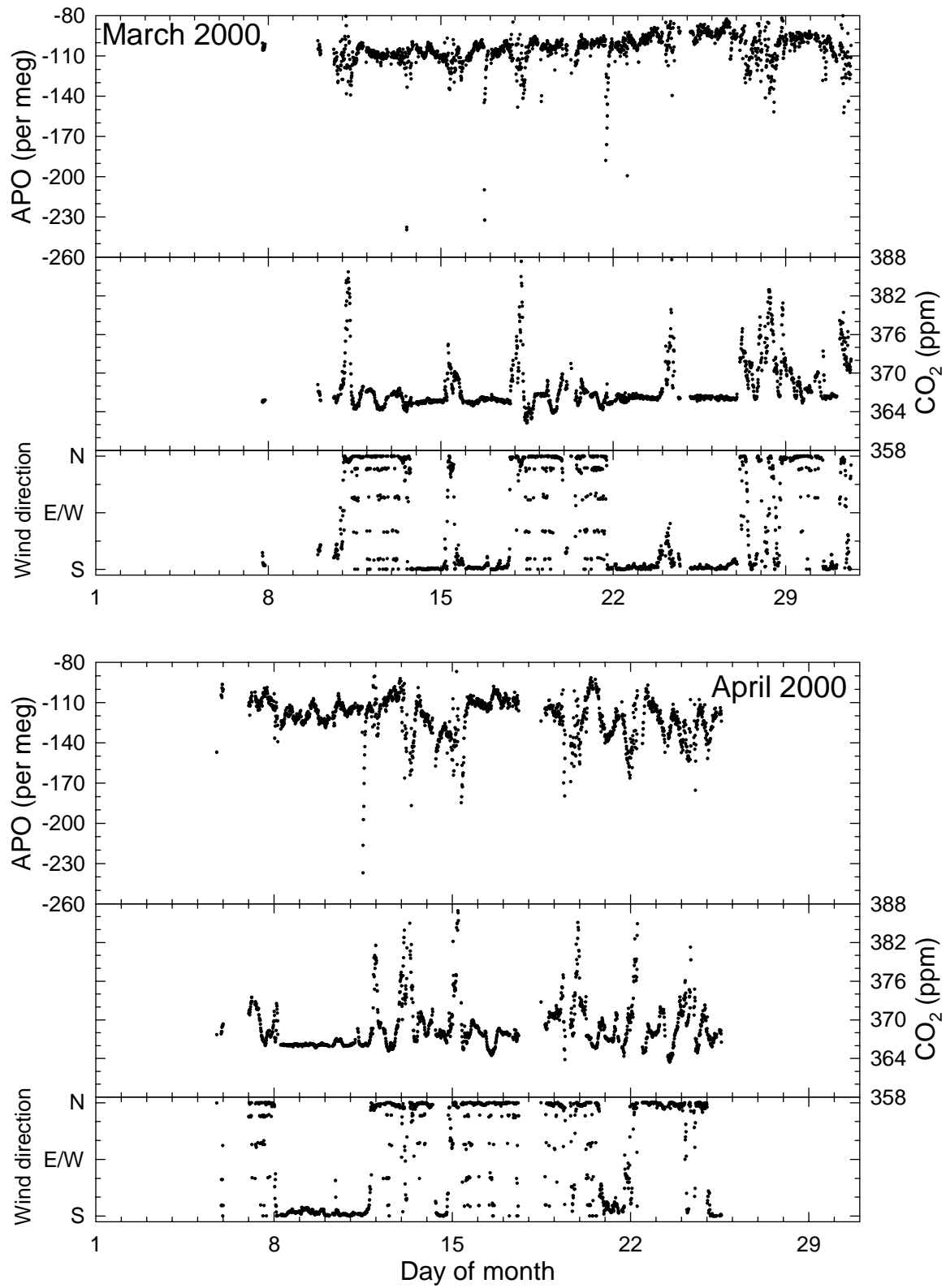


Figure 4.13e. APO, CO₂ and wind direction at Baring Head for March and April 2000.

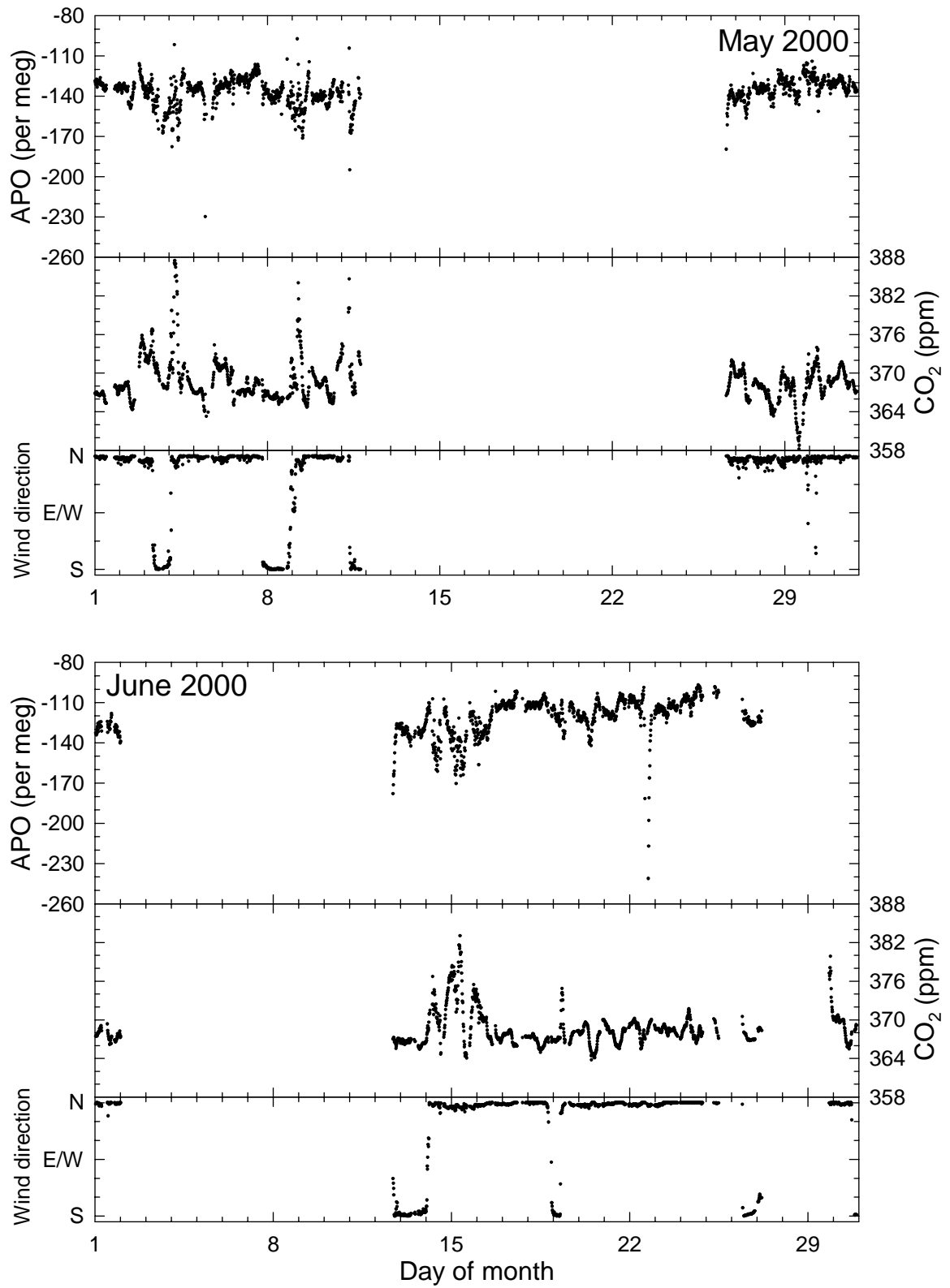


Figure 4.13f. APO, CO₂ and wind direction at Baring Head for May and June 2000.

barrier caused by air-sea gas exchange rates. Diurnal cycles can be seen in CO₂, typically only during northerlies, and these can reach amplitudes as high as 20 ppm, but 10 ppm is more typical.

4.4. Anomalous Events

An interesting feature was observed in the O₂/N₂ data over the period 3-5 July 1999. During this period meteorological conditions met “baseline” criteria, where such criteria are defined as wind direction in the appropriate sector (135° to 225°) and a wind speed above 20 km/h. This baseline criteria is set so that the air mass sampled at Baring Head, to a good approximation, will not have been influenced by local anthropogenic or land biotic sources or sinks of O₂ or CO₂. Generally at Baring Head, baseline conditions exist when the winds are from the south, recently derived from the Southern Ocean, and not having crossed the South Island of New Zealand.

The event that I analyze in detail here started at approximately 15:00, 3 July 1999 NZST when the wind direction at Baring Head suddenly changed from a northerly to a southerly, and continued until about 18:00, 5 July 1999 NZST, when the wind direction changed back to a northerly. During this entire event the wind speed was between 35 and 85 km/h, and the wind direction was between 165° and 210°, except for a brief, 2-hour period when it shifted to 230-240°. At the end of the event, as well as the wind direction change, wind speed dropped dramatically from about 55 km/h to 20 km/h, ambient temperature dropped by 4°C to 6°C, and ambient pressure increased by 6 mbar to 1016 mbar, indicative of a high pressure front moving in. In particular because this event occurred shortly after the continuous O₂/N₂ ratio time series began, I carefully

checked to ensure that there was no evidence of instrumental or calibration anomalies for the duration of this event.

As shown in Figure 4.14, O_2/N_2 was initially relatively constant, and about 15 per meg lower than expected when compared to results from our flask sampling program at Cape Grim. Then O_2/N_2 was observed to decrease in an approximately linear fashion over a period of approximately 18 hours by 80 per meg. Finally, the O_2/N_2 ratio steadied at a very low value of about -330 per meg, then the baseline event ended dramatically as the wind changed, and O_2/N_2 decreased further, before recovering again. In this latter case changes are clearly due to anthropogenic or land biotic sources and sinks. Unfortunately, at the beginning of the dramatic decrease in O_2/N_2 ratios at about 12:00, 4 July, there is a 2.5-hour gap in the data when the O_2 analyzer carried out a daily calibration cycle. Despite this missing data, I am confident that the existing data support the conclusion that a downward trend in O_2/N_2 began at about the same time that the calibration started. A second gap seen in the data at the same time on 5 July is the following day's calibration.

Also shown in Figure 4.14 is the CO_2 concentration over the same time period and on the same effective scale so that molar changes are comparable for both O_2 and CO_2 on a visual basis. Note that the CO_2 concentration scale has been reversed so that decreases in O_2/N_2 will have the same sign as increases in CO_2 concentration. These data appear to show that CO_2 was relatively constant over this time period, which is what one would generally expect during a baseline event. However, when I expand the CO_2 scale, as shown in Figure 4.15, a relatively significant increase in CO_2 of at least 1.5 ppm is observed. Unfortunately the Baring Head CO_2 analyzer was experiencing

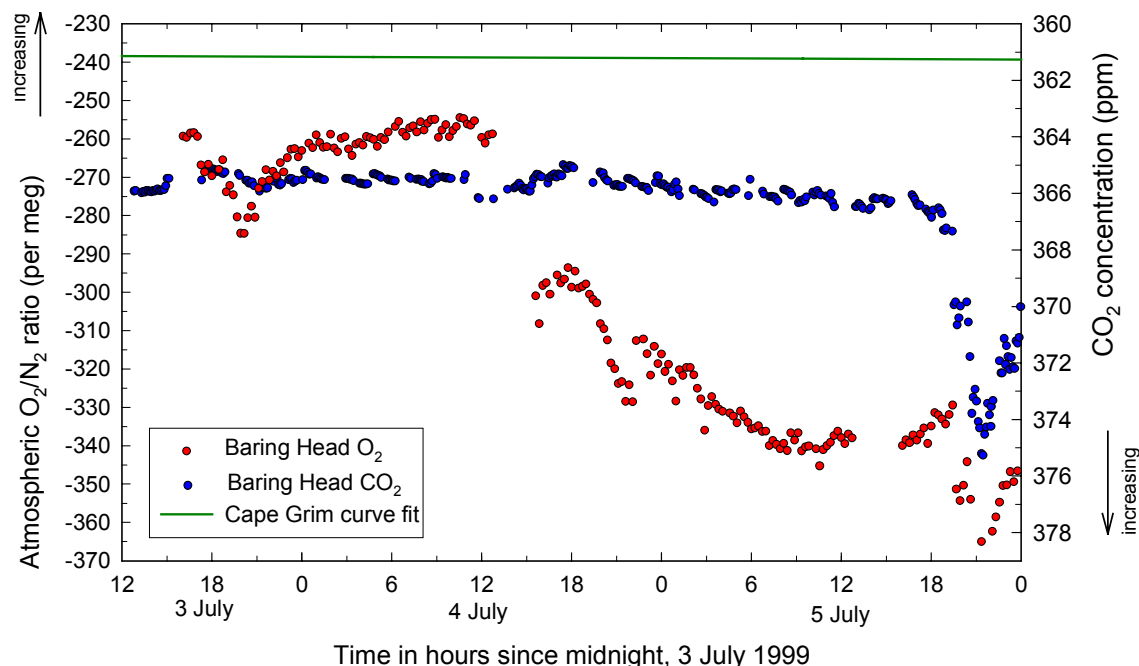


Figure 4.14. O_2/N_2 ratio and CO_2 concentration at Baring Head for 3-5 July 1999. Note that O_2/N_2 ratio and CO_2 concentration axes are reversed with respect to each other. In addition these axes are scaled so that changes in O_2 and CO_2 are comparable on a mole to mole basis. The green line shows the curve fit to the O_2/N_2 ratio data from flask samples collected at Cape Grim, Tasmania.

some technical problems during this time period, as illustrated by the abnormally noisy signal. Therefore a more precise determination on the exact increase in CO_2 concentration can not be made, however, it is clearly of the order of 1.5 ppm.

These changes in O_2/N_2 ratio and CO_2 concentration can not be attributed to land biotic or anthropogenic effects, because the observed $O_2:C$ molar ratio is approximately $-11:1$, instead of $-1.1:1$ that would be observed from land biotic effects, or $-1.4:1$ that would be observed from fossil fuel combustion. This leaves only oceanic processes that could be responsible for the observations.

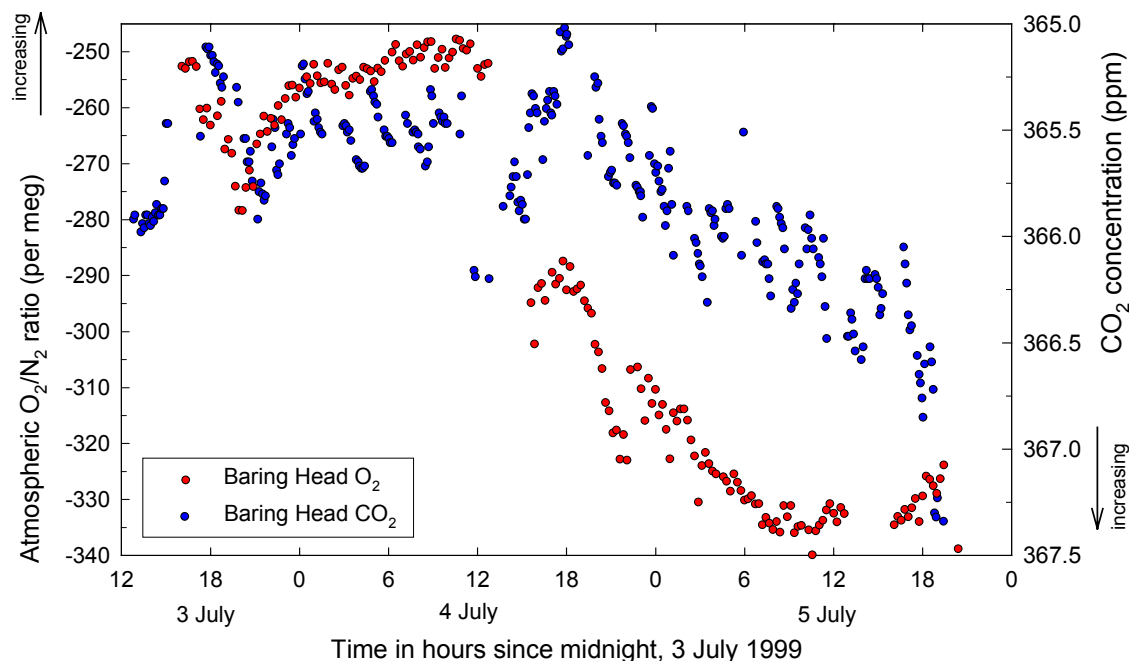


Figure 4.15. As for Figure 4.14, except the CO₂ axis has been blown up, showing that CO₂ concentrations increased at the same time that O₂/N₂ ratios decreased.

To help identify the origin of the sampled air, I have calculated 72-hour backward wind trajectories using the HYbrid Single-Particle Lagrangian Integrated Trajectory model, version 4 (HYSPLIT4), developed by the NOAA Air Resources Laboratory [Draxler and Hess, 1998]. This model uses 1° meteorological analyses from the National Center for Environmental Prediction as input fields. In Figure 4.16, I show one such trajectory calculation for air arriving at Baring Head at 12:00, 4 July 1999 NZST. This figure clearly shows that the air arriving at Baring Head was solely of oceanic origin, and from relatively high latitudes in the Southern Ocean.

There is some concern regarding the accuracy of such trajectory models in the southern hemisphere where direct observations are relatively sparse and the model must

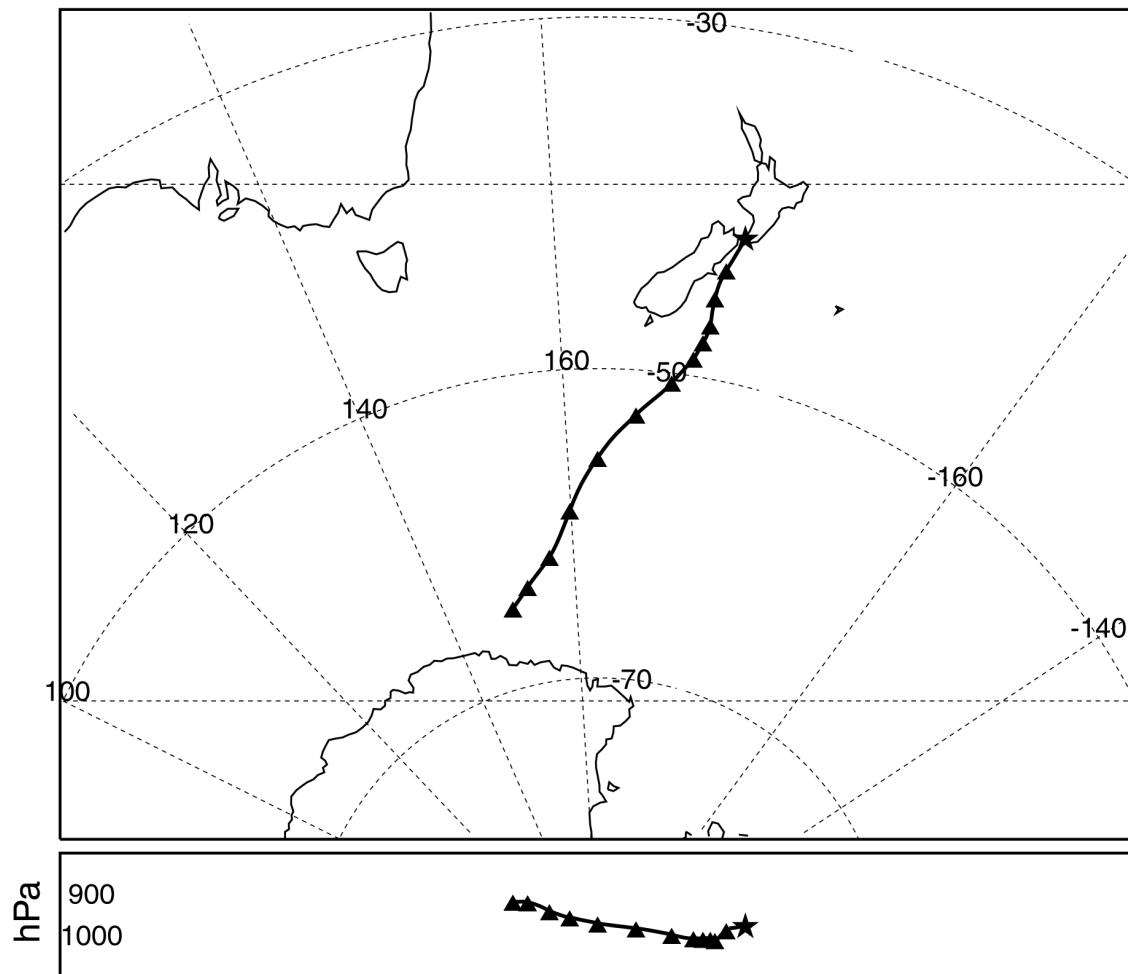


Figure 4.16. Three-day backward wind trajectory ending at 12:00 4 July 1999 at Baring Head, New Zealand. Calculated using the HYSPLIT program (see text). This shows that during this southerly event, wind was derived from high latitudes in the Southern Ocean and has not passed over any land mass, in particular missing the South Island of New Zealand.

rely heavily on satellite scatterometer winds and interpolation routines. Therefore I calculated back trajectories at many other times not shown here, including at the start and end of the baseline event, as indicated by the observed wind changes at Baring Head. The HYSPLIT model captured all of these observed wind changes remarkably

well, except that both the beginning and end of the baseline event occurred about 6 hours later in the model. These results provide confidence in the model's prediction of the origin of the air arriving at Baring Head in Figure 4.16. The model indicated that before the baseline event, the air originated from north of the North Island, whereas afterwards, although the wind at Baring Head was again a northwesterly, the air in fact originated from the southwest Pacific, but had traveled up across the South Island.

What oceanic process could cause such a dramatic drawdown in O_2/N_2 ratios as observed here? To highlight the magnitude of this effect, in this 18 hour period, O_2/N_2 decreased by about 80% of the seasonal amplitude observed at Baring Head, and CO_2 increased by about 100% of the amplitude of its seasonal cycle. I do not think that the processes involved could be a purely local effect around the region of Cook Strait, because the wind speed for the duration of the event was 35 km/h or higher, indicating that the sampled air mass was representative of a large region of the Southern Ocean, as further evidenced by the backward wind trajectory plot of Figure 4.16.

A strong oceanic upwelling event, perhaps off the east coast of the South Island, could bring O_2 -depleted waters to the surface, presenting a net O_2 demand to the atmosphere. Such deeper waters would have higher CO_2 concentrations owing to respiring organic matter, thus they could also present a net CO_2 supply to the atmosphere, in agreement with the observations at Baring Head. The CO_2 exchange with the atmosphere would be significantly buffered by the reactions of CO_2 with seawater to form carbonate and bicarbonate ions, thus explaining the very large negative $O_2:C$ ratio of $-11:1$ observed. Unfortunately I was unable to obtain satellite SST data to

support this upwelling hypothesis, since the entire New Zealand region was almost completely overcast during this time period.

Irrelevant of the causes of this event, such high resolution temporal sampling of O_2/N_2 ratios have shown that non-anthropogenic processes are capable of influencing O_2/N_2 ratios to a degree not previously suspected. This event also illustrates that additional care needs to be taken in assessing appropriate baseline conditions for flask sampling, not only for O_2/N_2 , ratio, but for atmospheric CO_2 sampling also. Without real-time continuous O_2/N_2 and CO_2 monitoring at Baring Head, and based only on the adopted criteria for baseline conditions, if a flask sample had been collected at 06:00 on 4 July 1999, a result 80 per meg higher in O_2/N_2 ratio and 1.5 ppm lower in CO_2 concentration would have been obtained compared to a sample collected at 06:00 on 5 July 1999.

The question now needs to be asked, are such significant oceanic impacts on O_2/N_2 ratios and CO_2 concentrations a unique feature to Baring Head, or could they be present at other baseline monitoring stations also? Because of the high wind speed, I suspect that the effect was regional as opposed to local, suggesting that other parts of the world could have similar processes occurring. Our flask data from Cold Bay, Alaska (Chapter 2) and data from Point Barrow, Alaska (M. Bender, personal communication) both exhibit high short-term variability compared to other sites, and this variability is most probably linked to oceanic processes similar to the event described here.

Two final points should be made about this event from 3-5 July 1999. First, NIWA personnel have an additional criteria to define a “baseline” event, which is that CO_2 concentrations must be steady as defined by at least six consecutive hours with

standard deviation below 0.1 ppm. This 3-5 July period did not in fact meet these requirements. It is not possible to determine whether this was because of the technical problems experienced by the CO₂ analyzer, or because the real atmospheric variability in CO₂ was greater than 0.1 ppm over six hours (M. Manning, personal communication). Therefore the only conclusion that can be made, is that the meteorological conditions were such that we would expect baseline conditions. The second point relates to the frequency of such events. From an analysis of the monthly plots of Figure 4.13, I did not find any other events with this magnitude change in O₂/N₂ ratios (or APO). Smaller, but still significant, changes during baseline conditions of the order of 20 to 30 per meg were observed on a more regular basis.

4.5. Determining the land biotic O₂:C ratio

The approximate chemical reaction describing photosynthesis and respiration is $\text{CO}_2 + \text{H}_2\text{O} \leftrightarrow \text{CH}_2\text{O} + \text{O}_2$, where the forward reaction represents photosynthesis and the reverse reaction represents respiration. However, CH₂O is only an approximate representation for organic matter because other elements such as nitrogen and sulphur are also present in small quantities. Therefore the actual land biotic O₂:C molar ratio in this equation is not -1.0 but closer to -1.1 [Severinghaus, 1995]. This value of -1.1 is little more than a guess, however (J. Severinghaus, personal communication).

In order to separate land biotic and oceanic components of the atmospheric O₂ signal, and to derive global land biotic and oceanic carbon sink estimates, this ratio needs to be well known. One method of determining this ratio is from analyzing the concurrent changes in atmospheric O₂/N₂ ratios and CO₂ concentrations, when such

changes can be assumed to be caused by the land biota only. Clearly such a calculation will only define the O₂:C ratio locally, but observations at several stations globally will help to define this ratio more precisely, and to obtain an idea on how much the ratio may vary on spatial and temporal scales. Baring Head is a good location to observe this ratio, since when the winds are from the north, changes in O₂/N₂ and CO₂ appear to be almost entirely due to land biotic processes.

4.5.1. Preliminary Analyses of Land Biotic O₂:C Ratios

I examined the Baring Head monthly plots of Figure 4.13 to find periods of persistent northerlies. One such period is from 3-10 November 1999. Figure 4.17 shows a plot of O₂/N₂ ratio versus CO₂ concentration for this period, where I filtered out all data that did not have a wind direction between 315° and 45°. These data resulted in an O₂:C ratio of 1.13 mol O₂ consumed per mol of CO₂ produced. The r^2 on these data was 0.91, showing a strong correlation between O₂ and CO₂ changes.

This value of 1.13 is in good agreement with the earlier work of *Severinghaus* [1995]. However, it is very preliminary, in that I have not yet examined how this ratio varies over different temporal scales. Further investigations will soon be carried out to observe how the ratio may vary on diurnal and seasonal time scales. Such investigations will allow us to report a global average number and its associated uncertainty with greater accuracy.

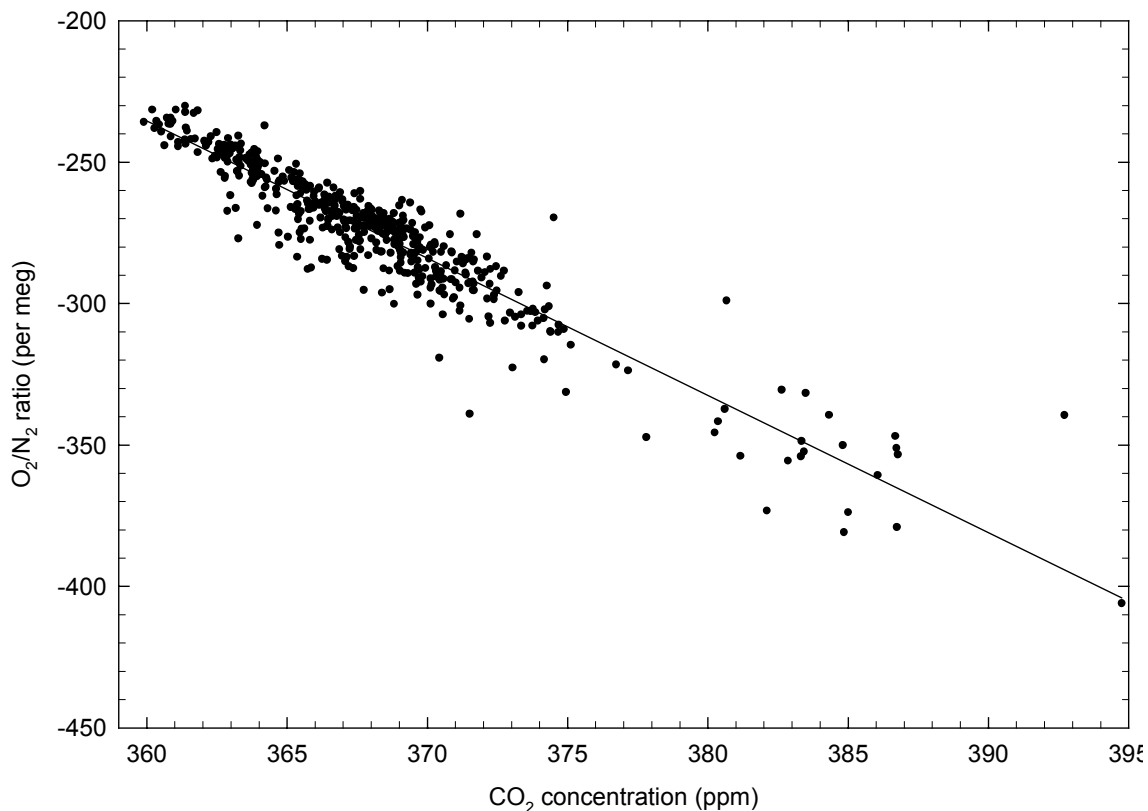


Figure 4.17. Shows the O₂/N₂ ratio correlation with CO₂ concentration for air arriving at Baring Head from 3-10 November 1999. These data have a slope of 1.13 mol O₂ consumed per mole of CO₂ produced, and have a good r^2 value of 0.91. Wind conditions during this time were persistent northerlies, indicating that the land biota is the main influence driving O₂/N₂ ratio and CO₂ concentration changes.

4.5.2. Computational Techniques Used to Derive O₂:C Ratios

An important point needs to be made concerning the computation of O₂:C ratios such as those derived in this dissertation and elsewhere. The method for determining such numbers from atmospheric measurements such as those presented here generally consists of plotting O₂/N₂ ratios against CO₂ concentrations and fitting a linear model to the data using a linear least squares fitting technique. Typically, such a fit is achieved by using standard functions available in popular commercial software packages such as

Microsoft Excel. Most of the functions in these packages assume an independent x variable and proceed to minimize the sum of the squares of the y data from the fitted linear model in an iterative fashion. But in fact, what the calculations presented here require, is a method which will simultaneously minimize the sum of the squares of both the x and y data from the linear model. I have written a program in Matlab which achieves such a computation, using a non-linear fitting technique to minimize the sum of the squares of both the x and y data from the linear model.

To demonstrate that such careful calculations are necessary in this work, I performed a sensitivity analysis. I used as my example the subset of data described above, from 3-10 November, 1999, with the results shown in Table 4.3. First, the standard linear least squares fitting function in Excel was employed, which minimizes the sum of the squares of the fitted linear model to the y data only, treating x as an independent variable. This computation was run twice, first with CO_2 as the independent variable, then with O_2 as the independent variable. As shown in the table, the difference between the two is large, greater than 0.1 mol O_2 per mol CO_2 .

The size of this difference depends directly on how closely the data fit the linear model, which can be quantified with the r^2 parameter (r^2 is the square of the Pearson product moment correlation coefficient and ranges from 0 to 1, where 1 indicates a perfect fit to the model). In the case of the data I used in this sensitivity analysis, my r^2 value was 0.91, demonstrating that the data are a good fit to the linear model, and demonstrating that even with a fit this good, large errors can be propagated when using an erroneous method for computing the $\text{O}_2:\text{C}$ slope.

Table 4.3. Comparison of Techniques for Computing O₂:C Ratios

Technique	y	x	-O ₂ :C molar ratio from fitted slope
Excel, linear fit	O ₂	CO ₂	1.027
Excel, linear fit	CO ₂	O ₂	1.132
Average of Excel	-	-	1.080
“perpendicular” fit	O ₂	CO ₂	1.083
Matlab, non-linear fit	O ₂	CO ₂	1.127
Matlab, non-linear fit	CO ₂	O ₂	1.128

The non-linear fitting program used in Matlab gave a result of 1.127 mol O₂ consumed per mol CO₂ produced. As a consistency check on this method, I ran the same data through the program, reversing the x and y variables, resulting in a value of 1.128. Another popular method commonly referred to as the “perpendicular fit” method also gave an erroneous result. The final point to be made from this analysis is that taking an average of the two Excel results is also not an appropriate method, giving 1.080 in this example. Instead, a technique which simultaneously minimizes the sum of the squares of both x and y variables from the fitted model is required.

4.6. References

- Ciais, P., P.P. Tans, M. Trolier, J.W.C. White, and R.J. Francey, A large northern hemisphere terrestrial CO₂ sink indicated by the ¹³C/¹²C ratio of atmospheric CO₂, *Science*, 269, 1098-1102, 1995.
- Draxler, R.R., and G.D. Hess, An overview of the HYSPLIT_4 modelling system for trajectories, dispersion, and deposition, *Aust. Met. Mag.*, 47, 295-308, 1998.
- Fan, S., M. Gloor, J. Mahlman, S. Pacala, J. Sarmiento, T. Takahashi, and P. Tans, A large terrestrial carbon sink in North America implied by atmospheric and oceanic carbon dioxide data and models, *Science*, 282 (5388), 442-446, 1998.
- Gille, S.T., D.P. Stevens, R.T. Tokmakian, and K.J. Heywood, Antarctic Circumpolar Current response to zonally-averaged winds, in *Journal of Geophysical Research*, 2000.
- Houghton, R.A., J.L. Hackler, and K.T. Lawrence, The US carbon budget: Contributions from land-use change, *Science*, 285 (5427), 574-578, 1999.
- Keeling, C.D., J.F.S. Chin, and T.P. Whorf, Increased activity of northern vegetation inferred from atmospheric CO₂ measurements, *Nature*, 382, 146-149, 1996.
- Keeling, R.F., Measuring correlations between atmospheric oxygen and carbon dioxide mole fractions: A preliminary study in urban air, *Journal of Atmospheric Chemistry*, 7, 153-176, 1988.
- Keeling, R.F., A.C. Manning, E.M. McEvoy, and S.R. Shertz, Methods for measuring changes in atmospheric O₂ concentration and their applications in southern hemisphere air, *Journal of Geophysical Research*, 103 (D3), 3381-3397, 1998.
- Keeling, R.F., S.C. Piper, and M. Heimann, Global and hemispheric CO₂ sinks deduced from changes in atmospheric O₂ concentration, *Nature*, 381, 218-221, 1996.
- Lowe, D.C., Atmospheric carbon dioxide in the southern hemisphere, *Aust. J. Clean Air*, 8, 12-15, 1974.
- Lowe, D.C., P.R. Guenther, and C.D. Keeling, The concentration of atmospheric carbon dioxide at Baring Head, New Zealand, *Tellus*, 31, 58-67, 1979.
- Manning, M.R., A.J. Gomez, and G.W. Brailsford, The New Zealand CO₂ measurement programme, in *Proceedings of WMO Meeting of Experts on CO₂ Measurement, Melbourne, 1 - 4 September, 1997*, edited by R.J. Francey, World Meteorological Office, 1999.

- Manning, M.R., A.J. Gomez, and K.P. Pohl, Atmospheric CO₂ record from in-situ measurements at Baring Head, in *Trends '93: A compendium of data on global change, ORNL/CDIAC-65*, edited by T.A. Boden, D.P. Kaiser, R.J. Sepanski, and F.W. Stoess, pp. 174-178, Carbon Dioxide Information Analysis Center, Oak Ridge National Laboratory, Oak Ridge, Tennessee, U.S.A., 1994.
- Murnane, R.J., J.L. Sarmiento, and C. Le Quere, Spatial distribution of air-sea CO₂ fluxes and the interhemispheric transport of carbon by the oceans, *Global Biogeochemical Cycles*, 13 (2), 287-305, 1999.
- Myneni, R.B., C.D. Keeling, C.J. Tucker, G. Asrar, and R.R. Nemani, Increased plant growth in the northern high latitudes from 1981 to 1991, *Nature*, 386 (6626), 698-702, 1997.
- Rayner, P.J., I.G. Enting, R.J. Francey, and R. Langenfelds, Reconstructing the recent carbon cycle from atmospheric CO₂, $\delta^{13}\text{C}$ and O₂/N₂ observations, *Tellus Series B-Chemical and Physical Meteorology*, 51 (2), 213-232, 1999.
- Sarmiento, J.L., T.M.C. Hughes, R.J. Stouffer, and S. Manabe, Simulated response of the ocean carbon cycle to anthropogenic climate warming, *Nature*, 393, 245-249, 1998.
- Schimel, D., J. Melillo, H. Tian, A.D. McGuire, D. Kicklighter, T. Kittel, N. Rosenbloom, S. Running, P. Thornton, D. Ojima, W. Parton, R. Kelly, M. Sykes, R. Neilson, and B. Rizzo, Contribution of increasing CO₂ and climate to carbon storage by ecosystems in the United States, *Science*, 287 (5460), 2004-2006, 2000.
- Severinghaus, J.P., Studies of the terrestrial O₂ and carbon cycles in sand dune gases and in Biosphere 2, Ph.D. thesis, Columbia University, New York, U.S.A., 1995.
- Severinghaus, J.P., M.L. Bender, R.F. Keeling, and W.S. Broecker, Fractionation of soil gases by diffusion of water vapor, gravitational settling, and thermal diffusion, *Geochimica et Cosmochimica Acta*, 60 (6), 1005-1018, 1996.

Appendix 1.
Baring Head oxygen system
LabVIEW programming

This appendix gives a brief outline of the LabVIEW program running the continuous atmospheric O₂ system at Baring Head, New Zealand. Programming structure is not discussed in any depth, but rather the structure of the output files generated.

The LabVIEW program was co-written by myself and Antony Gomez of NIWA (National Institute of Water and Atmospheric Research), New Zealand. It consists of 123 custom-written “vi”s or subroutines, contained in seven different libraries. The libraries group different classes of vi’s together, and are called:

FrontEnd.llb - start-up and user interface.

Globals.llb - definitions of all global variables.

Intrface.llb - digital and analog data acquisition interfacing routines.

SysInOut.llb - reading from and writing to various system and data files.

Process.llb - performs all calculations and controls all valve sequencing.

Simulate.llb - routines for running the program in a simulation mode.

Utility.llb - miscellaneous utility routines.

Four INI files define system variables and parameters, and are read into the program on start up. They are:

O2Sys.ini

O2Cycles.ini

O2WTanks.ini

O2Gases.ini

O2Sys.ini defines many operating parameters of the system such as the time periods for all air and calibration gas jogs and flushing intervals, and minimum or maximum criteria used before warning flags will be given on various gas handling operating parameters.

O2Cycles.ini is able to store six different sample air or calibration gas cycles, and contains information on how frequently to run each cycle, when each cycle is next scheduled to be run, and what valve switching protocol is used for each cycle.

O2WTanks.ini contains information on the past, current, and future working gases used by the system. The information contained in this file is written as a header to the raw data output files each day.

O2Gases.ini contains information on all of the long term calibration gases, including the high span (HS) and low span (LS) gases, and is also written to the header of the raw data output files each day.

In addition to controlling all solenoid valve sequencing, cycling of sample air and calibration gases, and acquisition of data, the LabVIEW program also generates five different categories of output files, including final calculations of atmospheric O₂/N₂ ratios and CO₂ concentrations in per meg and ppm units respectively. This real-time generation of O₂/N₂ and CO₂ data into atmospheric concentration units greatly facilitates data handling procedures and prompt analysis of the data. In addition it provides useful diagnostic information with which I am able to identify and resolve

potential problems, without being present on-site, nor requiring NIWA personnel to keep a close check on the system.

The five different categories of output files are:

- | | |
|---------------------|-----------------------|
| 1. YYYYMMDDHHMM.DAT | e.g. 199912050000.DAT |
| 2. YYYYMMDDHHMM.DIG | e.g. 199912050000.DIG |
| 3. YYYYMM.DIF | e.g. 199912.DIF |
| 4. YYYYHSL.S.DAT | e.g. 1999HSL.S.DAT |
| 5. YYYYSPAN.DAT | e.g. 1999SPAN.DAT |

1. YYYYMMDDHHMM.DAT is the primary raw data file, consisting of one row of raw data every 30 seconds and includes O₂ and CO₂ concentration information, and ambient meteorological data. A header in this file copies information from the O2WTanks.ini and O2Gases.ini files, detailing current information on working gases and calibration gases in use.

2. YYYYMMDDHHMM.DIG is the primary diagnostic data file, also consisting of one row of raw data every 30 seconds, and contains information on flowrates, pressures, and temperatures in the system. Both this file and the YYYYMMDDHHMM.DAT file include information on the present air sample or calibration cycle that is in operation, and on what airline or gas stream is passing through the O₂ and CO₂ analyzers at any given time. Both files also contain user-entered notes, as well as system-generated messages for various procedures, for example, if the system switches to UPS power, or if working gas pressure is low. Generally, there is one of each of these files for each day, and they are created at midnight. However, if the system is stopped and restarted, new files with the appropriate time stamp in the file name will be generated.

3. YYYYMM.DIF contains processed ambient air data. For each WT-Air-WT cycle (WT denotes working tank gas), one row of data is generated. With the valve switching sequence currently employed, this results in one row of data every 15 minutes. Raw O₂ data in Volts from each Air jog are averaged, and subtracted from an interpolated WT value. From the most recent HS/LS calibration information a value in per meg concentration units is reported, including a CO₂ dilution correction. CO₂ concentration (in both ppm units, and raw 'bits') and meteorological data are also averaged and reported for the duration of the ambient air jog. A new *.DIF file is generated each month. Data from figures 4.8 to 4.12 were derived from these monthly files.

4. YYYYHSL.S.DAT contains information on the HS/LS calibrations which are typically run once per day. Each HS or LS jog is represented by one row in this file. Similarly to the YYYYMM.DIF file, data is reported as the WT-HS-WT difference (or WT-LS-WT). Typically, 5 jogs each of HS and LS are run, hence there will be 10

rows of data per day in this file. This file is created at the start of each year, with data appended at the end of each daily calibration cycle.

5. YYYYSPAN.DAT shows one row of data for each time the HS/LS calibration cycle is run, typically once per day. The information contained in the YYYYHSL.DAT file is used to compute the paramagnetic analyzer O₂ span and the working gas concentration. The first jog of each HS and LS calibration is ignored in this calculation. The purpose of this file is to quickly show trends in the paramagnetic analyzer O₂ span, and in the working gas concentration over time. Data from this file were used to generate Figures 4.6 and 4.7. If extraneous values appear in this file, the YYYYHSL.DAT file provides additional information enabling the cause of the problem to be determined.

A description of the columns in each data file follows.

1. YYYYMMDDHHMM.DAT

DDMMYYYY - date.

HHMM - time.

Status - indicates whether calibration gas or ambient air is flowing through the analyzer. If calibration gas, which one is specified; and if air, informs on the status of the CO₂ system (needed for CO₂ corrections), i.e. running Airline 1, 2, or if the CO₂ system is on a calibration cycle.

O2_mV - average O₂ concentration in mV of 30 one-second data points.

O2_stddev - standard deviation of O₂ concentration in mV over the 30 second time interval.

O2_min - minimum O₂ concentration in mV over the 30 second time interval.

O2_max - maximum O₂ concentration in mV over the 30 second time interval.

O2_meg - running estimate of the average O₂ concentration for the 30 sec time interval, converted to approximate per meg units. No WT interpolation is made, since this calculation runs in real-time, hence it is only an approximation. A CO₂ correction is made.

CO2_bits - gives the raw output from the CO₂ analyzer in bits. This is the instantaneous output at the end of the 30 sec interval. If the CO₂ system is currently running a calibration cycle, this column will record the last CO₂ value before the calibration run started. If the O₂ system is running a calibration run, or working gas, this column will record "99999".

CO2_ppm - also taken directly from the CO₂ system, gives the estimated CO₂ concentration in ppm. Also an instantaneous value at the end of the 30 sec interval. If the CO₂ system is running a calibration, then as for CO₂_bits, this column will record the last ambient airline value, in ppm. However, if the O₂ system is on a calibration run or working gas, this column will record the assigned CO₂ concentration for that cylinder taken from the O2Gases.ini or O2WTanks.ini file.

Flag_Code - this is the binary-converted-decimal that records zero if there are no problems over the 30 sec interval, or a non-zero number otherwise, depending on what the problem is. Problems being monitored are:

- (1) Gas pressure low - flag TRUE if working gas pressure is < 300 psig.
- (2) Flow control bad - flag TRUE if MKS pressure controller reads > 5.08V or < 4.92V.
- (4) Pressure bad - flag TRUE if analyzer pressure < 3.5 psig.
- (8) Temperature bad - flag TRUE if analyzer temperature < 39°C or if 10 min standard deviation > 0.1°C.
- (16) Chiller temp. bad - flag TRUE if chiller temperature > -65°C
- (32) UPS on battery - flag TRUE if UPS is running on battery power.

Amb_Temp - instantaneous ambient temperature in °C, derived from CO₂ computer.

Amb_Press - instantaneous ambient pressure in mbar, derived from CO₂ computer.

Amb_RH - instantaneous ambient relative humidity in %, derived from CO₂ computer.

Wnd_Spd - instantaneous ambient wind speed in knots, derived from CO₂ computer.

Wnd_Dirn - instantaneous ambient wind direction in degrees, derived from CO₂ computer.

2. YYYYMMDDHHMM.DIG

DDMMYYYY - date.

HHMM - time.

Status - identical to Status column in YYYYMMDDHHMM.DAT file.

O2_mV - identical to O2_mV column in YYYYMMDDHHMM.DAT file.

F4_mL/min - instantaneous flowrate through the working gas flush four-way valve purge in mL/min (see Figure 4.4).

F5_mL/min - instantaneous flowrate through the O₂ analyzer bypass vent in mL/min (see Figure 4.4).

F6_mL/min - instantaneous flowrate through the O₂ analyzer in mL/min (see Figure 4.4).

AnalP_psi - instantaneous analyzer pressure in psig.

MKS_V - instantaneous reading of MKS pressure controller signal in Volts.

AnalT_C - instantaneous reading of analyzer temperature in °C.

TCntrl_V - instantaneous value of voltage being applied to the heater elements in V.

ChillerT_C - instantaneous reading of chiller temperature, taken from CO₂ computer in °C.

ValveState - indicates position of all computer controlled valves in system. That is: the 8-port Valco valve selecting a calibration gas (designated by letter A through H), and 6 solenoid valves (designated by 0 or 1's). Order is Valco valve; airline 1/airline2 four-way valve (V7 in Figure 4.4); calibration/air four-way valve (V9); working gas/air sample four-way (V14); working gas purge (V15); calibration fast purge (V10); and calibration slow purge (V12).

3. YYYYMM.DIF

DDMMYY - date.

HHMM - time.

HS_CylID - high span cylinder ID.

LS_CylID - low span cylinder ID.

WT_CylID - working gas cylinder ID.

Status - indicates what is happening on both O₂ and CO₂ systems during this O₂ air jog. Similar to the status flag in the YYYYMMDDHHMM.DAT files, but must now also account for the possibility of the CO₂ system switching to a different status during this O₂ jog.

Air-WT_mV - works and reports in mV, interpolates the working gas jogs on either side of the current air jog, and subtracts this interpolated value from the average of the air jog.

Error_mV - determines the error in Air-WT_mV by calculating the quadrature sum of errors on the air jog and the two working gas jogs before and after the current air jog.

Air-WT_meg - converts Air-WT_mV value from mV into per meg, using the most recently completed HS/LS calibration span data, and using CO₂_ppm (below) to make the appropriate CO₂ dilution correction. If there has been no completed HS/LS calibration in the preceding 48 hours, this column will record 99999.

Error_meg - converts Error_mV into per meg, using the most recently completed HS/LS calibration span data. Will record 999 if there has been no completed HS/LS calibration in the preceding 48 hours.

CO₂_Time - because of the asynchronicity of the CO₂ and O₂ systems, the time corresponding to the following CO₂ data is recorded.

CO₂_bits - similar to the CO₂_bits column in the YYYYMMDDHHMM.DAT file, except averaged over the O₂ air jog. Deals with possibilities of the CO₂ system switching to or from a calibration gas cycle during the O₂ air jog, or CO₂ being on calibration for the entire O₂ air jog. This column only calculates averages from the 30 second data when CO₂ is on an airline. It is assumed that no CO₂ spikes occur on switching between CO₂ airlines, or switching from a calibration cycle to an airline. And it is assumed that the O₂ airlines lag the CO₂ airlines by 3 minutes. If less than two CO₂ airline data records exist for the O₂ jog, the nearest valid CO₂ air data is used going backwards in time.

CO₂_ppm - similar to the CO₂_ppm column in the YYYYMMDDHHMM.DAT file, except averaged over the air jog. Deals with possibilities of the CO₂ system switching in the same manner as CO₂_bits described above.

Flag_Code - similar to the Flag_Code column in the YYYYMMDDHHMM.DAT file, with some modifications: stores a '0' if there are no problems for duration of the WT-Air-WT cycle. If there are one or more problems (as shown by the 30 sec Flag_Code entries in YYYYMMDDHHMM.DAT) for all or some of the WT-Air-WT cycle, then this column will store the average of all non-zero 30sec Flag_Code entries. In this way, more information is obtained on what the problem is, given the numbers assigned to each problem listed in Flag_Code in YYYYMMDDHHMM.DAT described above. If either or both of the working gas jogs have a standard deviation greater than 10 per

meg, 9000 will be added to this value. If CO₂_Time is more than 7 mins earlier than HHMM above, 90000 will be added to this value.

Amb_Temp - ambient temperature in °C, taken from CO₂ computer, averaged over air jog (does not include working gas jog or discarded section of air jog).

Amb_Press - ambient pressure in mbar, taken from CO₂ computer, averaged over air jog (does not include working gas jog, or discarded section of air jog).

Amb_RH - ambient relative humidity in %, taken from CO₂ computer, averaged over air jog (does not include working gas jog, or discarded section of air jog).

Wnd_Spd - ambient wind speed in knots, taken from CO₂ computer, averaged over air jog (does not include working gas jog, or discarded section of air jog).

Wnd_Dirn - ambient wind direction in degrees, taken from CO₂ computer, averaged over air jog (does not include working gas jog, or discarded section of air jog).

Calib_Used - shows the date and time of the calibration calculations that were used in calculating O₂ per meg values in this file. Time is the finish time of the HS/LS calibration, as also shown in the YYYYSPAN.DAT file.

4. YYYYHSL.S.DAT

DDMMYYYY - date.

HHMM - time.

Calib_CylID - high span or low span cylinder ID.

WT_CylID - working gas cylinder ID.

Calib-WT - similar to Air-WT_mV calculated in YYYYMM.DIF, except works on calibration jogs instead of air jogs. Units are mV.

Calib-WT_Error - determines the error for Calib-WT, similar to Error_mV calculated in YYYYMM.DIF. Units are mV.

Interim_Flag - diagnoses problems within a calibration jog. Reports over the interval of the current calibration jog and the working gas jog on either side of it. Returns a '0' if no problems; a '1' if any of the 30 second Flag_Codes were non-zero; a '2' if Calib-WT_Error is larger than 0.5 mV; or a '3' if '1' and '2' are both true.

5. YYYYSPAN.DAT

DDMMYYYY - date.

HHMM - time.

HS_CylID - high span cylinder ID.

LS_CylID - low span cylinder ID.

WT_CylID - working gas cylinder ID.

O2Span - is calculated when Cycle '3' is completed. Reports the O₂ analyzer span as determined from the declared concentrations of the HS and LS cylinders, and the completed calibration cycle. Units are per meg/mV.

O2Span_Error - Calculates the error in the O2Span based on a quadrature sum of errors. The initial errors worked with are the standard deviations of the arrays of HS-WT and LS-WT differences. Units are per meg/mV.

WTO2_meg - also calculated when Cycle '3' is completed. From the O2Span and from the HS and LS differences from the working gas in mV, a new daily working gas concentration is defined. Units are per meg.

WTO2_Error - is derived in a similar manner as O2Span_Error. As for O2Span_Error, the initial errors that are worked with are the standard deviations of the HS-WT and LS-WT difference arrays. Units are per meg.

Calib_Flag - diagnoses problems over the entire calibration cycle. Returns a '0' if no problems; a '1' if any of the 30 second Flag_Codes for the duration of the calibration were non-zero; a '2' if all the 30 second Flag_Codes are zero, but either O2Span_Error or WTO2_Error are larger than a specified amount (set to 0.05 per meg/mV, and 3 per meg respectively); or a '3' if both '1' and '2' are true.

Appendix 2.

Support

During the long course of my Ph.D. career, the support I have had from family, friends and colleagues has been overwhelming, as I have already mentioned in my acknowledgements. In many cases, such support has been both incredibly understanding, as well as uplifting and humorous, as the following email demonstrates, sent from a fellow Kiwi, Paul Drayton, who often had to wait months before I managed to reply to his emails.

Gidday Andrew,

Since I know you are very busy, I'll include a multi choice e-mail so that you can write back quickly.

1. I have finished this much of my thesis:

- A. All of it, but I can't decide what colour the cover should be.
- B. Most of it, except the appendices.
- C. A couple of main chapters.
- D. It's written on two cocktail napkins from happy hour last night.

2. I relax by:

- A. Partying with models.
- B. By watching TV, mostly movies starring models.
- C. By trying to remember what a model is.
- D. By running the computer model again to see if it works this time.

3. My apartment is:

- A. Spotless, since the maid comes daily.
- B. A little untidy, but I can still see the carpet.
- C. A Superfund site, where the mold in the bathroom has evolved into a new lifeform.
- D. A place I don't go, I now live in my office.

4. The best thing about writing a thesis is:

- A. Putting together all of my ideas into a dazzling Unified Theory of Everything.
- B. Putting together some things that were important at the time.
- C. Finding that my two finger typing is getting faster.
- D. Realising that my advisor will have to suffer by reading it, even if it's not as much as I suffered by writing it.

5. After finishing my thesis I will:

- A. Party like it is 1999 (again).
- B. Relax, and go out for a good meal.
- C. Sleep for three weeks and finally take a shower.
- D. Put on a jacket and gloves as Hell has just frozen over.

Mistakes found
If you find more, please email me at: andmalolo@gmail.com

1) Page 25:

I referenced Bender and Battle, 1999, but they got it wrong. Saying that 98% of the CO₂ in atmosphere/ocean system is in the ocean. They (and I) should have said carbon.

2) Page 84:

Says "...as shown in section 2.6 of this chapter", but actually, I never did talk about interannual variability of interhemispheric gradients.

3) Page 93:

Standard error calculations. I have no idea what I was thinking at the time, but this is NOT standard error.

4) Chapter 4, all data:

S1 versus S2 scale problem. Not sure if I have been consistent everywhere. I'm fairly sure that all Baring Head data is reported on S1 scale. Therefore, e.g. in comparisons with CGO data, must make sure that this is also on S1 scale.

5) Chapter 4:

Baring Head archive tank data does not have CO₂ correction applied. See my file "ArchiveRuns.xls", where this correction has now been applied. Note also that archive tanks in thesis are reported on SIO S1 scale – this is not "wrong", but one should be aware of it.

6) Page 131:

Murnane *et al.* statement, should say CO₂-enriched waters, not CO₂-depleted waters.

7) Page 136:

5,000 per meg/h should actually only be 200 per meg/h! (200 per meg/h corresponds to 40 ppm/h which is what the drift rate was after modifications of Chapter 3. 500 per meg/h is initial drift rate from factory specs. 5,000 per meg/h is from nowhere!).

8) Page 146:

Plumbing diagram of BHD setup – shows tee to paramagnetic bypass inside temperature-controlled environment – it should be, but in fact it is not!

9) Pages 172-177:

Figure 4.13 – months with less than 31 days still show data until the 31st – some sort of strange data processing bug.

10) Sections 4.5.1 and 4.5.2:

For all these fits, I did not weight O₂ relative to CO₂ at all. Need to rerun all fitting routines on molar basis, i.e. with O₂*0.2095.

Have now done this. Can see results on page 87 of my "Computer/Data Workbook #2".

11) Page 190:

Gomez, 1996 reference completely missing from Chapter 4 references.